

N O T I C E

THIS DOCUMENT HAS BEEN REPRODUCED FROM
MICROFICHE. ALTHOUGH IT IS RECOGNIZED THAT
CERTAIN PORTIONS ARE ILLEGIBLE, IT IS BEING RELEASED
IN THE INTEREST OF MAKING AVAILABLE AS MUCH
INFORMATION AS POSSIBLE



National Aeronautics and
Space Administration

Lyndon B. Johnson Space Center

Houston, Texas 77058

FEBRUARY 1979

INTRODUCTION TO THE APOLLO COLLECTIONS:

PART II

LUNAR BRECCIAS

PATRICIA E. MCGEE

CHARLES H. SIMONDS

JEFFREY L. WARNER

WILLIAM C. PHINNEY

(NASA-CR-162559) INTRODUCTION TO THE APOLLO
COLLECTIONS: PART 2: LUNAR BRECCIAS
(NASA) 206 p HC A10/MF A01 CSCL 03E

N80-15013

Unclas
G3/91 46523



INTRODUCTION TO THE APOLLO COLLECTIONS

PART II

LUNAR BRECCIAS

BY

P.E. McGee¹, C.H. Simonds², J.L. Warner³ and W.C. Phinney³

¹Lockheed Electronics Co., Inc.
Houston, Texas 77058

²Lunar Curatorial Laboratory
Northrop Services Inc.
Houston, Texas 77034

³NASA-Johnson Space Center
Houston, Texas 77058

TABLE OF CONTENTS

I. Introduction.....	1-10
II. Classification of Lunar Breccias.....	11-16
III. The Cratering Process.....	17-19
IV. Two-Component Thermal Model of Impact Breccia Lithification.....	20-21
V. A Discussion of Pristine Lunar Crustal Compositions.....	22-23
VI. Chemical Systematics of the Highland Breccias.....	24-30
VII. The Lunar Regolith.....	31-36
VIII. Petrogenesis of the Lunar Breccias.....	37-40
IX. Lunar Evolution.....	41-43
X. Petrographic Descriptions of the Lunar Breccias.....	44-177
XI. Geochemistry.....	178-189
XII. Bibliography.....	190-203

Introduction

The lunar breccias represent perhaps the most complex and challenging suite of lunar materials presently under study by lunar scientists. The combined efforts of scores of investigators in the fields of geology, geochronology, geophysics and geochemistry have produced an overwhelming collection of data, the evaluation of which has led to important observations and conclusions bearing on such pertinent issues as cratering processes, petrogenesis of the breccias and fractionation of the early lunar crust.

The purpose of this catalogue is to introduce a representative suite of lunar breccias to students and potential lunar sample investigators who have an interest in lunar rocks and the geology of the moon. The emphasis, as with the companion volume dealing with lunar igneous rocks, is on sample description and data presentation. Although some attempt is made to briefly familiarize the reader with the variety of existing petrogenetic models and the controversies related to each, the interpretive aspects of lunar breccias receive a secondary emphasis. This approach is intended to provide the basic petrographic, chemical and age data for a representative suite of these complex rocks while encouraging individual readers to seek additional, perhaps more detailed, sources of information (referenced throughout the catalogue) and ultimately to pursue their own investigation and evaluation of the existing data.

The samples chosen as representative were selected from a wide variety of chemical, petrographic and isotopic groupings. An attempt was made to choose samples which have undergone extensive scientific investigation, but data sets (especially geochemical) for some samples are embarrassingly small or nonexistent. Representative samples are listed in Table 1, together with a classification scheme based on matrix texture and mineralogy and the nature and abundance of glass present both in the matrix and as clasts. A calculus of the classification scheme (section II) which follows Table 1, describes the characteristic features of each of the breccia groups. In that section, the reader is made aware of alternative nomenclature and is urged to consult the referenced sources to avoid confusion which might result from differences in terminology.

Following the classification scheme is a discussion of the cratering process (section III) which describes the sequence of events immediately following an impact event, especially the thermal and material transport processes affecting the two major components of lunar breccias (i.e. clastic debris and fused material).

The section dealing with the cratering process is followed by a discussion of the two-component thermal model (section IV) of Simonds (1975) and Simonds et al. (1976) which describes the turbulent flow of impact melt and associated incorporation of clastic debris, the reaction of clasts with the melt, and the final equilibration of the clast-melt mixture. The model represents an important concept in the understanding of lunar breccias because it explains many of their observed petrographic and chemical features.

A discussion of pristine lunar crustal compositions (section V) has been included to emphasize the relationship between proposed crustal rock types and related rock types present as clasts in the lunar breccias.

A section dealing with the chemical systematics of highland breccias (section VI) serves to explain the chemical features of the breccias in terms of the compositional groupings established in the previous section.

Following the discussion of breccia chemistry, a brief discussion dealing with the process of regolith formation and modification (section VII) has been included to: 1) emphasize the significance of meteorite impact (both micrometeorite impact and large-scale basin forming impacts) as the single most important constructional and destructional process affecting the lunar surface and, 2) describe the major impact products which are common to all regolith samples and which have important implications relating to the problems of breccia petrogenesis. This section also contains a petrographic description of Apollo 11 regolith sample 10084, together with photomicrographs of the most commonly occurring constituents present in the sample.

A section dealing with breccia petrogenesis (section VIII) follows the discussion of the lunar regolith and represents perhaps the most important and certainly the most complex and controversial section. Although the purpose of this catalogue is basically descriptive in nature, it is important to introduce interested readers to the extremely numerous, infinitely complex, and commonly conflicting interpretations and evaluations which result from extensive studies of this suite of samples. Thus, this discussion attempts to relate the features (mainly descriptive) of each breccia group to presently existing petrogenetic models.

Following the section on petrogenesis is a brief outline of lunar evolution (section IX) based on interpretations of geological, geochronological, geophysical and geochemical data.

The main body of the catalogue (section X) contains the petrographic descriptions and descriptive data for individual breccia samples; sample numbers are listed in numerical order. Except for cases in which pertinent data is lacking, the format for each of the breccias is consistent and is presented in six categories:

1. A macroscopic description emphasizing such features as color, cohesiveness, porosity and extent of fracturing. This description is accompanied by "mug" shots (photographs of samples prior to cutting or chipping) of each sample and slab shots (photographs of the sawn surface) when they are available.
2. Lunar surface data which describes where and how the sample was collected and its orientation on the lunar surface (data of this type for the early Apollo missions [11 and 12] is typically nonexistent or, at best, highly speculative due to incomplete documentation during sampling on the lunar surface). A lunar map of the nearside of the moon (Figure 1) locates the landing sites for the Apollo missions and for the unmanned Ranger, Surveyor, Luna, and Lunokhod missions. Locations of described samples are shown on Figures 2, 3, 4, 5 and 6 which are detailed landing site maps for all Apollo missions except Apollo 11.
3. A new petrographic description of the important features of each breccia sample, including matrix characteristics and descriptions of included mineral and lithic clasts. Photomicrographs accompany the descriptions and serve to illustrate specific features of each breccia sample.
4. Graphical plots of mineralogical analyses including pyroxene quadrilaterals, Ab-An plots, and Fo-Fa plots for both matrix minerals and included clasts. A table containing modal data for each sample is also present. Mineralogical analyses and modal data are taken from the literature when such data are available and are referenced to the original work. Plots which contain no reference represent new data collected by the senior author.
5. Radiometric age data include crystallization ages determined by the Rb-Sr internal isochron method and the associated initial Sr isotope data. Ar^{40} - Ar^{39} plateau ages are included where such data are available. All age data are referenced to the original work.
6. A general reference list which refers readers to additional, perhaps more detailed sources of information, relating to various aspects of each particular sample. The list is not intended to be complete.

Following the petrographic descriptions and data is a table containing chemical analyses (section XI) of every breccia sample for which data are available. The table is divided into three sections which contain:

- 1) Major element chemistry based on X-ray fluorescence and gravimetric analyses.
- 2) Minor and trace element abundances for lithophile elements collected by isotope dilution mass spectrometry and neutron activation analyses.
- 3) Minor and trace element abundances for siderophile and chalcophile elements collected largely by radiochemical neutron activation analyses.

All analyses contained in the table are identified by a number which refers to the master reference list at the end of the catalogue.

A lengthy bibliography (section XII) represents the final section of the breccia catalogue. Bibliographic details are listed for all information referenced by number throughout the catalogue, including sources referenced (1) as additional reading in the section containing petrographic descriptions and data, (2) for graphical plots of mineral analyses and modal data, (3) for age data, and finally (4) for geochemistry.

Acknowledgements — We wish to thank J.A. Wood and J.T. Wasson for providing us with thin sections of sample 15445. L.E. Nyquist provided helpful assistance in the search for age data. D.P. Blanchard offered suggestions relating to REE data plots. We are indebted to L. Romero, A. Simmons, and S. Dorsett for typing the text and to G. Ryder and A. Cochran for helpful comments and advice. Work performed by P.E. McGee was supported by contract NAS 9-15800 between the Johnson Space Center and Lockheed Electronics Company, Inc. Work performed by C.H. Simonds was supported by contract NAS 9-15425 between the Johnson Space Center and Northrop Services Inc. for operation of the Lunar Curatorial Laboratory.

MANNED AND UNMANNED LUNAR LANDING SITES

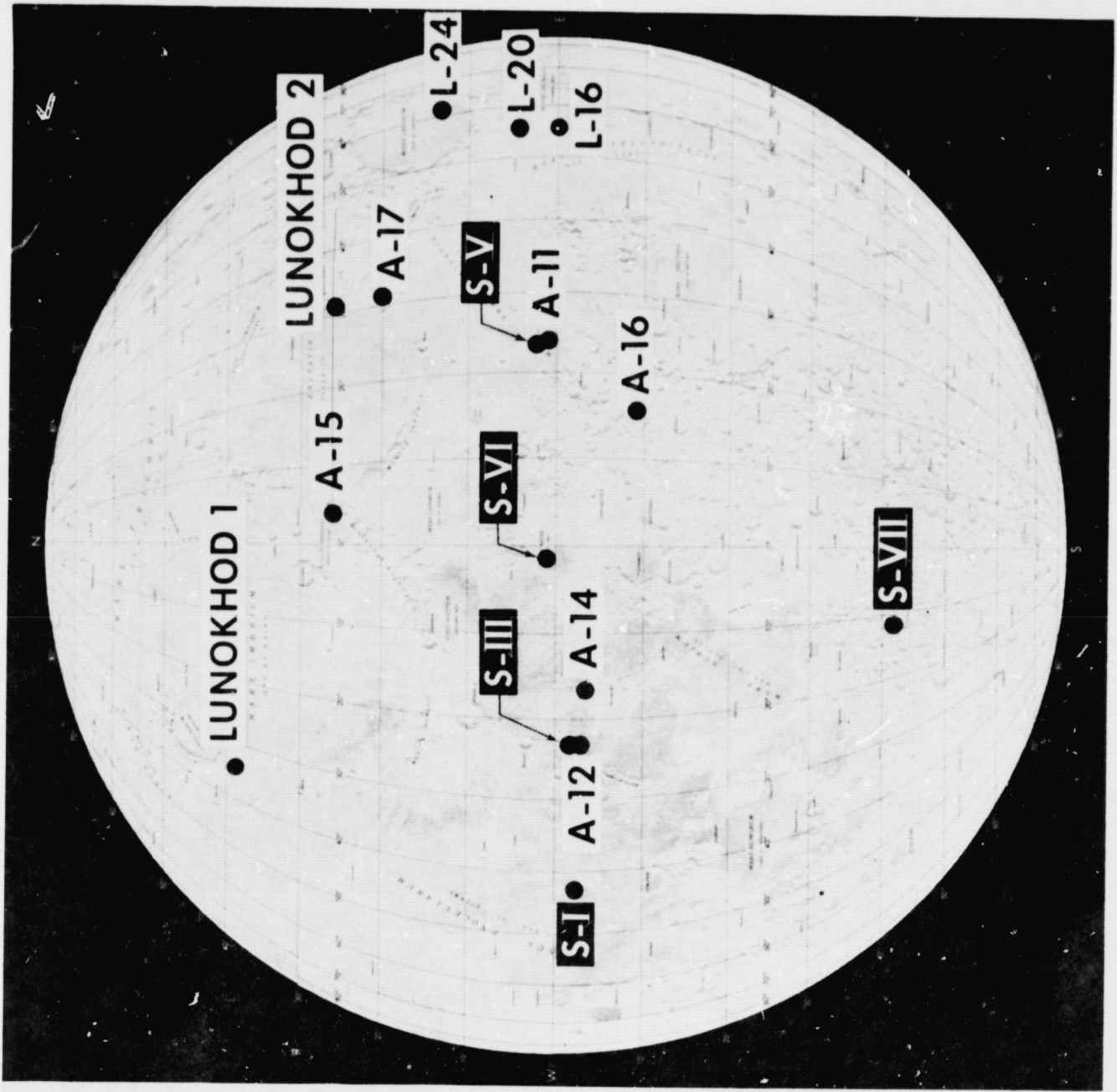


FIGURE 1

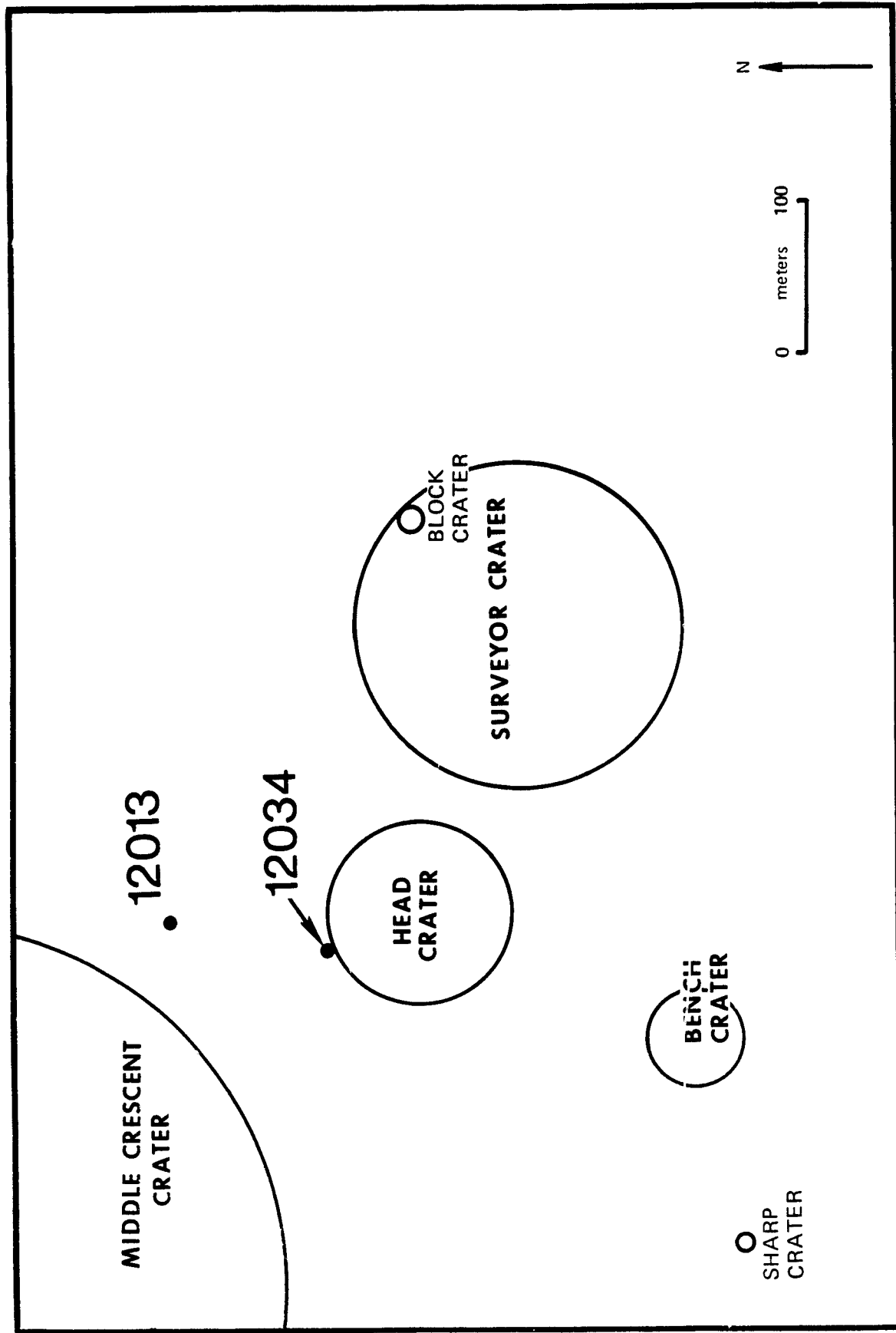


FIGURE 2. APOLLO 12 SAMPLE LOCATION MAP

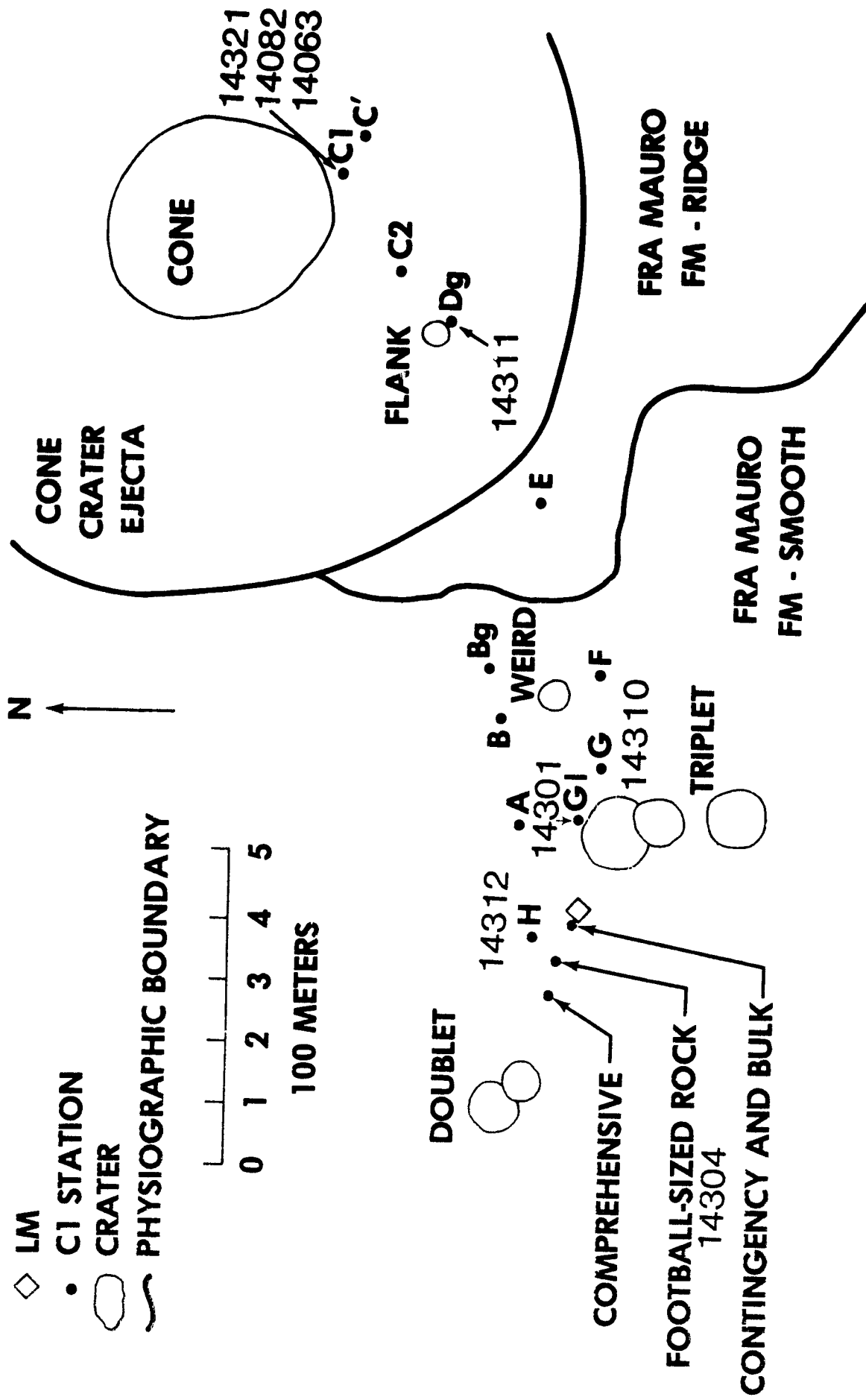


FIGURE 3. APOLLO 14 SAMPLE LOCATION MAP

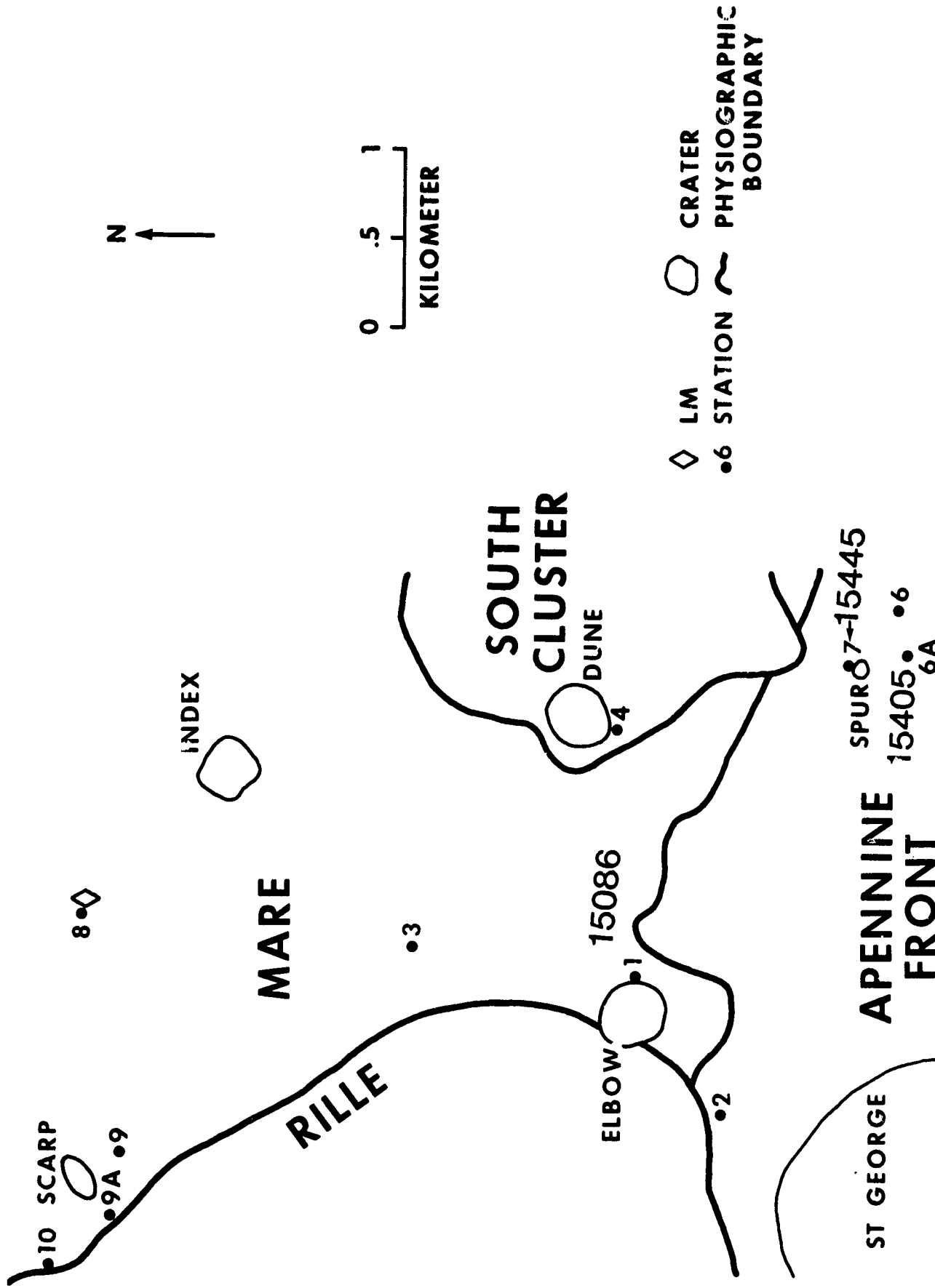


FIGURE 4. APOLLO 15 SAMPLE LOCATION MAP

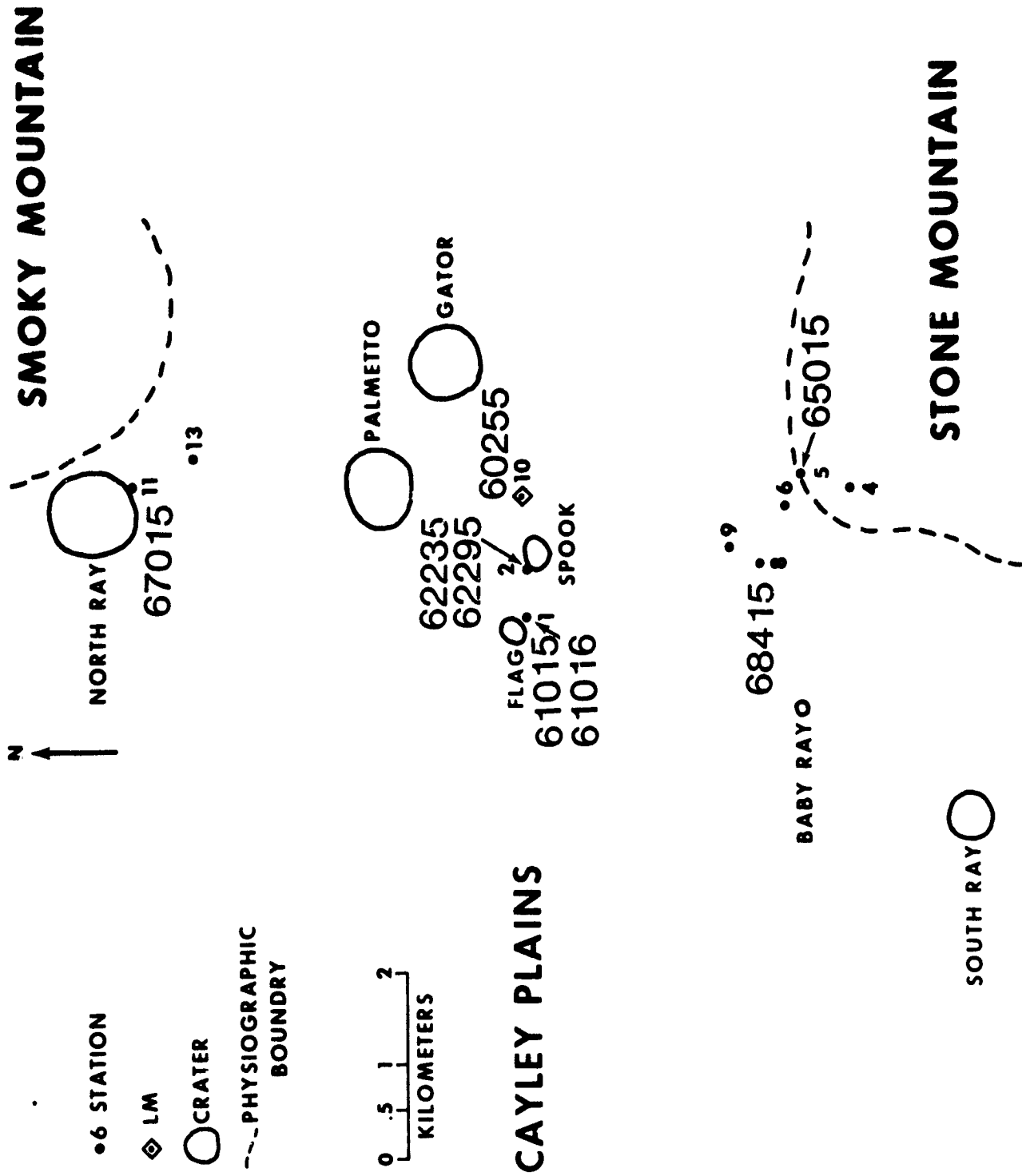


FIGURE 5. APOLLO 16 SAMPLE LOCATION MAP

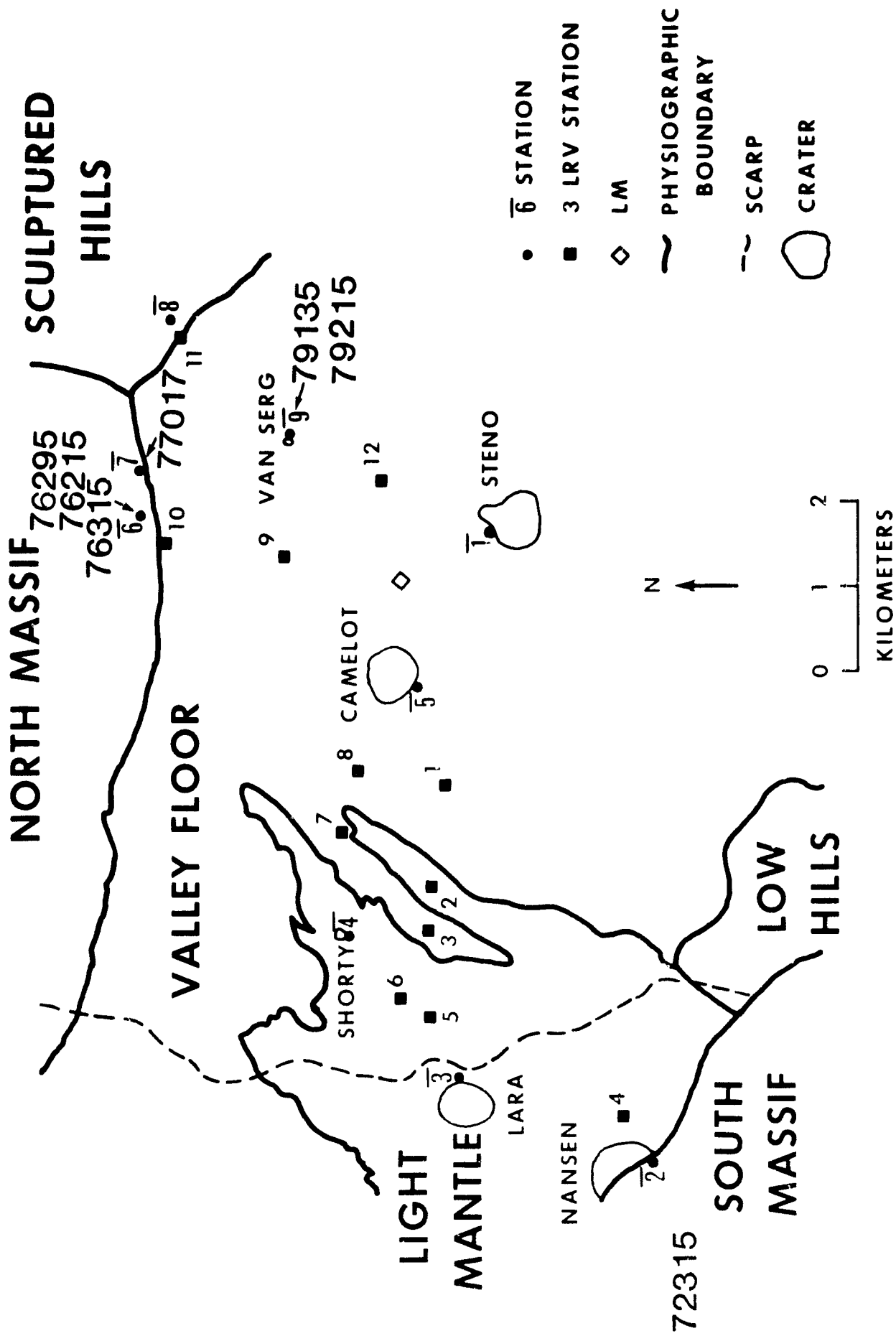


FIGURE 6. APOLLO 17 SAMPLE LOCATION MAP

Table 1. Classification of Lunar Breccias

- O FRAGMENTAL BRECCIAS
 - o Dark-Matrix

10060	15086
12034	60255
14301	79135
 - o Light-Matrix

14063	
14082	
67015	
- O CRYSTALLINE BRECCIAS
 - o Impact-Melt Breccias
 - o Clast-Free

14310	
68415	
 - o Clast-Bearing

15405	76315
61016	76295
62235	
62295	
65015	
72315	
76215	
 - o Clast-Rich

14304	14312
14311	14321
 - o Granulitic Impactites

77017	
79215	
- O BLACK AND WHITE BRECCIAS

12013	
15445	
61015	

Classification of Lunar Breccias

Lunar breccias are lithified aggregates of clastic debris and melt generated by meteoritic impact. One, or possibly all, of the following criteria are used to distinguish this group of rocks from endogenically produced (i.e. truly volcanic or plutonic) igneous rocks: (1) a clast-matrix texture (or a relatively clast-free texture with at least some vestiges of clasts, e.g. 68415); (2) a polymict clast assemblage (i.e. clasts of many types and compositions suggesting mixtures of several parental rock types); (3) an enrichment of trace siderophile elements relative to mare basalts and coarse-grained "pristine" rocks (suggesting contamination of pristine lunar material with meteoritic debris) and (4) a high metallic iron content relative to mare basalts and "pristine" rocks.

The breccia samples included in Table 1 have been studied petrographically with special emphasis on mineralogy and texture of the matrix and the extent of devitrification of glassy clasts. On the basis of these observations the breccias have been divided into three major groups: (1) Fragmental, (2) Crystalline, and (3) Black and White. Characteristic features of each breccia group (and subgroup) are discussed in the following section.

- 0 Fragmental breccias - Fragmental breccias are friable rocks which typically display a detrital texture, contain glass, and display a wide range of pyroxene and plagioclase compositions. The size distribution of fragments is typically seriate, ranging upward from less than 0.5 microns (observable with the SEM). Where a distinction between clast and matrix is not clear an arbitrary boundary is set at 39 microns for convenient manipulation of microscopic measurements. This also coincides with a natural clast-matrix break observed in crystalline breccias. Fragmental breccias are divided into two subgroups:
 - o Dark-matrix breccias - Dark-matrix breccias (alternatively referred to as regolith or soil breccias), which include the vitric-matrix breccias described by Waters et al. (1971), are dark to medium-dark brown-grey, friable to coherent rocks. They are the dominant rock type in the fragmental group and occur at all Apollo landing sites both on mare basalt flows and in the highlands. Dark-matrix breccias are fine-grained and typically porous, with micron-size intergranular voids which can best be viewed in reflected light or at magnifications of 300-3000X using a scanning electron microscope (Phinney et al. 1976). They are characterized by a detrital (i.e. minerals display a wide range

of chemical compositions) assemblage of mineral, lithic and glass clasts in a complex matrix of various types of mineral and lithic debris together with varying amounts (up to 50%) of brown glass as fragments or small interstitial patches. Agglutinate clasts are present in minor amounts. The volatile element content is typically high. Chemical compositions of dark-matrix breccias are similar to the composition of the local regolith at the site where the breccia was collected (Drake and Klein, 1973).

- o Light matrix breccias - Light-matrix breccias, described by Delano et al. (1973) and illustrated by the Apollo 14 "white rocks" and several samples from the Apollo 16 North Ray Crater, are light grey to tan, friable rocks. They are typically porous and are characterized by mineral and lithic clasts, together with rare orange-brown glass clasts in a detrital matrix of plagioclase, pyroxene, opaque minerals, rare orange-brown glass fragments and 1-3% colorless glass fragments. The light-matrix breccias are compositionally distinct from other breccias at both the Apollo 14 and 16 sites.

- 0 Crystalline breccias - Crystalline breccias are tough coherent rocks with textures which suggest both igneous (e.g. poikilitic, ophitic and subophitic) and subsolidus metamorphic (e.g. granulitic) origins. Plagioclase and pyroxene in breccias with igneous textured matrices display narrower compositional ranges than those observed in fragmental breccias but wider than those observed in breccias with granulitic textured matrices (Figures 7 and 8). Crystalline breccias are divided into two subgroups: (2a) Impact-melt breccias and (2b) Granulitic impactites. Impact-melt breccias may be further subdivided on the basis of total clast content and correlated variations in the morphology of matrix feldspar into clast-free, clast-bearing and clast-rich impact-melts.

- 0 Impact-melt breccias
 - o Clast-free impact-melts - Clast-free impact-melts, described by Simonds et al. (1977), are fine to medium-grained (feldspar laths 1 mm in length or more), subophitic rocks with igneous textures which contain complexly zoned feldspar megacrysts suggesting the presence of digested clasts. The matrices display isolated patches of finer-grained material.

 - o Clast-bearing impact-melts - Clast-bearing impact-melts, described by Simonds et al. (1977), are characterized by

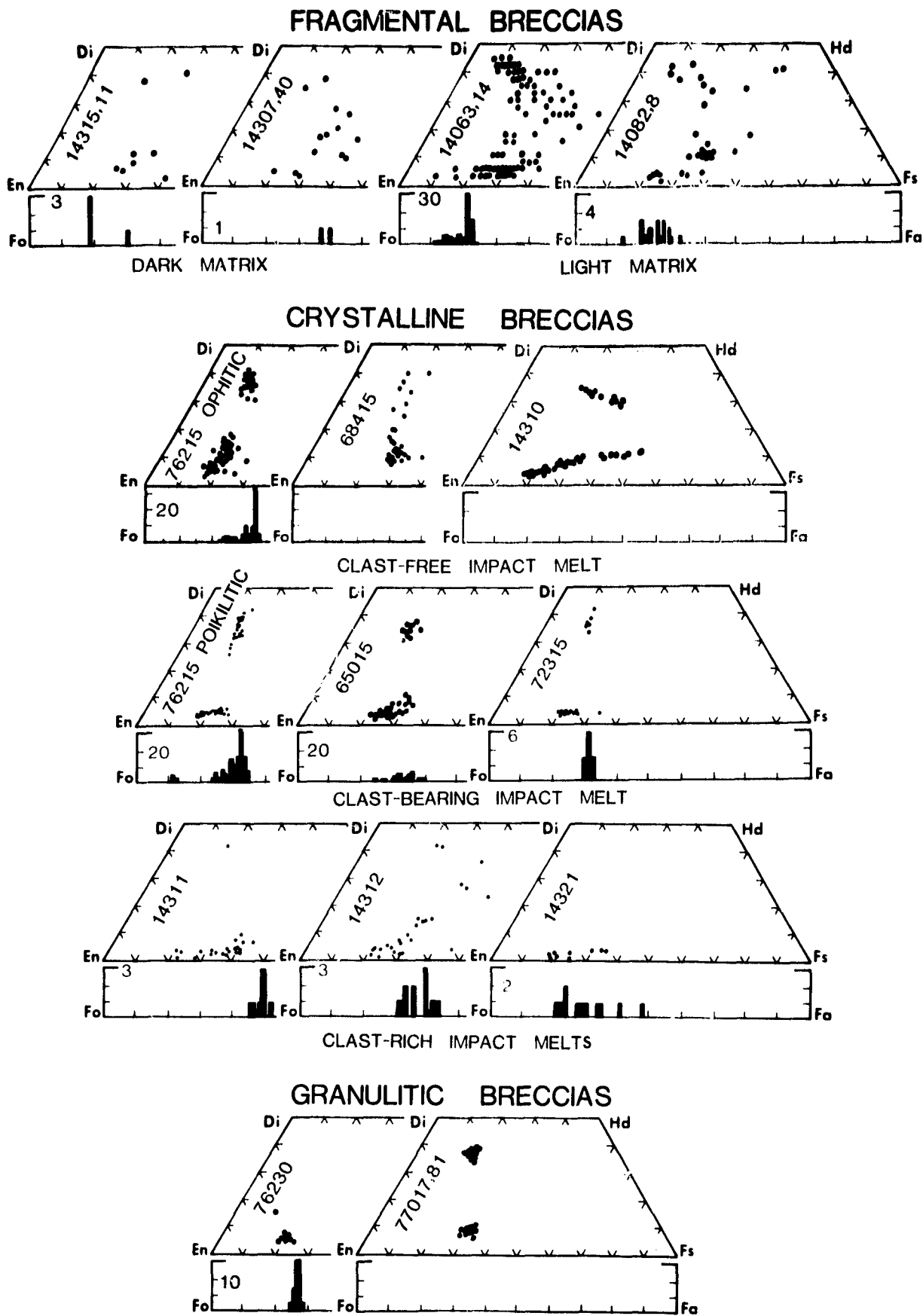
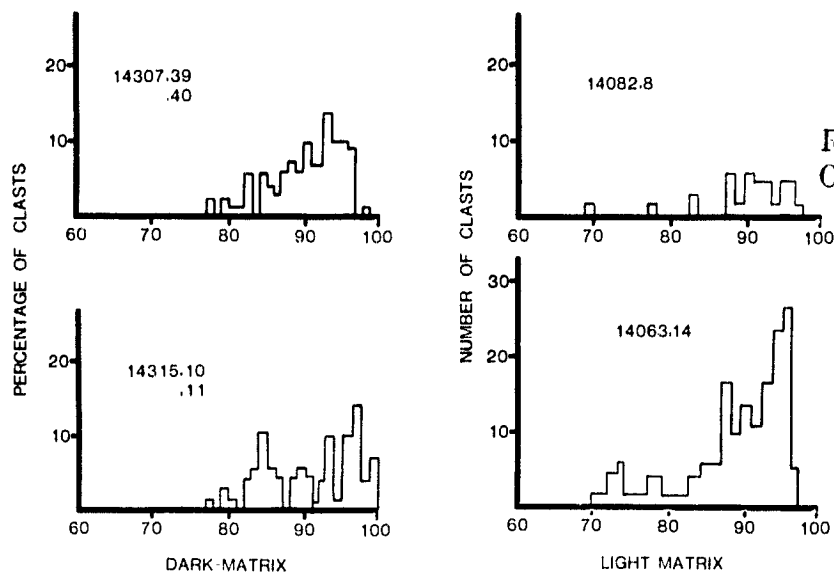
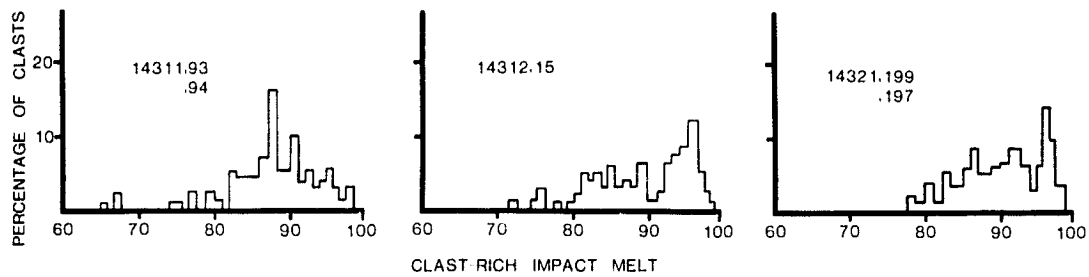
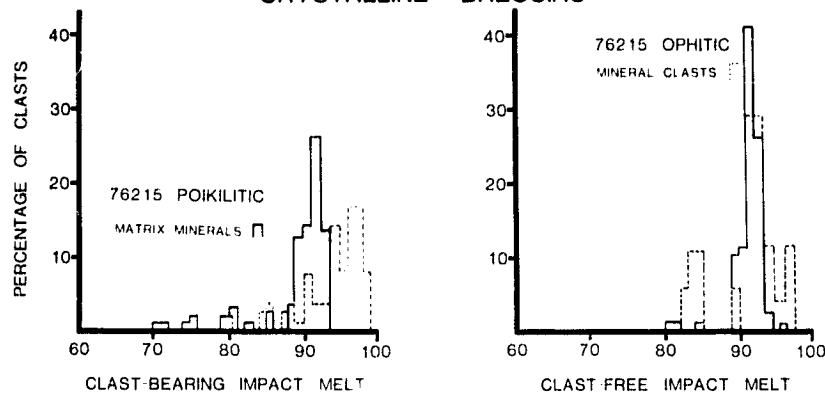


FIGURE 7. COMPOSITIONS OF MAFIC MINERALS IN FRAGMENTAL, CRYSTALLINE, AND GRANULITIC BRECCIAS.
 DATA FROM: SIMONDS (1975), SIMONDS et al. (1977), MCCALLUM et al. (1974),
 BENCE AND PAPIKE (1972), ALBEE et al. (1973)

FRAGMENTAL BRECCIAS



CRYSTALLINE BRECCIAS



GRANULITIC BRECCIA

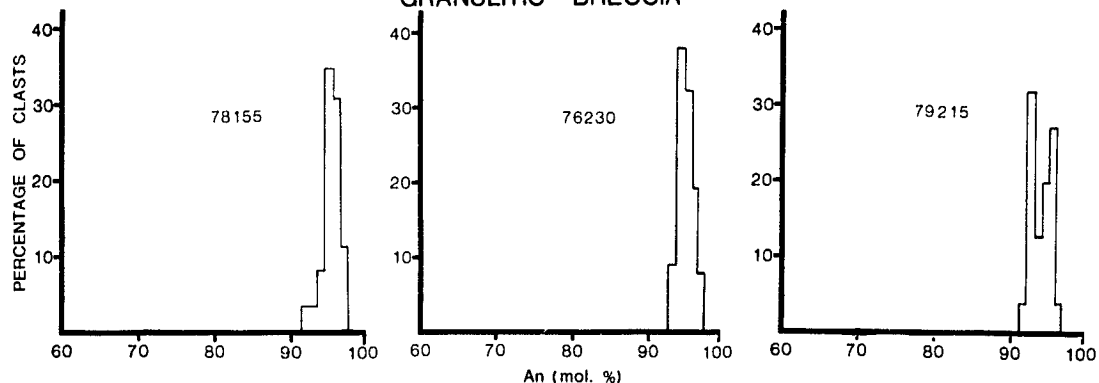


FIGURE 8. COMPOSITIONS OF PLAGIOCLASE GRAINS IN FRAGMENTAL, CRYSTALLINE AND GRANULITIC BRECCIAS.
DATA FROM: SIMONDS (1975); SIMONDS et al. (1977); BICKEL et al. (1976); BICKEL (1977).

very fine-grained poikilitic, subophitic, and ophitic textured matrices which contain 1-15% clasts. Refractory silicate minerals are the most common type of clast; glassy clasts are rare to nonexistent.

- o Clast-rich impact-melts - Clast-rich impact melts, including the Fra Mauro breccias described by Chao et al. (1972), are medium to dark grey, moderately coherent to coherent breccias which display anhedral matrix textures varying on a scale of a few millimeters; they contain 15% to 50% clasts. Mineral clast populations are less biased towards refractory minerals than in the clast-bearing melts. Lithic clasts are common. Glass clasts are rare.

- o Granulitic impactites - Granulitic impactites, described by Warner et al. (1977), are typically characterized by granoblastic or poikiloblastic textures that display smooth crystal boundaries between anhedral and equant grains of plagioclase, pyroxene, and olivine meeting at 120° triple junctions. Relict grains of these same minerals occur as monocrystalline and polycrystalline fragments which are coarser grained than the surrounding matrix. Their bulk compositions typically approximate anorthositic norites or troctolites.

- o Black and White breccias - Black and white breccias (found only at the Apollo 15 and 16 landing sites), described by Wilshire et al. (1973), typically contain two distinct lithologies: (1) anorthosite or anorthositic troctolite and (2) clast-bearing impact-melt. The impact-melt lithology (black) is typically interpreted as intrusive into the anorthositic lithology; rare samples contain three distinct lithologies and display obscure clast-host relationships. Unique sample 12013, a granitic breccia, is included in this group although it differs from other members of the group in texture, composition, and the relationship between light and dark lithologies.

The Cratering Process

Lunar breccias are aggregates of fragmental debris and melt generated by meteorite impact and consolidated in the ejecta and fall-back blankets of lunar craters. As most of the features unique to impact-lithified rocks may be explained in terms of processes occurring after the passage of a shock wave when various materials are intimately mixed, it is important to review the sequence of events immediately following the impact to better understand the thermal and material transport processes affecting the various components. The cratering process can be divided into four phases as suggested by Shoemaker (1963), Gault (1964), Dence et al. (1968) and Simonds et al. (1978):

(1) Meteorite collision and passage of compressive shock wave:

The compressional shock wave expands radially outward from the point of impact. Peak shock pressures are over 3 megabars at the point of impact and decay exponentially outward as $r^{-3.5}$ (Dence et al. 1977) (estimates range from r^{-2} to $r^{-5.5}$) where r is the distance from the point of impact (Grieve et al., 1977). The compressive phase lasts until the shock wave is reflected off the upper edge of the impacting projectile. The wave propagates at velocities up to about 8 km/sec in the highly compressed region near the point of impact, falling off to the acoustic velocity of the rocks (5-6 km/sec) when shock pressures decay below 100 kb.

(2) Rarefaction: A rarefaction wave follows the compressional wave with essentially the same velocities. The highly inelastic compression is followed by a sudden release of pressure which generates internal friction raising the temperature of the rocks. Rocks subjected to peak pressures over 600 kb begin to melt and those over 1 megabar are totally melted. Some, subjected to very high pressures (~ 2 megabars), will be vaporized. Rocks subjected to peak compressional pressures of 200-400 kb will have their feldspar vitrified to maskelynite (less compressible pyroxene and olivine will show only fracturing) and will be heated to temperatures of a few hundred degrees centigrade. Rocks subjected to pressures less than 100 kb will be fractured and planar deformation features will be produced in the feldspar and quartz. Although the volume of rock melted is only a few percent of the volume excavated, the heat of the melt (originally melt and vapor) represents about 1/3 of the total kinetic energy of the impacting meteorite (O'Keefe and Ahrens, 1975).

(3) Excavation: The momentum of the meteorite is transmitted to the target rocks; melt generated near the point of impact is accelerated to over 2 km/sec and the fragments at the periphery of the excavation are accelerated to a few tens of meters/sec. The motion of material in the crater is generally downward and outward. The downward and outward motions are deflected as excavation proceeds to form a parabolic cavity. Flow is stagnant directly under the impact; rocks immediately below the cavity contain maskelynite (200-400 kb peak shock pressure).

Diabase → Granite (24 km/sec)

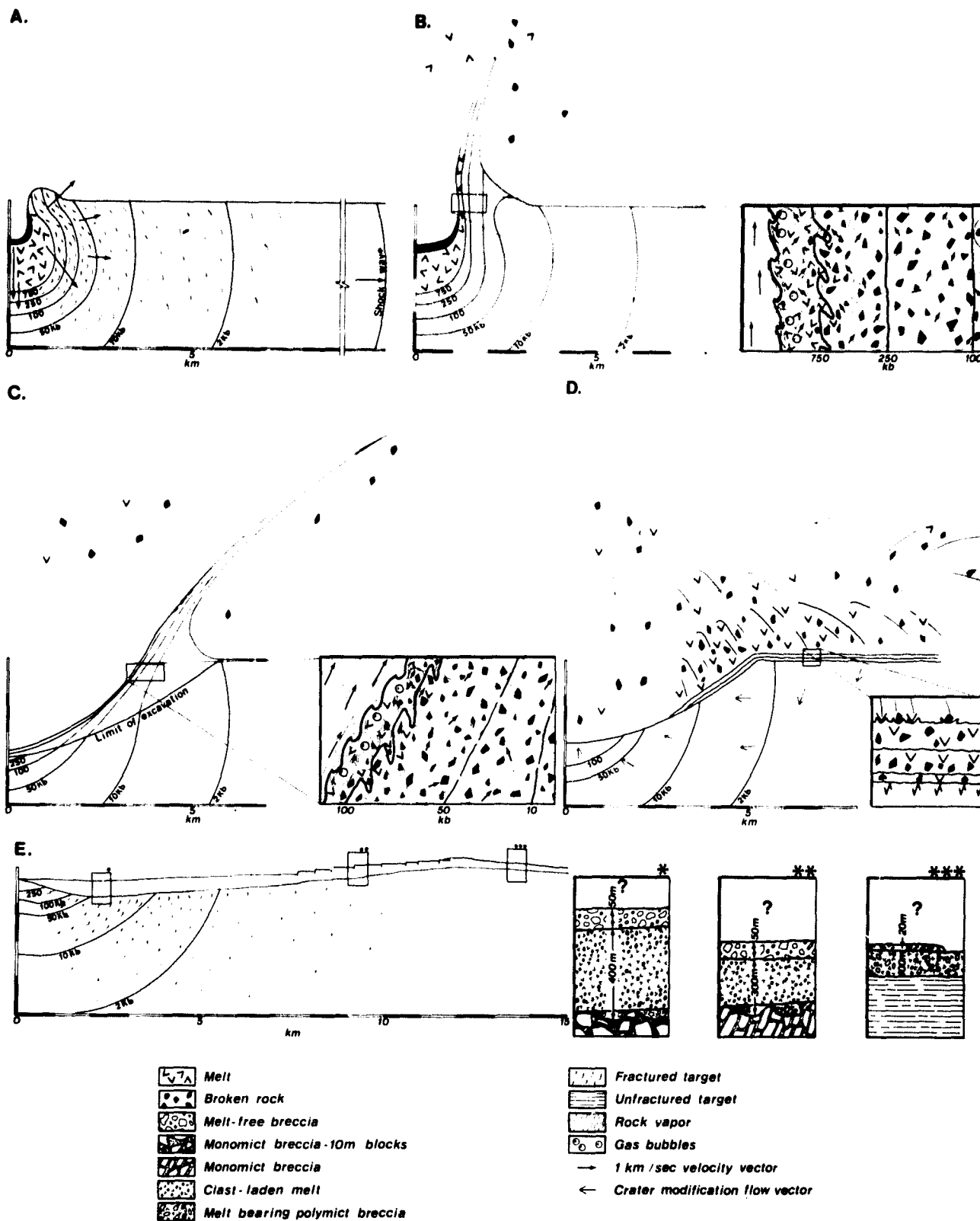


Figure 9. Cross section of model impact into a hard rock target showing: a) meteorite collision and passage of shock wave; b) ejection of debris; c) formation of parabolic cavity; d) small-scale impact and mixing by debris excavated during primary impact event; d) final stragrapy of crater prior to erosion. (Adapted from Kieffer and Simonds, 1979).

Detailed discussions of the flow directions are given by O'Keefe and Ahrens, (1975). Relatively unshocked materials from the surface and near the edge of the excavation are the first deposits on the rim. These materials are then overlain by more highly shocked materials from deeper in the excavation to form an inverted stratigraphy (Shoemaker, 1963). Melt from the center of the crater near the point of impact overruns and pushes the less shocked materials so that eventually the melt and included debris lines the excavated cavity as a thin sheet and spills out over the edge of the excavation. The melt is so hot that it is superheated; the excess energy is dissipated by the digestion of much of the incorporated debris.

(4) Readjustments: The final phase of cratering involves the collapse of the rim and movements of the basement rocks such as the uplift of a central block. Melosh (1976) has argued that the relatively shallow slopes of the excavation should be stable if the rocks have typical values for the coefficient of internal friction. Seismic shaking is one of the possible mechanisms suggested to lower the rocks' effective coefficients of internal friction to the point that the slopes are not stable. Such shaking would last only a few minutes even for the larger impacts. Another possible mechanism involves excess ground water pressures due to the rapid unloading of the crust. This mechanism is of little importance on the moon (due to the absence of water) but may be significant on Mars and the Earth. Presently, no data exists to uniquely support either of the suggested mechanisms and resolution of the problem awaits future experimental work. The occurrence of the melt sheet over collapse features is a further indication that the readjustments take place within minutes of the crater's formation because the melt becomes quite viscous within minutes of emplacement. For a more complete discussion of cratering physics, the reader is referred to the volume Impact and Explosion Cratering (1977), particularly the summaries by Dence et al. (1977), Grieve et al. (1977) and Cooper and Sauer (1977).

Two-Component Thermal Model for Impact Breccia Lithification

During the excavation phase of the cratering process, the mixture of melt and fragmental debris is in turbulent motion due to 1) the acceleration of the melt by the shock wave to velocities higher than those of the less shocked, slower moving debris which is overrun and mixed with the melt and 2) local velocity gradients in both the melt and fragmental debris due to different proportions of different minerals and diffraction of waves around local heterogeneities. Petrographic and chemical interpretations of the breccias formed as a result of this complex and turbulent flow, suggest that the two-component thermal model of Simonds (1975) and Simonds et al. (1976) closely approximates actual conditions. The model is characterized by a two-stage cooling history involving (1) a rapid first-stage thermal equilibration between small clasts and the surrounding melt, and (2) a second-stage of slow heat loss from the melt to the surroundings. The thermal model can be divided into four stages as follows:

1) Production of a superheated silicate melt formed near the point of impact and cold, unshocked, fragmental debris formed some distance from the point of impact. Several lines of evidence suggest that the melt was initially superheated. Systematic variations in the abundance and populations of various clast types, together with the biasing of clast populations to refractory materials, can be explained by the fusion of lower-melting point phases into an initially superheated melt. Studies of glasses from the Ries impact crater (Hörz, 1965; El Goresy, 1965) suggest several hundred degrees of superheat. The inferred temperature of the clasts is based on the lack of features in feldspar clasts indicative of shock pressures over 100 kbar. Maximum post-shock temperatures associated with such pressures are about 200-300° (Ahrens and O'Keefe, 1972).

2) Rapid mixing of the melt-clast mixture. Observations of impact-melt samples show that clasts and melt are mixed on a submillimeter scale so that no 1mm² of a thin section is free of clasts. Chemical analyses show that impact-melt samples are essentially homogeneous and free of the compositional variations present in the target rocks. Calculations by Onorato et al. (1977) suggest that for clasts with a median grain size of 0.10 mm, thermal equilibration of the clast-melt mixture will occur in times on the order of 100 seconds. Thus, the process of mixing clasts must not only be extremely violent and efficient (as suggested by observations of clast distributions discussed above), but must occur relatively rapidly (i.e., before thermal equilibration of the clast-matrix mixture initiates crystallization).

3) Rapid thermal equilibration of the clast-melt mixture and digestion of low-melting point clasts. The finely comminuted (<1 mm) and evenly distributed clasts absorb large quantities of heat from the surrounding melt in seconds. This rapid quenching of the melt produces a flood of small subhedral to euhedral feldspar nuclei (as observed in most impact-melts). Feldspar crystallization releases sufficient latent

heat to both raise the temperature of enclosed clasts and buffer the melt's temperature to the range between the liquidus and the solidus. As the clasts approach chemical equilibrium the smaller, lower melting point clasts are preferentially digested, altering the melt's composition.

4) Matrix crystallization and loss of heat to the surroundings. When the temperature of the melt falls below the liquidus, feldspar begins to crystallize releasing latent heat to slow or stop the temperature decrease and digest much of the lower-melting point clastic debris. Thus, for all but extremely high clast abundances (e.g., the Apollo 14 clast-rich impact-melt breccias) the drop in temperature will cease slightly below the liquidus. Experimental crystallization of plagioclase melts at near liquidus temperatures (Lofgren, 1974) produced the subhedral and euhedral plagioclase tablets observed in the Apollo 16 and 17 poikilitic and subophitic impact-melt breccias. The clast-rich Apollo 14 impact-melts are inferred to have crystallized at sub-solidus temperatures. Loss of heat to the surroundings begins after the melt reaches a thermal-equilibration and crystallization begins. Due to the dimensions involved this heat transfer is orders of magnitude slower relative to the melt-clast transfer.

A Discussion of Pristine Lunar Crustal Compositions

Petrogenetic studies of lunar breccias focus on two broad categories of problems: 1) studies of the cratering process and its subsequent modification of the lunar crust and 2) studies seeking evidence relating to the early fractionation of the moon. Cratering process studies are matrix-oriented with an emphasis on clast-matrix interactions and the degree to which chemical variations in the target are homogenized in the breccias. Lunar fractionation studies are clast-oriented and seek to identify pristine lunar materials (i.e., materials with low siderophile element abundances, low incompatible element concentrations, "cumulate" textures, >4.2 b.y. ages, low $^{87}\text{Sr}/^{86}\text{Sr}$). These pristine materials occur in breccias either as 1) ancient clasts which represent direct remnants of the lunar crust (e.g., plutonic rocks) or as 2) relatively young clasts (3.95 AE, Nyquist 1977) with pristine chemical compositions suggesting that they are late differentiates of the lunar crust (e.g., non-brecciated KREEP materials). KREEP is a basaltic chemical composition characterized by an enrichment in potassium (K), rare-earth elements (REE), and phosphorus (P).

Estimates concerning the types and relative abundances of pristine lunar crustal compositions have been established by the compilation of analyses of bulk rocks together with clasts and lithic fragments from regolith samples (Wood, 1975; Warren and Wasson, 1977; Bickel and Warner, 1978). Table 2 presents the composition of proposed pristine samples established by these studies which are believed to define the compositions of major portions of the highland crust.

The plutonic rocks (anorthosite, troctolite and dunite) are characterized by cumulate textures and chemically homogeneous minerals suggesting long annealing times at a depth of several kilometers in the lunar crust. Age determination studies of the dunite and troctolite samples placed them at over 4.2 billion years; this age is believed to reflect a period of crushing and annealing between 4.0-4.3 b.y. which followed the initial crystallization at 4.3-4.6 b.y. The primitive $^{87}\text{Sr}/^{86}\text{Sr}$ (0.6990) of the lunar anorthosites suggest that they are also products of the early lunar differentiation. Samples of non-brecciated pristine KREEP are characterized by basaltic textures (Dowty et al., 1976; Irving, 1977) with peritectic compositions suggesting that they are either partial melts from the lunar interior (Irving, 1977) or a late stage fractionation product (Shih, 1977). The 3.95 b.y. age for these samples represents either an extrusion age or an age of impact-melting.

Table 2. Major elements expressed as oxides in weight percent for
pristine rocks or clasts assumed to represent compositional groupings

wt. %	Anorthosite	Anorthositic Gabbro	Troctolite	Dunite	Quartz Monzodiorite	KREEP Basalt	Norite
SiO ₂	44.10	44.40	42.90	39.90	57.40	52.40	49.5
TiO ₂	.02	<0.07	.05	.03	1.10	1.78	0.16
Al ₂ O ₃	35.50	26.20	20.70	1.50	13.20	17.80	20.87
FeO	.20	4.20	5.00	11.30	11.20	8.60	5.05
MnO	—	—	.07	.10	—	0.10	0.08
MgO	.10	10.90	19.10	43.60	3.40	7.10	11.76
CaO	19.70	14.30	11.40	1.10	9.00	9.90	11.71
Na ₂ O	.30	0.36	.20	<.02	1.00	0.96	0.35
K ₂ O	<.01	<0.06	.03	—	1.90	0.57	0.06
Cr ₂ O ₃	.003	0.064	.10	.30	—	0.21	0.23
Total	99.93	100.55	99.55	97.85	98.20	99.42	99.77
Reference	1	2	3	4	5	6	7
	15415	15455 "clast"	76535	72415	15405 "clast"	15382	78235

1) LSPET (1972); 2) Taylor et al. (1973); 3) Rhodes et al. (1974); 4) LSPET (1973)
5) Taylor et al. (1976); 6) Dowty et al. (1976); 7) Winzer et al. (1975)

Chemical Systematics of Highland Breccias

To adequately constrain and better understand models of breccia petrogenesis it is necessary to study the chemical systematics of the highland breccias in relation to the compositional groupings established in the previous discussion. Investigations of this nature have demonstrated that the chemical composition of highland breccias plot along a trend which joins an aluminous basalt or "KREEP" composition (CaO = 10-12 wt. %; Al₂O₃ = 17 wt. %) to an anorthositic composition (CaO = 19-20 wt. %; Al₂O₃ = 35-36 wt. %). A plot of the breccias included in this study is shown on CaO vs. Al₂O₃ diagram (Figure 10). The data closely approximates the above trend (with the exception of several dark-matrix breccias and a clast-rich Apollo 14 sample). Figure 11, shows these same compositions plotted in terms of the normative percentages of silica, plagioclase and olivine. The trend is equivalent to the one displayed in the previous CaO/Al₂O₃ diagram. Figure 12, illustrates the variations in the FeO/MgO ratio among the breccias included in this study and serves to illustrate that a simple KREEP-anorthosite mixing cannot explain all of the observed compositions. A chondrite normalized plot for the rare earth and several additional large ion lithophile (LIL) elements for breccias from this study are shown in Figures 13 and 14. The consistent slope displayed by all of the non-mare breccias (lighter REE's enriched over heavier REE's) suggests a probable genetic correlation. The abundances of LIL elements in the breccias is inversely related to the Al₂O₃ content so that basaltic breccias (17-20 wt. percent Al₂O₃) have high LIL element concentrations and anorthositic breccias (30-36 wt. percent Al₂O₃) have low LIL element concentrations. Systematic fractionation of the LIL elements and negative Sr and Eu anomalies suggests that the LIL concentrations are controlled by plagioclase-liquid equilibria. The high concentrations of volatile siderophile elements in the lunar breccias relative to the mare basalts or coarse-grained plutonic rocks (1 to 3 orders of magnitude) is illustrated by the gold histogram plot in Figure 15. These concentrations are interpreted as evidence of meteoritic contamination (Anders et al., 1973); inversely, low siderophile element concentrations suggest pristine, uncontaminated compositions.

Interpretations of the chemical systematics of the highland breccias include the following alternatives.

- 1) Anorthosite and KREEP compositions represent two of the major "primary" rock types in the highlands and chemically diverse breccias are the result of various amounts of mixing of the end members. Variations of this model include one or more additional end members (e.g. dunite and/or spinel-bearing anorthositic troctolite) (Schonfeld, 1974).

- 2) Repetitive impacts should have homogenized the bulk chemistry of the breccias to that of the local average highlands (anorthositic gabbro plus KREEP) composition, the partial melting of which corresponds to a peritectic liquid with a KREEP composition. The range of breccia chemistry is explained by impact-generated partial melting with some subsequent separation of melt and residue (Warner et al., 1974).

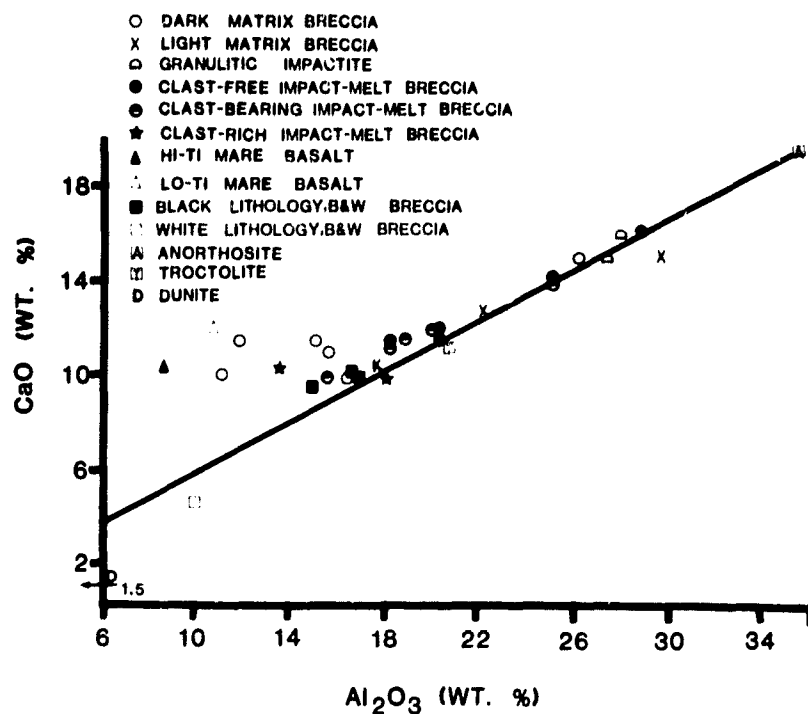


Figure 10. $\text{CaO}-\text{Al}_2\text{O}_3$ plot for representative lunar breccias. Anorthosite, troctolite, dunite, high and low-Ti mare basalt and KREEP (K) samples are plotted for reference.

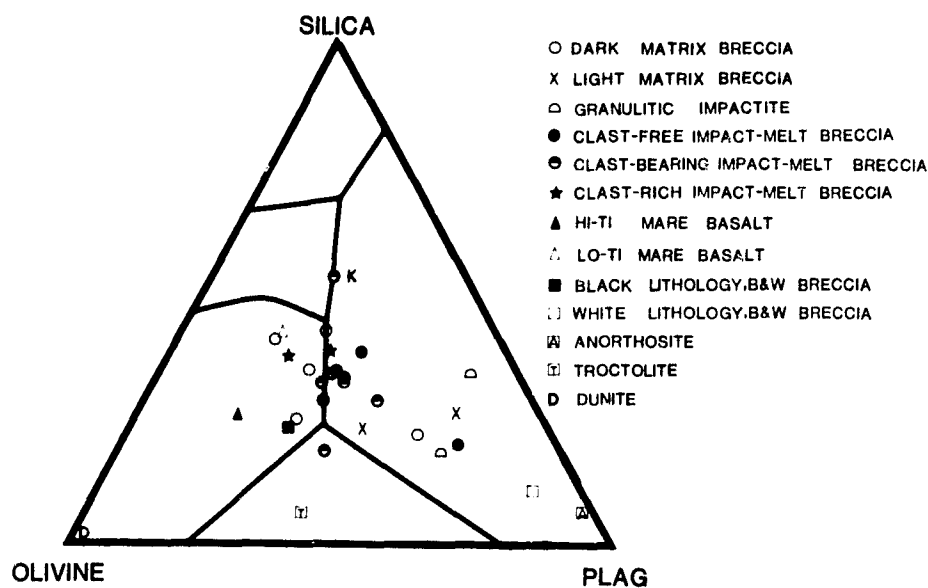


Figure 11. Plot of representative lunar breccias and reference samples on the Olivine-Silica-Anorthite pseudoternary liquidus diagram. KREEP sample 15382 is represented by the symbol K.

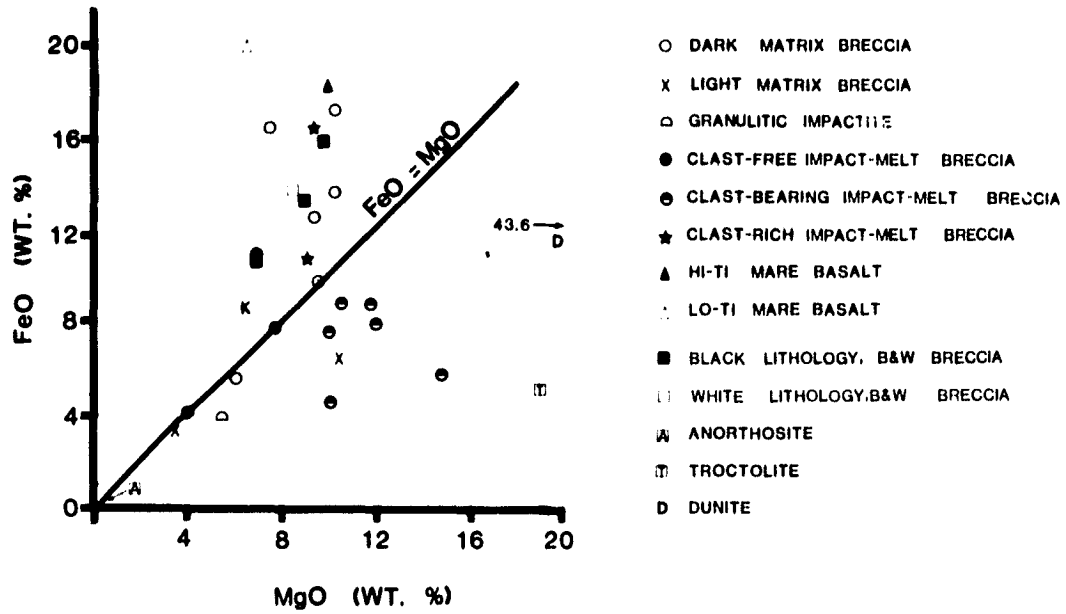


Figure 12. FeO-MgO plot of representative lunar breccias and reference samples. KREEP sample 15382 is represented by the symbol K.

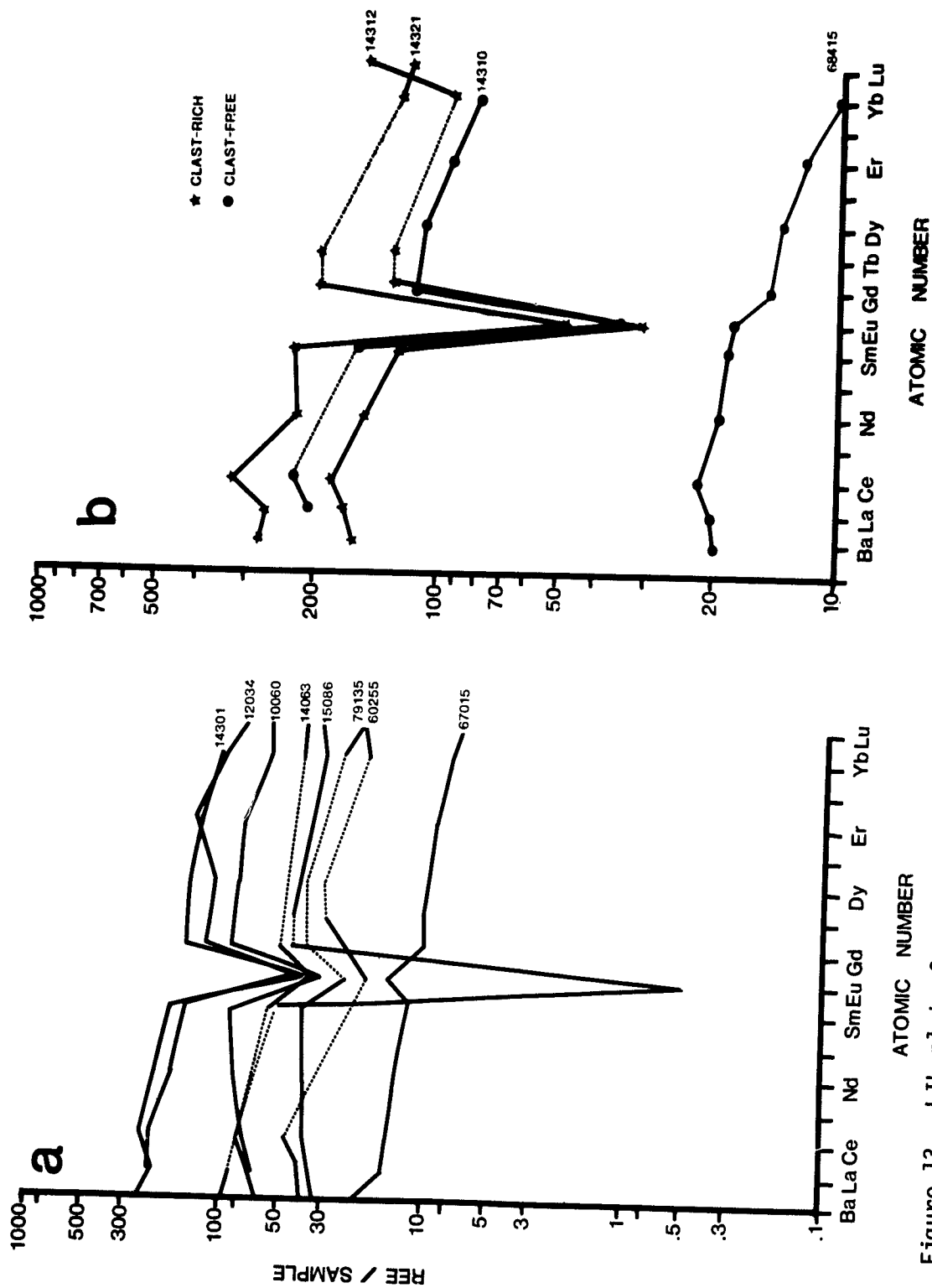


Figure 13. LIL plot of representative lunar breccias a) fragmental breccias
b) clast-free and clast-rich impact-melt breccias.

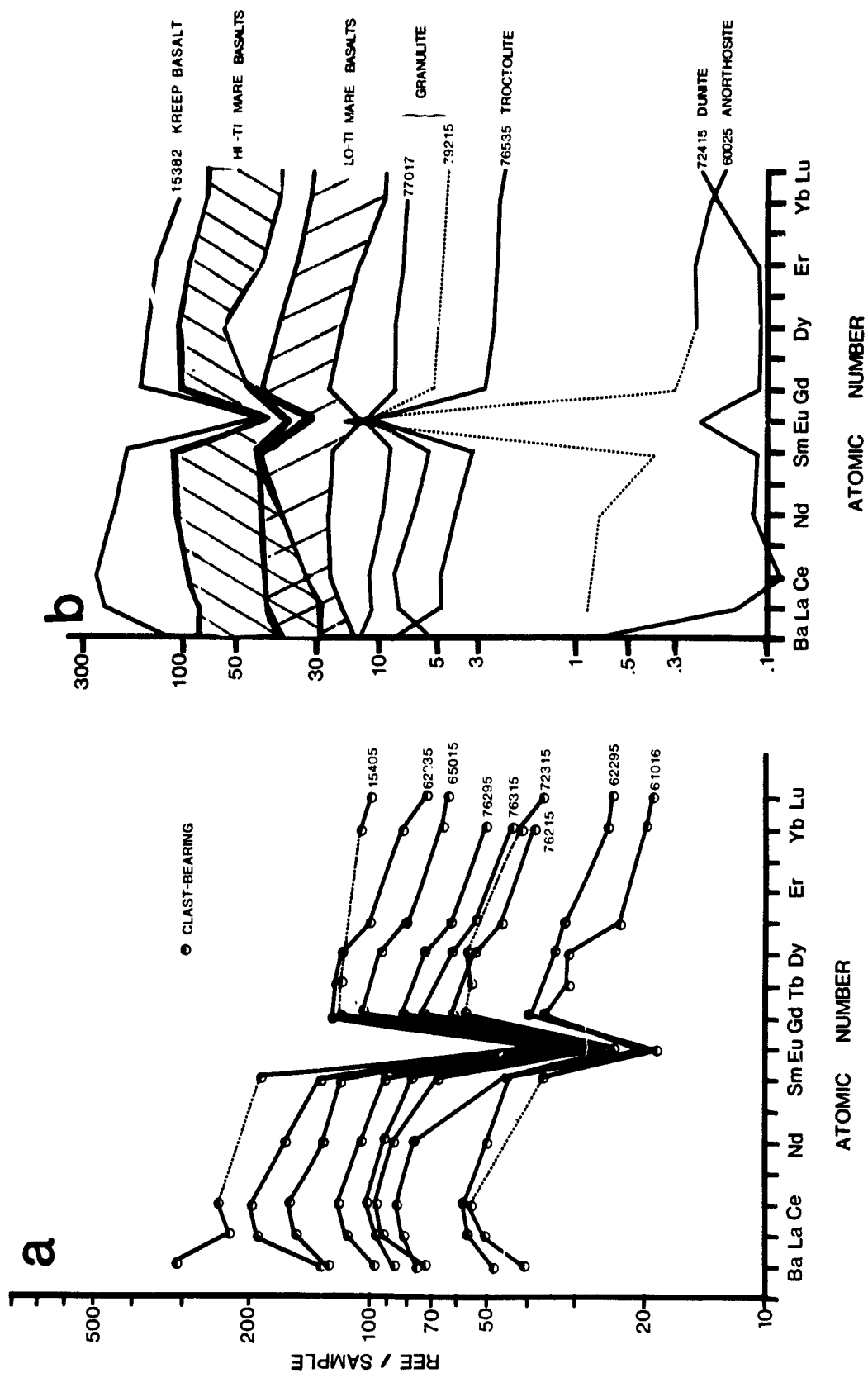


Figure 14. LIL plot of representative lunar breccias and reference samples. a) clast-bearing impact-melt breccias b) granulitic impactites and reference samples.

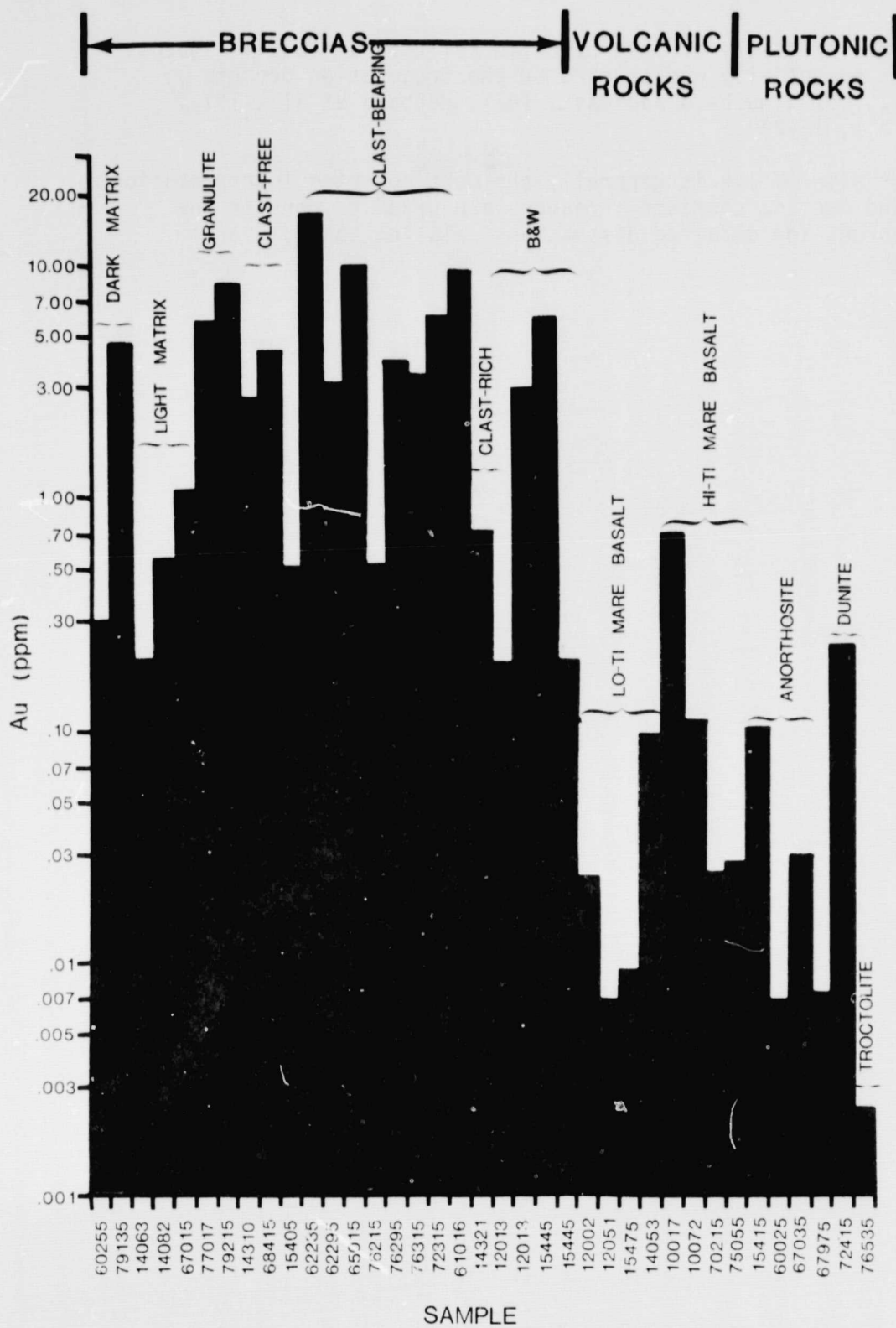


FIGURE 15. Plot of gold abundances (ppm) for representative lunar breccias, basalts and plutonic rocks.

3) The bulk chemistry of most breccias reflects a "fossil" igneous rock chemistry essentially undisturbed by the brecciation process (Haskin et al., 1973; Hubbard and Gast, 1971; Hubbard et al., 1972; Lindstrom et al., 1972).

The first alternative is generally the most accepted interpretation of the highland breccia chemistry; readers are urged to consult the referenced sources for detailed discussions relating to additional interpretations.

The Lunar Regolith

This discussion of the lunar regolith emphasizes the role of impacts in modifying the lunar crust and illustrates the components formed by impacts (common to all regolith samples) which have major implications for the problems of breccia petrogenesis, particularly for the dark-matrix fragmental breccias.

Lunar regolith is the term applied to the layer of weakly coherent, fragmental, impact-generated debris which overlies the bedrock on the lunar surface. It is composed of poorly sorted material ranging in size from the finest dust particles to blocks which may be several tens or hundreds of meters across. The thickness of the regolith generally increases with the age of the underlying bedrock ranging from 2-5 meters at Apollo 12 and 15 (~ 3.2 AE) to 3-6 meters at Apollo 11 (~ 3.6 AE). In the non-mare regions, the thickness is even greater because the base of the regolith grades into breccias produced by intense meteorite bombardment that affected the rocks to a depth of several kilometers. Thicknesses of the least consolidated regolith at non-mare sites range from 8.5 meters to 12 meters at Apollo 14 and 16 (~ 3.85 AE) to 10 to 15 meters at Apollo 17 (~ 3.65 AE).

The dominant processes of regolith formation are the comminution of coherent rock masses by repetitive impacts (yielding destructional fragments) and the reaggregation of small particles by bonding with glass (yielding constructional fragments). Debris initially excavated by one crater-forming impact is subsequently crushed, fused, mixed, and transported by additional impacts which range in magnitude from frequent, small-scale micrometeorite events producing pits microns to millimeters across to rare, large-scale impact events, producing craters 10's to 100's of kilometers across.

Destructional fragments include glass, lithic, and individual mineral fragments derived from pre-existing rocks by impact comminution. The absence of chemical weathering on the Moon leaves the fragments fresh and unaltered, angular to sub-rounded and relatively equant.

Constructional fragments, called agglutinates, form as a result of the mixing of splashes of impact melt (produced by micrometeorite impact) with previously deposited regolith material. Studies by Hartung et al., (1972) have shown that much of the material impacting the lunar surface is in the form of micrometeorites which erode exposed rocks and form millimeter-size craters in the regolith that produce splashes of melt. The splashes of melt thus produced solidify with included destructional fragments producing agglutinates. These agglutinates are characterized by heterogeneous mixtures of comminuted glass, mineral and lithic debris bonded by vesicular, flow-banded, heterogeneous glass. The bonding glass typically makes up over half of the volume of each agglutinate particle and contains vesicles ranging upward in size to several centimeters; most agglutinate fragments are less than 1 millimeter in diameter. The flow-banded glass contains trails of immiscible iron metal

particles ranging in size from $.002 \mu\text{m}$ to $1 \mu\text{m}$. The included metal particles distinguish agglutinitic fragments from comminuted dark-matrix breccia fragments, which appear similar to the untrained observer. Morphologically, the agglutinates range from simple, irregular, ameboid shapes to complex branching forms. Lunar regolith samples contain from 0 to 60 percent of agglutinate fragments. The agglutinate content in regolith samples decreases rapidly with depth; at 20 cm below the surface agglutinate abundances rarely exceed 10%.

Most regolith samples contain a small percentage (1 percent or less) of fragments of both clear and devitrified glasses as spheres, fragments of spheres, and dumbbell-shaped forms which are interpreted as volcanic in origin. The Apollo 15 green glass (15426) and Apollo 17 orange glass (74220) described in the companion volume are two such examples. The homogeneity of the glass and uniformity of the chemical composition, together with the lack of shock features and included rock fragments argues against an impact origin for these fragments and supports the generally accepted belief that the fragments are the result of lava fountaining (Heiken et al., 1974).

The enriched siderophile trace element abundances of regolith samples suggest that up to several percent of most samples consist of meteoritic material, although an unambiguous identification of fragments ultimately derived from an impacting meteorite is difficult. Iron metal fragments, the regolith components most likely to represent meteoritic derivatives, have chemical compositions comparable to those of metal grains within breccia samples. Consequently, interpretations of their immediate source remain speculative.

An important concept of regolith formation is that of maturity, the measure of regolith exposure time at the immediate lunar surface. Heiken (1975) has shown that the agglutinate content of the regolith increases with surface exposure time and can therefore be used as a measure of regolith maturity. Immature soils are characterized by recently comminuted, fresh ejecta or volcanic deposits. Mature soils are characterized by comminuted material together with abundant agglutinates. Submature soils are intermediate between immature and mature soils. Agglutinates in different horizons of core samples can be used to determine the extent of reworking of regolith components; most cores show a progressive decrease in agglutinate content downward for the first half meter below the lunar surface. In addition to the increase in agglutinate content with age, the soil also 1) adsorbs a layer of the solar wind gases H and He, 2) becomes finer-grained (materials $>1 \text{ mm}$ are systematically eliminated, 3) increases its content of metallic iron, and 4) sustains damage to the outer few tens of microns of more and more of the individual grains due to energetic atoms ejected by the sun during solar flares.

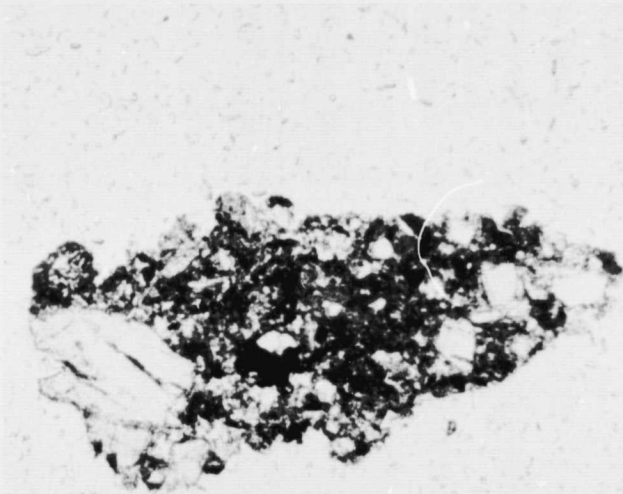
Regolith samples returned from the Apollo 11 site are basically similar to soils at other Apollo sites and typically reflect the make-up of the local bedrock. The soils are composed of the following types of particles: 1) agglutinates; 2) lithic fragments; 3) mineral fragments and 4) various glasses. Studies of the Apollo 11 regolith samples have shown them to be composed predominantly of basaltic debris derived from the excavation of local high Ti basaltic bedrock together with a small but significant amount of chemically and mineralogically exotic components possibly derived from material under the flood basalts or from distant sites (possibly the highlands to the south). A petrographic description of Apollo 11 regolith sample 10084 follows and serves to illustrate the common constituents of lunar surface soils.



10084 <1mm Fines

Sample 10084 consists of fine-grained, poorly sorted, medium dark gray portion of the Apollo 11 soil less than 1 mm in diameter (Figure a). The sample was collected by the Apollo 11 astronauts in the last few minutes of lunar surface activity near the lunar module. It is characterized by mineral fragments of plagioclase and augite, together with lesser amounts of olivine, ilmenite and Fe-Ni metal blebs. Homogeneous glass fragments in a variety of colors are present as well as heterogeneous fragments decorated with schlieren and mineral fragments. Fine-grained to coarse-grained basaltic fragments are abundant, together with significant members of micro-breccia fragments and agglutinates. Several anorthositic rock fragments were observed (Wood et al., 1970) but are not common. The major constituents of 10084 are shown in Figures 16A through 16F. Table 3 gives the modal composition of grain size fractions of Apollo 11 soil 10084,106 (von Engelhardt et al., 1971).

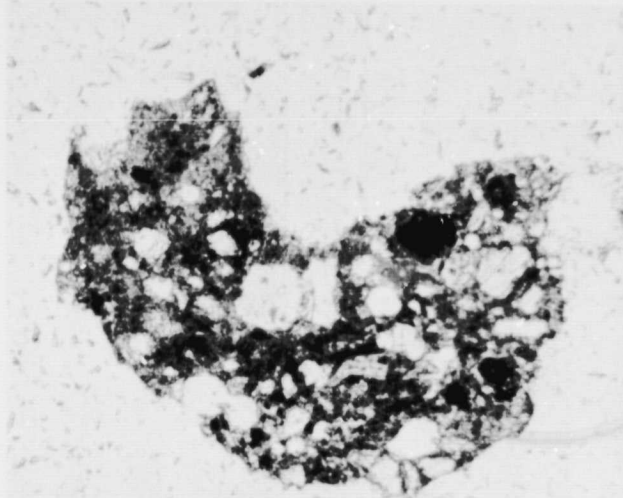
SOIL BRECCIA TRANSMITTED LIGHT



10084 0.05MM

16A

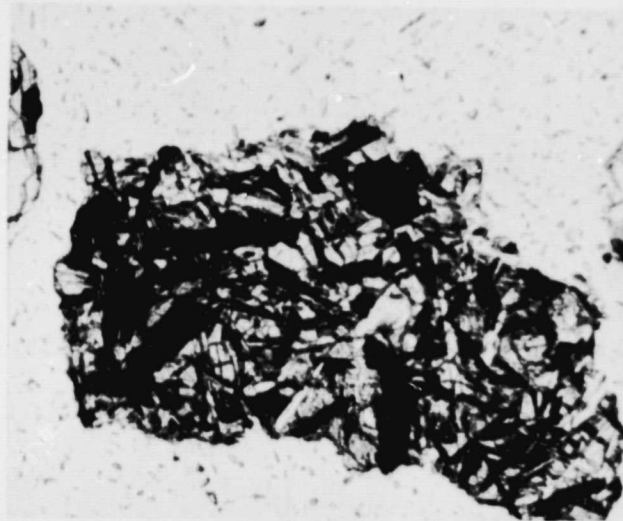
AGGLUTINATE TRANSMITTED LIGHT



10084 0.05MM

C

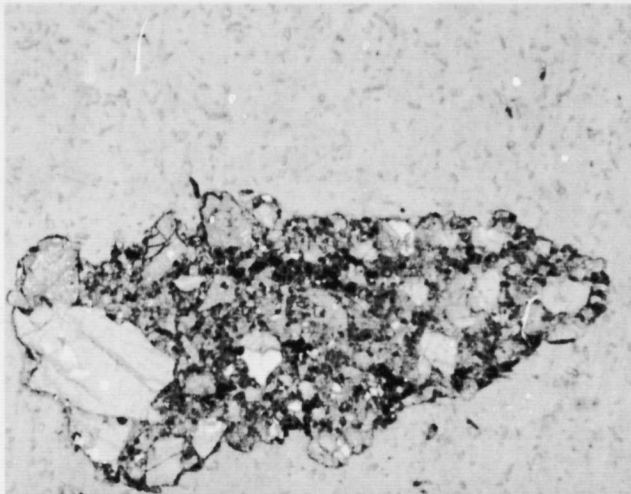
BASALT FRAGMENT TRANSMITTED LIGHT



10084 0.05MM

E

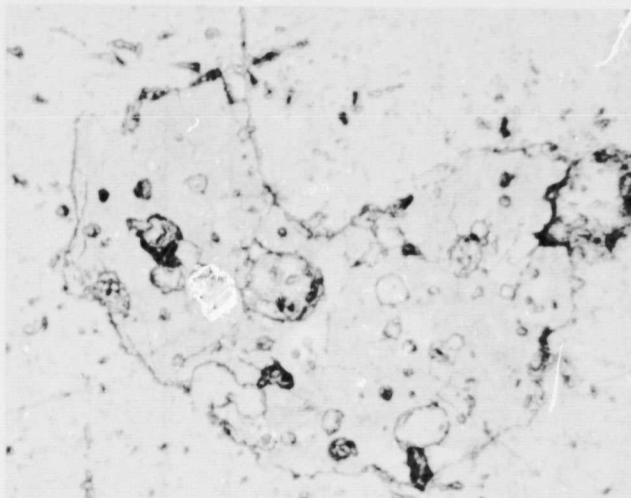
SOIL BRECCIA REFLECTED LIGHT



10084 0.05MM

B

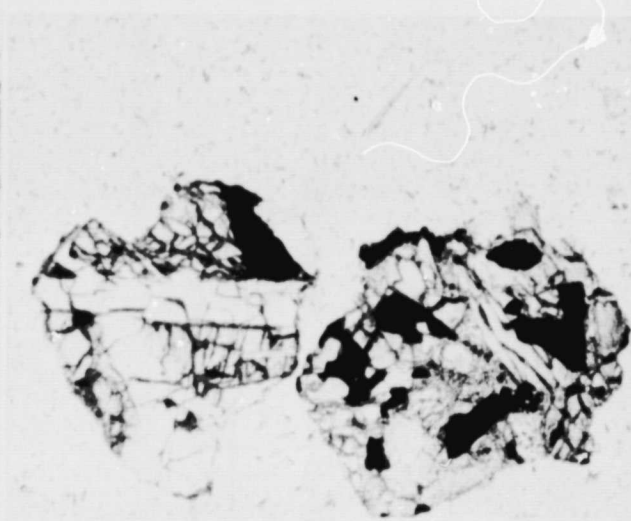
AGGLUTINATE REFLECTED LIGHT



10084 0.05MM

D

BASALT FRAGMENT TRANSMITTED LIGHT



10084 0.1MM

F

Table 3. Modal composition of grain size fractions of Apollo 11 soil (10084,106)

	10-20 μm	20-63 μm	63-125 μm	125-250 μm
Basalt	—	—	4.5	19
Anorthosite	—	—	—	1.5
Breccia	—	—	11.	24.
Agglutinates	—	—	34.	30.
Glass fragments, dark	23	31	4.1	4.4
Glass fragments, light	11	5.1	2.8	3.1
Regular glass bodies	4.0	1.0	1.1	1.3
Pyroxene + olivine	30	35	31	12
Plagioclase	22	19	8.6	2.4
Opakes	10 ²	9.2 ²	2.0	2.4

¹Some agglutinates included in "opakes"; ²Including some agglutinates

adapted from von Engelhardt et al. 1971

Petrogenesis of Lunar Breccias

The major objective of this catalogue, a general introduction to the lunar breccias, depends upon interpretations of chemical, petrographic, and mineralogic features of the breccias. The following sections of text attempt to relate these features to presently existing models of breccia petrogenesis.

Dark-matrix breccias

The dark-matrix breccias are an extremely heterogeneous suite of lunar breccias with physical and chemical characteristics that suggest mixing of components from diverse sources. They contain abundant fragmental material and shock-melted glasses, together with minor amounts of relatively large (up to 1 mm), nickel-enriched iron blebs. Collectively these features indicate that the fragmental material was generated by meteoritic impact.

Several lines of evidence suggest that dark-matrix breccias are the lithified equivalent of the lunar soil. Similarities in the bulk chemical composition, as illustrated in Table 4, and in the types and relative proportions of fragments between the dark matrix breccias and the lunar regolith at each respective site support this interpretation. Also the incorporation of agglutinates (common constituents of the regolith) into the dark-matrix breccias suggest that these breccias contain at least some lunar soil. The low abundance of agglutinates (0-3%) in the dark-matrix breccias at each of the Apollo landing sites relative to the regolith (up to 58% for a mature regolith, Heiken, 1974), suggests the following alternatives: (1) that soil making up the dark-matrix breccias was very immature; (2) that only a small portion of the incorporated regolith was agglutinate-rich; (3) that agglutinates are destroyed or obscured by breccia-making processes; (4) that the protolith of the breccias was not regolith. The exact mechanics of dark-matrix breccia lithification are uncertain but probably a number of processes are operative. Chao et al., (1972), Christie et al., (1973), and Kieffer (1975) have proposed models for the lithification of soil by shock waves, arguing that the interaction of shock waves and grain boundaries in porous aggregates results in the formation of glass at these boundaries, a feature which has in fact been observed by Christie et al. (1973). Other investigators (McKay and Morrison, 1971; Waters et al., 1971; Simonds, 1973; Uhlmann et al., 1975; Phinney et al., 1976) argue that the lithification involves thermal welding or sintering either between grains or by small impact-produced glass fragments formed near the point of impact. The SEM investigation of matrices of very friable glass-poor soil clods (Phinney et al., 1976) revealed filaments, 1-3 μm films of glass and apparent sintering between the clastic debris. The fact that these features are not associated with any clearly recognizable glass suggests lithification by shock (as discussed by Kieffer,

1975). Moderately coherent microbreccias to tough vitric-matrix breccias display 10-100 μm glassy patches to continuous glassy matrices with KREEP-enriched composition which do not appear to originate from shock melting of the clastic debris. Correlated gradations in coherence, porosity, glass content, glass texture, apparent sintering, grain size, and grain shape in matrices from friable soil clods through coherent microbreccias and tough vitric breccias to tough crystalline breccias are compatible with Simonds et al. (1976) two-component thermal model for breccia lithification. Thus, if shock lithification is a viable process it must be important only for the very friable soil clods and micro-breccias.

Light-matrix breccias

The physical and chemical characteristics of light-matrix breccias (as in the case of dark-matrix breccias) indicate a complex formational history characterized by the mixing of both local and foreign components. The breccias are characterized by a detrital matrix which hosts single mineral grains (predominantly plagioclase), lithic clasts representative of the anorthosite-troctolite-norite (ANT) suite, and rare orange-brown glass. The unrecrystallized nature of the matrix suggests that these breccias are not annealed, yet they lack characteristic features of the dark-matrix regolith breccias such as glassy or devitrified spheres and brown glass in the matrix. The Apollo 14 light-matrix breccias are plagioclase-rich and KREEP-poor suggesting that they are possibly derived from pre-existing crustal rocks uncontaminated by KREEP. Unambiguous identification of the precursor of the light-matrix breccias or the processes involved in their formation is not possible at this time.

Crystalline Matrix Breccias

The impact-melt crystalline-matrix breccias, were initially thought to be made by simply metamorphosing the dark matrix breccias (Warner, 1972; Warner et al., 1973, 1974; Phinney et al., 1972). Later investigations, including SEM petrography (Phinney et al., 1976) and thermal models (Simonds, 1975; Simonds et al., 1976) suggest that the crystalline-matrix breccias were not made in this manner. For example, at the Apollo 14 site, Simonds et al., (1977) pointed out that the dark-matrix breccias are systematically depleted in MgO and enriched in Al_2O_3 when compared with the Apollo 14 crystalline-matrix breccias. Stöffler et al., (1976) used clast population data (for Apollo 14 breccias) to show that the dark-matrix breccias are not the protoliths of the crystalline-matrix breccias because the former contain less than 6% mineral clasts whereas the crystalline-matrix breccias contain 10-20% mineral clasts; thus, to produce crystalline-matrix breccias from dark-matrix breccias it would be necessary to create clasts. Similar patterns exist for the dark-matrix and crystalline-matrix breccias at both the Apollo 16 and 17 sites.

Comparison of clast-rich impact-melt breccias from the Apollo 14 site with clast-bearing impact-melt breccias from the Apollo 16 and 17 sites (Simonds et al., 1977) revealed correlated variations in matrix texture, volume fraction of matrix, and abundances of clast types and refractory mineral clasts. These correlations between suites of impact-melt breccias from widely separated sites suggest that: 1) similar formational processes are responsible for both the clast-bearing and clast-rich impact-melts and 2) systematic characteristics exist between impact-melt breccias produced by different impact events. The observed correlations are compatible with the two-component thermal model of Simonds (1975) and Simonds et al., (1976). Thermal calculations by Onorato et al., (1977) suggest that the degree of clast-digestion (resulting in the biasing of clast populations to refractory minerals) is a function of the initial equilibration temperature of the clast-melt mixture. The observed textural sequence from clast-rich impact-melts (Apollo 14) through clast-bearing impact melts (Apollo 16 and 17) to clast-free impact-melts can be explained in terms of a progressive increase in the amount of superheated melt relative to incorporated debris, resulting in variations in the temperature of the clast-melt mixture following the initial thermal equilibration; thus, plagioclase morphology is indirectly related to the equilibration temperature of the clast-melt mixture. Subhedral and euhedral plagioclase tablets observed in the Apollo 16 and 17 subophitic and poikilitic impact-melt breccias have been experimentally reproduced by Lofgren (1974) at near-liquidus temperatures. Anhedral matrix textures observed in several Apollo 14 clast-rich impact-melt breccias are inferred to have crystallized at temperatures below the solidus due to greater amounts of cold clastic debris resulting in subsolidus equilibration temperatures.

Granulitic impactites

Based on criteria outlined in a previous section (enriched siderophile element abundances, presence of vestigial clasts) this suite of granulitic samples is interpreted to have an impact origin (Warner et al., 1977). Although an unambiguous identification of some criteria is difficult due to the subsequent thermal metamorphic event experienced by these samples, the following features of individual granulitic samples serves as evidence to support an impact origin.

The investigation of sample 79215 (Bickel et al., 1976; Morgan et al., 1975; McGee et al., 1978) revealed a clast-matrix texture with polymict clast assemblages and an enrichment in trace siderophile elements, satisfying two criteria for an impact interpretation. Isolated regions with textures and modes which differ from the matrix (see petrographic description) are interpreted as lithic clasts although the mineral compositions have been homogenized.

Sample 77017 has been interpreted by Ashwal (1975) as an igneous rock, however, Morgan et al., (1974b) report an enrichment in trace siderophile element abundances corresponding to a group associated with the final lunar bombardment (Higuchi and Morgan, 1975). Also a detailed petrographic study by McCallum et al., (1974) describes the rock as a breccia which contains anorthositic and troctolitic lithic clasts, together with single mineral clasts of rounded olivine and plagioclase.

Sample 78155 described by Bickel (1977) satisfies all of the criteria for an impact produced rock. It displays a clast-matrix texture, is polymict and is characterized by an enrichment in trace siderophile element abundances corresponding to a poorly defined siderophile group of Higuchi and Morgan (1975).

Granulitic clasts present in sample 73215 (James and Hammarstrom, 1977; Blanchard et al., 1977) also display enriched trace siderophile element abundances and are interpreted as granulitic impactites.

Black and White breccias

Because many of the samples from this group are composed of lithologies other than those described in the classification section (i.e. anorthositic and impact-melt), a discussion of the petrogenesis of individual samples will be included with the petrographic description.

Lunar Evolution

The combined geological, geochronological, geophysical and geochemical evidence gained from the investigation of the lunar rocks (both mare and highland) has resulted in the following scenario of lunar history:

a) Formation of the moon at 4.6 AE (1AE = 10^9 years) closely followed by almost total melting of the outer 200-300 km with subsequent fractionation to produce a crust and mantle. A well-established 4.55 AE age for a single dunite sample 72417, apparently represents an early lunar differentiation (Figure 17). Although unequivocal ages for lunar anorthositic rocks are hard to establish due to their low radioisotope content, results suggest that they crystallized 4.3-4.6 AE ago and that their primitive $\text{Sr}^{87}/\text{Sr}^{86}$ ratios (~ 0.6990) are compatible with formation during early lunar differentiation. Residual liquids (KREEP) from the early fractionation period have evolved initial $^{87}\text{Sr}/^{86}\text{Sr}$ values of 0.701 which suggests separation of this material or of a parental material at approximately the same time as the anorthosites.

b) A period of intense lunar bombardment by planetary debris from ~ 4.2 AE until 3.84 AE producing the large mare basins. This bombardment ended between 4.05-3.84 AE, a period referred to as a terminal lunar cataclysm (Tera and Wasserburg, 1974) (note the frequent occurrence of ages during that time frame, Figure 18). The crystalline age at $3.95 \pm$ AE for the pristine KREEP sample (15382) possibly represents remelting although it is unclear whether the KREEP composition existed in a lower crustal layer formed during the early differentiation or whether it represents a partial melt from the lunar interior present on the surface as an early basaltic flow (Gast 1972, Weill et al., 1974).

c) A period of mare flooding occurring ~ 3.9 -3.2 AE. High-Ti mare basalts (Apollo 11 and 17) range in age from 3.9-3.6 AE while most other basalts have ages less than 3.4 AE. Differences in $^{87}\text{Sr}/^{86}\text{Sr}$ values for mare basalts suggest a two-stage history for most systems with distinct sources varying in Rb/Sr by a factor of ~ 4 -5.

d) A period of quiescence from ~ 3.2 AE ago until the present with only sporadic small crater forming impacts.

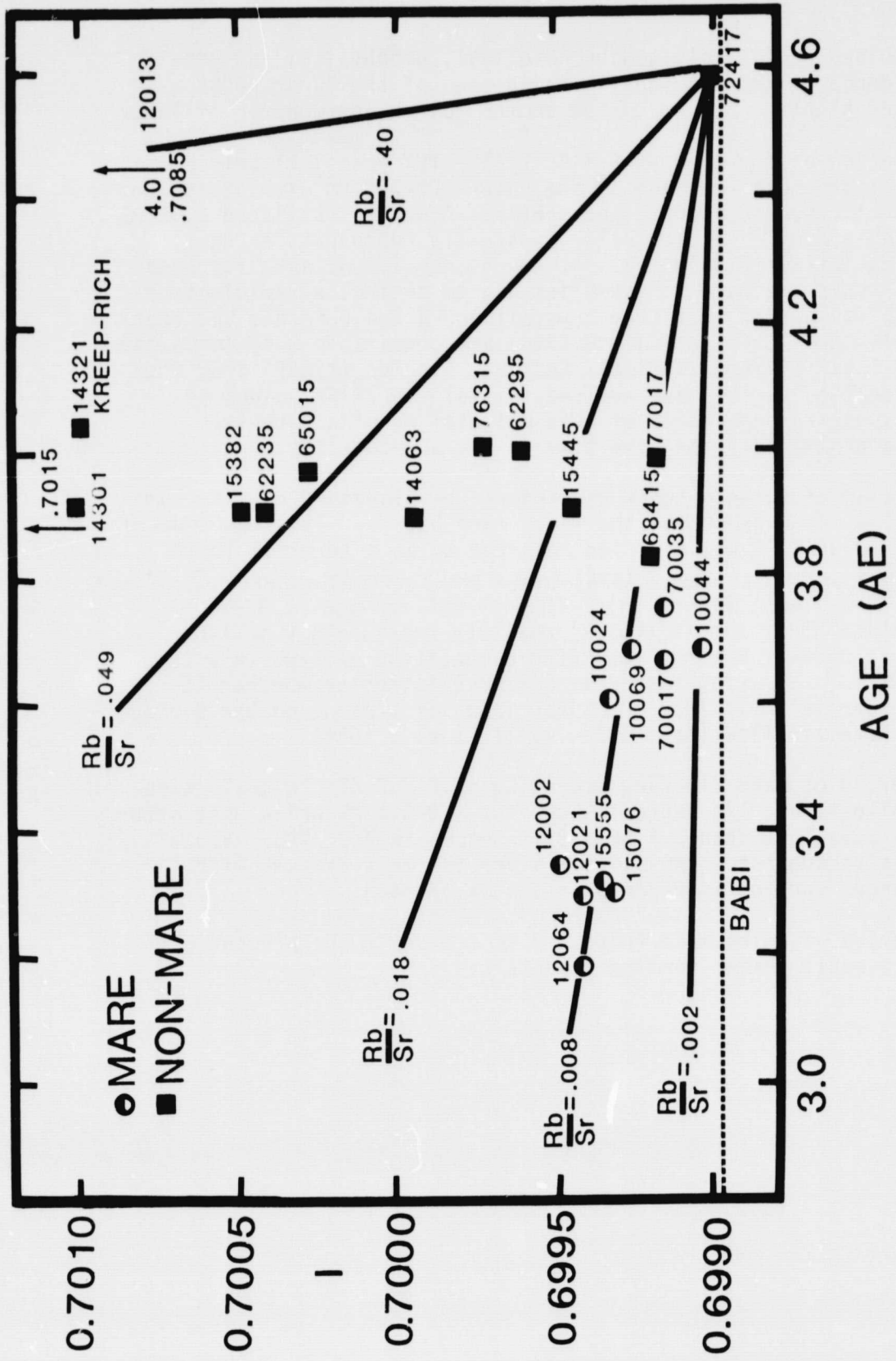


FIGURE 17. (T, I) diagram for lunar breccias and reference samples. Evolution for a hypothetical "first stage" from formation of the Moon to crystallization of the lavas is shown by the series of lines radiating from (T, I) = 4.6 AE, BABI). Adapted from Nyquist (1977).

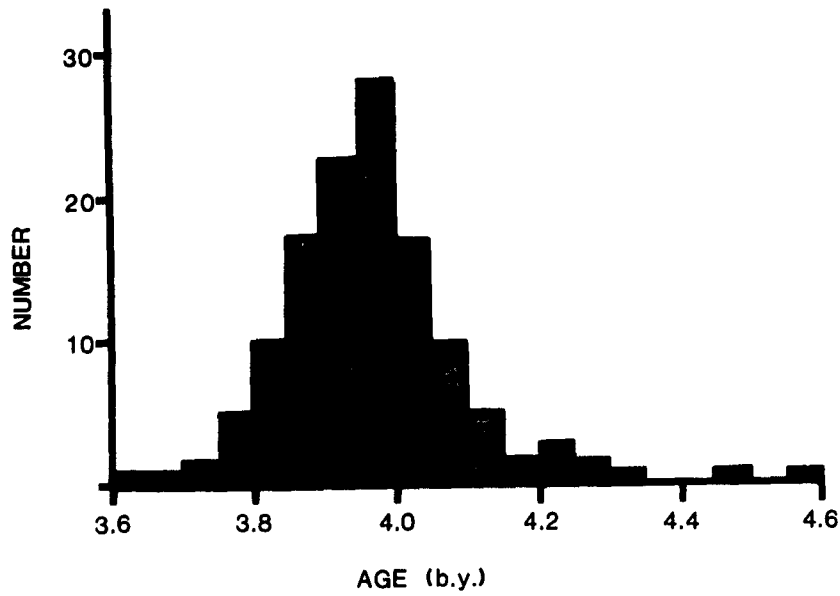


Figure 18. Distribution of highland ages as determined from $^{87}\text{Rb}/^{87}\text{Sr}$ isochrons and the $^{39}\text{Ar}-^{40}\text{Ar}$ plateaus, using data from the literature. Some ages in the 3.6-3.8 range may be younger igneous mare rocks transported to the highlands by distant impacts. A few ages >4.2 b.y. appear to have survived the intense rate heavy bombardment. Adapted from Wetherill (1975).

ROCK DESCRIPTIONS

10060- A typical "soil" breccia from Apollo 11.



Sample 10060 is a medium-grey rounded to subrounded rock (5x5x4.5 cm) believed to have been collected 10 to 15 meters away from the lunar module near the rim of the large double crater.

10060 DARK-MATRIX BRECCIA

Sample 10060 is a porous, fragmental-matrix breccia characterized by a detrital assemblage of mineral, lithic and glass clasts contained in an opaque brown matrix of mineral and lithic debris with minor brown glass (Figure a). The overall texture is seriate with grain sizes ranging from less than a micron to several millimeters. The matrix (material 39 microns and less) consists of a complex mixture of brown glass fragments (~5%) in various stages of devitrification, abundant micron-size mineral fragments, and various types of lithic debris. Sample 10060 is porous, with micron-size intergranular voids which can best be viewed in reflected light. Probably the most complete description of the glassy and porous nature of the matrix of fragmental-matrix breccias is given by Phinney et al. (1976).

The glass-clast population is characterized by abundant homogeneous orange-glass clasts and spheres or parts of spheres, with angular clasts being more abundant than spheres. Both clasts and spheres are commonly fractured. Some of the orange-glass clasts have compositions which resemble that of the Apollo 17 orange glass 74220 described in the companion volume. Other homogeneous glass clasts may be yellow, green or colorless. Green glass occurs most commonly as spheres and represents a small proportion of the total glass content. The spheres are compositionally similar to Apollo 15 green glass 15426 described in the companion volume. Colorless glass is present as individual clasts and commonly as a coating on mineral and lithic clasts or on other glass clasts. Heterogeneous glass in a variety of colors, occurs most commonly as irregularly shaped clasts which commonly contain schlieren formed by trains of sub-micron size debris. The glass may be vesicular or non-vesicular and contains mineral fragments and Fe-Ni blebs (Figure b).

Pink sub-calcic augites and pigeonites derived mostly from local mare basalts are the most common mineral clasts, occurring as angular grains which rarely display shock features. Angular plagioclase clasts are common, some with flame textures; rare maskelynite clasts are also present.

Basaltic fragments (up to 1.5 mm) are the predominant lithic clast type in 10060 (Figure c). Ophitic and subophitic textures similar to basalts 10020 and 10044 respectively are most common, followed by fine and medium-grained intersertal textures similar to basalts 10049 and 10017. The basaltic clasts often contain pore spaces in the form of angular voids enclosed by silicate minerals. Anorthositic clasts, generally less than 0.6 mm across, are observed but are not a common constituent. They are characterized by sub-rounded plagioclase grains which meet at 120° angles. Clasts (from 0.2 mm to 1.0 mm across) of poikilitic, impact-melt rock similar to 76015 are observed in section 10060,39 (Figure d). They are characterized by matrices of interlocking pigeonite oikocrysts hosting plagioclase grains. Clasts similar to the granulitic impactite 79215 were observed by Wood et al. (1970) but are not observed in section 10060,39.

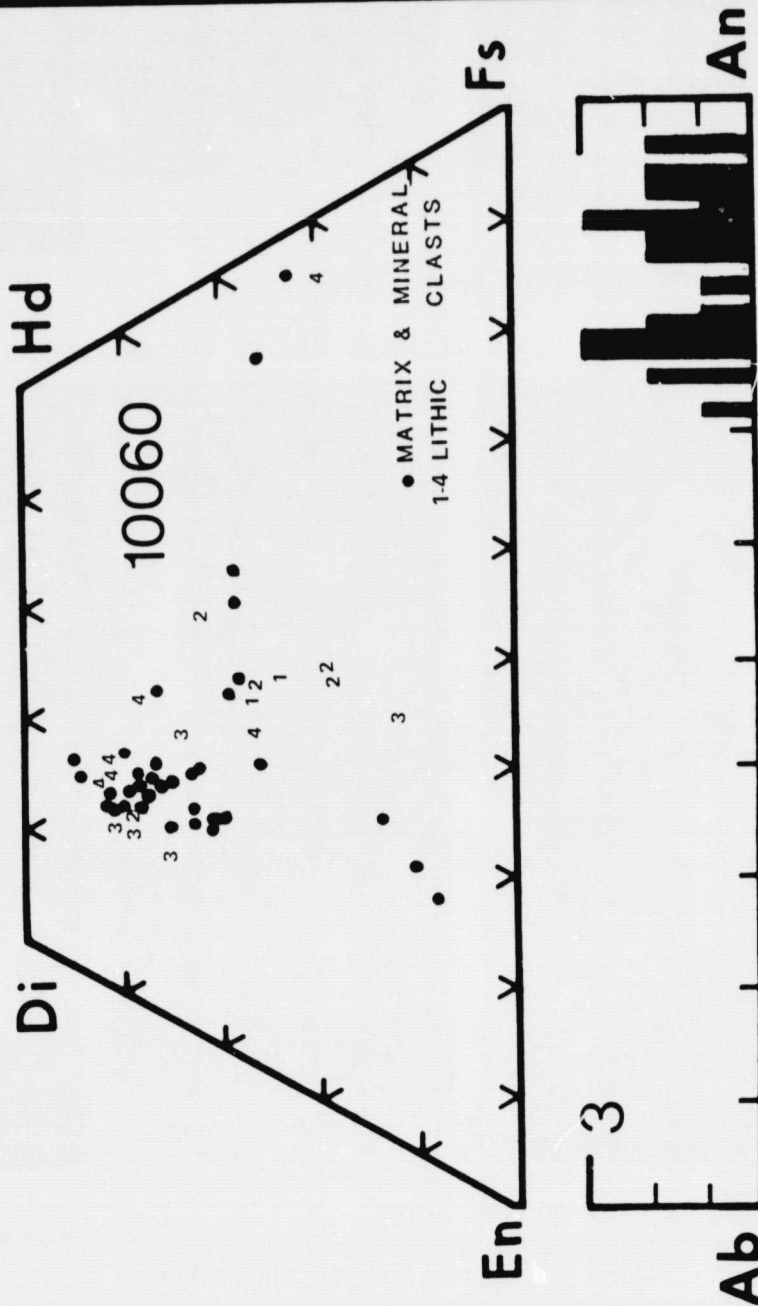
References: Agrell et al. (1970); Wood et al. (1970); Cameron (1970); Chao et al. (1971); Phinney et al. (1976).

10060,32

MODAL ANALYSES (VOL. %)

MATRIX (<39μ)	55.0
CLASTS (>39μ):	
PLAGIOCLASE	1.2
MAFIC	2.3
OPAQUE	.4
HETEROGENEOUS GLASS	2.6
HOMOGENEOUS GLASS	0.5
DEVITRIFIED GLASS	4.4
FRAGMENTAL BRECCIA	3.7
CRYSTALLINE BRECCIA	—
GRANULITIC	TR
OTHER METAMORPHIC	—
MARE BASALT	29.8
HIGHLAND BASALT	TR
CRUSHED	—
PORE SPACE	TR
OTHER	—

REFLECTED LIGHT



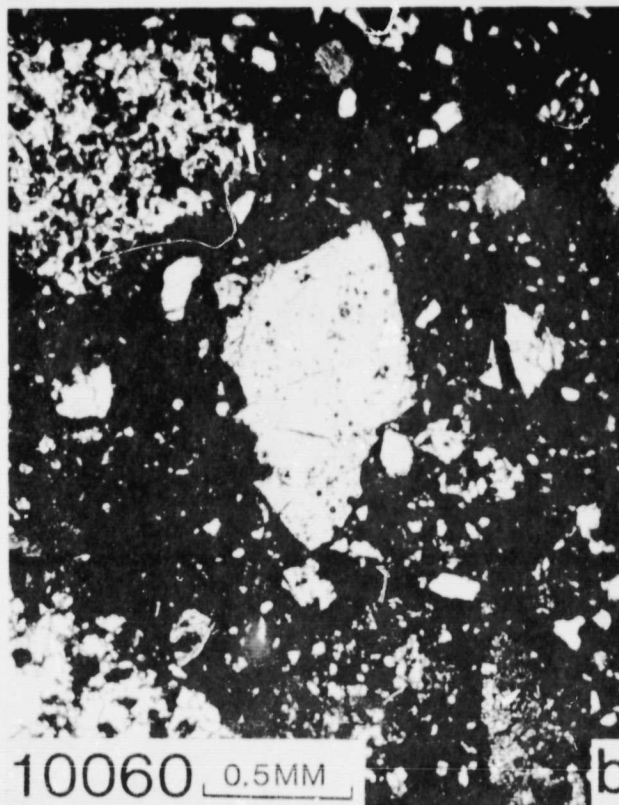
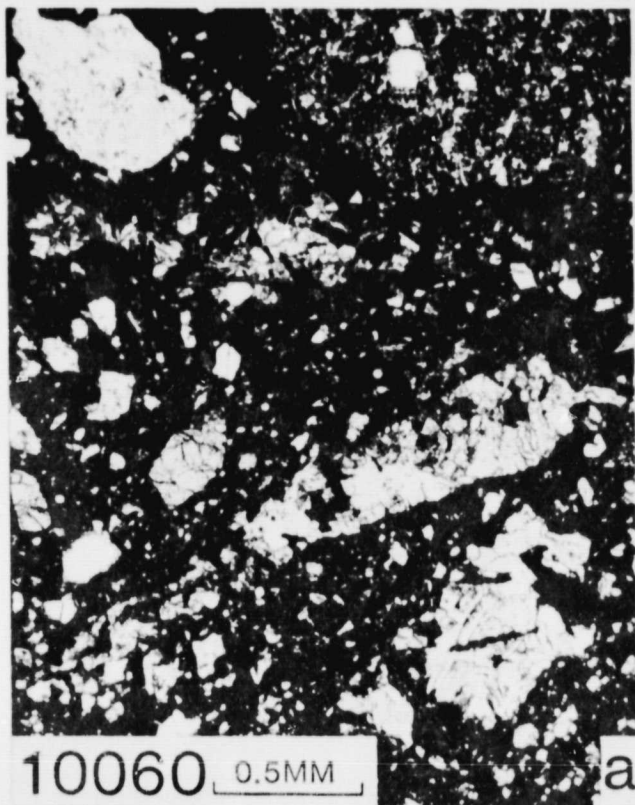


Figure 10060a. Typical view of 10060; transmitted light.

Figure 10060b. Debris-laden heterogeneous glass clast; transmitted light.

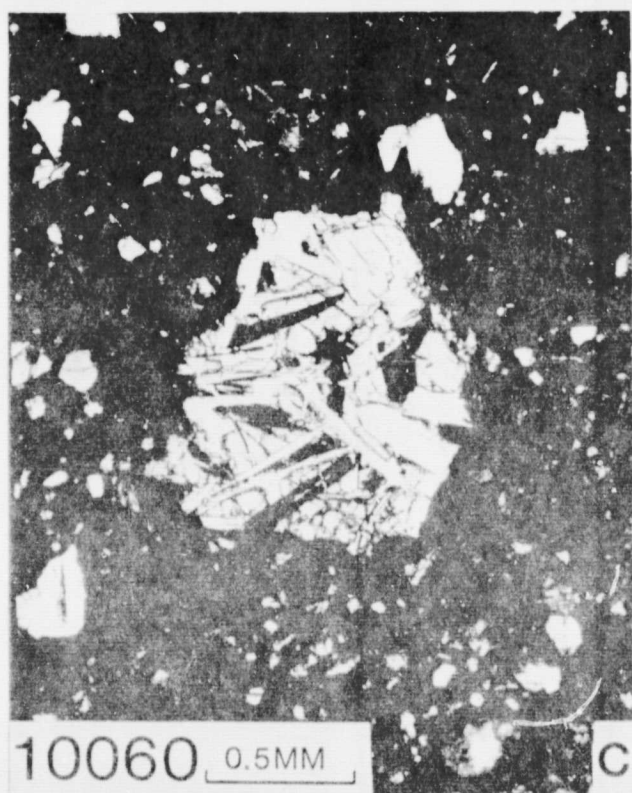


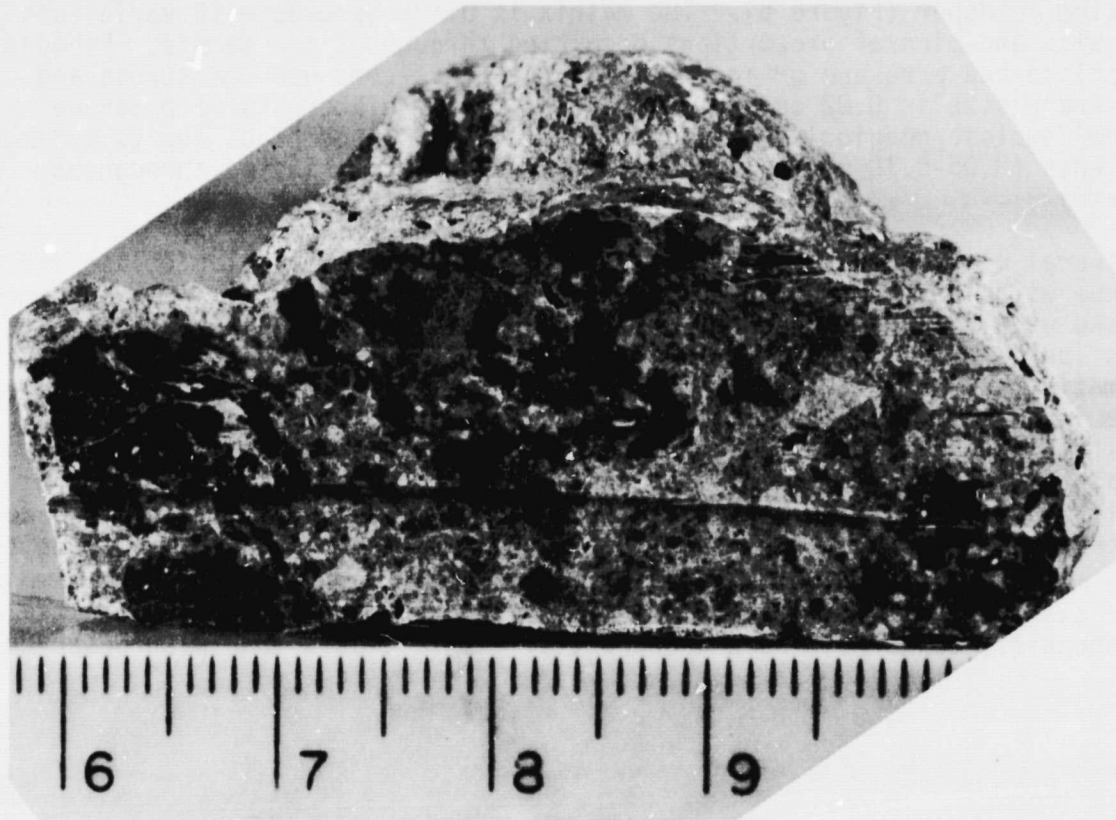
Figure 10060c. Basalt clast; transmitted light.

Figure 10060d. Poikilitic, impact-melt rock clast; transmitted light.

12013- A unique lunar breccia with a "granitic" composition. Several hypotheses including liquid immiscibility have been suggested for the differentiation of the two main lithologies (light and dark grey breccias). The rock contains the most highly evolved $^{87}\text{Sr}/^{86}\text{Sr}$ of any lunar material.



Sample 12013 is a light-grey angular rock (4x3x2 cm) with dark patches. Neither its location or orientation on the lunar surface is known.



12013 BLACK AND WHITE BRECCIA

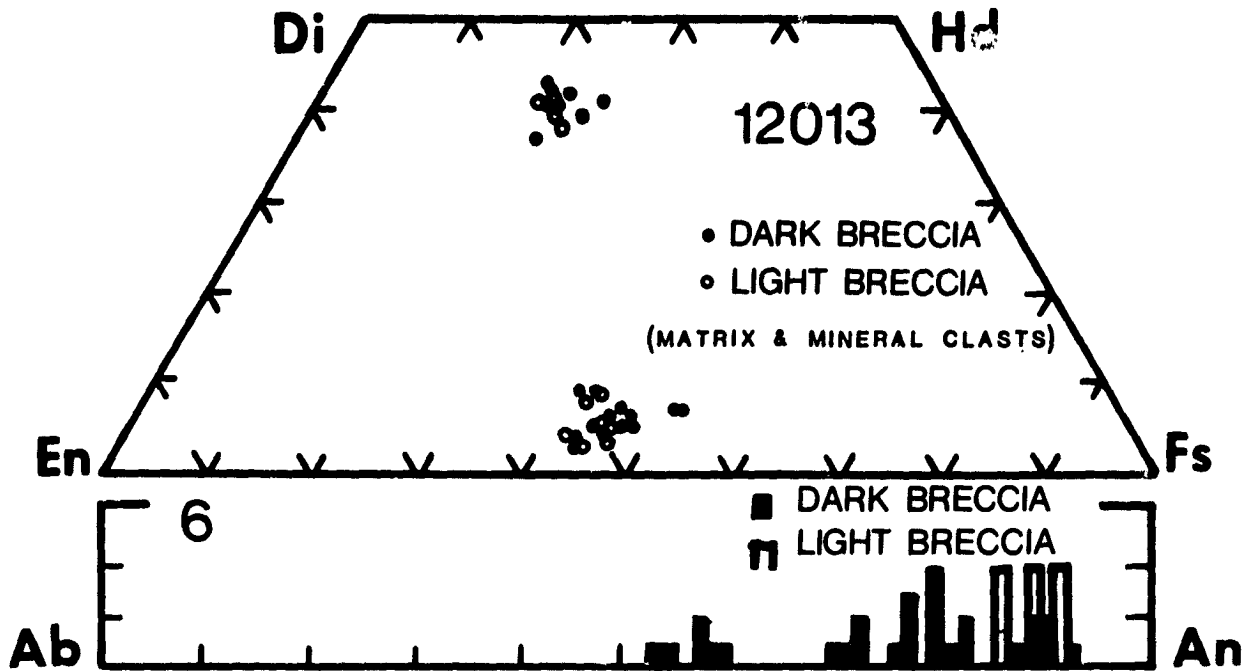
Sample 12013 is a black and white breccia characterized by three distinct lithologies: 1) light-grey breccia, 2) dark-grey breccia and 3) felsite (Figure a). The black and white appearance of the breccia is the result of different mineral assemblages in each of the three lithologies: the light-grey breccia is dominated by pyroxene and plagioclase and encloses rare patches and stringers of felsite; the dark-grey lithology is also composed of plagioclase and pyroxene but contains abundant opaque mineral grains; the felsite consists of intergrowths of quartz and potassium feldspar. Vesicles (0.05-0.15 mm) and vugs (up to 0.5 mm) occur in the dark-grey breccia and in the felsite. Only rare, irregularly shaped vugs (0.15 mm) are observed in the light-grey breccia.

It is evident from the photograph of the cut slab of sample 12013 that boundary relationships between the three lithologies are complex. In hand specimen the felsite occurs as almost equidimensional patches distributed throughout the light-grey breccia. The combination of these two lithologies (light-grey breccia and felsite) comprises the largest percentage of the rock and encloses irregularly shaped patches and streaks or schlieren of dark-grey breccia. In some areas, however, patches of felsite occur within the dark-grey breccia. Characteristics of each lithology are presented below.

Light-grey breccia

The light-grey breccia is characterized by a granoblastic matrix displaying equigranular grains of plagioclase and pyroxene; interstices are filled with potassium feldspar (Figure b). The matrix is heterogeneous with variations in grain size and mineral proportions occurring throughout the sample. Rounded plagioclase and pyroxene grains typically do not exceed 0.05 mm across and the average size is 0.02 and 0.03 mm across. Rare oikocrysts of pyroxene (0.1 mm) enclose plagioclase grains. Irregularly shaped blebs (up to 0.2 mm) and blades (0.05-0.10 mm) of ilmenite are randomly distributed throughout the matrix.

The mineral clast population is seriate and is dominated by plagioclase and pyroxene with less commonly occurring ilmenite. Clasts of olivine, described by Drake et al. (1970), were not observed in section 12013,6. Plagioclase clasts (up to 0.4 mm in length) are subangular to angular and typically lack deformation or recrystallization features. Some grains appear clouded due to minute inclusions of opaque minerals. Rare clasts of plagioclase display recrystallization features; several clasts display undulatory extinction. Clasts of pyroxene are typically subangular (up to 0.2 mm) and clouded by sub-micron size opaque mineral inclusions. Opaque mineral clasts are rounded and irregularly shaped and do not exceed 0.2 mm in section 12013,6. Ilmenite is the most common opaque phase; troilite occurs rarely throughout the sample. Lithic clasts in section 12013,6 are typically basaltic and display ophitic and subophitic textures. Rare anorthositic lithic clasts are also observed.



12013,6 Lt-grey breccia MODAL ANALYSES (VOL. %)	
MATRIX (<39 μ)	66.7
CLASTS (>39 μ):	
PLAGIOCLASE	9.9
MAFIC	2.0
OPAQUE	—
HETEROGENEOUS GLASS	—
HOMOGENEOUS GLASS	—
DEVITRIFIED GLASS	—
FRAGMENTAL BRECCIA	—
CRYSTALLINE BRECCIA (Dk-grey)	10.0
GRANULITIC	—
OTHER METAMORPHIC	—
MARE BASALT	—
HIGHLAND BASALT	3.1
CRUSHED	—
PORE SPACE	TR
OTHER (Felsite)	8.0

REFLECTED LIGHT

12013,6 Dk-grey breccia MODAL ANALYSES (VOL. %)	
MATRIX (<39 μ)	68.0
CLASTS (>39 μ):	
PLAGIOCLASE	16.0
MAFIC	1.5
OPAQUE	—
HETEROGENEOUS GLASS	—
HOMOGENEOUS GLASS	—
DEVITRIFIED GLASS	—
FRAGMENTAL BRECCIA	—
CRYSTALLINE BRECCIA (Lt-grey)	8.35
GRANULITIC	—
OTHER METAMORPHIC	2.3
MARE BASALT	—
HIGHLAND BASALT	—
CRUSHED	—
PORE SPACE	1.6
OTHER (Felsite)	2.0

REFLECTED LIGHT

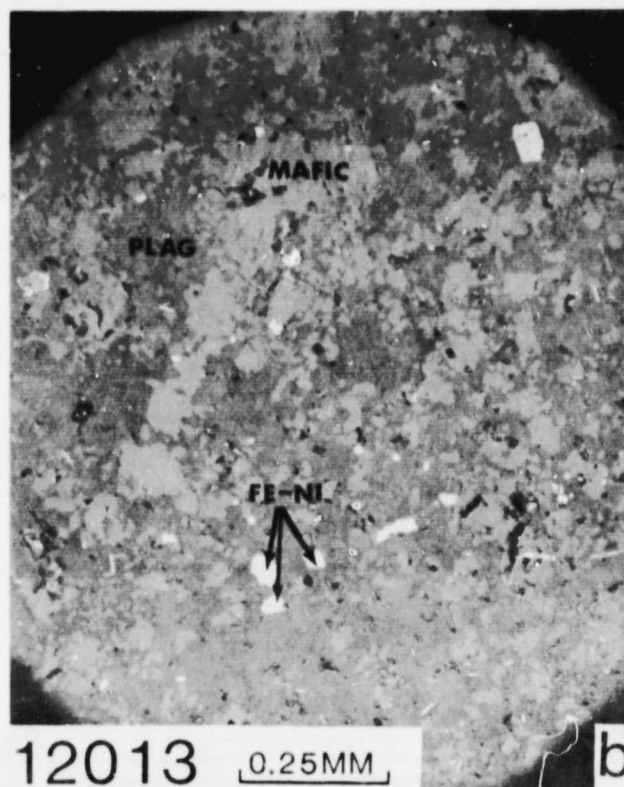
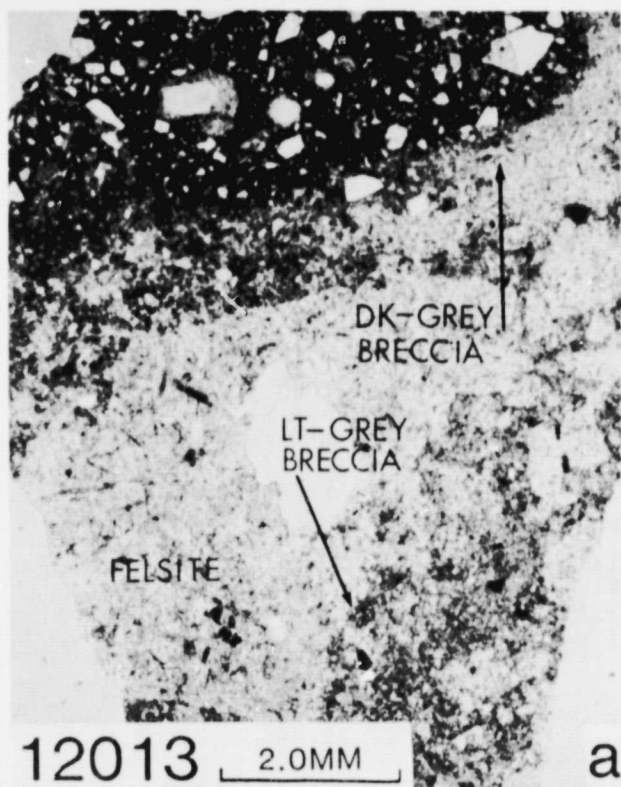


Figure 12013a. Typical view of 12013; transmitted light.

Figure 12013b. Typical matrix of light-grey breccia; reflected light, dark-grey, plagioclase; light-grey, mafic; white, Fe-Ni metal; black, vugs and plucked areas.

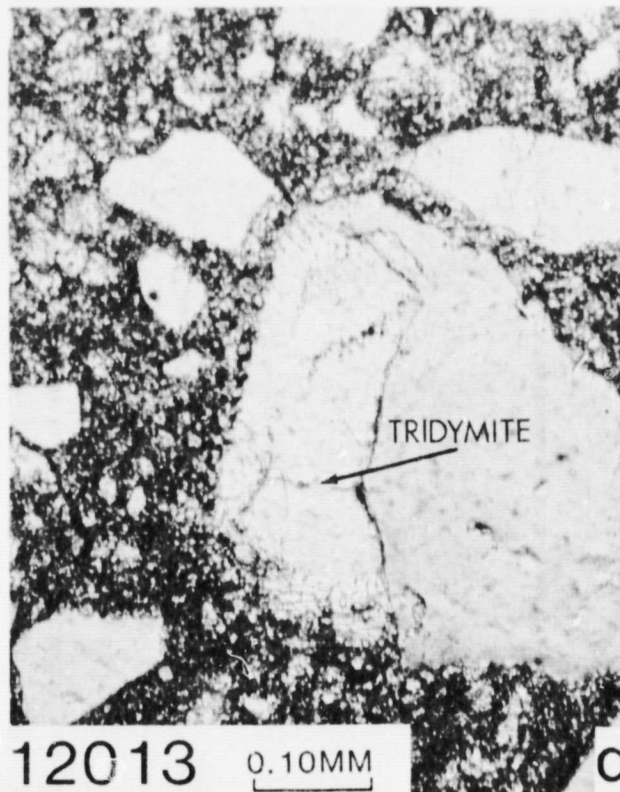
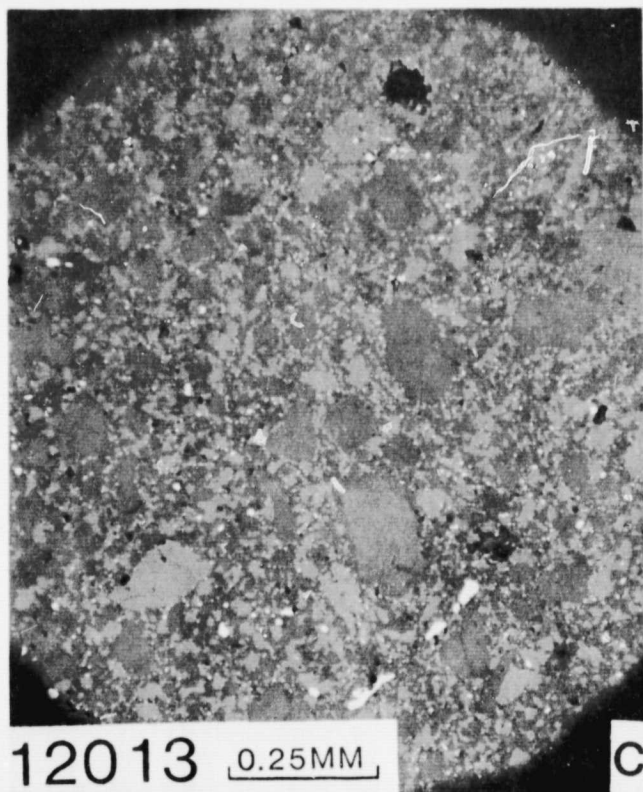


Figure 12013c. Typical matrix of dark-grey breccia; reflected light. Color key same as (b).

Figure 12013d. Tridymite grain in vug; transmitted light.

Dark-grey breccia

The dark-grey breccia is characterized by a fine-grained granoblastic matrix of plagioclase, pyroxene and ilmenite which hosts mineral and lithic clasts (Figure c). The size distribution of matrix minerals and mineral and lithic clasts is distinctly bimodal. Matrix plagioclase and pyroxene grains are typically 6 to 10 μm and ilmenite rarely exceeds 2 μm . Mineral and lithic clasts range from 0.05 to 0.6 mm. Vesicles up to 0.5 mm are common in the dark-grey lithology. The vesicles are commonly partially or completely surrounded by patches of feldspar. The mineral clast population is dominated by subangular to angular plagioclase (as in the light-grey breccia) but the proportion of plagioclase to pyroxene is much higher than in the light-grey breccia. Plagioclase clasts in the dark-grey breccia are also larger (up to 0.6 mm) than in the light-grey breccia. They are typically unfractured and undeformed although rare clasts display fine recrystallization features. Clasts of angular pyroxene do not exceed 0.2 mm and are also undeformed. Rare pyroxene clasts consist of aggregates of recrystallized grains. Fine exsolution lamellae are common in most pyroxene clasts. Irregularly shaped clasts of ilmenite (up to 0.2 mm) are present but are relatively uncommon. One large subrounded grain of tridymite 0.4 mm across was observed in section 12013,6 (Figure d); minerals present in trace abundances include apatite, whitlockite and zircon (Drake et al. 1970).

Lithic fragments in the dark breccia lithology in section 12013,6 are typically granoblastic and have mineral assemblages which resemble the light-grey breccia. The patches occur at the edge of section 12013,6 making it impossible to determine if the patches are clasts or portions of the light-grey breccia. Anorthositic fragments reported by Drake et al. (1970) are not present in section 12013,6.

Feldspar

The feldspar lithology is characterized by intergrowths of quartz and potassium feldspar; quartz typically occurs as acicular needles (up to 0.3 mm long) forming a network of interconnected crystals (Figure e). Interstices are filled with potassium feldspar. Both the quartz and potassium feldspar are clouded with numerous opaque inclusions. Pyroxene is randomly distributed throughout the feldspar as irregularly shaped grains (0.1-0.2 mm) or as elongated blades up to 1.0 mm in length. Ilmenite typically occurs as blades 0.1 mm long although some irregularly shaped grains (0.1-0.2 mm) are present. Troilite is relatively common, occurring as 10-20 μm blebs scattered throughout the feldspar; Fe-Ni metal is rarely found in association with the troilite. Minerals present in trace amounts include apatite, whitlockite, zircon and chromian ulvöspinel.

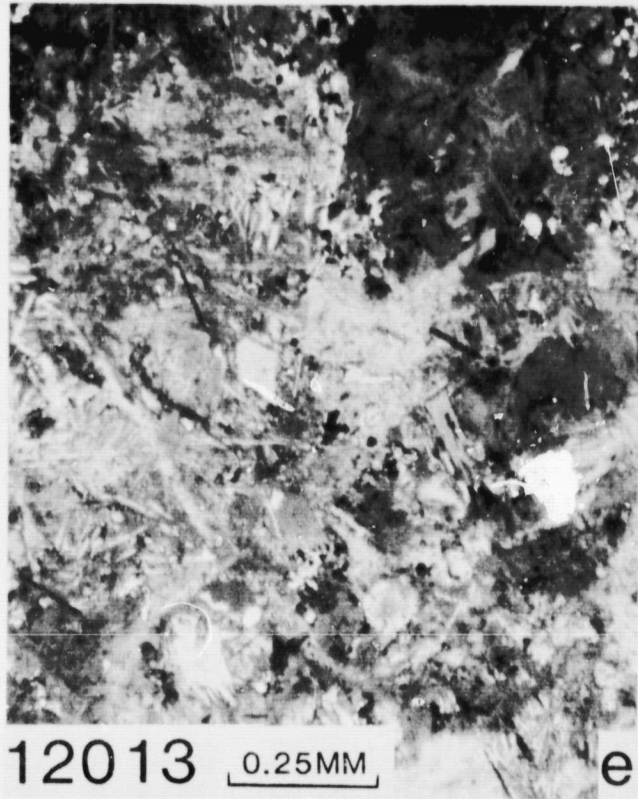


Figure 12013e. Felsite; transmitted light (crossed polarizers).

Discussion

Textural relationships in sample 12013 suggest that the felsite and the dark-grey breccia matrix crystallized from co-existing immiscible melts. High REE and P concentrations in the dark-grey breccia matrix and high K, Ba and Rb concentrations in the felsite are possibly due to silicate liquid immiscibility (Quick et al. 1977). However, although the major element chemistry data for both lithologies is compatible with a silicate liquid immiscibility relationship, some aspects of the REE chemistry are inconsistent with that relationship.

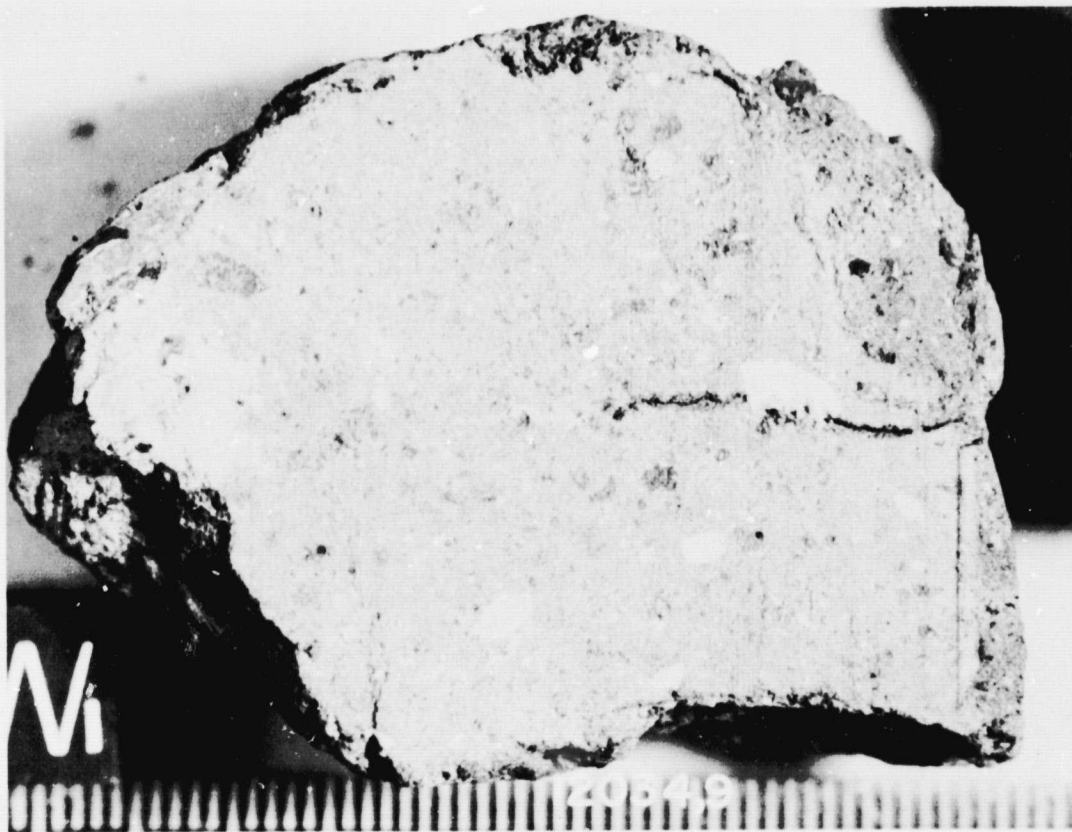
Quick et al. (1977) propose the following 2 models to explain the origin of sample 12013: 1) The dark-grey breccia melt and the felsite melt were produced by an impact event which completely melted genetically-related rocks and mixed them with clastic debris to form the light-grey breccia and the dark-grey breccia. (Quick et al. suggest an impact into a differentiated basaltic intrusion with late-stage granophyres). 2) The felsite melt and the dark-grey breccia melt were produced in an impact event which partially melted two genetically-unrelated rocks.

References: Drake et al. (1970); James (1970); Quick et al. (1977).

Age Data: Light-lithology
Rb-Sr isochron - 3.99 ± 0.05 ; I_{Sr} - 0.7085 (Lunatic Asylum, 1970)
Dark-lithology
Model I_{Sr} - 0.7001 at 4.0 AE (Lunatic Asylum, 1970)



Sample 12034 was collected on the northwest rim of Head Crater from the bottom of a 15 cm trench dug by astronauts Conrad and Bean.



12034 DARK-MATRIX BRECCIA

Sample 12034 is a fragmental matrix breccia similar in appearance to the Apollo 11 fragmental matrix breccias but with a much lower porosity. It consists of a variety of glass, mineral and lithic clasts contained in a matrix of brown glass fragments and comminuted debris (Figure a). The texture is seriate with fragments ranging in size from the limit of resolution up to 2.0 millimeters. Brown glass fragments dominate the less than 0.05 millimeter size fraction. Waters et al. (1971) noted the stratified nature of sample 12034 which can best be observed at low magnifications in reflected light (Figure b).

The glass-clast population in sample 12034 is extremely diverse, ranging from colorless, pale green, yellow or orange homogeneous glass to partially to completely devitrified glass clasts, some with included mineral grains. Orange glass is characteristically devitrified and, except for the smaller clasts (<0.20 mm), commonly contains mineral debris. Subrounded to rounded fragments of maskelynite and devitrified maskelynite occur commonly as inclusions in the large (>0.60 mm) devitrified glass clasts. Devitrification features in glass clasts take the form of variolitic clusters of plagioclase needles and more commonly axiolitic intergrowths of tightly packed plagioclase and pyroxene crystals.

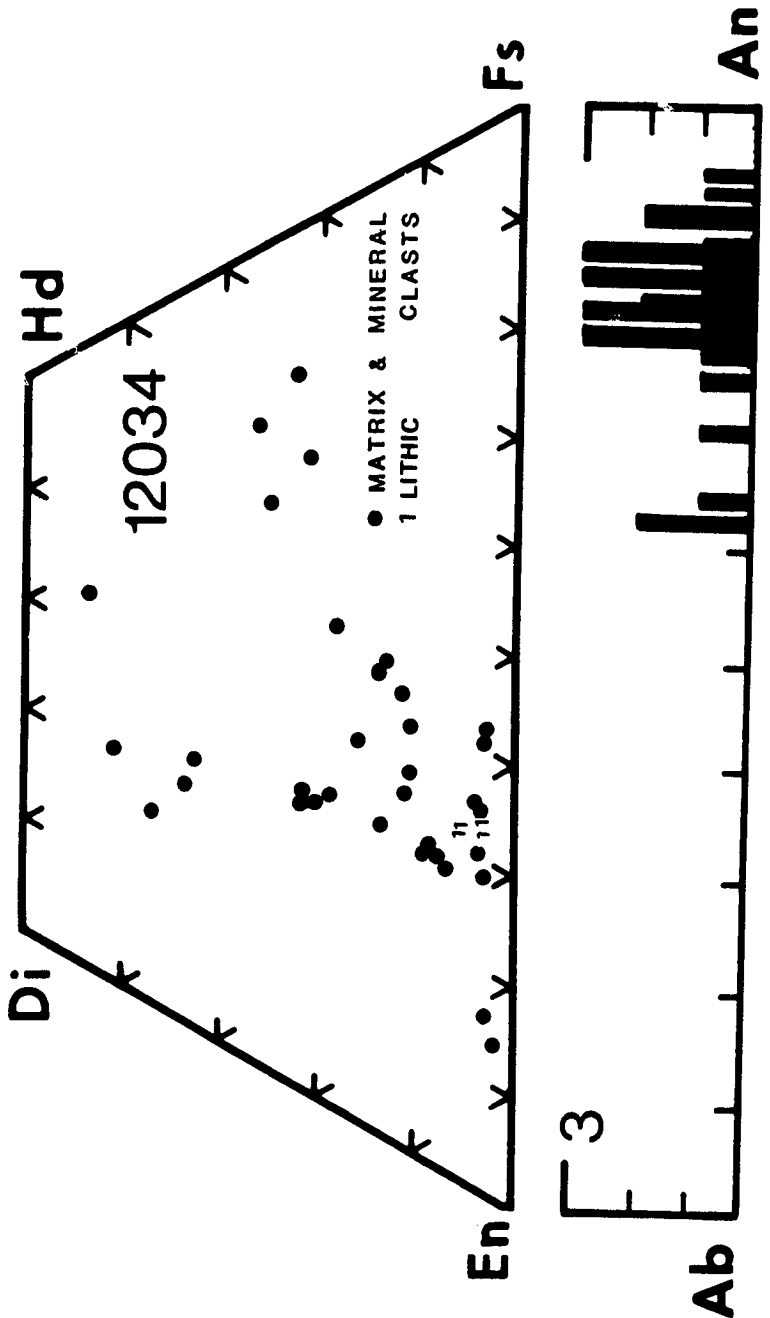
Lithic clasts display a more restricted range of types; the most commonly occurring are basalts and dark-matrix breccias. Several clasts of ophitic basalt were observed together with clasts which display vitrophyric textures. Clasts of cataclastic anorthosite (similar to 60025) are relatively common; many contain grains that are partially or completely maskelynitized. Clasts of dark-matrix breccia are relatively common; they are most easily observed in reflected light where very subtle differences between the clast itself and the host breccia are apparent. Waters et al. (1971) note the presence of lithic clasts of anorthositic gabbro although none were observed in section 12034,33 which was studied here.

References: Waters et al. (1971); Chao et al. (1971); Phinney et al. (1976).

12034

MODAL ANALYSES (VOL. %)

MATRIX (<39 μ)	53.49
CLASTS (>39 μ):	
PLAGIOCLASE	7.39
MAFIC	4.06
OPAQUE	.73
HETEROGENEOUS GLASS	22.71
HOMOGENEOUS GLASS	TR
DEVITRIFIED GLASS	1.11
FRAGMENTAL BRECCIA	.40
CRYSTALLINE BRECCIA	4.75
GRANULITIC	—
OTHER METAMORPHIC	—
MARE BASALT	5.96
HIGHLAND BASALT	—
CRUSHED	—
PORE SPACE	—
OTHER	—



REFLECTED LIGHT

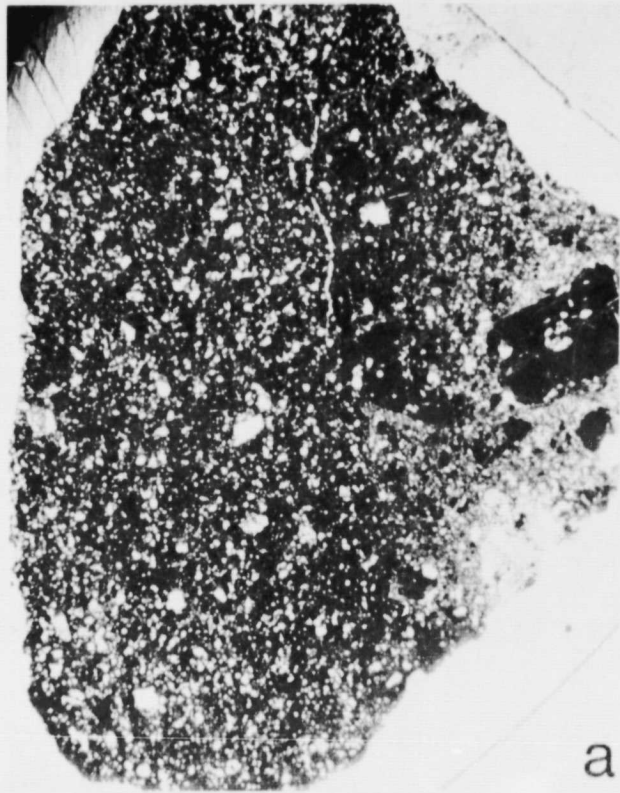
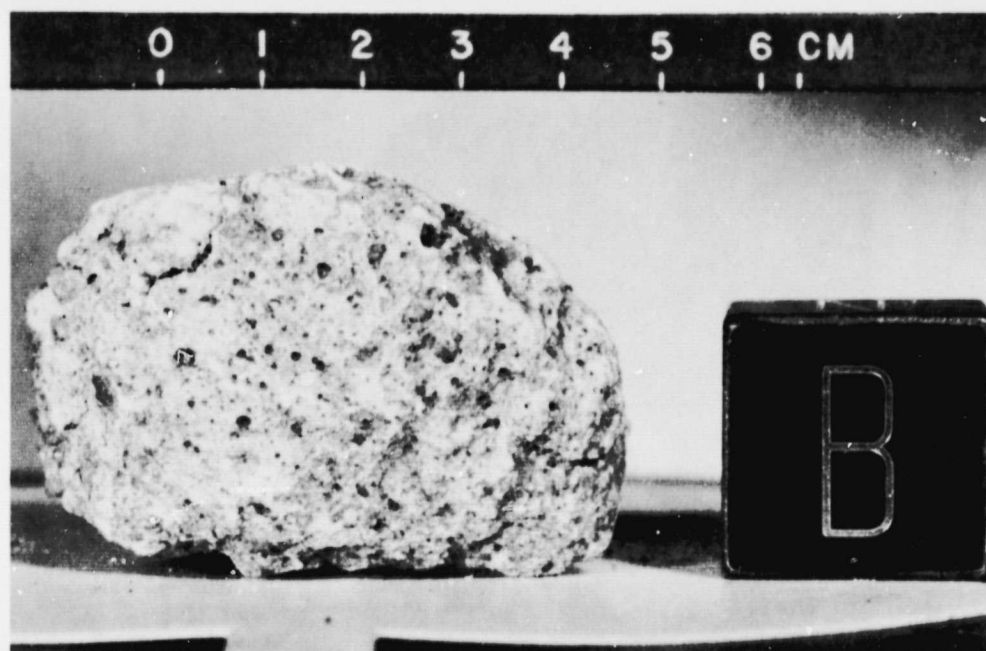


Figure 12034a. Typical view of 12034; transmitted light.



Figure 12034b. Same view as (a); reflected light.

14063- One of a small number of highly feldspathic breccias from Apollo 14.



Sample 14063 is a very light-grey subangular to subrounded rock (1.5x1.7x1.2 cm) collected at Station C1.

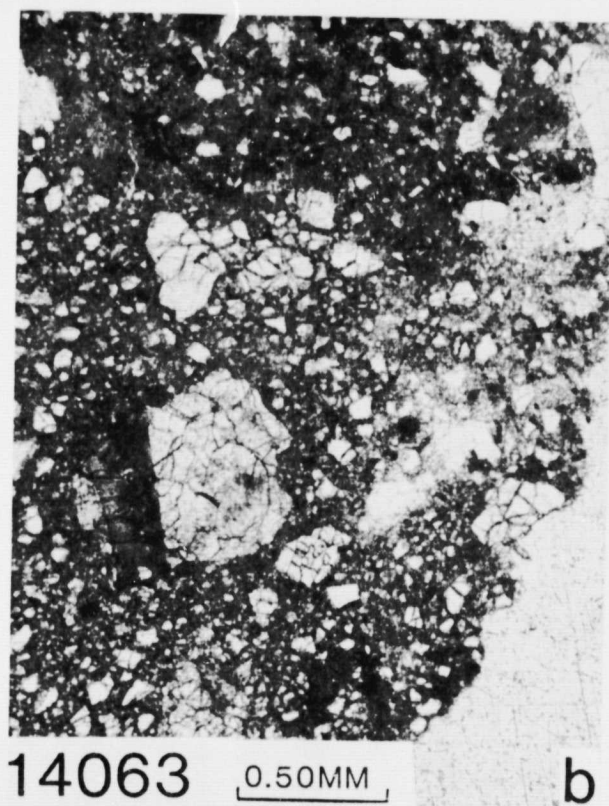
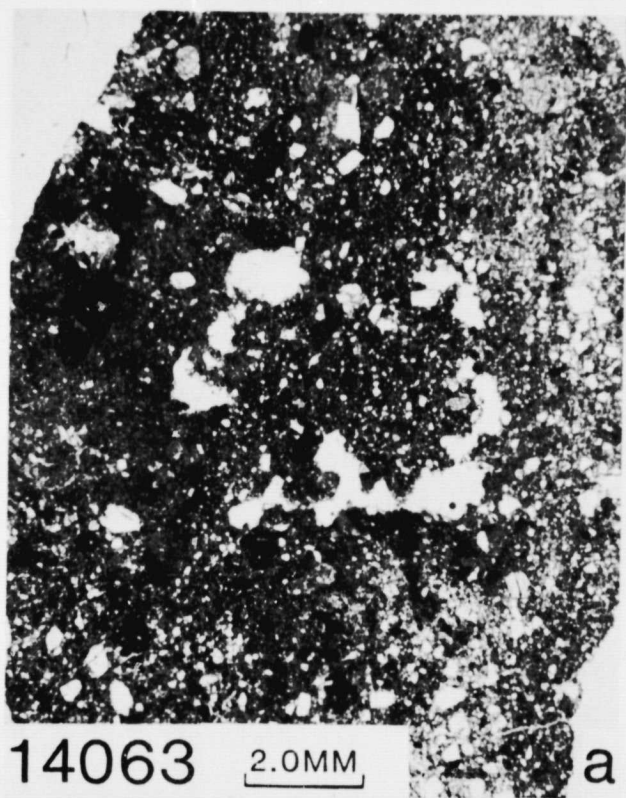


Figure 14063a. Typical view of 14063; transmitted light.

Figure 14063b. Olivine breccia; transmitted light.

14063 LIGHT-MATRIX BRECCIA

Sample 14063 is a complex light-matrix breccia characterized by several distinct lithologic units, each differing in texture and/or composition (Figure a). Steele and Smith (1976) describe six units in section 14063,14, four of which are recognized in section 14063,13 used in this study. The four units include 1) medium-grained olivine breccia (Figure b), 2) noritic breccia containing lithic clasts with approximately 70% lath-shaped plagioclase (0.05 mm) and 30% poikilitic pyroxene (Figure c), 3) a glassy unit which appears to be intrusive into the noritic breccia (Figure d) and 4) a polymict breccia (Figure e).

The polymict breccia comprises the largest area in section 14063,13 and is characterized by mineral clasts of plagioclase, pyroxene, spinel, olivine and opaques together with lithic clasts of dark-matrix breccia and noritic breccia (equivalent to clasts in unit 2); several devitrified glass clasts are observed. The matrix consists of <39 μ m mineral and lithic debris with only minor amounts of glass. The unit has a seriate texture with components ranging in size from the limit of resolution up to 1.30 mm. Pore space occurs as irregularly shaped vugs up to 2.0 mm across and as small intergranular voids which are most easily observed in reflected light at high magnification. Plagioclase, the most common mineral clast type, is characterized by subrounded to angular clasts which commonly display fracturing; rare clasts display undulatory extinction. Pyroxene clasts (up to 0.40 mm) are typically angular, display fracturing and some have exsolution lamellae. Spinel clasts, up to 0.15 mm, are relatively uncommon although their size and pink color make them very conspicuous. Ilmenite occurs randomly as angular grains (up to 0.10 mm) and Fe-Ni metal occurs as 5-10 μ m blebs scattered throughout the matrix. Clasts of dark matrix breccia up to 0.5 mm occur commonly in this unit and typically display rounded or ovoid shapes. Noritic breccia clasts (up to 0.5 mm) are also present but occur less commonly than the dark-matrix clasts. Finally, clasts of partially to completely devitrified orange-brown glass (0.50 mm) are relatively common. Most glass clasts contain mineral debris.

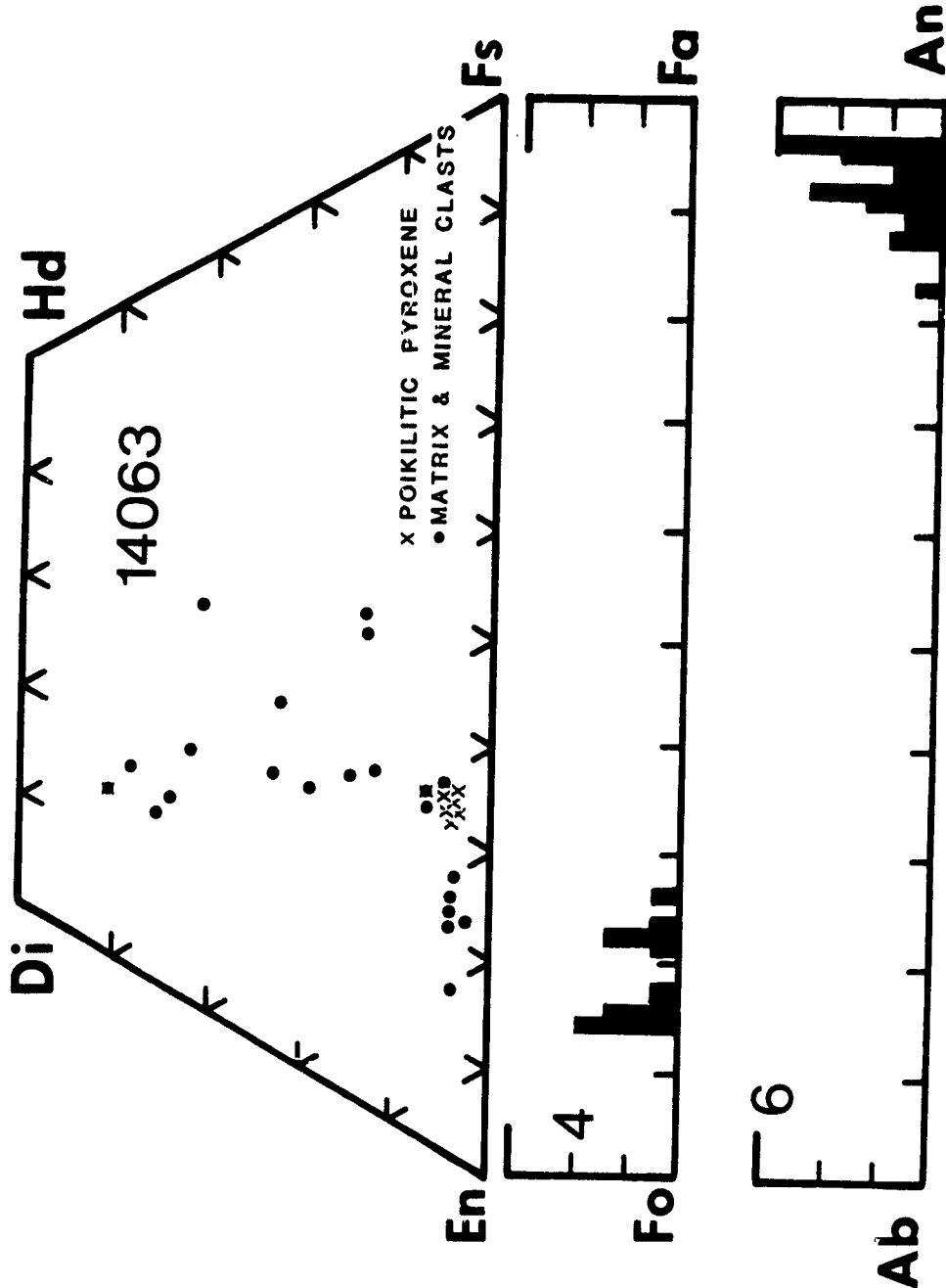
The noritic breccia is the second most dominant lithology in section 14063,13. It is characterized by abundant lithic clasts of noritic breccia (up to 2.5 mm across) together with rare clasts of dark-matrix breccia in a matrix dominated by single mineral clasts and lithic debris derived from the noritic breccias. Boundary relationships between the noritic breccia and the polymict breccia are locally sharp but may also be gradational (Figure f).

The glassy unit (which appears to be intrusive into the noritic breccia) is compositionally indistinct from the noritic breccia. It is fine grained and glassy, contains few clasts >0.03 mm and at higher magnification (400X) is observed to contain abundant 5 μ m blebs of ilmenite. One large (0.50 mm) shocked and partially melted clast of plagioclase (Figure d) is enclosed within the unit.

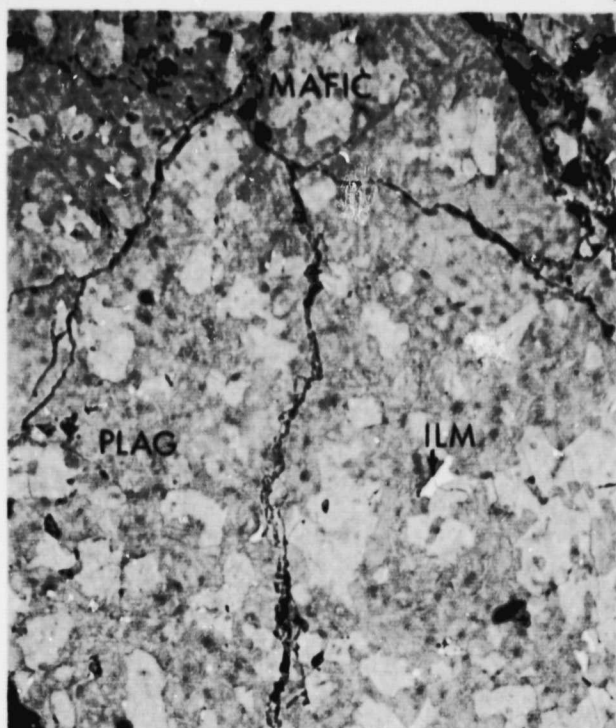
The olivine breccia is characterized by an almost monomict assemblage of angular olivine grains (up to 0.40 mm across). The largest grains are crushed and many grains in the 0.10 mm size range display fractures. Angular plagioclase grains (typically 0.10 mm and less with rare 0.30 mm grains)

14063,51
MODAL ANALYSES (VOL. %)

MATRIX (<39 μ)	73.0
CLASTS (>39 μ):	
PLAGIOCLASE	9.0
MAFIC	5.5
OPAQUE	TR
HETEROGENEOUS GLASS	TR
HOMOGENEOUS GLASS	TR
DEVITRIFIED GLASS	—
FRAGMENTAL BRECCIA	7.5
CRYSTALLINE BRECCIA	1.0
GRANULITIC	1.0
OTHER METAMORPHIC	2.0
MARE BASALT	TR
HIGHLAND BASALT	0.5
CRUSHED	0.5
PORE SPACE	—
OTHER	TR



REFLECTED LIGHT
Simonds et al. (1977)



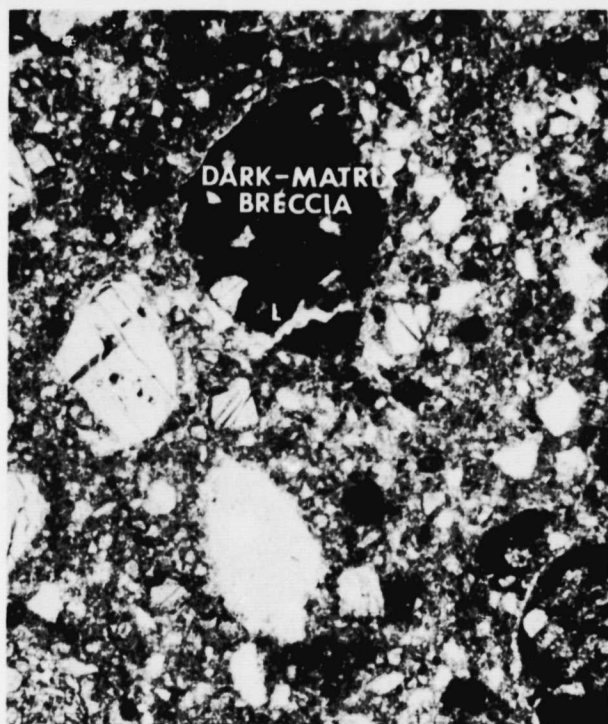
14063 0.10MM c



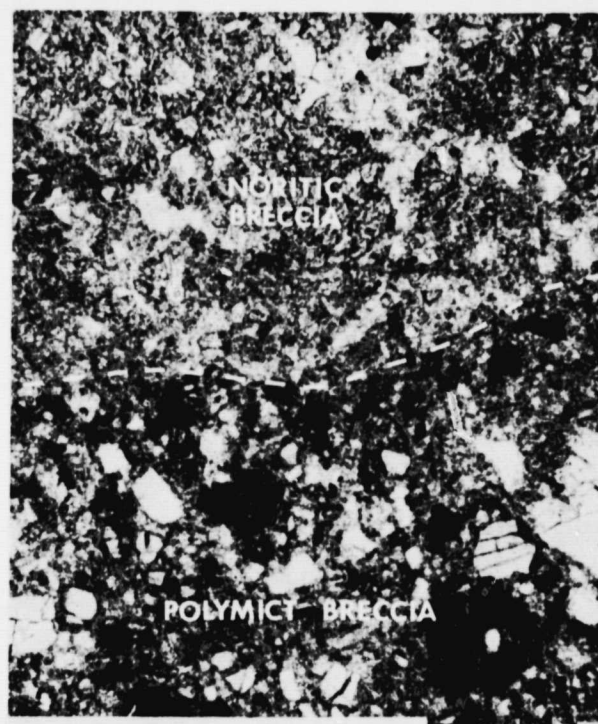
14063 0.50MM d

Figure 14063c. Poikilitic noritic breccia; reflected light. Dark-grey, plagioclase; light-grey, mafic; white, ilmenite.

Figure 14063d. Vitric intrusive unit with enclosed partially melted plagioclase clast; transmitted light.



14063 0.50MM e



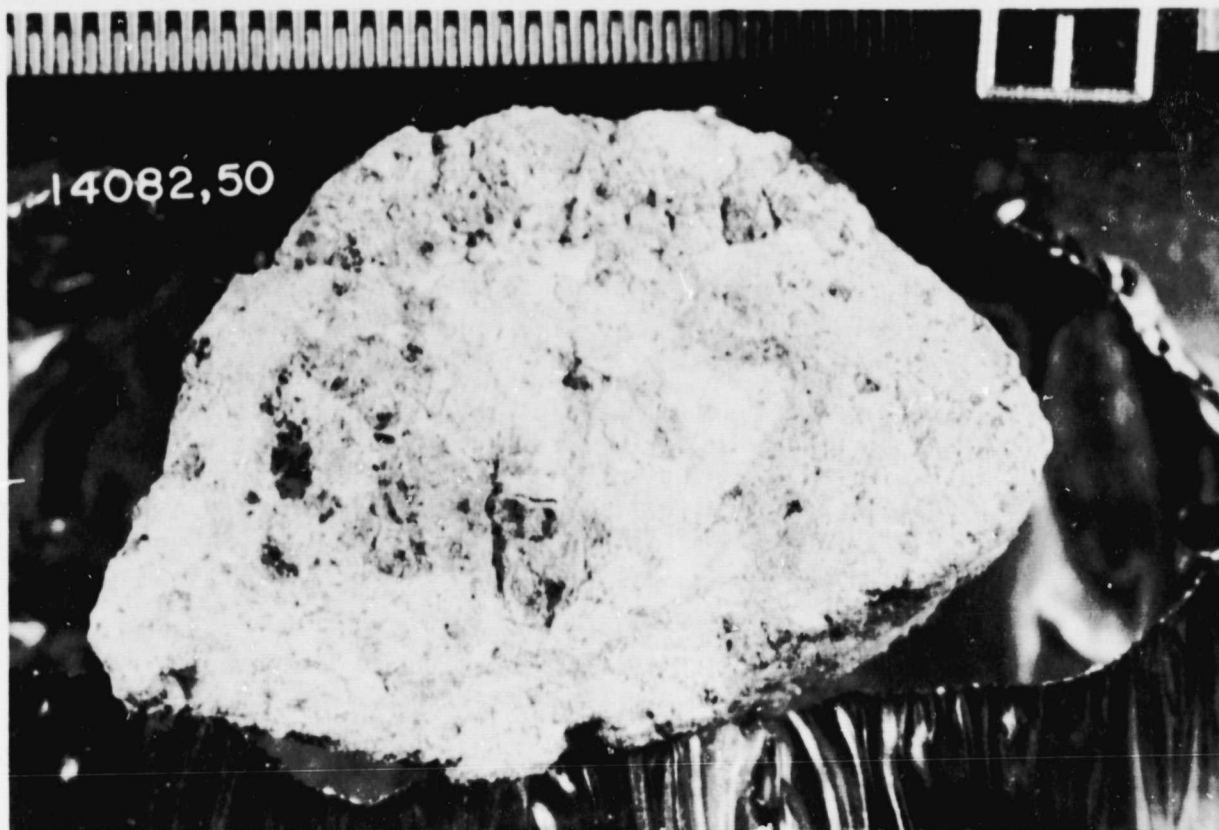
14063 0.50MM f

Figure 14063e. Typical polymict breccia with enclosed dark matrix breccia clasts; transmitted light.

Figure 14063f. Gradational boundary between noritic breccia and polymict breccia; transmitted light.

comprise approximately 5% of the breccia; most grains are fractured. Rare grains of chromite (0.05 mm) occur randomly throughout the breccia.

References: Warner (1972); Quaide and Wrigley (1972); Steele and Smith (1976).



Sample 14082 is a very light-grey blocky to slightly slabby rock (6.0x3.6x2.0 cm) collected at Station C1.

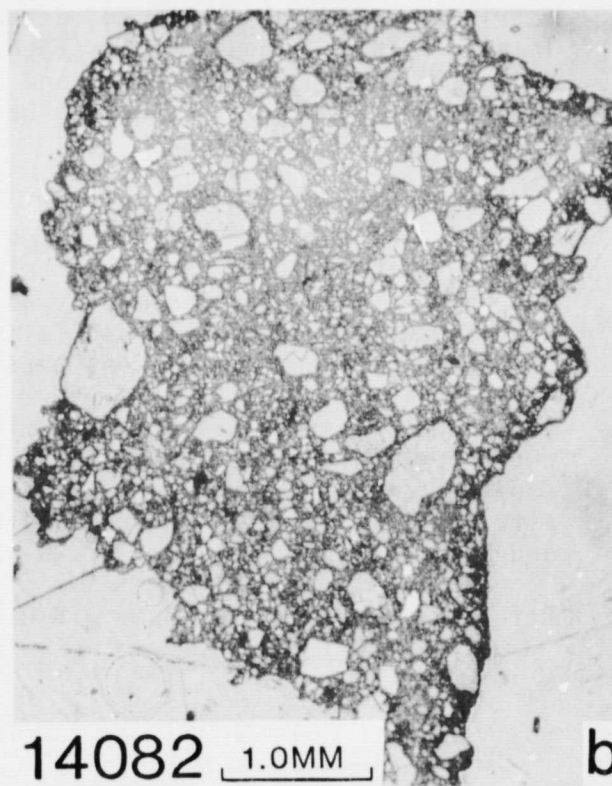


Figure 14082a. Typical view of 14082; transmitted light.

Figure 14082b. Same view as (a); reflected light.

14082 LIGHT-MATRIX BRECCIA

Sample 14082 is a light-matrix breccia with a relatively well-mixed matrix, although some sections appear to consist of monomict zones. In general the breccia is polymict and porous, and consists mainly of mineral clasts and small lithic clasts (Figure a). Two sections, 14082,7 and 14082,12 were investigated to illustrate the somewhat variable nature of the sample. Section 14082,7 displays the most homogeneous matrix and widest variety of clasts. It is characterized by a seriate texture, with materials ranging in size from the limit of resolution up to 0.3 mm. The matrix (material <39 μm) consists of plagioclase, pyroxene, olivine and opaque mineral grains, together with patches of colorless glass. The extremely porous nature of the matrix is best illustrated by a reflected light photomicrograph (Figure b).

Plagioclase, the most common mineral clast type, is present as subangular to subrounded clasts (up to 0.30 mm). Fracturing is uncommon and only rare clasts display undulatory extinction. Pyroxene and olivine clasts are subangular to subrounded (up to 0.3 mm). Rare clasts display lamellae; however, none of the spectacular exsolution features described by Ryder and Bower (1976) were observed in the sections investigated by the author. Rare, irregularly shaped clasts of ilmenite (up to 0.1 mm) are present. Micron-size blebs of Mg-spinel and Fe-Ni metal are present in the matrix.

A variety of lithic clasts are present in section 14082,7. Several vitric matrix breccias (up to 1.0 mm) are characterized by mineral and lithic debris in a dark brown glassy matrix (Figure c). Two impact-melt breccias with poikilitic textures (Figure d) and several clasts with basaltic textures similar to the high-alumina mare basalt clasts described by Ryder and Bower (1976a) were also observed.

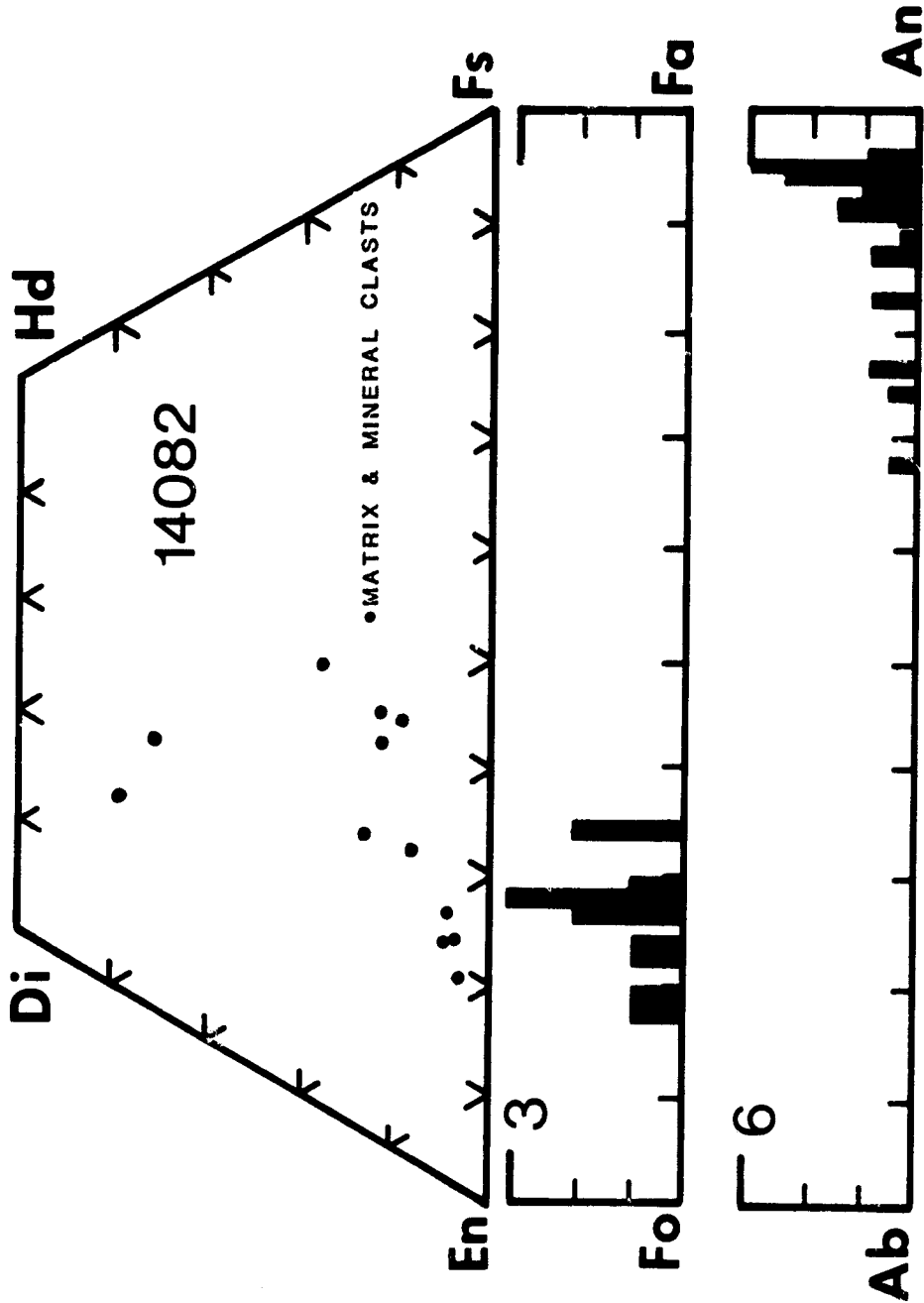
Section 14082,12 is distinguishable from 14082,7 in that it is nearly monomict and contains a much more restricted lithic clast population. The texture is seriate with material ranging in size from the limit of resolution up to 2.0 mm. The section is dominated by angular plagioclase grains, most of which are fractured; rare clasts display undulatory extinction. Clasts of angular, fractured pyroxene are present but are much less abundant than the plagioclase.

The lithic clast population is dominated by poikilitic textured impactites which contain plagioclase laths (.05-.10 mm) enclosed in pyroxene oikocrysts together with clasts of angular plagioclase (up to 0.3 mm). Two clasts of vitric-matrix breccia are present (0.15 mm) and are characterized by mineral and lithic debris in a dark brown glassy matrix.

References: Ryder and Bower (1976a).

14082, 10
MODAL ANALYSES (VOL. %)

MATRIX (<39 μ)	71.0
CLASTS (>39 μ):	
PLAGIOCLASE	10.5
MAFIC	2.0
OPAQUE	TR
HETEROGENEOUS GLASS	TR
HOMOGENEOUS GLASS	TR
DEVITRIFIED GLASS	—
FRAGMENTAL BRECCIA	3.5
CRYSTALLINE BRECCIA	7.0
GRANULITIC	1.5
OTHER METAMORPHIC	—
MARE BASALT	TR
HIGHLAND BASALT	3.0
CRUSHED	1.5
PORE SPACE	TR
OTHER	TR



REFLECTED LIGHT
Simonds et al. (1977)

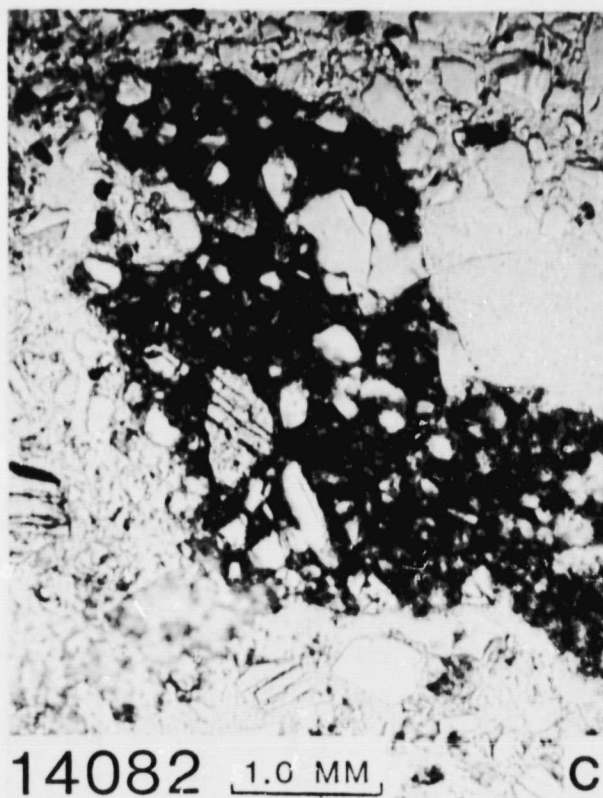


Figure 14082c. Vitric matrix breccia clast; transmitted light.

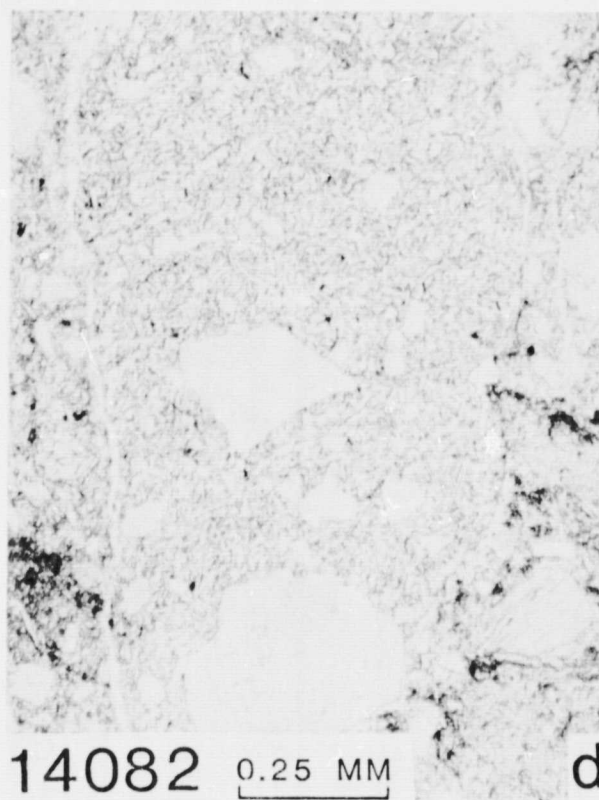
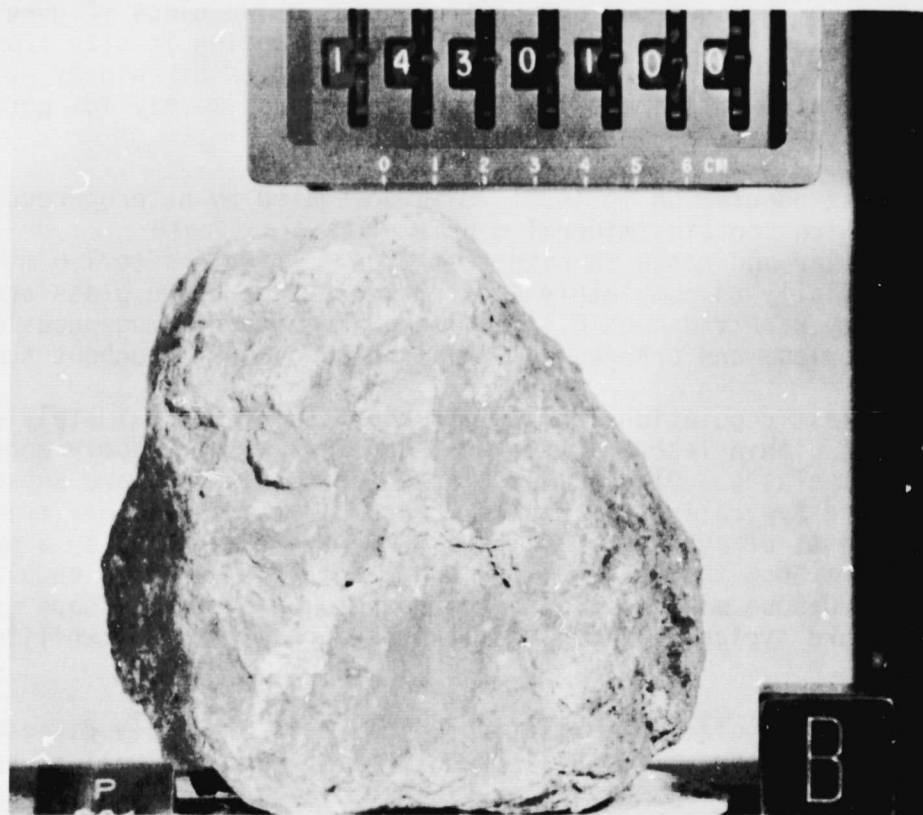


Figure 14082d. Poikilitic impact-melt clast in 14082; transmitted light.

14301- A typical Apollo 14 "soil" breccia.



Sample 14301 is a medium grey subrounded rock (12.5x12.0x8.0 cm) collected at Station G1.

14301 DARK-MATRIX BRECCIA

Sample 14301 is a fragmental-matrix breccia characterized by abundant lithic clasts (~50%), many of which are larger than one millimeter (Figure a). The matrix consists of a complex mixture of mineral and lithic fragments together with fragments of homogeneous and heterogeneous brown glass (Figure b). The texture of the sample is seriate with fragments ranging in size from the limit of resolution up to 5 millimeters. SEM studies by Phinney et al. (1976) show that the matrix of sample 14301 contains approximately 10% porosity which typically exists as intergranular pore space.

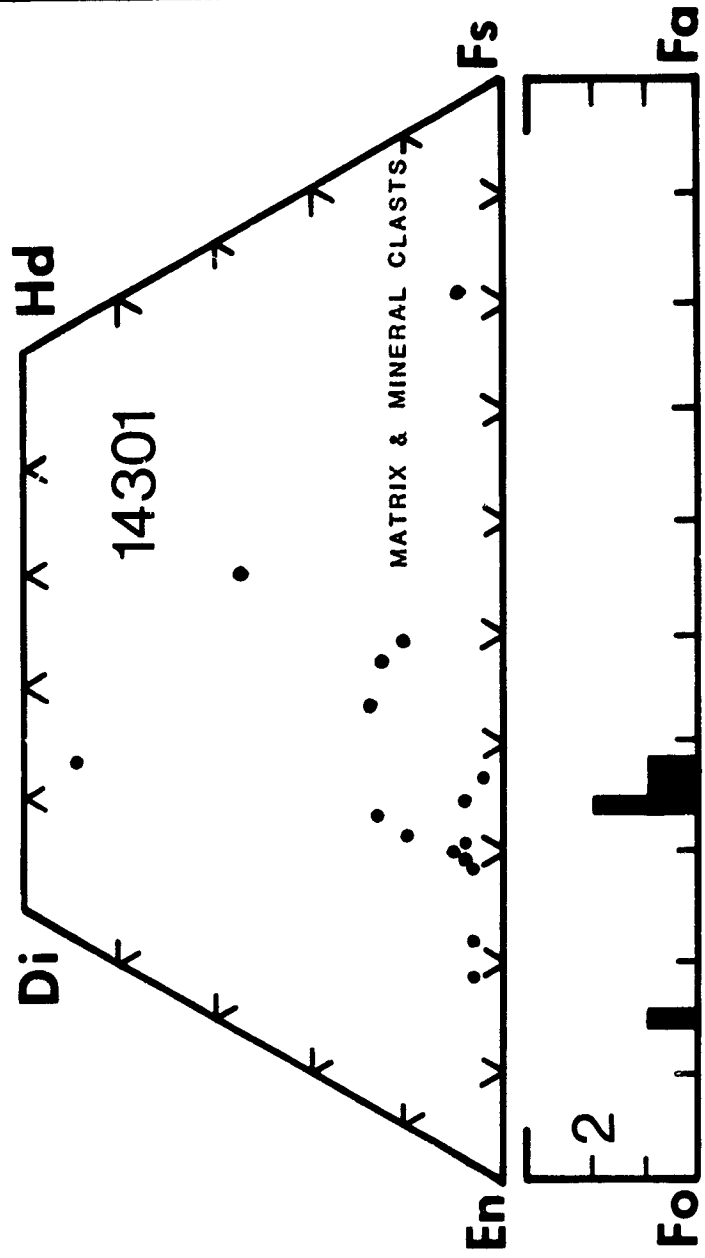
The glass clast population in 14301,78 is dominated by heterogeneous orange-brown glass which contains mineral debris. The clasts are typically angular and range in size from 0.04 millimeters to 1.5 millimeters. Clasts of partially to completely devitrified orange-brown glass are relatively common but they rarely exceed 0.1 millimeter in size. Homogeneous angular clasts of colorless and orange-brown glass also occur throughout the matrix.

The mineral clast population in 14301,78 consists of approximately equal percentages of plagioclase and pyroxene, together with randomly occurring opaque mineral clasts. Plagioclase clasts (up to 0.25 mm) are subangular to angular and are typically unfractured. Rare clasts display devitrification features. Clasts of pyroxene (up to 0.20 mm) typically display a more fractured appearance than plagioclase and range in shape from angular to sub-rounded. Opaque mineral clasts are rounded or ovoid in shape (up to 0.15 mm) and are typically ilmenite although rare clasts of troilite are also observed.

The lithic clast population in section 14301,78 is extremely diverse consisting of both crystalline and fragmental breccia clast types as well as basaltic and granulitic textures. Crystalline matrix breccias are the most abundant clast type and typically display matrices characterized by granular to lath-shaped plagioclase, anhedral to subhedral pyroxene and scattered ilmenite (Figure c); vesicles or vugs are typically present. A less abundant crystalline breccia type (equivalent to the equant-textured group 5 of Warner, 1972) is characterized by a matrix of interlocking equant grains of plagioclase and pyroxene (6-10 microns) with scattered disseminated blebs of ilmenite microns). Granulitic clasts are the second most abundant lithic type in section 14301,78. One large (4.5 mm) dunite clast (Figure d) consists of polygonalized olivine; a second, possibly related clast (2.6 mm) consists of polygonalized olivine and devitrified plagioclase. Several smaller (0.25 mm) clasts of cataclastic anorthosite are also observed in section 14301,78. Fragmental-matrix breccia clasts are relatively uncommon although one large (0.20 mm) fragmental-matrix clast is observed. The clast was coated by orange-brown debris-laden glass, similar to the heterogeneous orange-brown glass found as discrete clasts. Finally, basaltic clasts constitute a

14301, 13, 78
MODAL ANALYSES (VOL. %)

MATRIX (<39μ)	46.0
CLASTS (>39μ):	
PLAGIOCLASE	2.0
MAFIC	2.5
OPAQUE	TR
HETEROGENEOUS GLASS	1.0
HOMOGENEOUS GLASS	TR
DEVITRIFIED GLASS	—
FRAGMENTAL BRECCIA	5.0
CRYSTALLINE BRECCIA	28.5
GRANULITIC	10.0
OTHER METAMORPHIC	1.5
MARE BASALT	3.5
HIGHLAND BASALT	TR
CRUSHED	TR
PORE SPACE	TR
OTHER	—



REFLECTED LIGHT
Simonds et al. (1977)

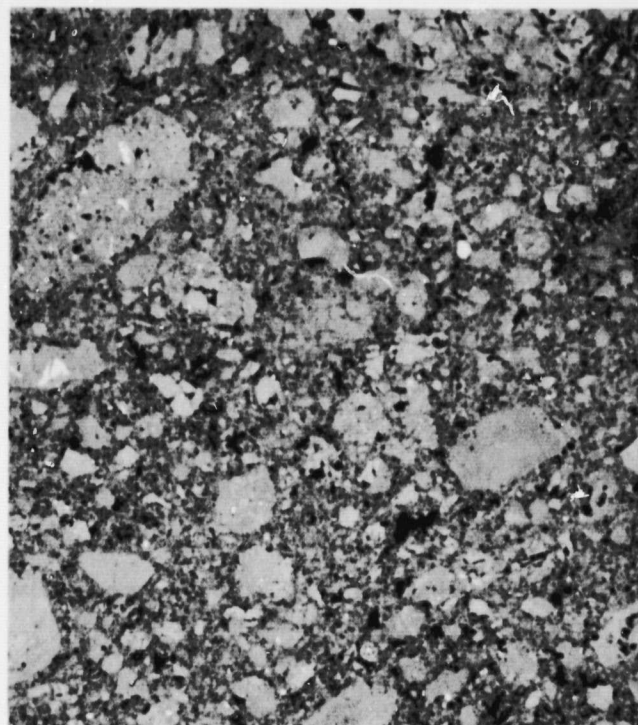
14301 2.0MM14301 0.25MM b

Figure 14301a. Typical view of 14301; transmitted light.

Figure 14301b. Typical view of matrix; reflected light.

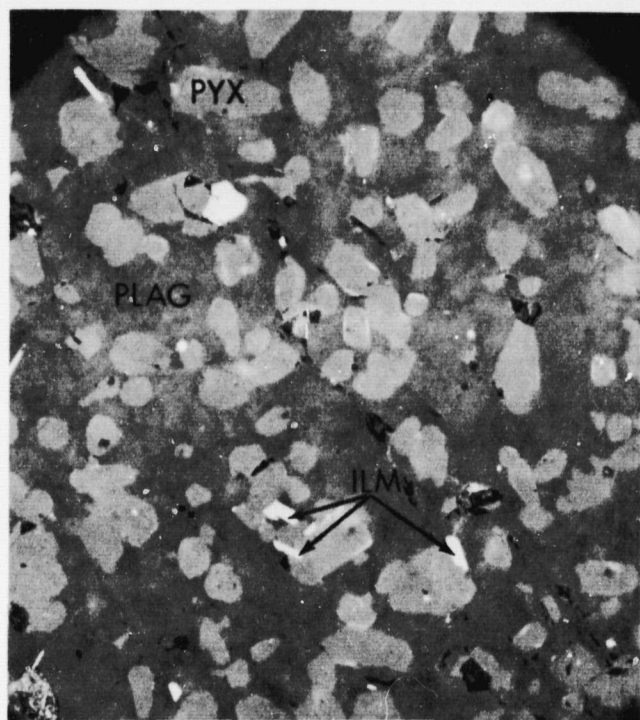
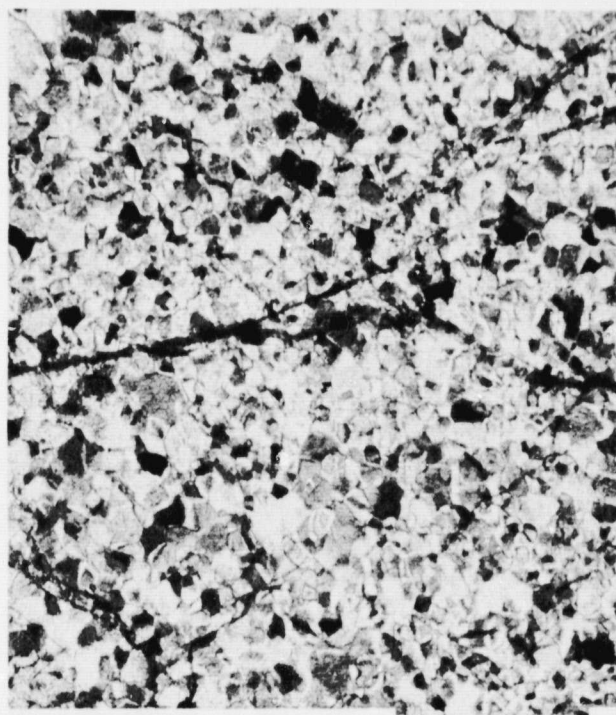
14301 0.05MM14301 0.25MM d

Figure 14301c. Crystalline matrix breccia clast; reflected light. Dark-grey, plagioclase; light-grey, pyroxene; white, ilmenite.

Figure 14301d. Dunite clast with polygonalized olivine; transmitted light (crossed polarizers).

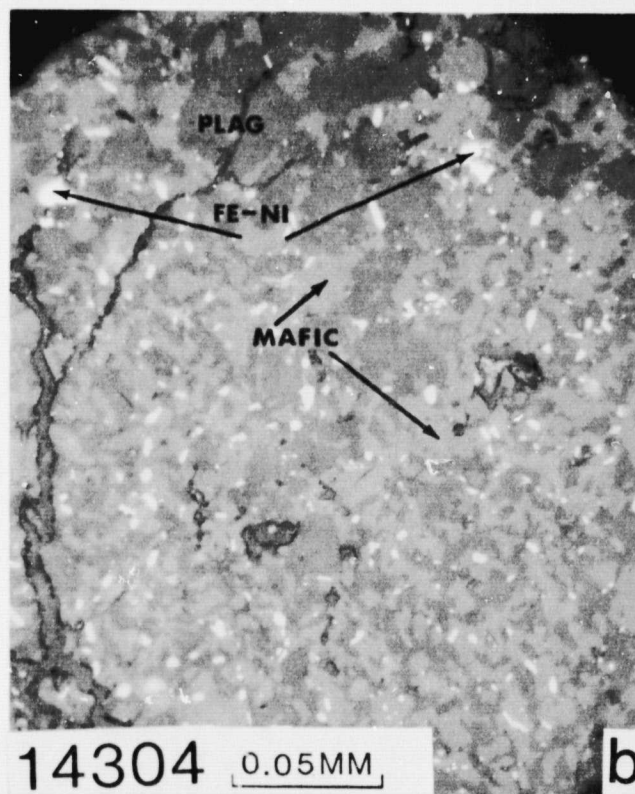
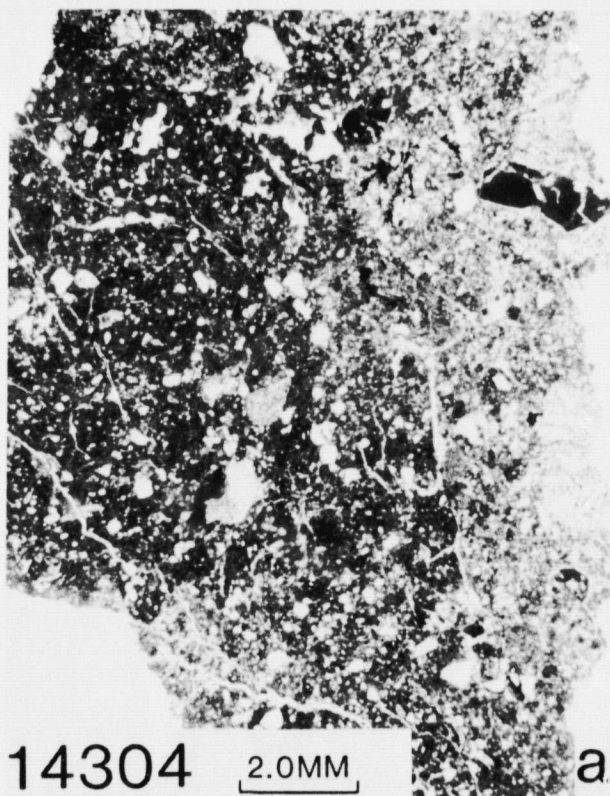
small percentage of the lithic clast population in 14301,78. The clasts are typically mare basalts with ophitic textures, although one small (0.3 mm) vitrophyric basalt is also present.

References: Warner (1972); King et al. (1972); Simonds et al. (1977).

14304- A clast-rich, KREEP-rich, impact-melt breccia from Apollo 14 which is texturally and compositionally unique from rocks collected at other landing sites.



Sample 14304 is a light-grey subangular rock (20x11x10 cm) with clasts which was collected near Station 14 during the first extra-vehicular activity (EVA) period.



14304 2.0MM

a

14304 0.05MM

b

Figure 14304a. Typical view of 14304; transmitted light.

Figure 14304b. Typical view of matrix; reflected light.

14304 CLAST-RICH IMPACT-MELT BRECCIA

Sample 14304 is a clast-rich impact-melt breccia characterized by a wide range of mineral and lithic clast types in a recrystallized matrix (Figure a). Warner (1972) describes the rock as a high-grade group 6 breccia with an "equant to euhedral" matrix texture (Figure b). At low magnification (in transmitted light) the matrix displays irregularly shaped patches of lighter and darker areas (Figure a), the result of fewer and larger ilmenite grains in the coarser-grained lighter areas as compared with more abundant and smaller ilmenite grains in the finer-grained darker areas. Pore space is present in the form of micron-size intergranular voids and irregularly-shaped vugs up to 0.75 mm across. No glass clasts are present.

The mineral clast population in section 14304,14 is dominated by subangular to subrounded clasts of plagioclase (up to 0.70 mm) which commonly display fracturing, undulatory extinction and granulation along fractures. Several plagioclase clasts display devitrification features; rare plagioclase clasts display overgrowth rims. Mafic mineral clasts, predominantly pyroxene together with minor olivine, occur as angular to rounded clasts (up to 0.30 mm) which are typically highly fractured and may rarely contain abundant opaque mineral inclusions. Opaque mineral clasts include irregularly shaped grains of ilmenite (0.10 mm and less), amoeboid-shaped troilite grains (0.10 mm and less) and micron-size blebs of Fe-Ni metal scattered randomly throughout the matrix.

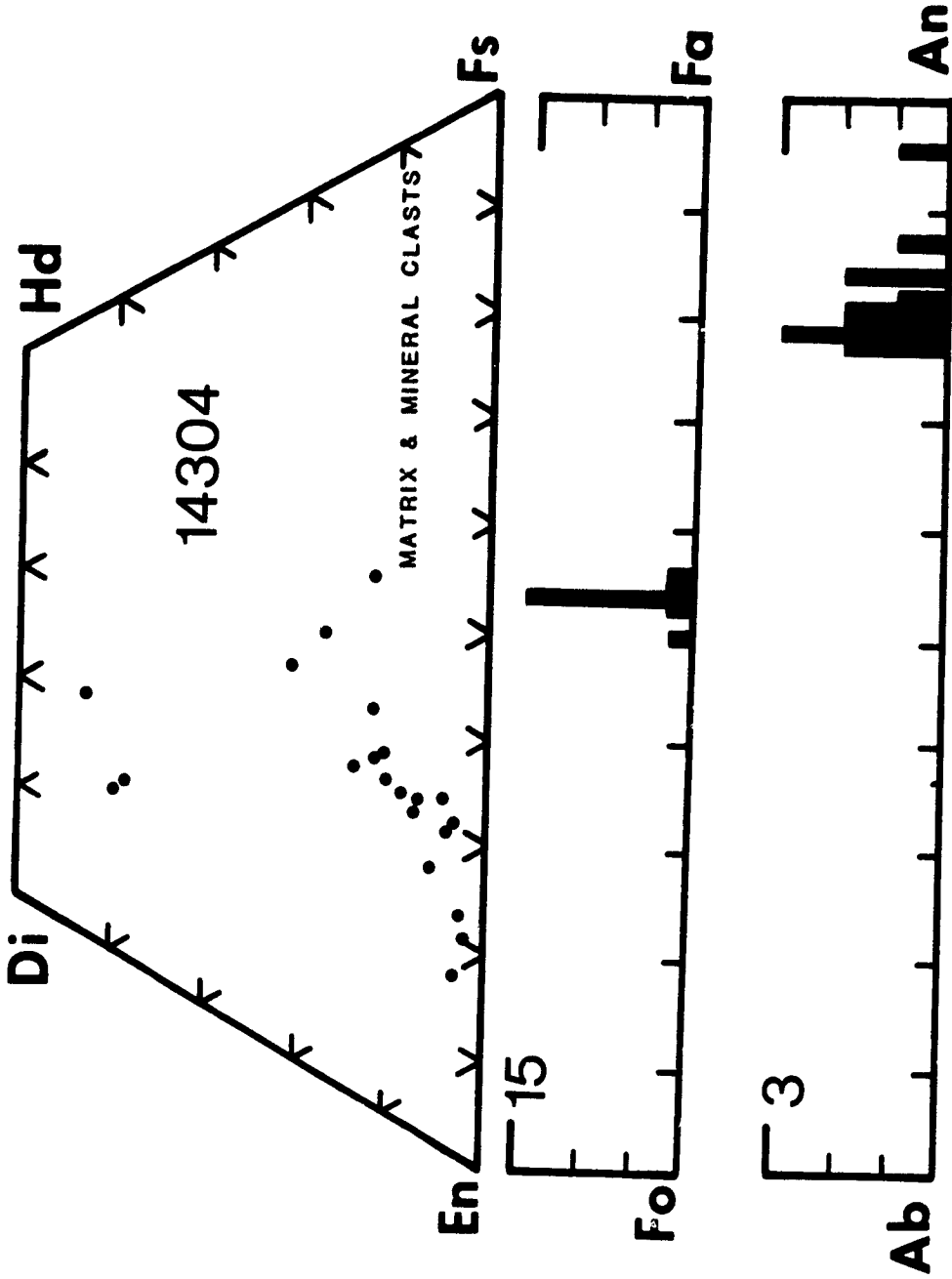
Lithic clasts in section 14304,14 are commonly the crystalline matrix breccia type with equant and euhedral textures similar to the matrix in which they are enclosed; the crystalline breccia clasts may be more easily observed in reflected light (Figures c & d). Both highland and mare basalt types are present as clasts (up to 1.0 mm) in section 14304,14 and are typically characterized by ophitic textures. One clast (0.80 mm) consisting of poikilitic pyroxene enclosing lath (.05-.10 mm) and tablet-shaped (.03 mm) plagioclase grains was also observed (Figure e).

References: Chao et al. (1972); Warner (1972); Simonds et al. (1977).

14304,2
MODAL ANALYSES (VOL. %)

MATRIX (<39μ)	74.0
CLASTS (>39μ):	
PLAGIOCLASE	3.0
MAFIC	5.0
OPAQUE	TR
HETEROGENEOUS GLASS	—
HOMOGENEOUS GLASS	—
DEVITRIFIED GLASS	—
FRAGMENTAL BRECCIA	—
CRYSTALLINE BRECCIA	6.0
GRANULITIC	2.0
OTHER METAMORPHIC	—
MARE BASALT	TR
HIGHLAND BASALT	10.0
CRUSHED	—
PORE SPACE	TR
OTHER	—

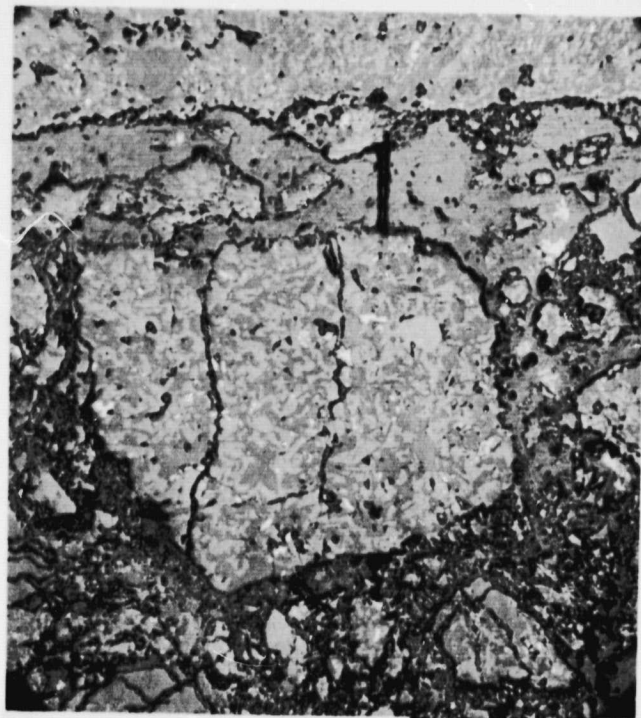
Simonds et al. (1977)
REFLECTED LIGHT





14304 0.10MM

c



14304 0.10MM

d

Figure 14304c. Crystalline matrix breccia clast; reflected light.

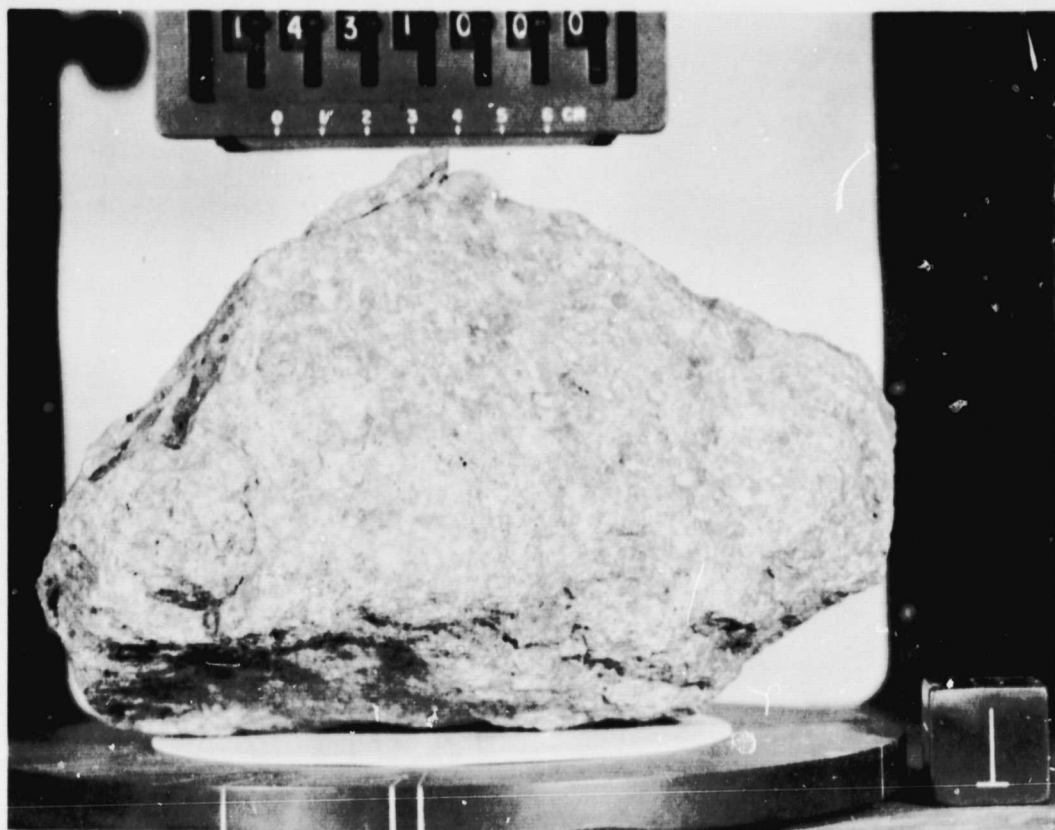
Figure 14304d. Crystalline matrix breccia clast; reflected light.



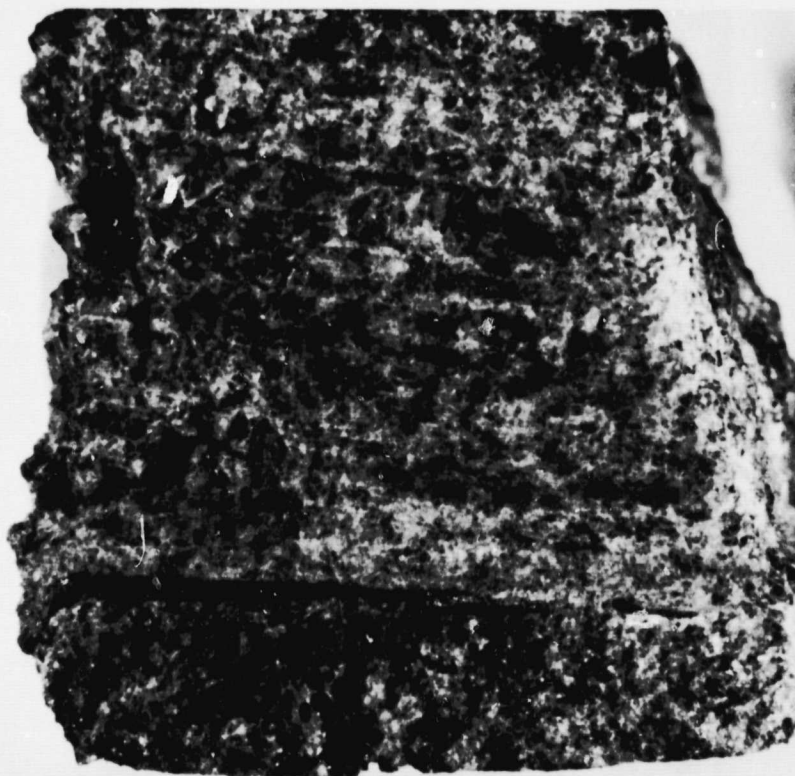
14304 0.10MM

e

Figure 14304e. Poikilitic pyroxene clast enclosing lath- and tablet-shaped plagioclase; transmitted light (crossed polarizers).



14310- A clast-free, KREEP-rich impact-melt breccia from Apollo 14 characterized by a higher Al_2O_3 content than most other Apollo 14 breccias.



Sample 14310 is a medium grey blocky rock (19x14x11 cm) collected at Station G during the second extravehicular activity period.

14310 CLAST-FREE IMPACT-MELT BRECCIA

Sample 14310 is a clast-free impact-melt breccia characterized by subophitic intergrowths of lath-shaped plagioclase and anhedral to subhedral pyroxene grains with interstitial glassy mesostasis (Figure a). Relatively large (0.5-1.0 mm), blocky subhedral crystals of plagioclase are randomly scattered throughout the sample and are interpreted as clasts. Local finer-grained patches of needle-like plagioclase laths are intergrown with the surrounding igneous-textured matrix and possibly represent thermal, compositional or nucleation heterogeneities. Pore space is present as angular voids enclosed by silicate minerals.

Plagioclase is the dominant mineral phase in sample 14310 and occurs in several forms. Lath-shaped plagioclase (.05x1.0 mm), intergrown with pyroxene, rarely displays albite or carlsbad twinning. The laths commonly project into the outer rims of pyroxene crystals and smaller plagioclase laths (.015x2.0mm) may be partially enclosed within them. Needle-like plagioclase crystals (0.1-0.2 mm) occur in clusters with interstitial anhedral pyroxene (0.1 mm) and complex mesostasis in the local finer-grained areas. Finally, blocky, nearly equant crystals of plagioclase (0.5-1.0 mm) (Figure b) are randomly scattered throughout the sample. The crystals, interpreted as clasts, lack twinning and commonly have smaller plagioclase laths projecting into them.

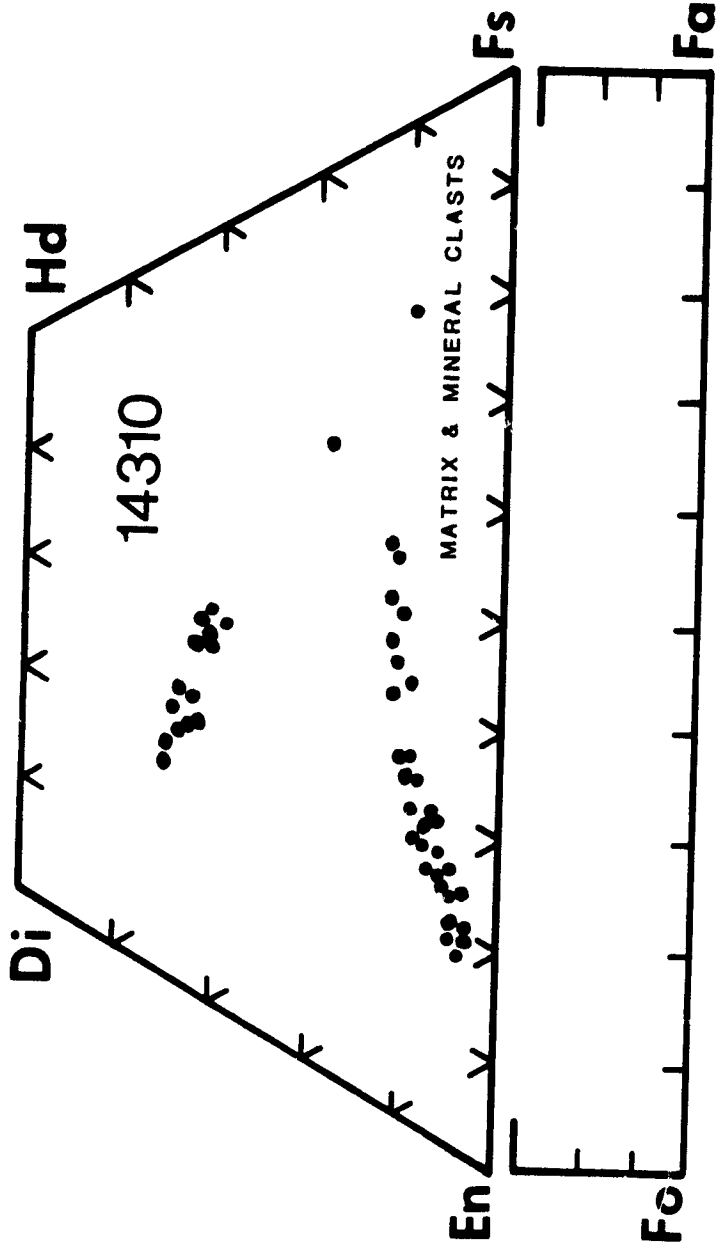
The mesostasis is a complex mixture of pale brown to colorless glass, skeletal or fibrous ilmenite crystals (Figure c), fine-grained pyroxenes, chromian ulvospinel, troilite, apatite, whitlockite and schreibersite. Rare plates of tranquillityite are also observed in the mesostasis.

References: James (1973); Bence and Papike (1972); Ridley et al. (1972); Meyer (1977); Simonds et al. (1977).

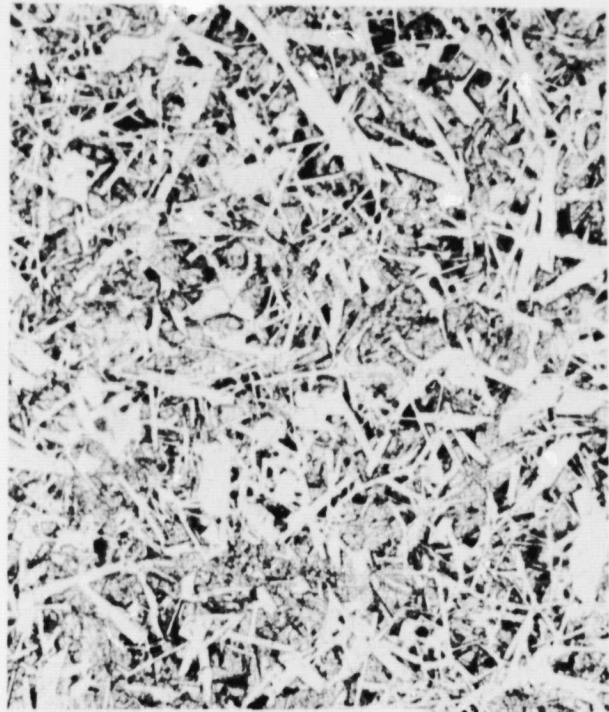
Age Data: Rb-Sr isochron $-3.93 \pm .04$; $I_{Sr} = .70035$ (Compston et al. 1971)
 $-3.94 \pm .03$; $I_{Sr} = .70041$ (Mark et al. 1974).

14310
MODAL ANALYSIS (VOL. %)

MATRIX (>39%)	
PLAGIOCLASE	55.0
MAFIC	35.0
OPAQUE	2.5
OTHER (silica minerals + mesostasis)	6.0
CLASTS (>39%)	
PLAGIOCLASE	<1.0
MAFIC	
OPAQUE	
FRAGMENTAL BRECCIA	
CRYSTALLINE BRECCIA	
GRANULITIC	
OTHER METAMORPHIC	
MARE BASALT	
HIGHLAND BASALT	
CRUSHED	
PORE SPACE	



REFLECTED LIGHT



14310 1.00MM

a

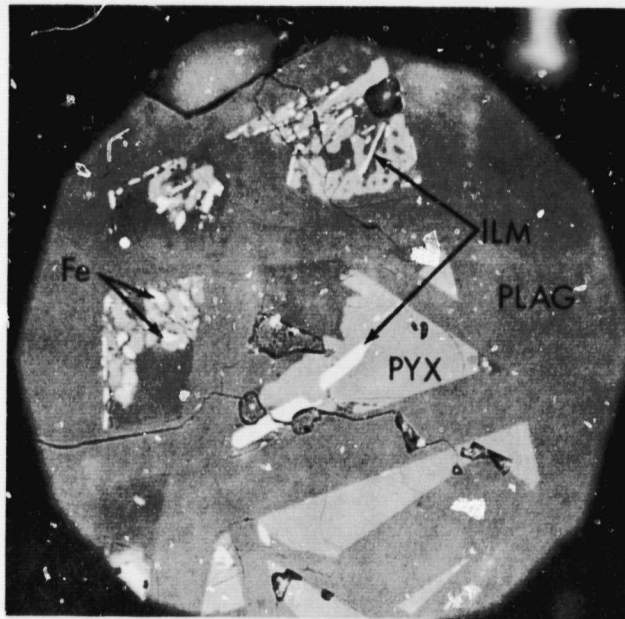


14310 0.5MM

b

Figure 14310a. Typical view of 14310; transmitted light.

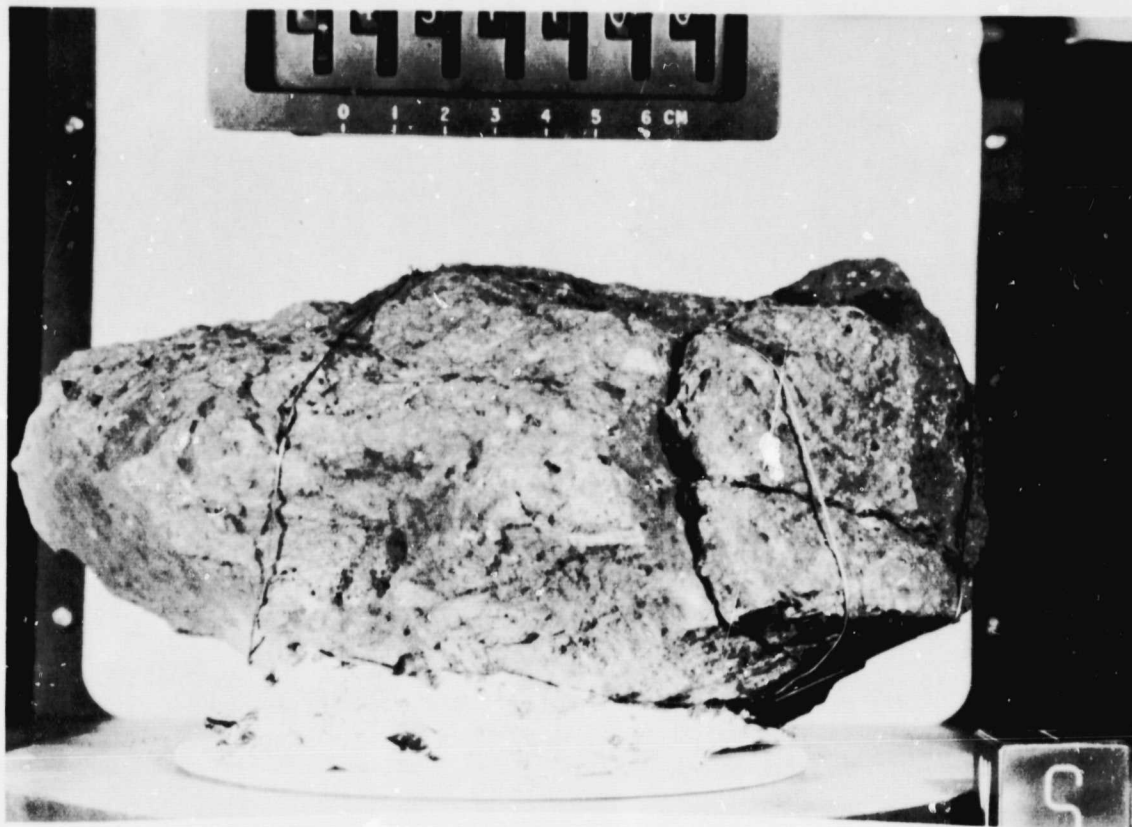
Figure 14310b. Plagioclase clast in 14310; transmitted light (crossed polarizers).



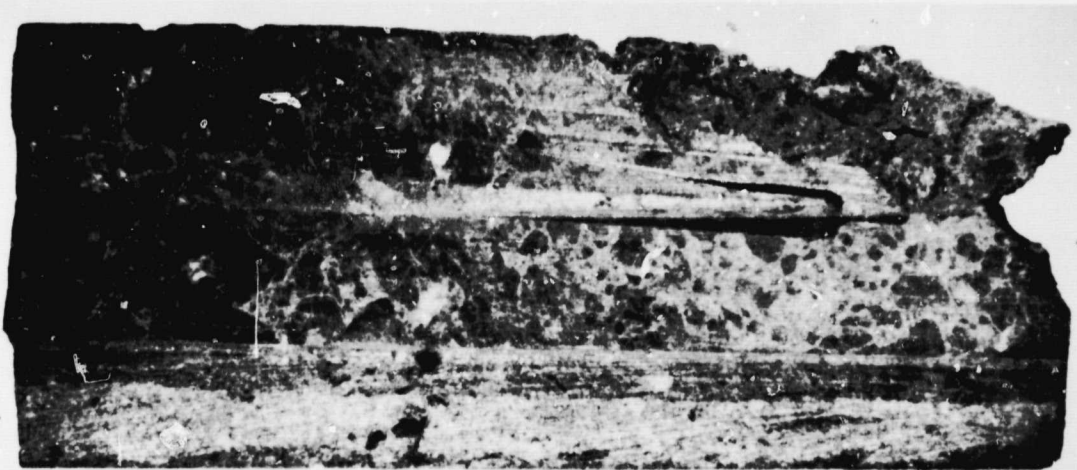
14310 0.05MM

c

Figure 14310c. Mesostasis in 14310; reflected light.



14311- A clast-rich impact-melt breccia with a composition (KREEP) and texture unique to breccias at the Apollo 14 site. The rock contains abundant post crystallization fractures due to a post formational cratering event.



Sample 14311 is a grey subrounded rock (20.0x12.5x9.1 cm) collected at Station Dg during the second EVA-period.

14311 CLAST-RICH IMPACT-MELT BRECCIA

Sample 14311 is a clast-rich impact-melt breccia characterized by a wide range of mineral and lithic clast types in an annealed crystalline matrix (Figure a). The matrix, (Group 5 of Warner 1972) which is composed of equant grains of plagioclase, pyroxene and ilmenite (5-10 μm) (Figure b), contains lighter colored regions (when viewed at low magnification in transmitted light) also composed of equant grains of the same mineral types except with a coarser grain size (10-15 μm) and fewer grains of ilmenite. Pore space is common and typically occurs as irregularly shaped vugs scattered throughout the sample; intergranular pore space is extremely rare. No glass clasts are observed.

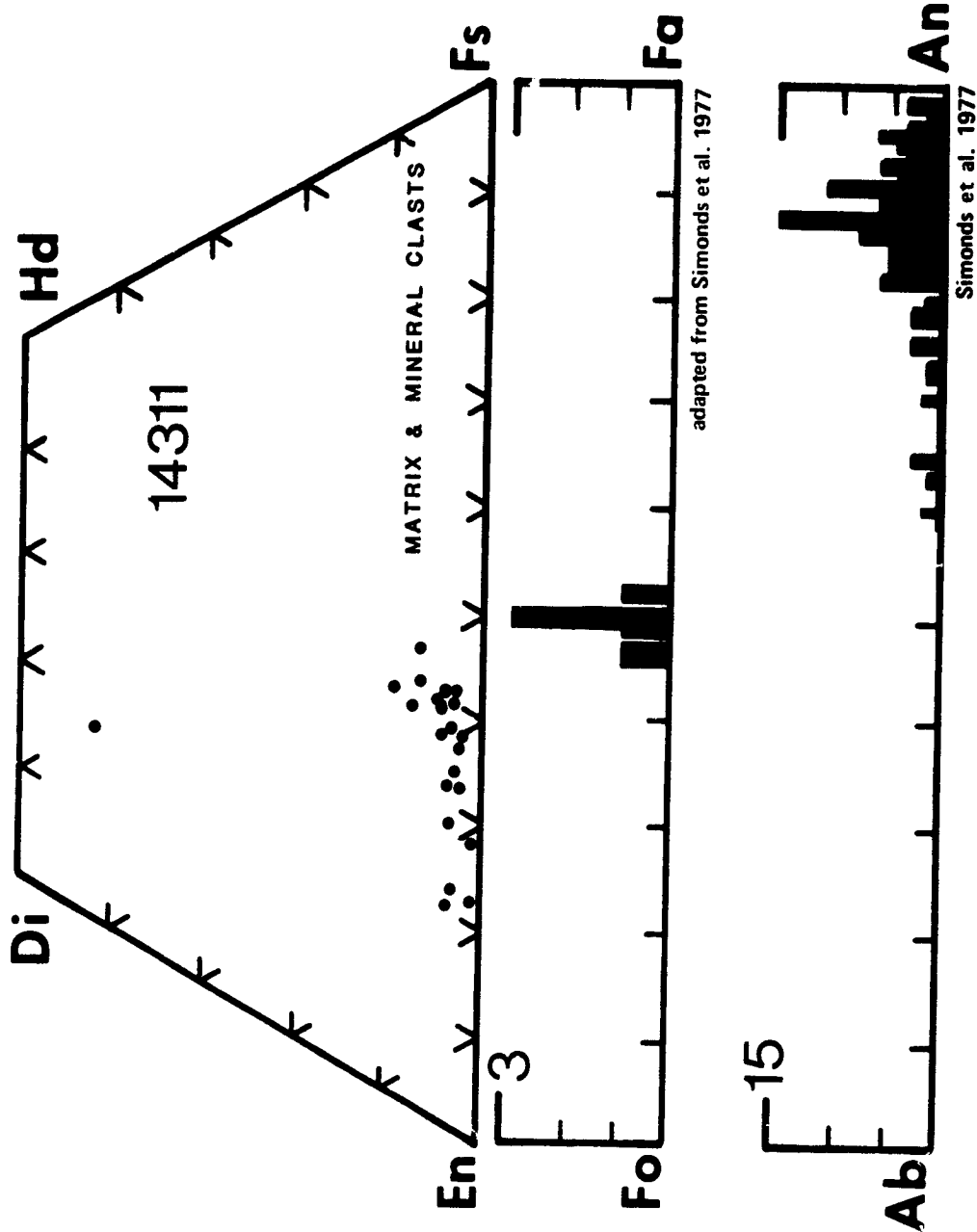
Mineral clasts in sample 14311 include plagioclase, pyroxene, olivine and ilmenite. Pink spinel clasts discussed by Warner (1972) are not observed in section 14311,94. Plagioclase clasts are subangular to subrounded with a seriate size distribution and typically display rims characterized by a higher concentration of ilmenite grains than the surrounding matrix (Figure c). Many clasts are highly fractured and display twin lamellae offset by the fractures. Some clasts are recrystallized and consist of aggregates of plagioclase grains. Unfractured clasts may be inclusion-free or may appear clouded due to micron-size blebs of opaque minerals. Pyroxene clasts are typically angular and are also clouded due to minute opaque minerals. Rare clasts display fine exsolution lamellae. Olivine clasts in sample 14311 are most commonly subrounded and display complex reaction rims as described by Cameron and Fisher (1974). The rims commonly consist of a mantle of elongate pyroxene grains, blebs of ilmenite and interstitial plagioclase surrounded by the equigranular matrix texture (Figure d).

Lithic clasts in sample 14311 are predominantly anorthositic and basaltic. Basalt clasts are typically fractured and may display signs of recrystallization. Clasts of anorthosite may be either unfractured or cataclastic. Rare clasts (1.0 mm) of a subophitic-poikilitic impact melt breccia similar to the Apollo 17 Station 6 boulder samples are observed in section 14311,94 (Figure e).

References: Warner (1972); Cameron and Fisher (1974); Simonds et al. (1977).

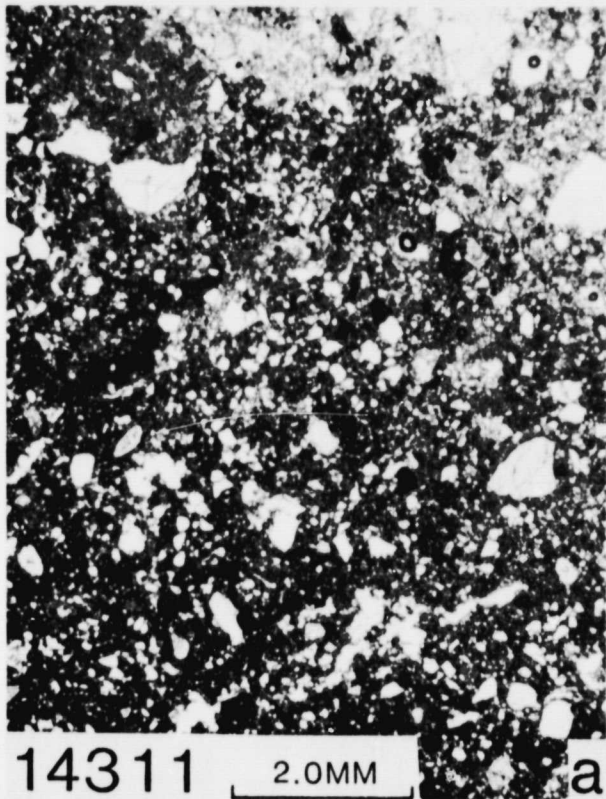
14311,94
MODAL ANALYSES (VOL. %)

MATRIX (<39μ)	75.0
CLASTS (>39μ):	
PLAGIOCLASE	6.5
MAFIC	3.0
OPAQUE	—
HETEROGENEOUS GLASS	—
HOMOGENEOUS GLASS	—
DEVITRIFIED GLASS	—
FRAGMENTAL BRECCIA	—
CRYSTALLINE BRECCIA	2.5
GRANULITIC	4.5
OTHER METAMORPHIC	—
MARE BASALT	TR
HIGHLAND BASALT	—
CRUSHED	0.5
PORE SPACE	8.5
OTHER	TR



Simonds et al. (1977)

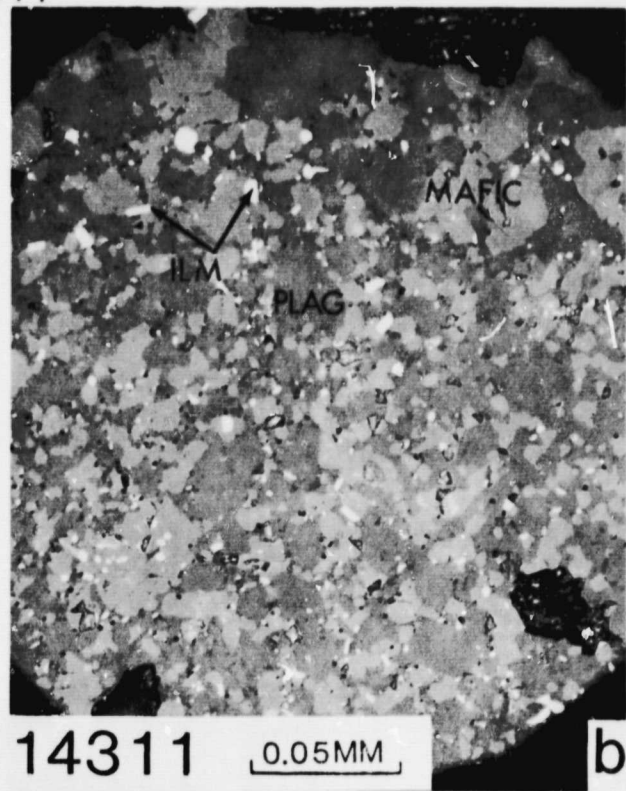
REFLECTED LIGHT



14311

2.0MM

a



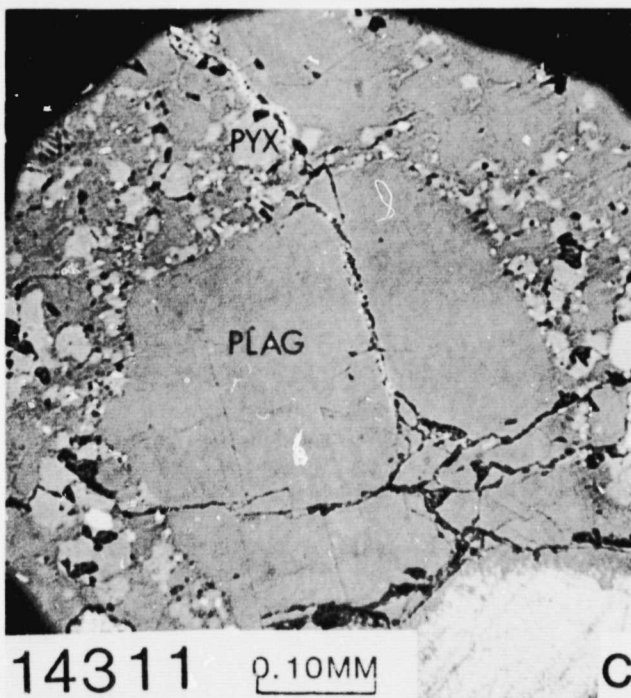
14311

0.05MM

b

Figure 14311a. Typical view of 14311; transmitted light.

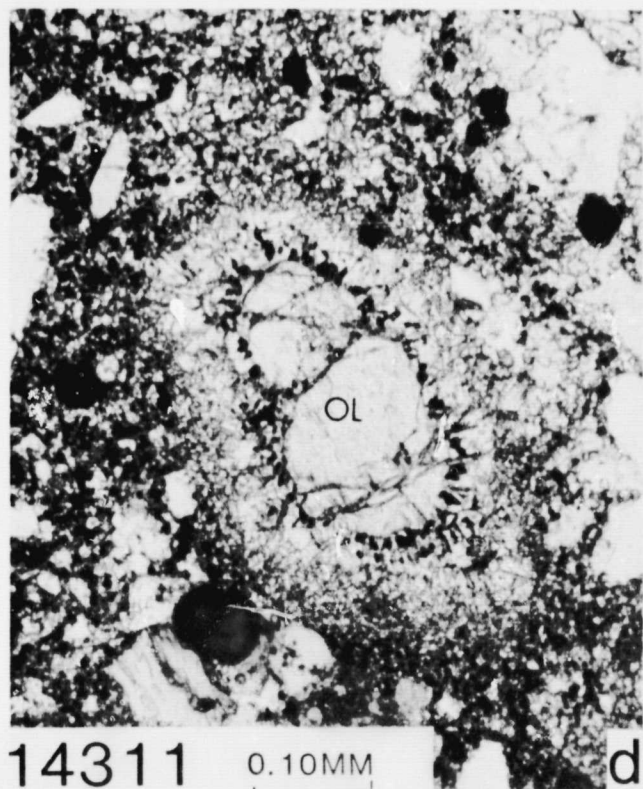
Figure 14311b. Typical matrix of 14311; reflected light. Dark-grey, plagioclase; light-grey, pyroxene; white, ilmenite.



14311

0.10MM

c



14311

0.10MM

d

Figure 14311c. Plagioclase clast with reaction rim; note higher concentration of ilmenite (white) in rim as compared to surrounding matrix; reflected light. Dark-grey, plagioclase; light-grey, pyroxene; white, ilmenite.

Figure 14311d. Olivine clast with reaction rim; transmitted light.

14311

86

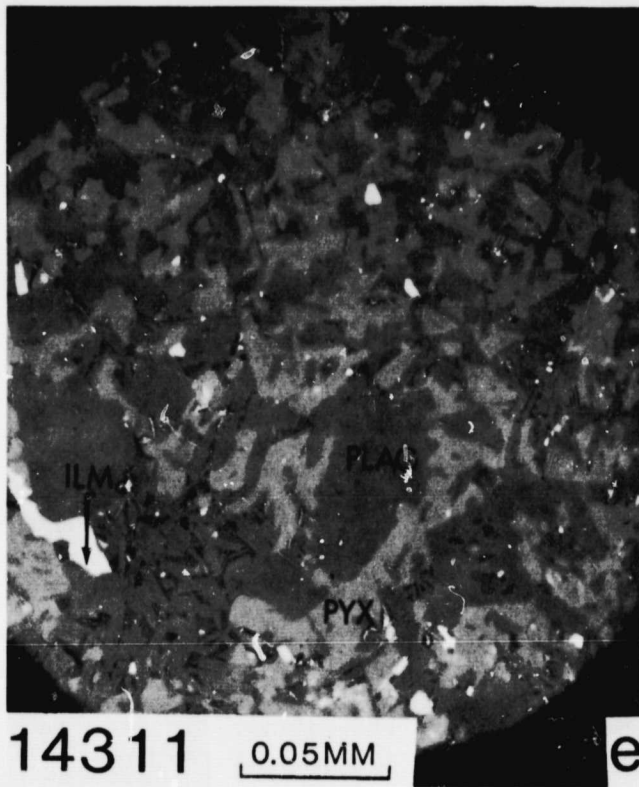
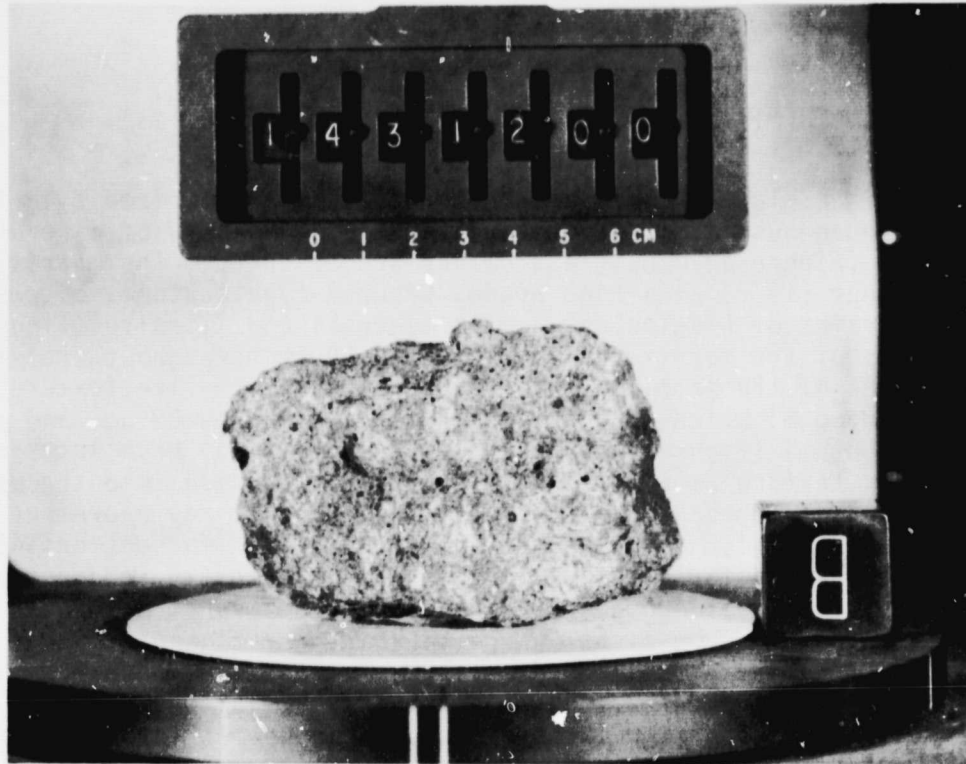
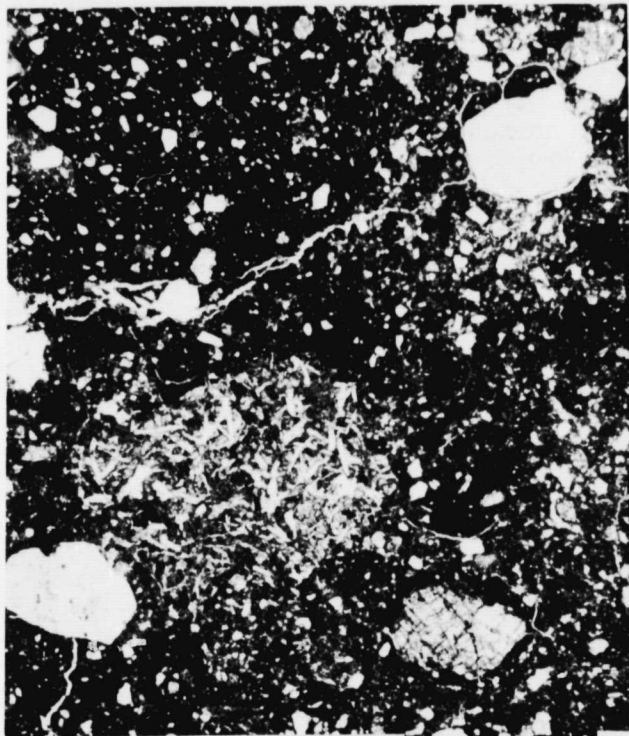


Figure 14311e. Poikilitic impact-melt clast; reflected light.
Color key as in (c).

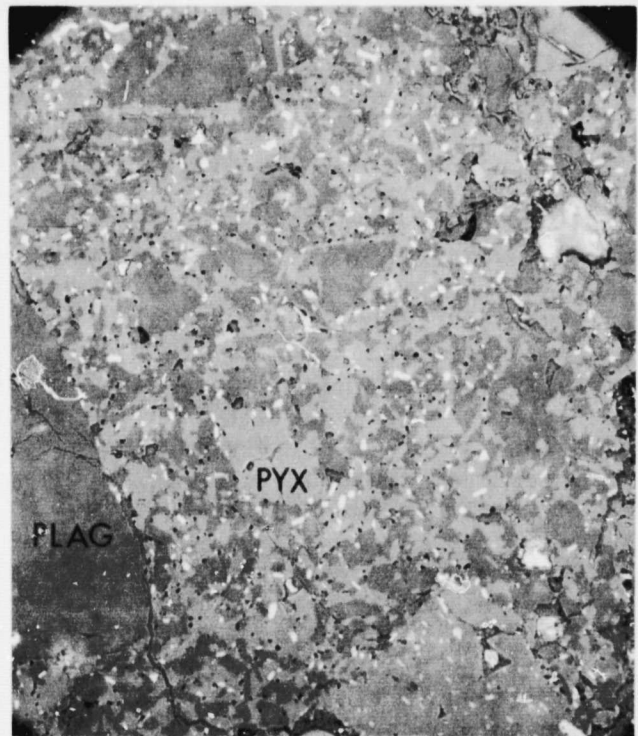
14312- A clast-rich, KREEP-rich impact-melt breccia from Apollo 14 which is texturally and compositionally unique from rocks collected at other landing sites; the breccia has a smaller proportion of clasts than similar Apollo 14 breccias.



Sample 14312 is a medium-grey rock (9x6x4 cm), partially coated with glass, which was collected from the top of "Turtle Rock" at Station H.



14312 2.0MM



14312 0.05MM

Figure 14312a. Typical view of 14312; transmitted light.

Figure 14312b. Typical matrix in 14312; reflected light. Dark-grey, plagioclase; light-grey, pyroxene; white, ilmenite.

14312 CLAST-RICH IMPACT-MELT BRECCIA

Sample 14312 is a clast-rich impact-melt breccia characterized by a fine-grained heterogeneous matrix which contains a wide variety of mineral and lithic clasts (Figure a). No glass clasts are observed. The matrix, described by Warner (1972) as a high grade, Group 7-type texture, displays equant to euhedral grains of plagioclase, mafic minerals and ilmenite (Figure b). The grain size of the matrix varies from 5 to 30 μm throughout the sample. Several regions of the matrix display an igneous sheath-like texture (similar to Warner's Group 8) which consist of plagioclase laths (30 μm) and mafic minerals (20-30 μm) (Figure c). Ryder and Bower (1976d) have interpreted the igneous matrix texture as a melt phase which is intrusive into the more commonly occurring euhedral texture. Alternatively it may represent a zone which is less clast-rich than the surrounding matrix. In section 14312,15 (the only section available to us which contained both the igneous and the euhedral matrix textures) boundary relationships between the two textures are not distinct. In some cases where boundary relationships are more distinct, the igneous texture appear as isolated blob-like patches within the euhedral matrix and do not display intrusive relationships. Ryder and Bower (1976d), noting the circular patches of igneous matrix in section 14312,14, suggest that they possibly represent molten globules which were incorporated into the breccia during assembly and subsequently injected into other regions of the matrix.

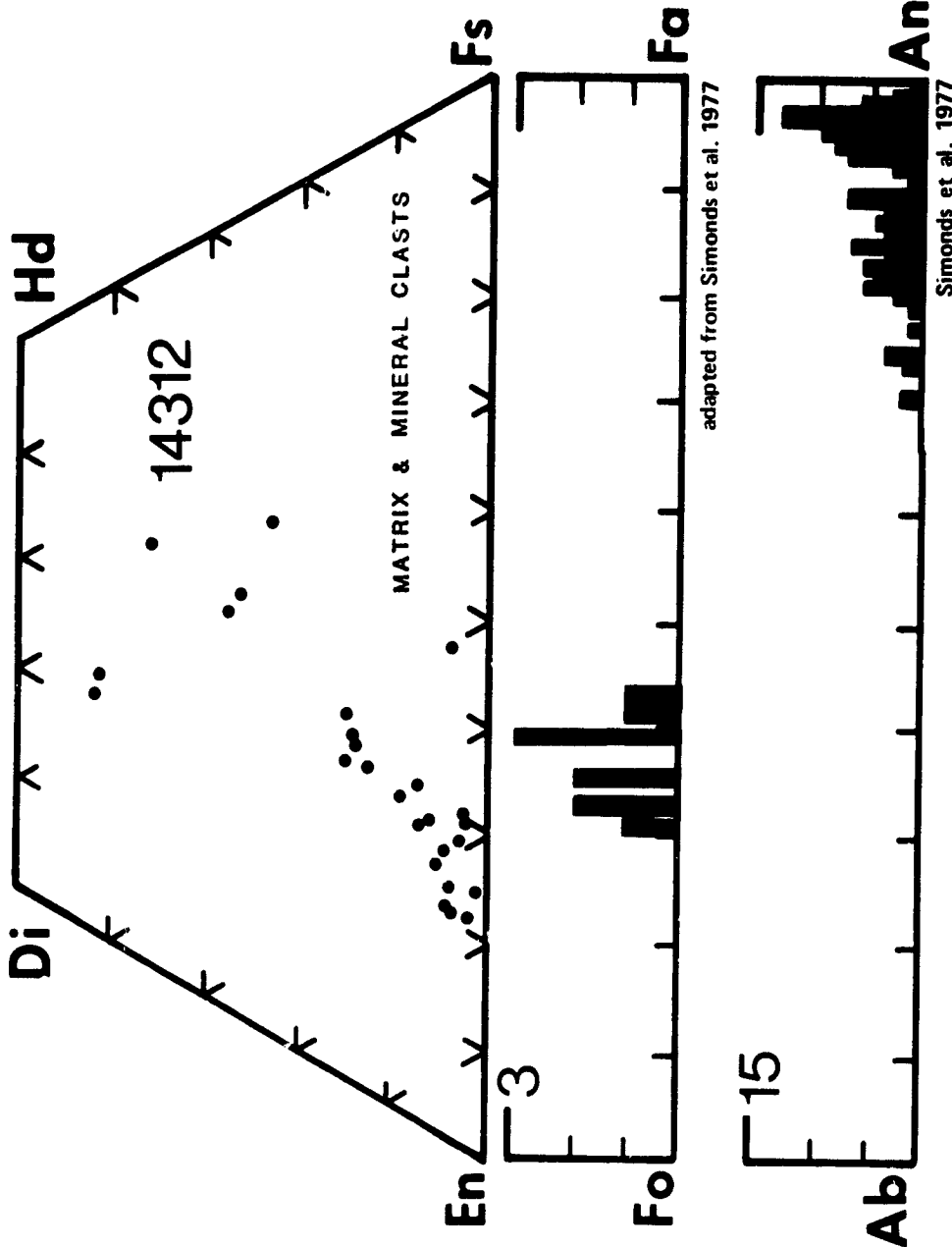
Mineral clasts in sample 14312 are abundant and consist dominantly of plagioclase with minor pyroxene, olivine, pink spinel, ilmenite and Fe-Ni metal. Most clasts display interdigitating contacts with the matrix; fracturing is common among all of the mineral clast types. Plagioclase clasts are typically subrounded and subangular (.04-2.0 mm) and commonly display undulatory extinction. Several clasts display partial maskelynitization and rare grains of maskelynite are observed in section 14312,15. Clasts of devitrified maskelynite are common throughout the sample. Aggregates of polygonal plagioclase grains are also observed in section 14312,15. High and low-calcium pyroxene clasts are subangular (up to 1.5 mm) and are also typically fractured. Pyroxene clasts with exsolution lamellae and/or twin lamellae are observed in section 14312,17 but are relatively rare. Olivine clasts are subangular to subrounded and commonly display overgrowth rims. Other olivine clasts occur as fractured, polygonalized aggregates. Ilmenite occurs as irregularly shaped clasts typically less than 0.2 mm. Troilite also occurs as irregularly shaped and rounded grains up to 0.1 mm; blebs of Fe-Ni metal occur in association with the troilite clasts.

Dark-colored crystalline matrix breccias, with matrix textures similar to the euhedral matrix of 14312, are the most common lithic clast type in section 14312,15 (Figure d). Because the breccias have a texture similar to the matrix, boundary relationships are often indistinct and may best be viewed in reflected light. One large (3.5 mm across) ophitic textured basalt clast is present in section 14312,15 and is characterized (in order of abundance) by plagioclase, clinopyroxene, olivine and opaques. Several small basalt clasts

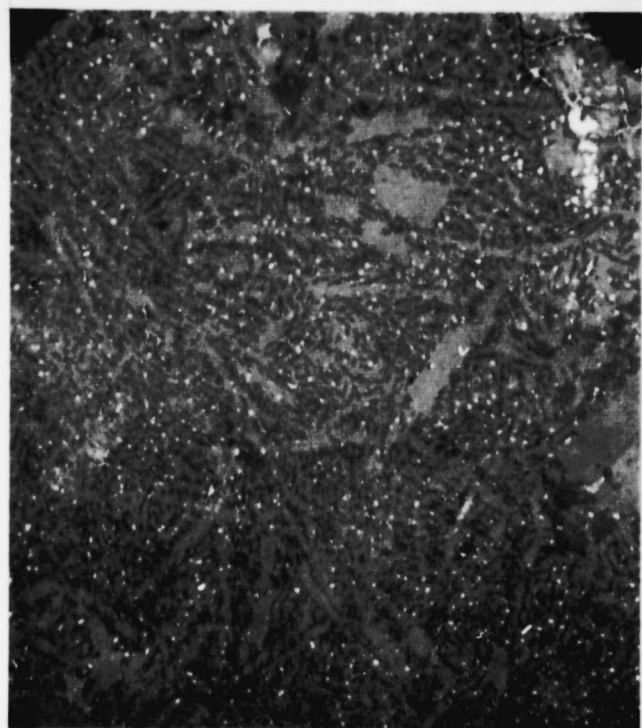
14312.15
MODAL ANALYSES (VOL. %)

MATRIX (<39μ)	75.0
CLASTS (>39μ):	
PLAGIOCLASE	10.0
MAFIC	3.0
OPAQUE	TR
HETEROGENEOUS GLASS	—
HOMOGENEOUS GLASS	—
DEVITRIFIED GLASS	—
FRAGMENTAL BRECCIA	1.0
CRYSTALLINE BRECCIA	2.0
GRANULITIC	3.0
OTHER METAMORPHIC	0.5
MARE BASALT	TR
HIGHLAND BASALT	5.0
CRUSHED	0.5
PORE SPACE	0.5
OTHER	—

Simonds et al. (1977)
REFLECTED LIGHT



adapted from Simonds et al. 1977

14312 0.05MM

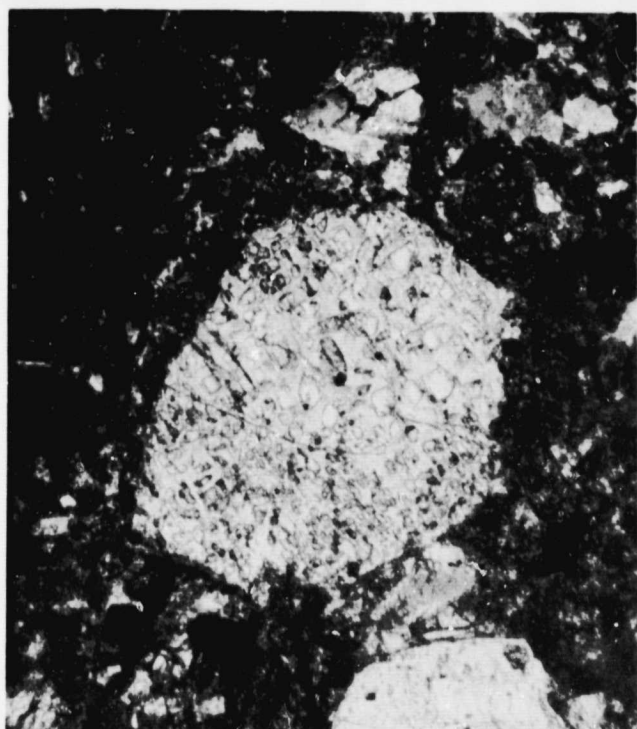
c

14312 0.25MM

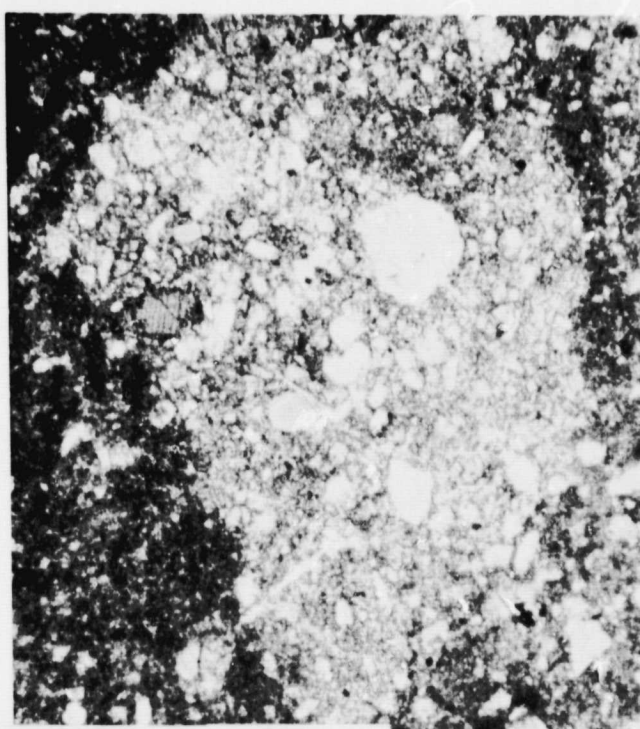
d

Figure 14312c. Matrix with igneous sheath-like texture; reflected light.
Color key same as in (b).

Figure 14312d. Crystalline matrix breccia clast in 14312; transmitted light.

14312 0.25MM

e

14312 0.25MM

f

Figure 14312e. Poikilitic pyroxene clast enclosing plagioclase tablets;
transmitted light.

Figure 14312f. "Light-matrix" breccia clast in 14312; transmitted light.

14312

90

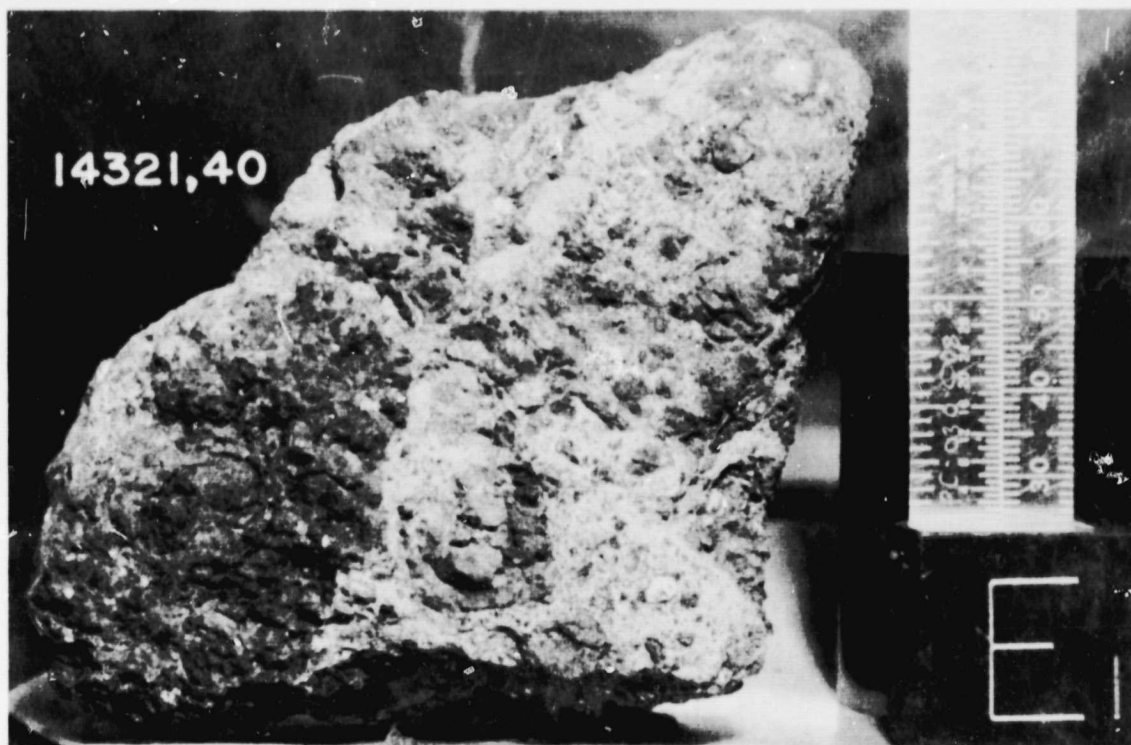


14312 0.25MM

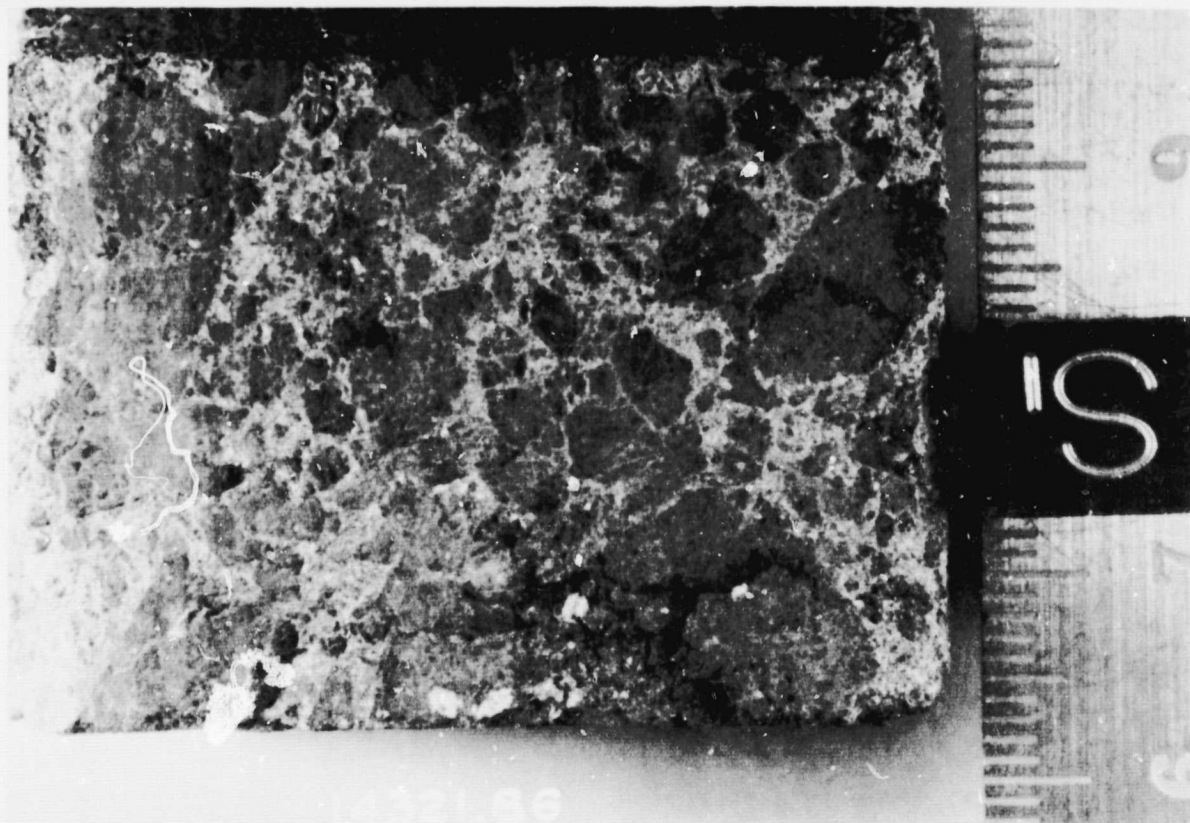
Figure 14312g. Coarse grained lithic troctolite clast in 14312; transmitted light.

(with ophitic textures) are observed in section 14312,15. Poikilitic norite clasts are a relatively common clast type in sample 14312 and consist of stubby (.05-.1 mm) plagioclase grains enclosed within poikilitic pyroxene grains (Figure e). Several clasts which resemble the Apollo 14 "white rocks" are observed in section 14312,17 (Figure f). They are characteristically coarser-grained than the dark-matrix crystalline breccias discussed earlier and contain colorless glass in the matrix. Coarse-grained ANT (anorthosite-troctolite-norite) clasts are common in sample 14312. Anorthosite clasts are characterized by plagioclase grains meeting at 120° triple junctions. Troctolite clasts display plagioclase and olivine grains with smooth boundary relationships (Figure g).

References: Warner (1972); Ryder and Bower (1976d); Simonds et al. (1977).



14321- A clast-rich, impact-melt breccia from Apollo 14 which contains abundant aluminous mare basalt clasts. It is the third largest rock returned by the Apollo missions.



Sample 14321 is a light-grey subrounded rock (23x23x17 cm) with clasts which was collected at Station C1 from the hummocky ejecta blanket of Cone crater.

14321 CLAST-RICH IMPACT-MELT BRECCIA

Sample 14321 is a complex impact-melt breccia consisting of dark-grey microbreccia clasts (microbreccia III of Grieve et al. 1975) and basaltic clasts bonded together by a light matrix which also hosts single mineral clasts of plagioclase, pyroxene, olivine, ilmenite spinel, Fe-metal, and troilite (Figure a). The light matrix displays a detrital texture (Figure b) although isolated patches in the matrix display an equant to euhedral texture suggesting at least some annealing. SEM studies by Phinney et al. (1976) show that sample 14321 contains about 15-20% porosity in the form of 10-20 μm vugs.

The dark-grey microbreccia constitutes the largest proportion of clastic material in the light-matrix and displays a matrix with a salt and pepper appearance characterized by equant to euhedral laths of plagioclase, pyroxene and ilmenite (Figure c).

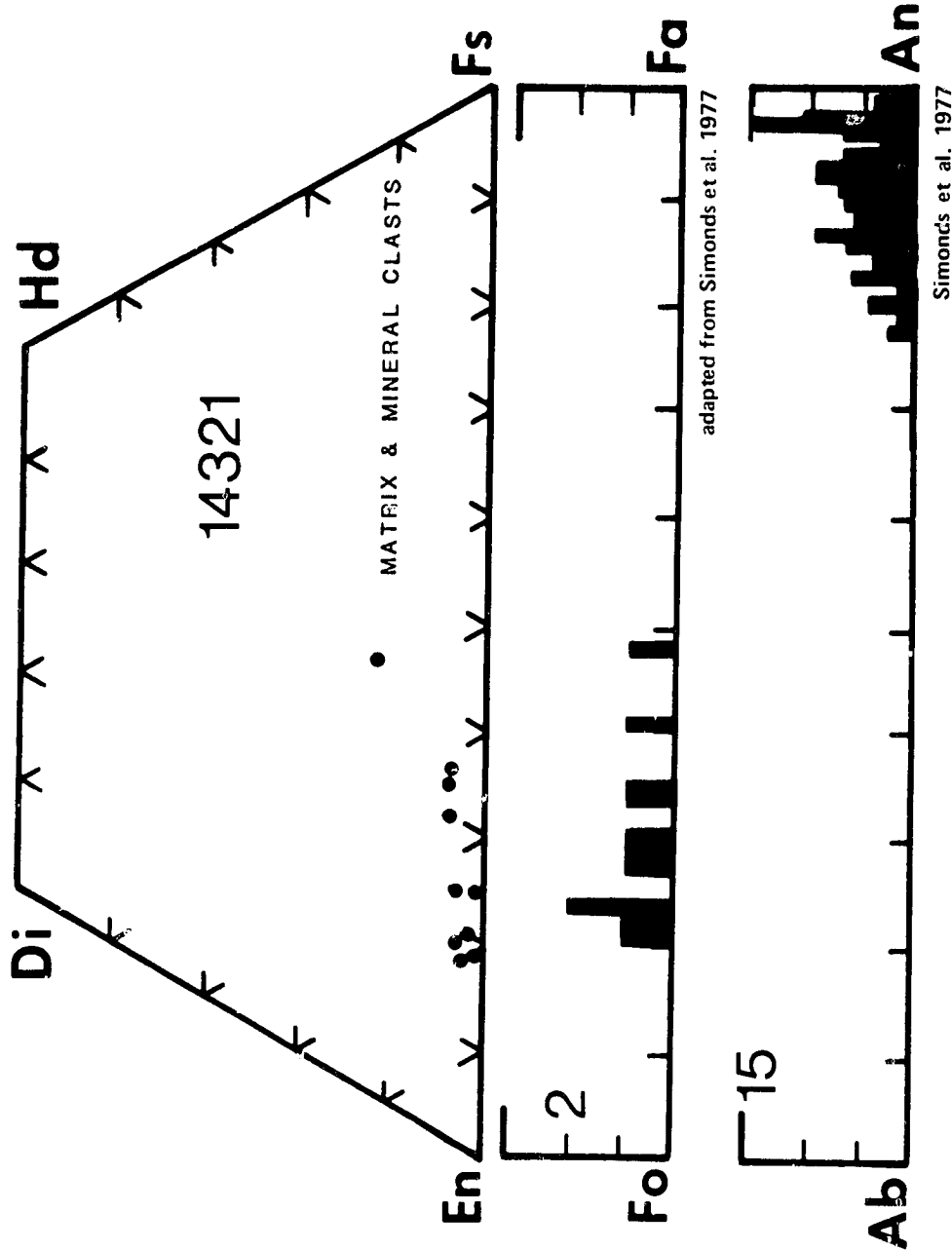
Single crystal clasts in the dark-grey breccia include plagioclase, pyroxene, olivine, ilmenite and Fe-metal together with trace abundances of troilite, apatite, whitlockite and zircon. Plagioclase and pyroxene are typically sub-angular to rounded and display a seriate size distribution; pyroxene clasts up to 2.0 mm and plagioclase clasts up to 3.5 mm are observed. Pyroxene clasts commonly display exsolution lamellae and reaction rims. Reaction rims are also present on many of the plagioclase clasts and twin-lamellae are often offset by fractures. Clasts of devitrified plagioclase glass are relatively common. Rounded clasts of olivine (up to 1.6 mm) are observed and are relatively common, many are zoned. Clasts of ilmenite (up to 1.0 mm) are the most typical opaque mineral type and are commonly angular or irregularly shaped. Anhedral troilite grains occur randomly in the dark-grey microbreccia and typically are 0.05 mm or less. Fe-Ni metal as micron size blebs may occur in association with troilite; discrete metal blebs also occur scattered throughout the microbreccia and as inclusions in olivine clasts.

Lithic clasts in the dark-grey microbreccia are dominated by noritic microbreccias and by rounded clasts (typically 1.5 mm) of norite which display granulitic and poikilitic textures (Figure d). The noritic microbreccias are characterized by plagioclase and pyroxene clasts in a matrix of plagioclase and pyroxene with minor amounts of olivine, ilmenite, Fe-metal and troilite; some clasts display a crystallized matrix with poikilitic pyroxene (Figure e). These noritic microbreccias are typically enclosed within clast-poor microbreccia unit (microbreccia 2 of Grieve et al. 1975) which is mineralogically and chemically identical to the dark-grey breccia except for the lower clast content. The clast-poor rims are interpreted as accretionary structures by Grieve et al. 1975 and frequently rim both mineral clasts as well as lithic clasts in 14321 (Figure f). The rounded norite clasts are probably the unfractured equivalent of the noritic microbreccias. Other lithic clasts in the dark microbreccia include devitrified brown glass fragments with rhyolitic compositions.

14321,97
MODAL ANALYSES (VOL. %)

MATRIX (<39 μ)	66.0
CLASTS (>39 μ):	
PLAGIOCLASE	9.5
MAFIC	4.0
OPAQUE	—
HETEROGENEOUS GLASS	0.5
HOMOGENEOUS GLASS	—
DEVITRIFIED GLASS	—
FRAGMENTAL BRECCIA	2.5
CRYSTALLINE BRECCIA	5.5
GRANULITIC	2.5
OTHER METAMORPHIC	4.5
MARE BASALT	—
HIGHLAND BASALT	3.5
CRUSHED	1.0
PORE SPACE	0.5
OTHER	—

Simonds et al. (1977)
REFLECTED LIGHT



94

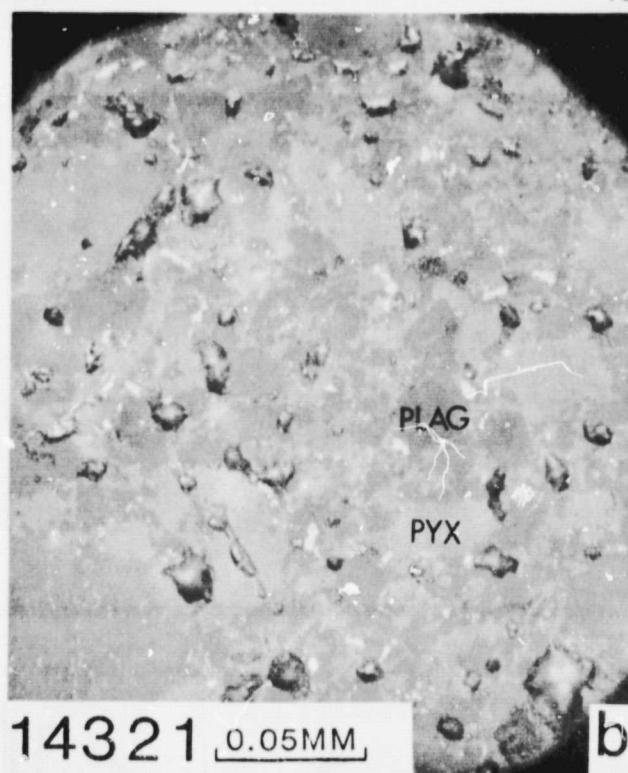
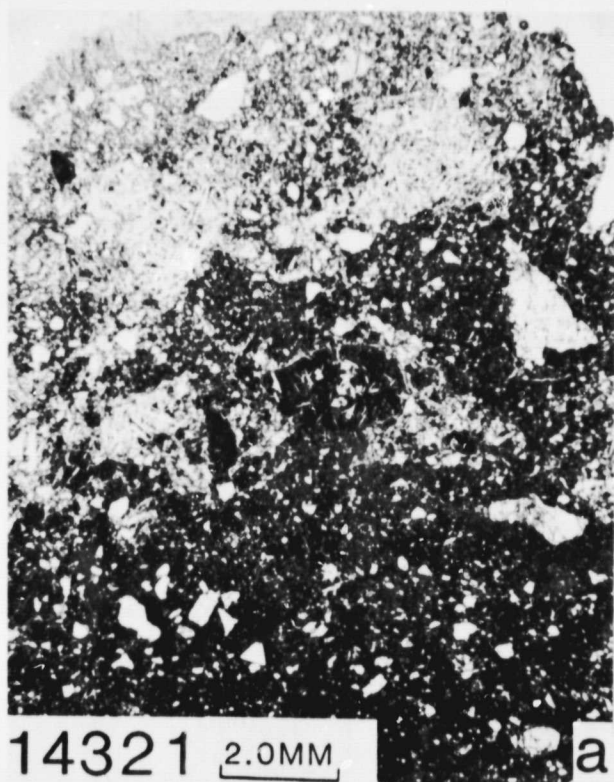


Figure 14321a. Typical view of 14321; transmitted light.

Figure 14321b. Detrital textured light matrix; reflected light. Dark-grey, plagioclase; light-grey, pyroxene; white, ilmenite.

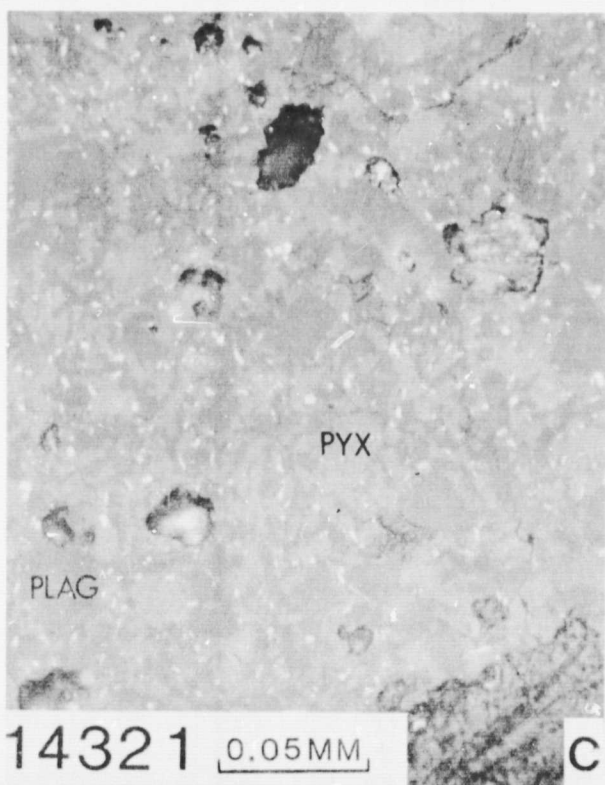
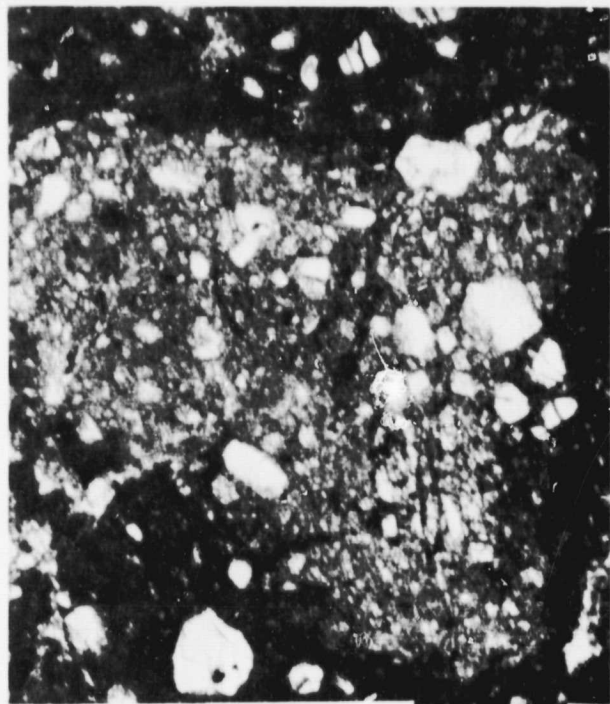


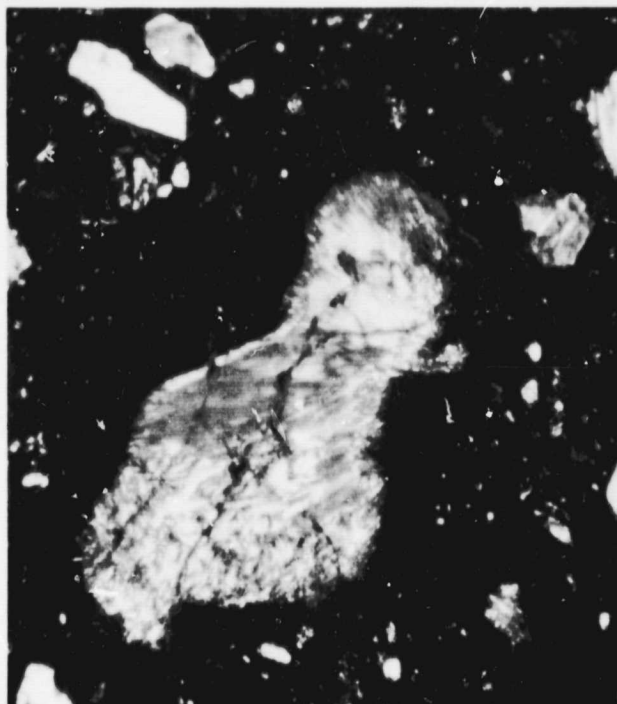
Figure 14321c. Dark-grey microbreccia clast; reflected light. Color key as in (b).

Figure 14321d. Poikilitic norite clast; transmitted light.



14321 0.25MM

e

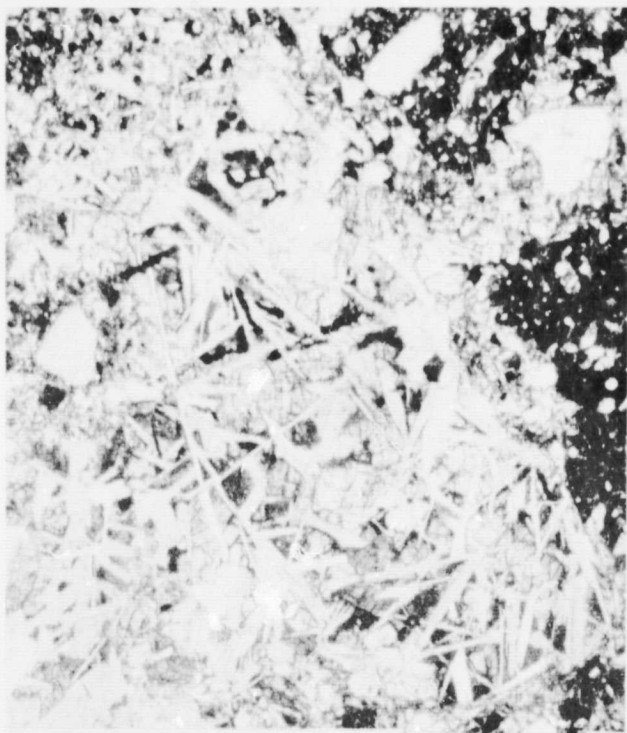


14321 0.25MM

f

Figure 14321e. Poikilitic noritic microbreccia; transmitted light.

Figure 14321f. Devitrified maskelynite clast with clast-poor rim; transmitted light.



14321 0.50MM

g



14321 0.50MM

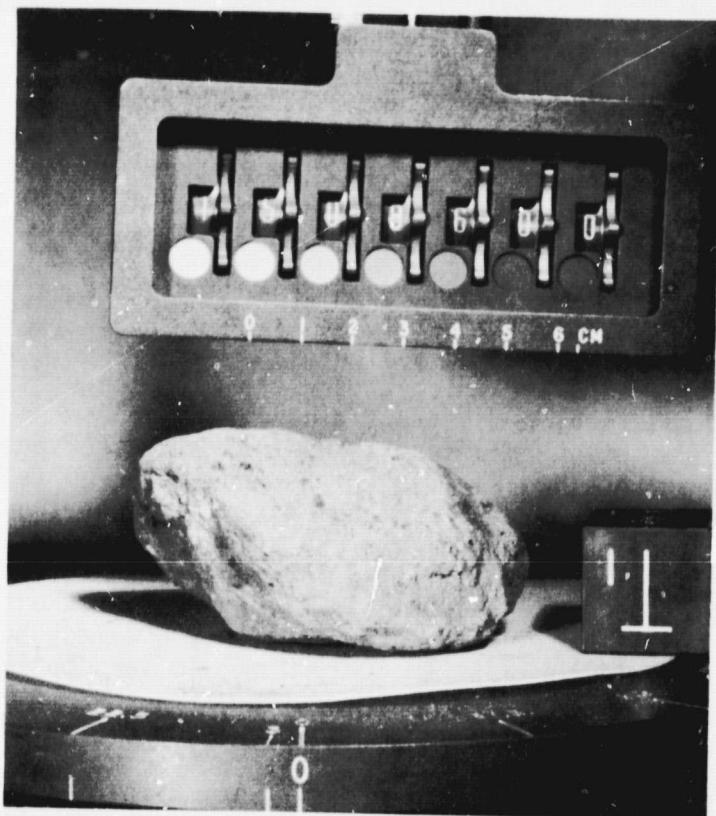
h

Figure 14321g. Basalt clast; transmitted light.

Figure 14321h. Basalt clast; transmitted light.

Mare-like basaltic clasts are present both in the light matrix and the dark microbreccia clasts of 14321. They display a variety of textures ranging from glassy and vitrophyric to fine to medium grained ophitic basalts (Figures g and h). Clasts up to 3.0 mm in size are observed. Pyroxene grains are typically strongly zoned with pigeonite cores and augite rims.

References: Duncan et al. (1975b); Grieve et al. (1975). Phinney et al. (1976)



15086- A typical Apollo 15 "soil" breccia.

15086 DARK-MATRIX BRECCIA

Sample 15086 is a fragmental-matrix breccia characterized by diverse populations of mineral, glass and lithic clasts set in a matrix of light to dark brown glass fragments and comminuted mineral and lithic debris (Figures a and b). The texture is seriate with material ranging in size from the limit of resolution up to 3.0 millimeters. Pore space is common and occurs in the form of irregularly shaped vugs 0.4 to 2.5 millimeters across.

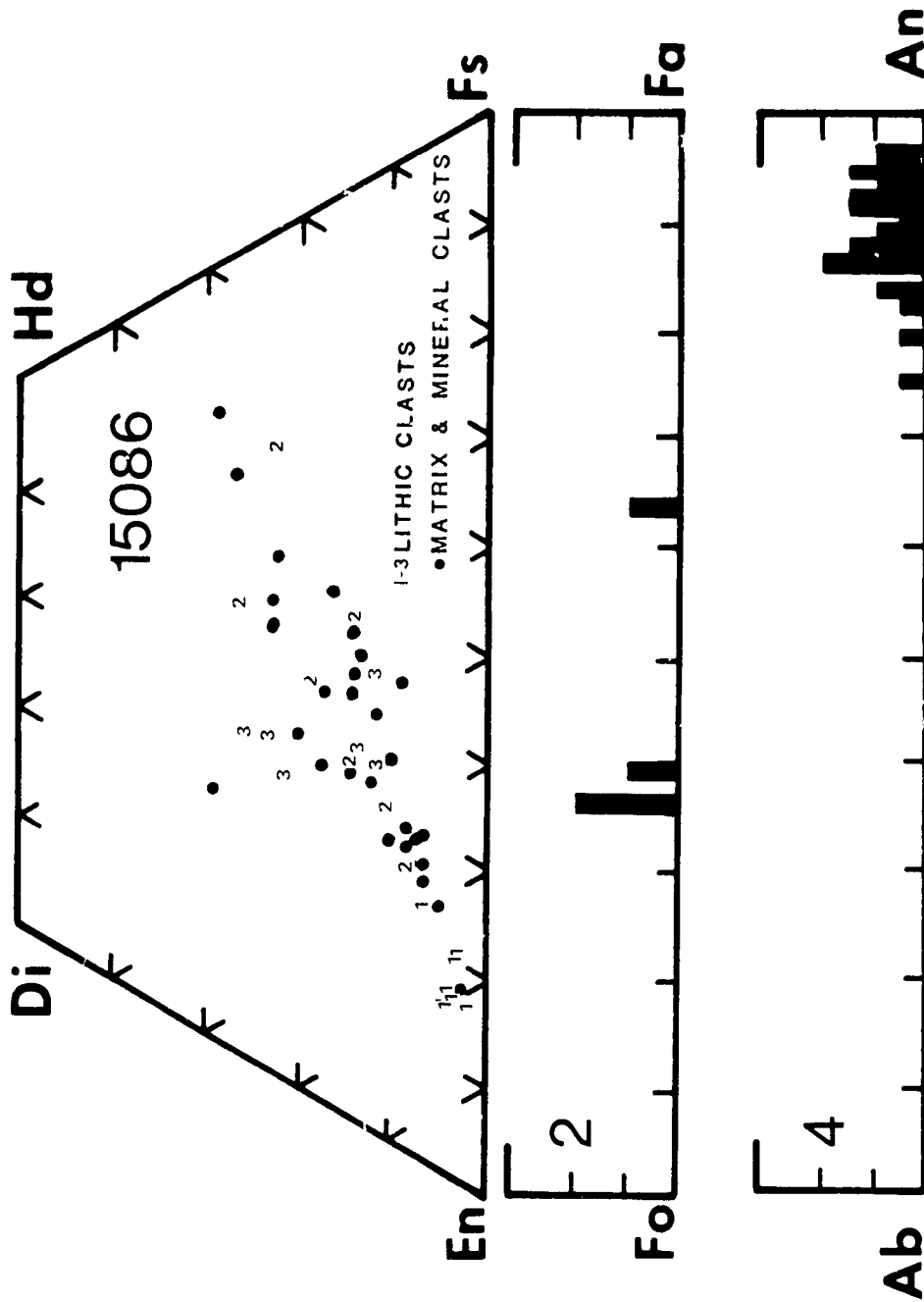
One of the most striking features of 15086 is the abundance of homogeneous glass spheres (0.05-0.2 mm), most of which are pale green in color and have compositions comparable to the Apollo 15 green glasses (Drake and Klein, 1973). Spheres of colorless and yellow glass are present, together with spheres of devitrified glass which appear brown to opaque in transmitted light. Angular clasts of homogeneous glass are also common and include pale green, yellow, orange and colorless types. As with the spheres, compositions of pale green fragments are similar to the Apollo 15 sample 15426 while colorless glasses typically have an anorthositic composition (Drake and Klein, 1973). Devitrified angular fragments are common and occur as brown to opaque clasts composed of clusters of tightly intergrown pyroxene needles and glass (Figure c). Heterogeneous glass clasts, i.e. fragments containing schlieren and/or mineral and lithic debris, are relatively uncommon but constitute some of the larger glass clasts (0.60-1.60 mm) in section 15086,39 (Figure d).

Mineral clasts include pyroxene, plagioclase and minor occurrences of olivine. Most clasts display some evidence of shock; fracturing of the clasts is common and many clasts display undulatory extinction. Rare clasts of ilmenite and troilite are observed although pyroxene and plagioclase constitute the largest percentage of mineral clasts.

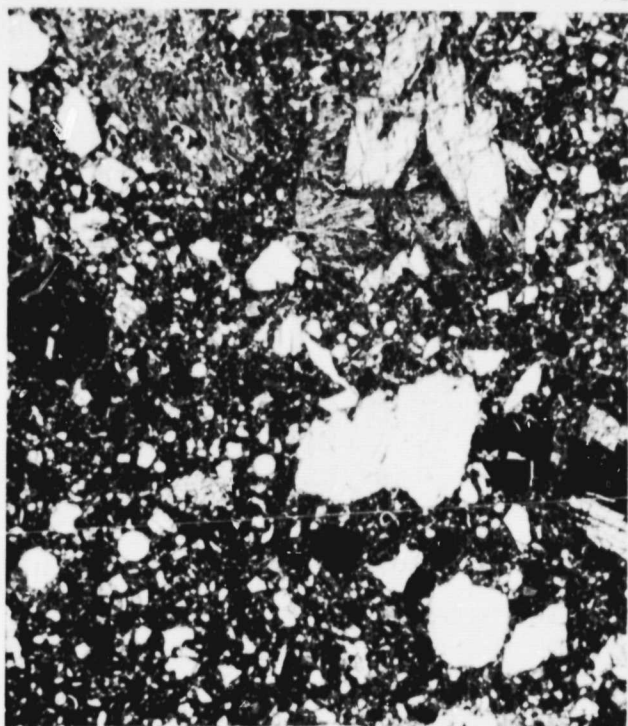
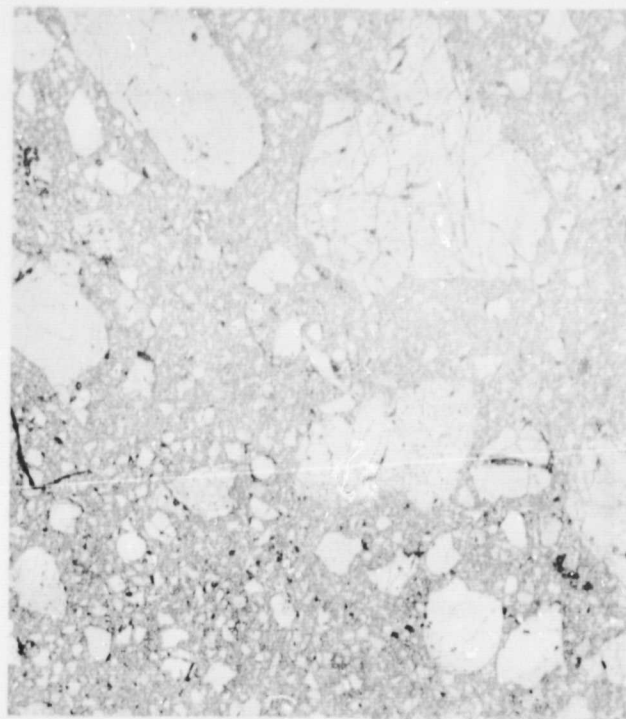
Lithic clasts in sample 15086 are dominated by basaltic rocks with a variety of textures. Vitrophyric varieties are present and consist of euhedral phenocrysts of pyroxene (up to 2.0 mm) set in an opaque matrix of brown glass (Figure e). A second type of basalt is characterized by subhedral to anhedral pyroxene grains and subhedral plagioclase laths with interstitial brown glass (Figure f). A third texture consists of euhedral phenocrysts of pyroxene (2.0x0.4 mm) with complex zoning trends in a matrix of acicular intergrowths of plagioclase and pyroxene with minor ilmenite. Many clasts are totally recrystallized and consist of plumose intergrowths of plagioclase, pyroxene and ilmenite. Drake and Klein (1973) reported textures of this type with KREEP compositions. Less commonly occurring fragments in 15086,39 include one poikilitic plagioclase basalt and rare anorthositic gabbros. No breccia fragments were observed in section 15086,39.

References: Drake and Klein (1973).

15086 MODAL ANALYSES (VOL. %)	
MATRIX (<39 μ):	65.5
CLASTS (>39 μ):	
PLAGIOCLASE	5.9
MAFIC	5.2
OPAQUE	.3
HETEROGENEOUS GLASS	1.4
HOMOGENEOUS GLASS	1.1
DEVITRIFIED GLASS	1.8
FRAGMENTAL BRECCIA	—
CRYSTALLINE BRECCIA	.5
GRANULITIC	—
OTHER METAMORPHIC	—
MARE BASALT	2.3
HIGHLAND BASALT	16.0
CRUSHED	—
PORE SPACE	—
OTHER	—



REFLECTED LIGHT

15086 1.0MM15086 1.0MM

a

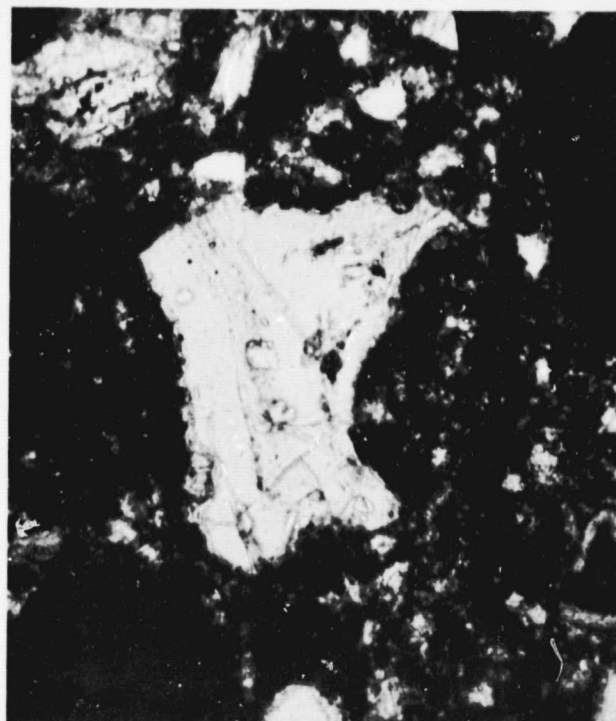
b

Figure 15086a. Typical view of 15086; transmitted light.

Figure 15086b. Same view as (a); reflected light.

15086 0.1MM

c

15086 0.10MM

d

Figure 15086c. Devitrified glass clast; transmitted light.

Figure 15086d. Heterogeneous glass clast with schlieren; transmitted light.

15086 0.25MM

e

15086 0.25MM

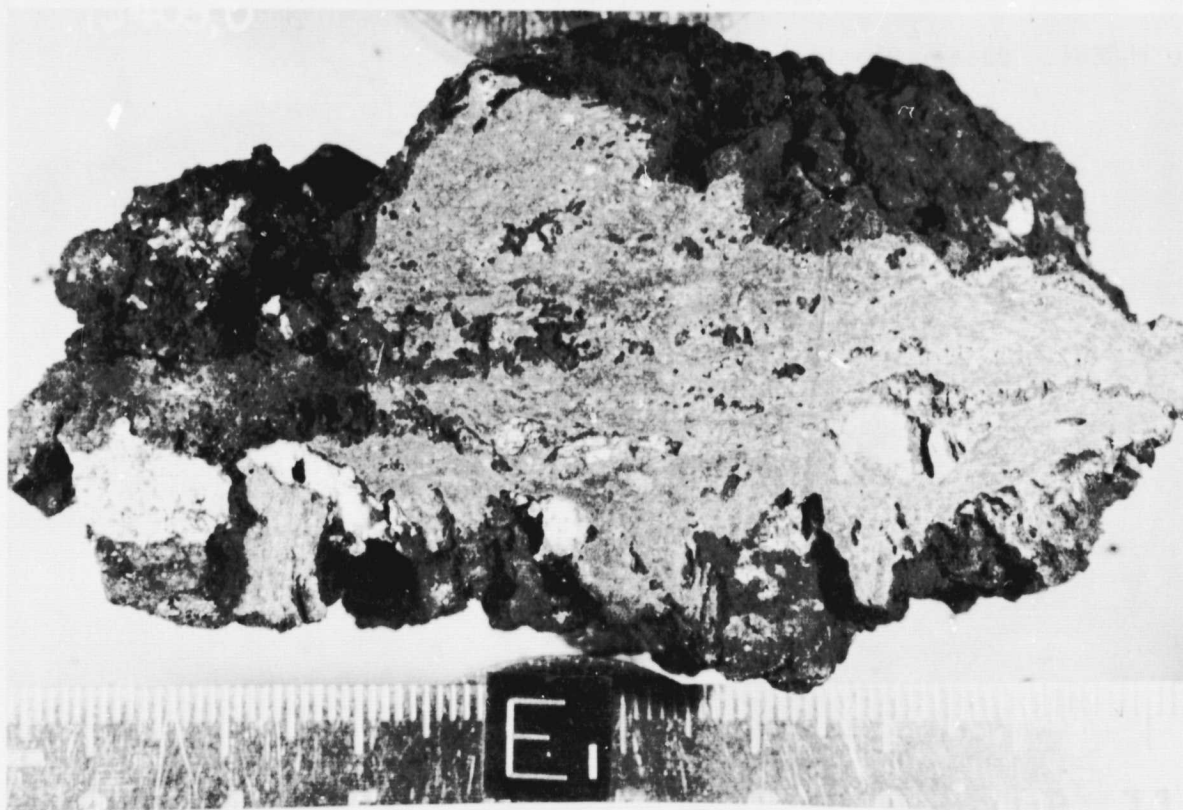
f

Figure 15086e. Vitrophyric basalt clast; transmitted light.

Figure 15086f. Basalt clast; transmitted light.



15405- A clast-bearing impact-melt breccia from Apollo 15 which contains several granite-like clasts.



Sample 15405 is a dark-grey angular rock with light-grey clasts which was chipped from a 3 meter boulder at Station 6A.

15405 CLAST-BEARING IMPACT-MELT BRECCIA

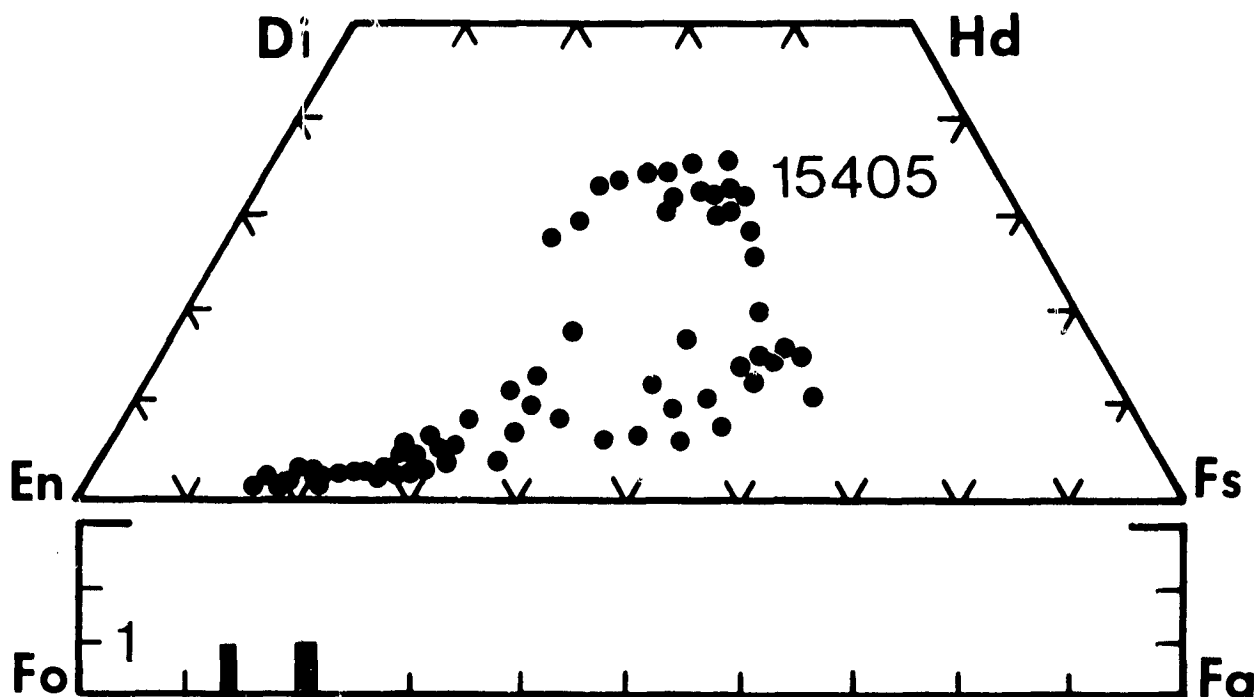
Sample 15405 is a clast-bearing impact-melt rock characterized by an igneous-textured matrix of tightly intergrown plagioclase, pyroxene and ilmenite laths (Figure a). Mineral clasts of plagioclase and pyroxene, together with lithic clasts of granite, KREEP-rich quartz-monzodiorite and KREEP-basalts occur throughout the sample (Figure b). No glass clasts are observed. Irregularly shaped vugs (up to 0.15 mm) and curving, sometimes interconnecting fractures (up to 0.2 mm wide) are relatively common.

Plagioclase and pyroxene are the dominant mineral clast types, ranging in size from 0.05 mm up to 0.35 mm; clasts less than 0.05 mm are rare. Plagioclase clasts are angular and typically display fracturing and/or undulatory extinction. Several plagioclase clasts display twin lamellae; in some cases the lamellae are offset by the fractures. Pyroxene clasts are also angular and fractured and are less abundant than plagioclase clasts.

The lithic clast population is characterized by the conspicuous absence of breccia fragments and rocks representative of the ANT-suite. It is restricted to granites, lithophile trace element rich quartz monzodiorites, and Apollo 15 type KREEP basalts. Granitic clasts are coarse-grained (>1.0 mm) and are typically extensively crushed (Figure c). They consist dominantly of untwinned plagioclase, clinopyroxene, a silica mineral (cristobalite?), and K-Feldspar. Ilmenite, Fe-metal, troilite, chromite and phosphate are present in minor amounts. Plagioclase grains commonly enclose opaques and irregular patches of silica glass. Discrete grains of silica (cristobalite?) display perlitic fractures and also occur intimately intergrown with K-Feldspar. Ilmenite is present as irregular grains and angular forms (up to 1.0 mm). Irregularly shaped grains typically occur in association with a Si-K-rich glassy mesostasis containing both euhedral pyroxenes and phosphate. Fe-metal and troilite occur in the mesostasis and as blebs enclosed within pyroxene. Chromite is rare as are phosphate phases which typically occur only in association with ilmenite.

Clasts of lithophile trace element rich quartz monzodiorite (up to 1.0 cm) are characterized by coarse-grained (>1.0 mm) basaltic textures which lack mesostasis and are typically fractured. Plagioclase grains are typically lath-shaped and twinned; pyroxene grains are typically subrounded to rounded, unzoned and display exsolution lamellae. The clasts also contain a silica mineral, possibly cristobalite, together with K-Feldspar, ilmenite and whitlockite. K-Feldspar and silica are typically intergrown; silica may occur as discrete grains although individual grains of K-Feldspar are rare. Ilmenite is present as relatively large grains which sometimes display wormy intergrowths with K-Feldspar and silica. Fe-metal blebs, probably with a low Ni content, occur enclosed within pyroxene grains.

Basaltic-textured KREEP-rich clasts are abundant in sample 15405 and commonly display subophitic textures ranging in grain size from coarse (plagioclase and pyroxene grains (>1.0 mm) (Figure d) to fine grains (less than 100 μm). Plagioclase occurs as twinned laths and blocky grains; some laths are slightly



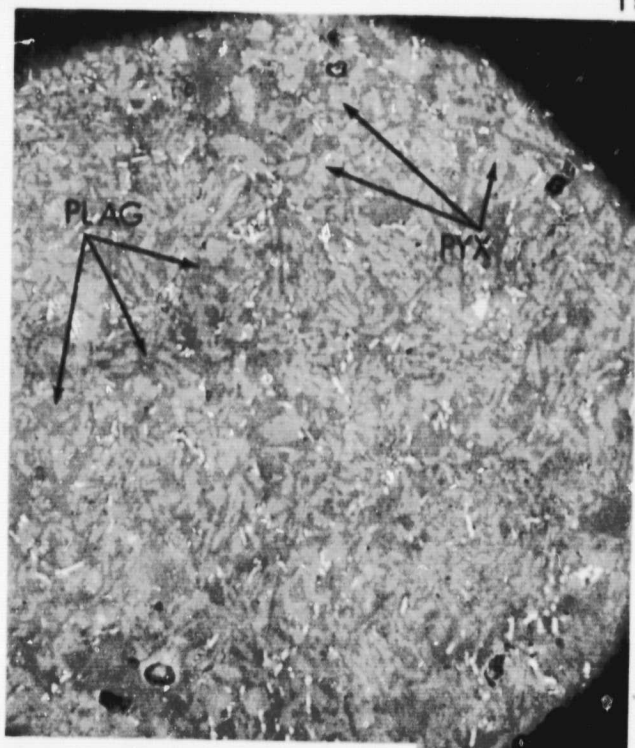
Ryder and Bower 1976C

15405 QTZ MONZODIORITE	
MODAL ANALYSIS(VOL. %)	
PLAGIOCLASE	34.8
MAFIC	35.9
QUARTZ	15.0
K-FELDSPAR	11.0
ZIRCON	0.6
WHITLOCKITE	0.8
ILMENITE	1.6
METAL	0.2

Taylor, G.J. 1976

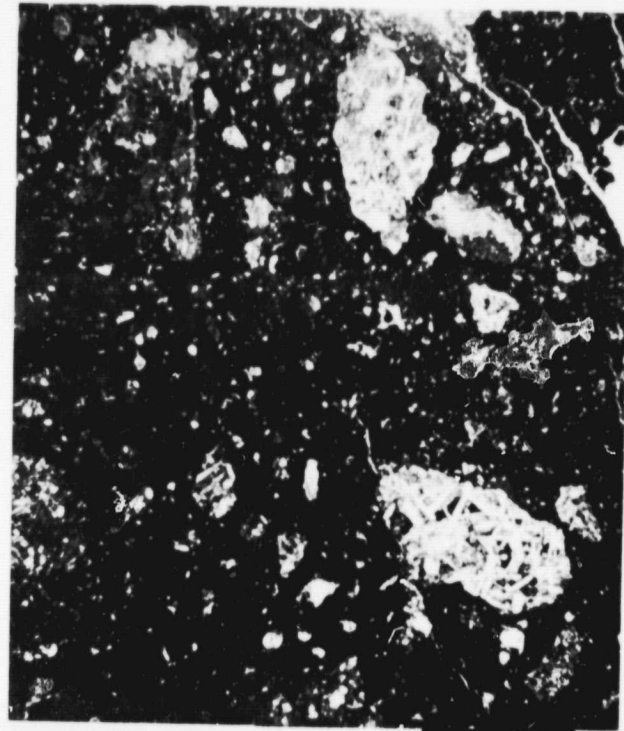
15405 KREEP BASALT	
MODAL ANALYSIS(VOL. %)	
PLAGIOCLASE	50.0
PYROXENE	40.0
ILMENITE	
CRISTOBALITE(?)	
PHOSPHATE	10.0
GLASS	
ZIRCON	

Ryder and Bower 1976b



15405 .025MM

a

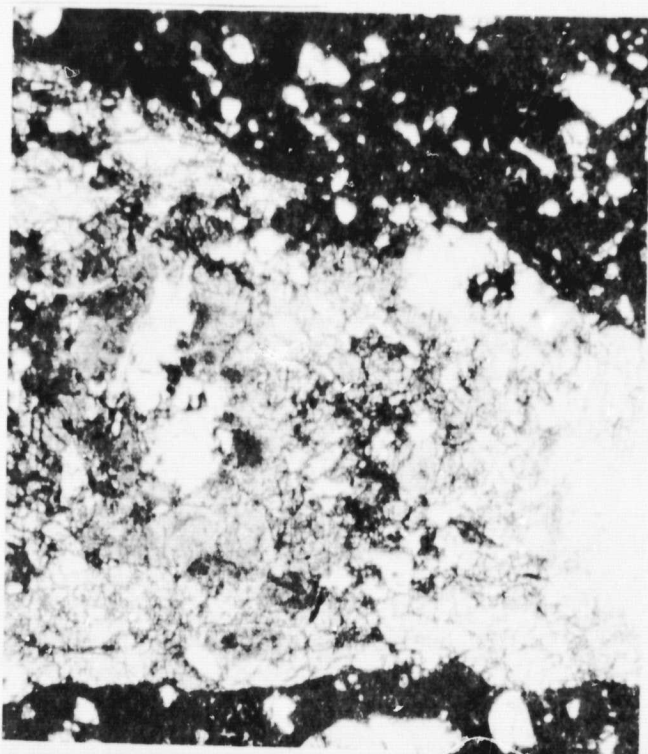


15405 2.00MM

b

Figure 15405a. Typical matrix in 15405; reflected light. Dark-grey, plagioclase; light-grey, pyroxene; white, ilmenite.

Figure 15405b. Typical view of 15405; transmitted light.



15405 0.50MM

c



15405 0.50MM

d

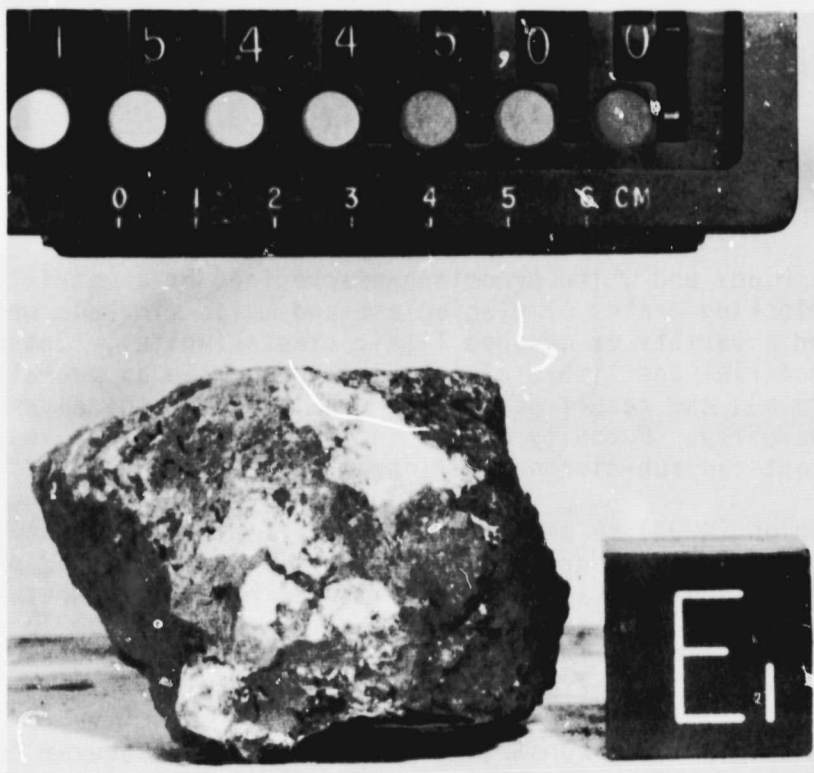
Figure 15405c. Fractured granitic clast in 15405; transmitted light

Figure 15405d. Basaltic KREEP clast; transmitted light.

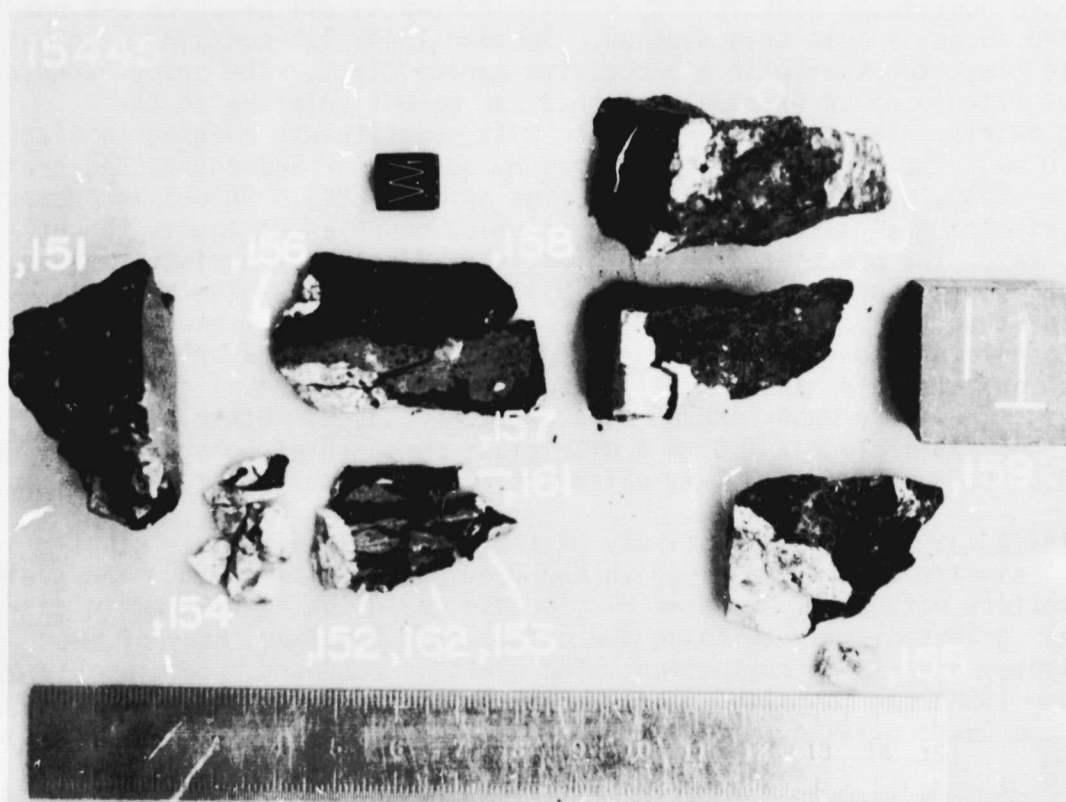
curved. Pyroxenes are consistently zoned from $En_{84}Wo_2$ through pigeonites to augites; some grains contain optically identifiable orthopyroxene cores. Interstitial phases include cristobalite(?), ilmenite and a phosphate mineral and brown glass. Fe-metal and troilite blebs are extremely rare.

Fragments of olivine vitrophyre described by Ryder and Bower (1976b) were not observed in the sections studied by the author.

References: Ryder and Bower (1976b and c); Ryder (1976).



15445- A clast-rich melt breccia enclosing a unique suite of pristine products of early lunar fractionation.



Sample 15445 is a dark-grey to black angular rock with white clasts which was collected inside the rim of Spur crater at Station 7.

15445 BLACK AND WHITE BRECCIA

Sample 15445 is a black and white breccia characterized by a matrix (black) of anhedral interlocking grains of plagioclase and mafic minerals which hosts mineral clasts and a variety of crushed lithic clasts (white). Interfingering zones of matrix material and lithic clasts give the sample an overall foliated appearance (Figure a), the result of differences in mineralogical and chemical composition and porosity. Porosity occurs in the matrix as rare vesicles and in some lithic clasts as sub-micron size intergranular voids.

At high magnification (400X) in reflected light the matrix is observed to contain 10-20 μm size anhedral grains of plagioclase, olivine, and pink spinel (Figure b). Ilmenite and Fe-metal occur as irregularly shaped grains or blebs typically less than 10 μm in size. Subhedral olivine grains (up to 60 μm in length) (Figure c) occur randomly throughout the matrix and suggest the presence of at least some silicate melt.

Mineral clasts in sample 15445 consist predominantly of subangular to subrounded grains of plagioclase and olivine. Many clasts display overgrowth rims (up to 20 μm) and have interdigitating contacts with the matrix. Relatively large blebs of Fe-Ni metal (up to 0.15 mm) occur randomly throughout the matrix.

Sample 15445 contains a wide variety of lithic clasts, all of which are not represented in any single thin section. Section 15445,135 contains a spinel troctolite clast together with a brecciated norite clast. The spinel troctolite clast (Figure d) is extremely crushed and porous relative to the enclosing matrix. The texture is seriate with constituents ranging in size up to 0.20 mm. The clast is characterized by subangular and subrounded grains of olivine (50%), plagioclase (30%) and pink spinel (20%). Spinel is present as aggregates of grains (0.20 mm and less) which occur as stringers throughout the clast. The brecciated norite clast also displays a seriate texture with constituents ranging in size up to 0.40 mm (Figure e). The clast is more porous than the matrix but has been annealed to some extent. The clast contains angular to subrounded grains of plagioclase (65%) and orthopyroxene (35%) with only trace amounts of silica and Fe-metal. Fe-metal forms a continuous vein-like network around some pyroxene clasts. Other clasts in section 15445,135 include a 1.0 mm dunite clast composed of polygonal olivine grains (0.05-0.08 mm) and a 3.5 mm cataclastic anorthosite clast.

Section 15445,139 is composed entirely of a brecciated anorthosite clast (Figure f) similar to that observed in the previous section (135). The grain size is seriate with some uncrushed plagioclase grains up to 0.25 mm in size. The largest grains display twinning and offset twin lamellae; many of the grains display undulatory extinction. The clast is composed predominantly of plagioclase (95%) but contains pyroxene (5%) in isolated regions. Opaque minerals and Fe-Ni metal occur in trace amounts only.

15445 SPINEL TROCTOLITE
 MODAL ANALYSIS (VOL. %)

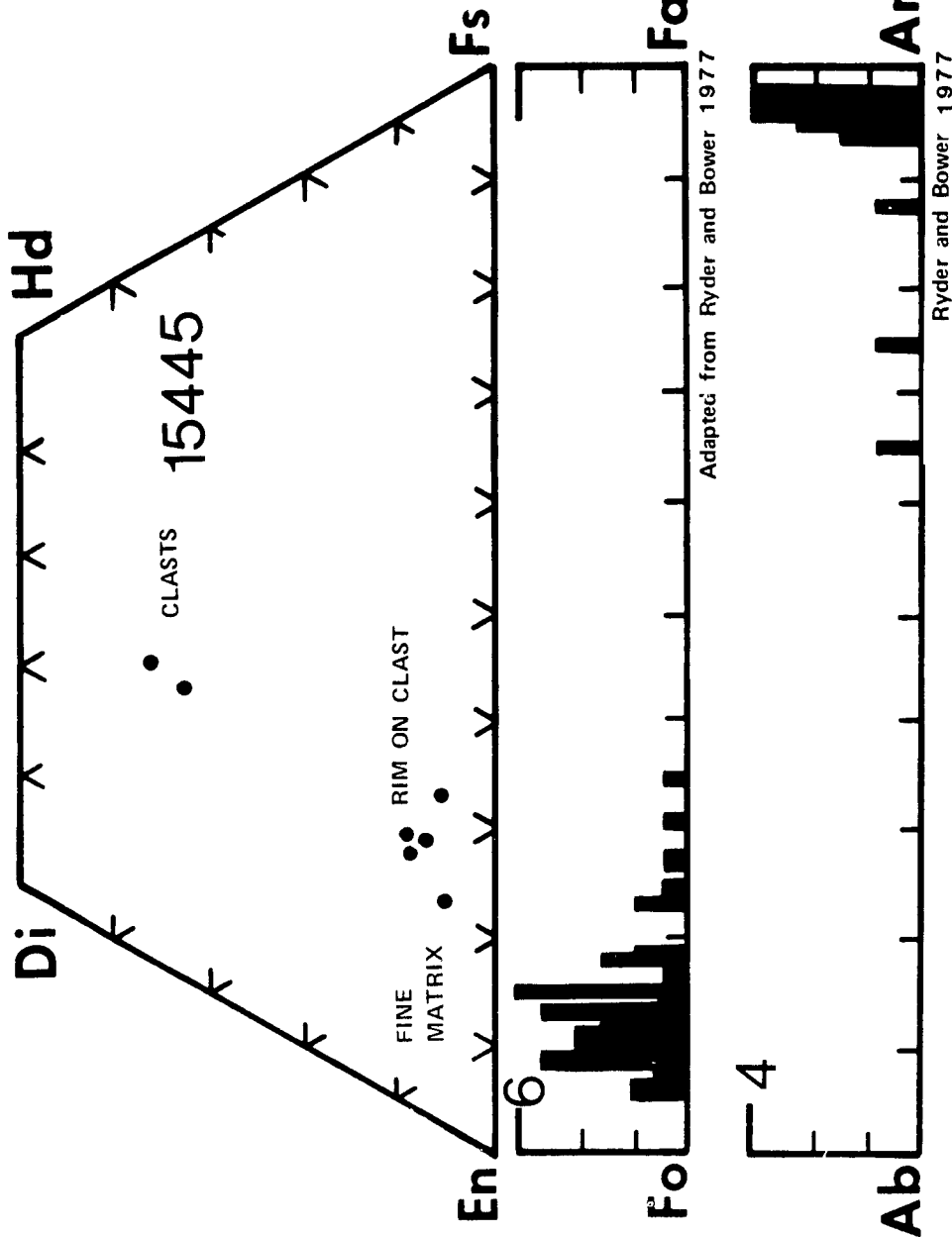
PLAGIOCLASE	30-40.0
PYROXENE	—
OLIVINE	50.0
PLEONASTE	10-20.0
OPAQUE	TR

Ryder and Bower 1977

15445 NORITE
 MODAL ANALYSIS (VOL. %)

PLAGIOCLASE	60-65.0
Low-ca PYROXENE	35-40.0

Ryder and Bower 1977

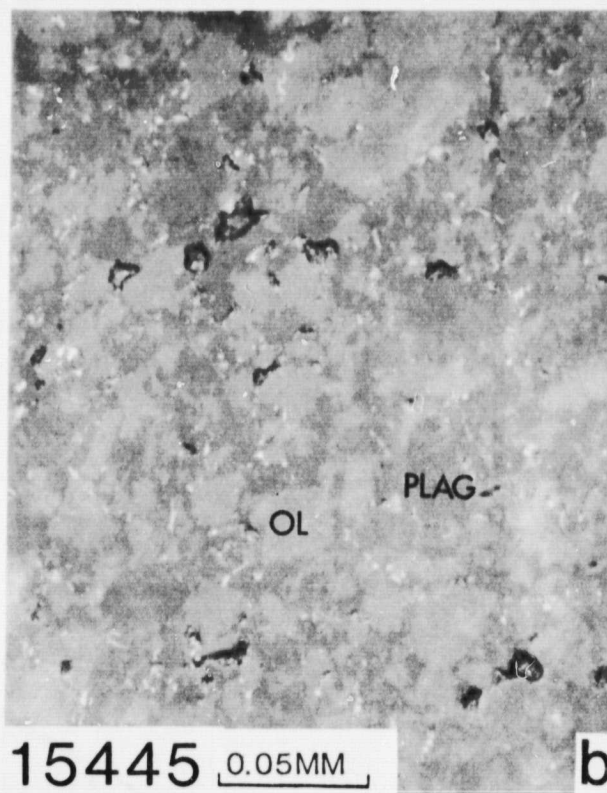




15445

2.0MM

a



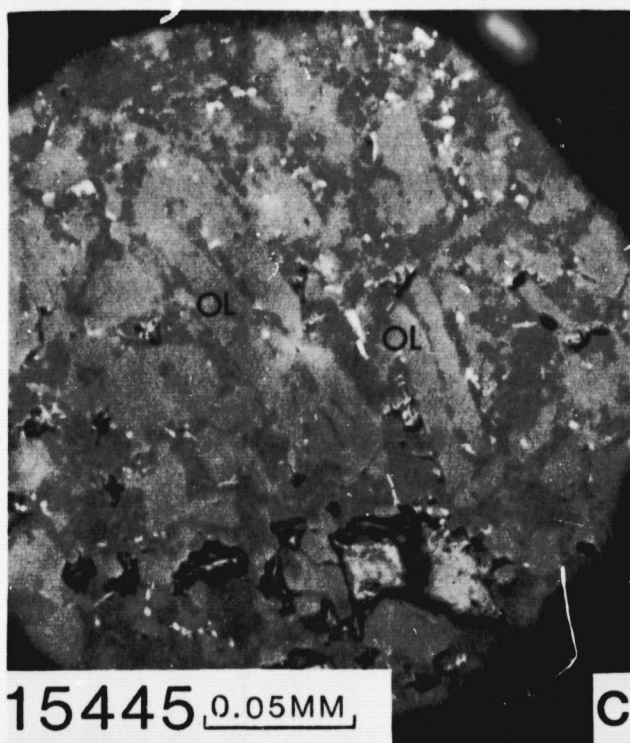
15445

0.05MM

b

Figure 15445a. Typical view of 15445; transmitted light.

Figure 15445b. Typical matrix in 15445; reflected light. Dark-grey, plagioclase; light-grey, olivine; white, ilmenite.

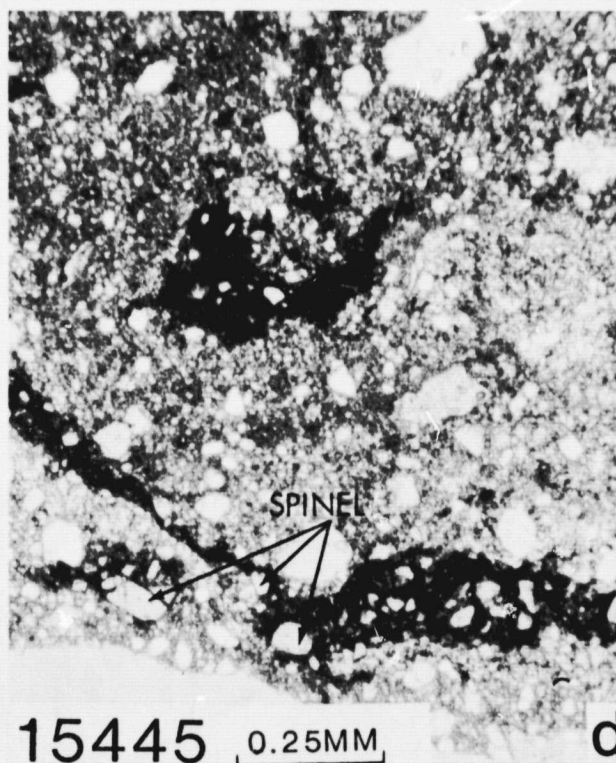


15445

0.05MM

c

Figure 15445c. Euhedral olivine grains in matrix; reflected light. Color key same as in (b).

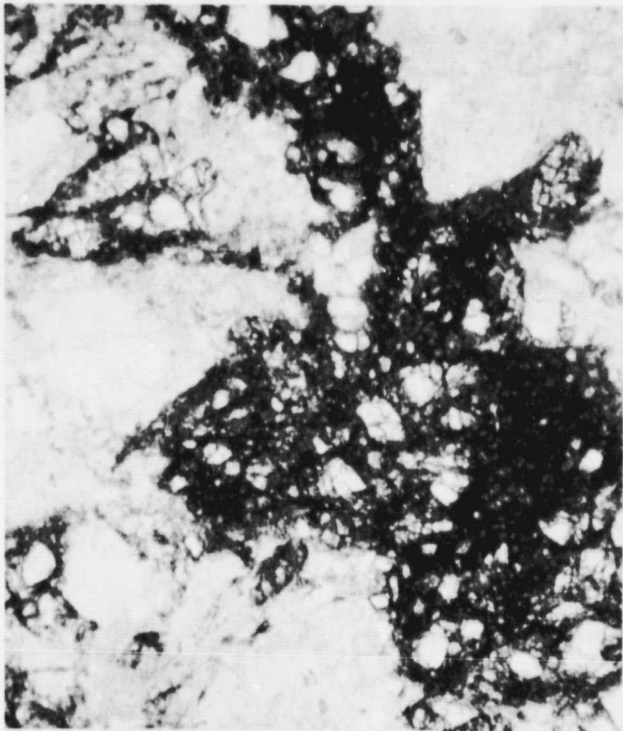


15445

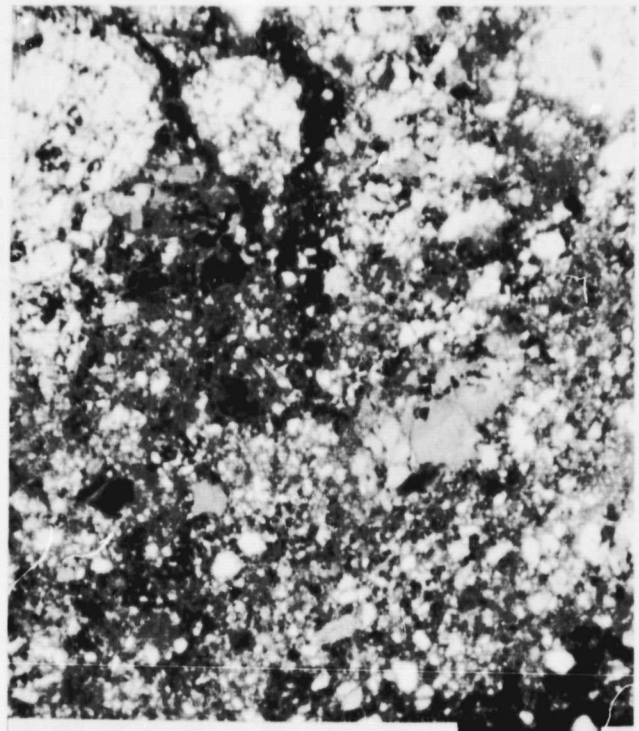
0.25MM

d

Figure 15445d. Spinel-troctolite clast; transmitted light.

15445 0.25MM

e

15445 0.25MM

f

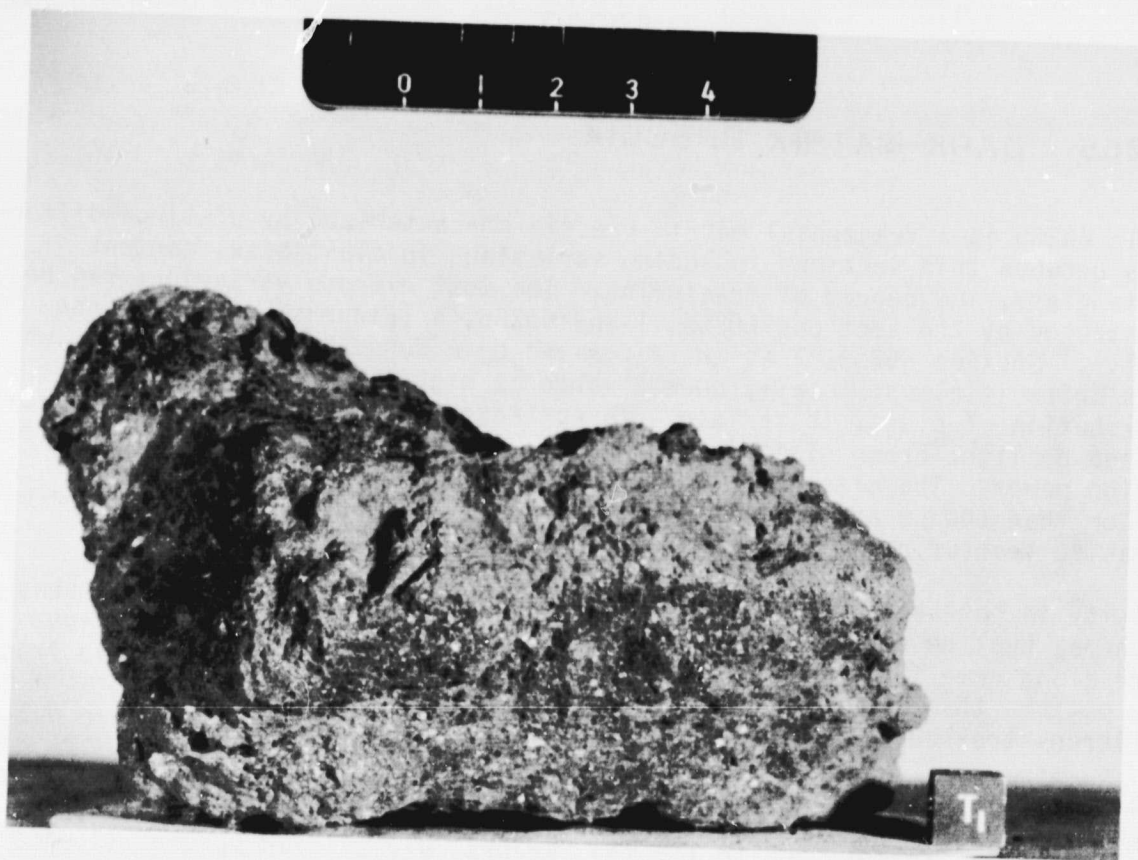
Figure 15445e. Brecciated norite clast; transmitted light.

Figure 15445f. Brecciated anorthosite clast; transmitted light.

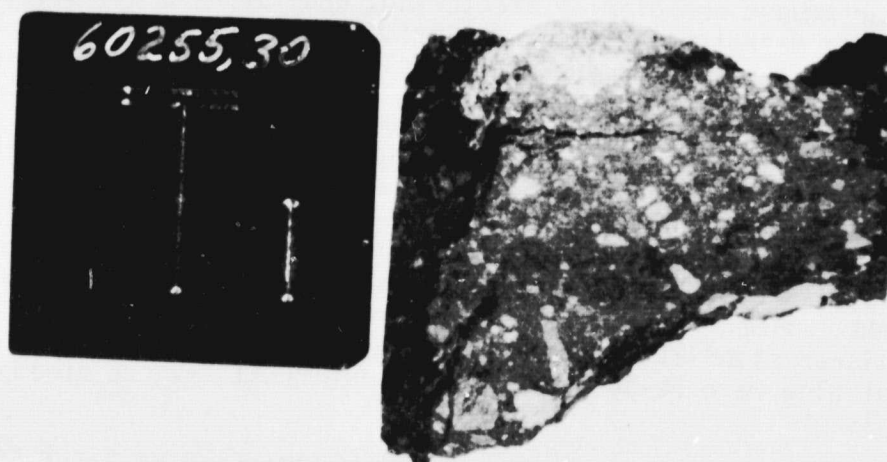
Finally, section 15445,144 consists of a spinel-troctolite clast petrographically similar to clast A in section 15445,135. It consists of a seriate size assemblage of olivine, plagioclase, and pink-spinel minerals up to 0.10 mm. Fe-Ni metal is present as micron-size blebs. The clast is crushed and intimately mixed with matrix material.

Ryder and Bower (1977) propose that sample 15445 is a fragment of an impact-melt sheet produced by the Imbrium impact event.

References: Ryder and Bower (1977); Ridley et al. (1973).



60255- A typical Apollo 16 "soil" breccia.



Sample 60255 is a light-grey subangular rock (12x9x7 cm) believed to have been collected near the lunar module approximately 30 to 40 meters south to southwest of the lunar-module-Y footpad.

60255 DARK-MATRIX BRECCIA

Sample 60255 is a fragmental matrix breccia characterized by distinct differences between thin sections including variations in clast size, content of matrix glass, and degree of fracturing. The most extreme variations can be illustrated by the sections 60255,71 and 60255,14 (Figures a and b respectively). Section 60255,71 is characterized by a dense matrix of dark brown glass which is almost totally unresolvable at high power (400X). The size distribution of clasts is seriate. In contrast, section 60255,14 is characterized by light brown glass in the matrix, fragments of which are resolvable at high power. The clast size distribution is also seriate, but clasts smaller than 100 μm are most abundant. Clasts in this section display more pervasive fracturing than those in 60255,71.

Porosity in both sections is limited to micron to millimeter-size fractures which may best be viewed in reflected light. Rare irregularly shaped vugs occur along some fractures. Section 60255,71 displays a more extensive fracture pattern than 60255,14; rare veinlets are filled with debris and schlieren-streaked glass.

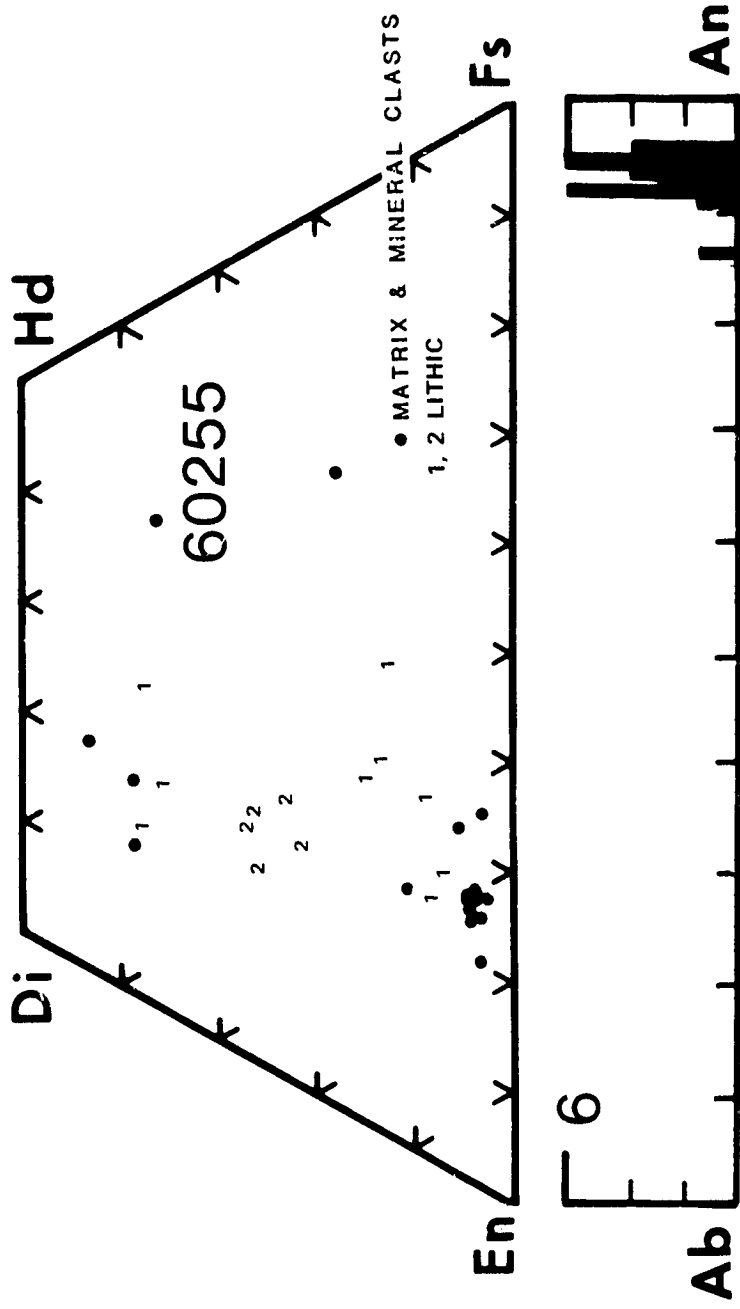
Glass clasts are common to both sections and are typically angular, colorless to pale-green, homogeneous and schlieren-free. Both sections display rare colorless glass spheres (up to 1.5 mm), several devitrified spheres (typically .10 mm in diameter) and debris-filled orange glass clasts (typically less than 0.2 mm). Homogeneous orange glass clasts are rare; one clast 0.35 mm long was observed in section 60255,14.

Plagioclase is the most common mineral clast in both sections. Most clasts are subangular or equant and display fracturing, undulatory extinction, and partial to complete maskelynitization; devitrification features are rare. Pyroxene is the second most abundant mineral clast and typically occupies a more restricted size range in both sections. Clasts in section 60255,71 are commonly 0.2 mm and less and in section 60255,14 are typically 0.1 mm and less. All clasts show fracturing to some extent; clasts in section 60255,14 are more extensively fractured. Subangular to equant morphologies are common to both sections. Opaque grains account for less than 1 percent of the clast population in each section. Fe-Ni metal and troilite occur as rounded and irregular blebs up to 0.20 mm ranging downward in size to sub-micron size blebs. Ilmenite and ulvospinel occur as rounded clasts which are typically micron sized although rare clasts up to 0.15 mm are present. Both sections display rare Fe-Ni metal grains with "rust" stains on adjacent silicate minerals.

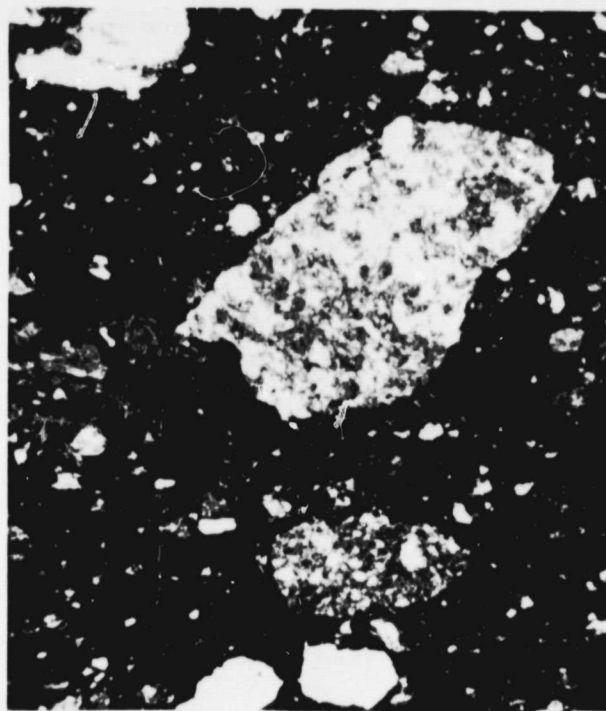
Lithic clasts dominate the clast population, accounting for at least 50 percent of the clasts in each of the two sections. Crushed gabbroic anorthosites (Figure c) and poikilitic textured impact melt rocks (Figure d) are the most common types; section 60255,14 displays an 8.0 mm clast of poikilitic impact-melt rock. Anorthositic clasts are common to both sections and are similar to

60255,14
MODAL ANALYSES (VOL. %)

MATRIX (<39.1)	28.0
CLASTS (>39.1):	
PLAGIOCLASE	17.0
MAFIC	3.0
OPAQUE	TR
HETEROGENEOUS GLASS	—
HOMOGENEOUS GLASS	2.0
DEVITRIFIED GLASS	—
FRAGMENTAL BRECCIA	—
CRYSTALLINE BRECCIA	—
ANORTHOSITE	5.0
OTHER METAMORPHIC (gabbroic anorthosite)44.5 MARE BASALT	—
HIGHLAND BASALT	TR
CRUSHED	—
PORE SPACE	—
OTHER	—

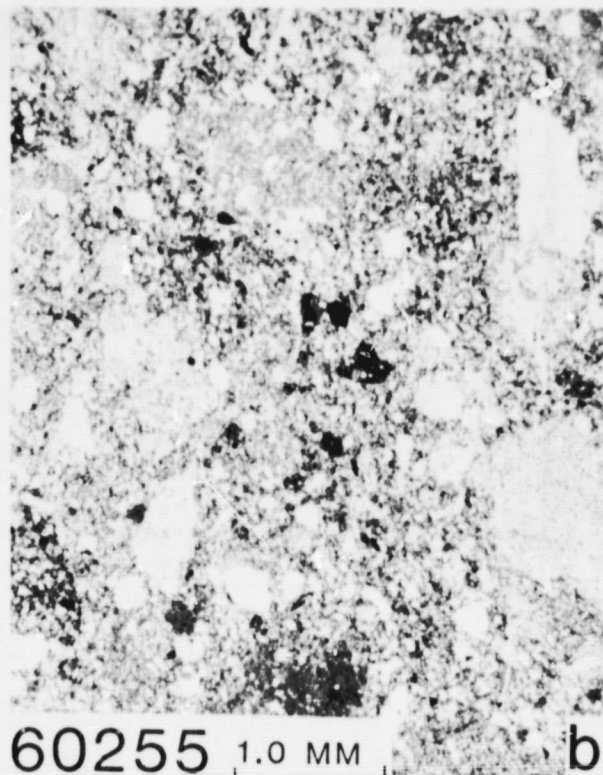


adapted from LSPEI 1972



60255 1.0 MM

a

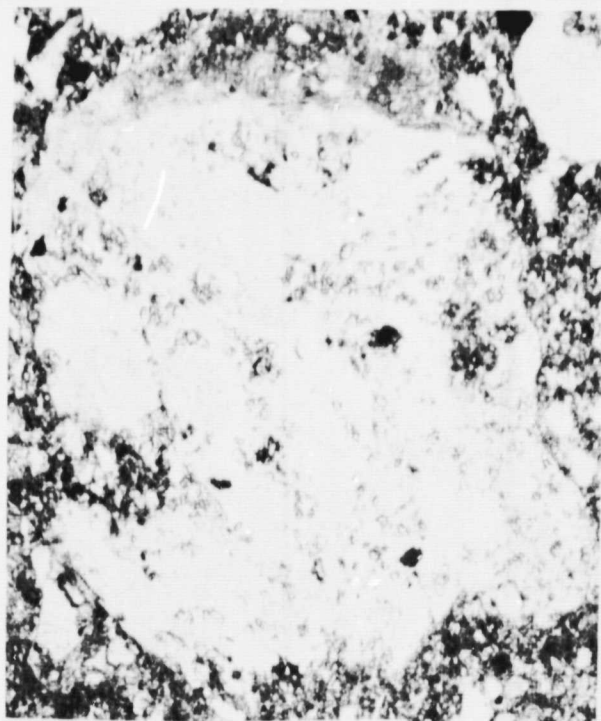


60255 1.0 MM

b

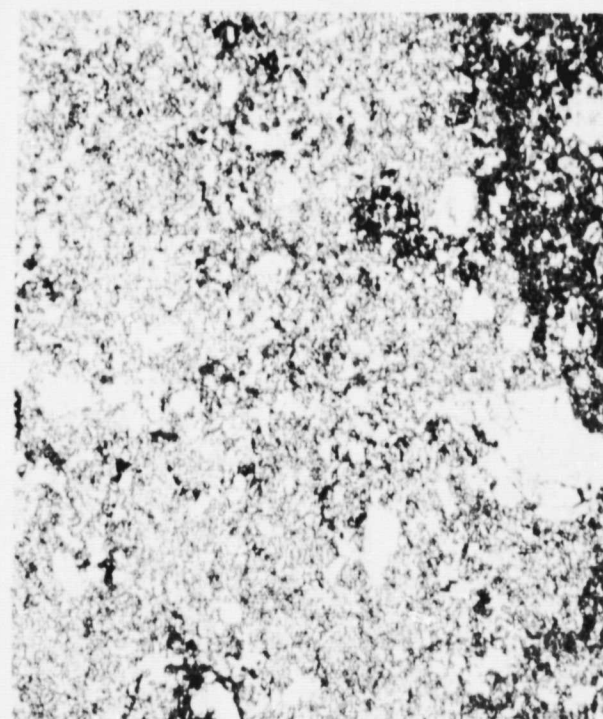
Figure 60255a. Typical view of 60255,71; transmitted light.

Figure 60255b. Typical view of 60255,14; transmitted light.



60255 0.25 MM

c



60255 0.50 MM

d

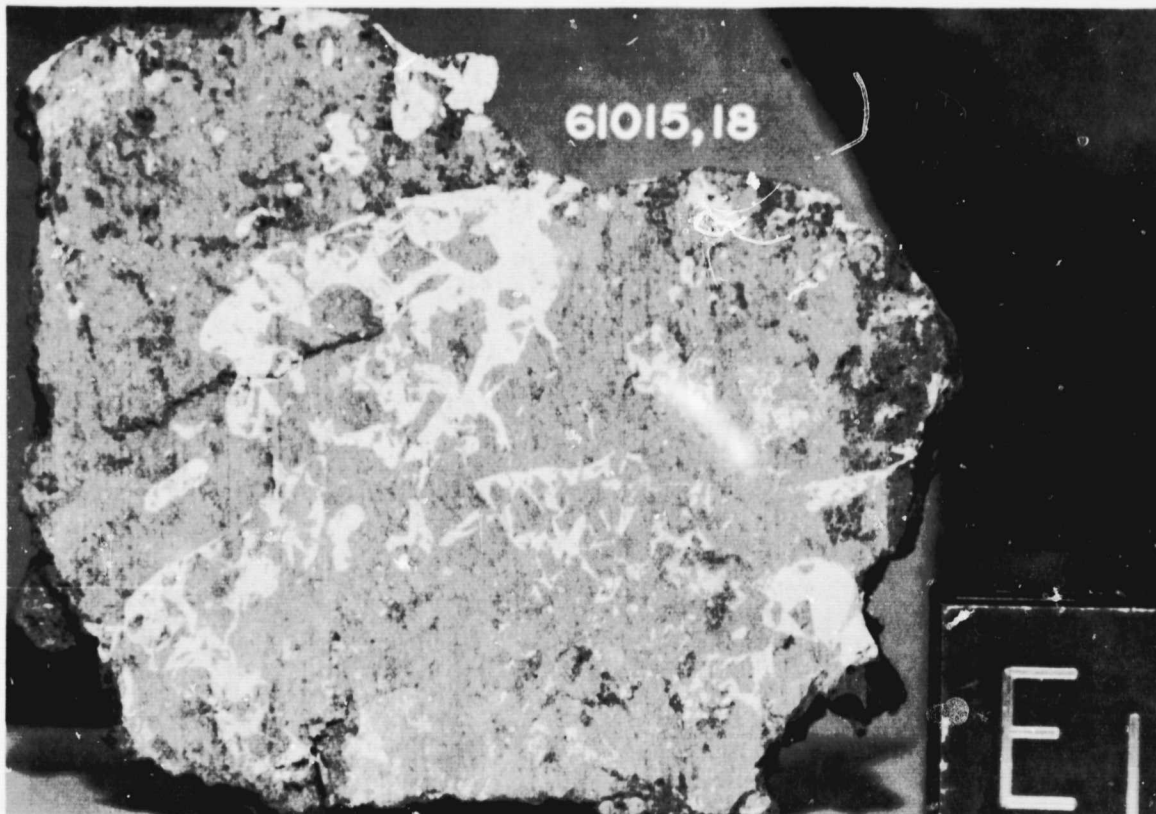
Figure 60255c. Crushed gabbroic anorthosite clast; transmitted light.

Figure 60255d. Poikilitic impact-melt clast; transmitted light.

cataclastic anorthosite 60025 described in the companion volume. Some of the anorthosite clasts may represent shocked plagioclase clasts. Basalt clasts, with vitrophyric, poikilitic and ophitic textures are present ranging in size up to 1.3 mm; section 60255,71 contains a 4.5 mm basaltic clast with a sub-ophitic texture.



61015- An Apollo 16 black and white breccia which consists of cataclastic, chemically pristine anorthosite which has been invaded by a pyroxene-rich impact-melt.



Sample 61015 is a medium-grey, angular to subrounded rock (15x12x10 cm) which was collected at Station 1, on the rim of Flag crater, 10 meters south of Plum crater.

61015 BLACK AND WHITE BRECCIA

Sample 61015 is a black and white breccia characterized by cataclastic anorthosite and clast-bearing impact melt; the impact melt lithology appears to have intruded the anorthositic lithology (Figure a). The igneous-textured impact melt lithology is characterized by clusters of tightly intergrown plagioclase laths (.025-.075 mm) and subhedral to anhedral pyroxene crystals (up to 0.5 mm) in a dark glassy mesostasis (Figure b). Plagioclase is the most common mineral clast type in the impact melt lithology and occurs as subangular clasts up to 0.15 mm across. Pyroxene is present as angular clasts up to 0.15 mm across but occurs only as a minor clast type (<10% of mineral clast population).

The cataclastic lithology is composed of cataclastic anorthosite displaying extremely fractured and deformed plagioclase grains. The largest grains are up to 1.0 mm across but most grains occupy the 0.3 to 0.5 mm size range. Rare anhedral mafic grains (up to 0.5 mm) occur interstitial to plagioclase grains.

A glass coating of flow-banded brown glass (in transmitted light) covers a portion of sample 61015. Figure c shows a glass vein which intersects both the anorthositic and the impact melt lithology.

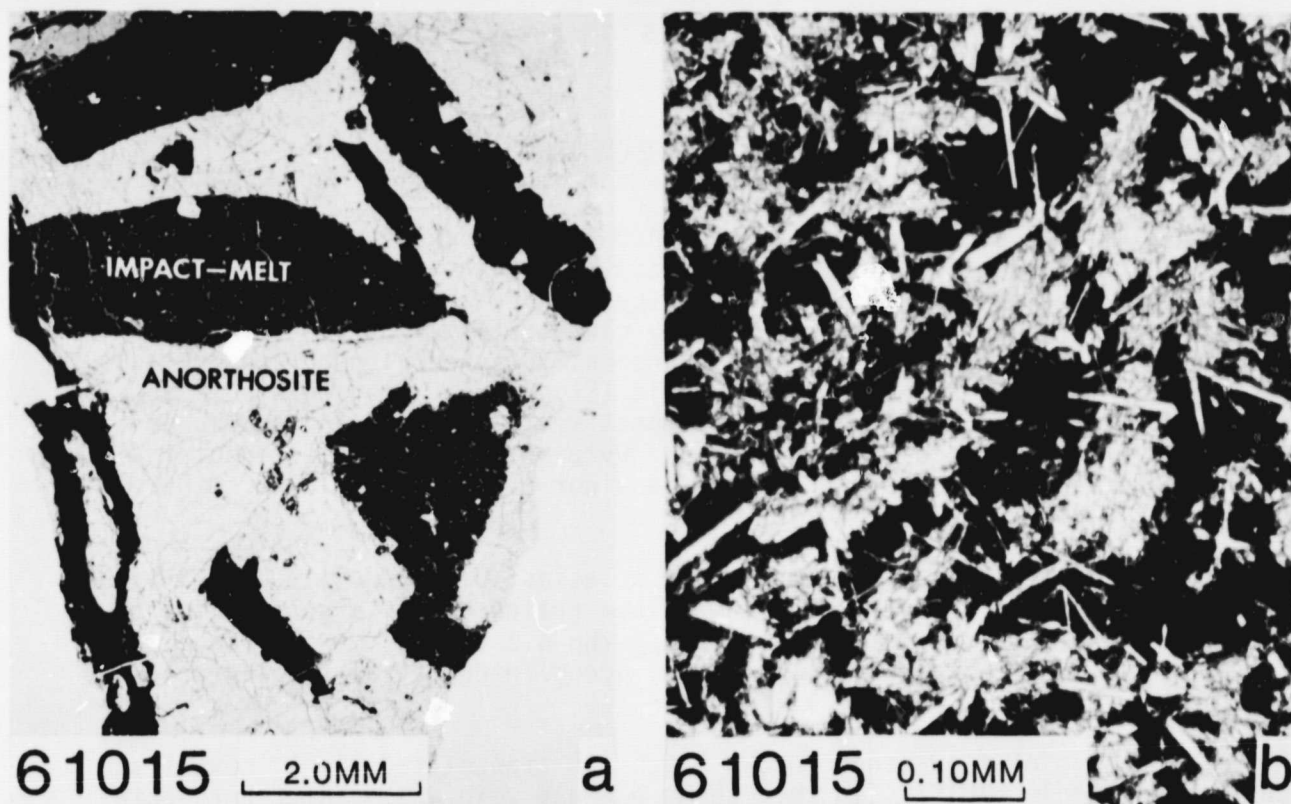


Figure 61015a. Typical view of 61015; transmitted light.

Figure 61015b. Impact-melt matrix; transmitted light.

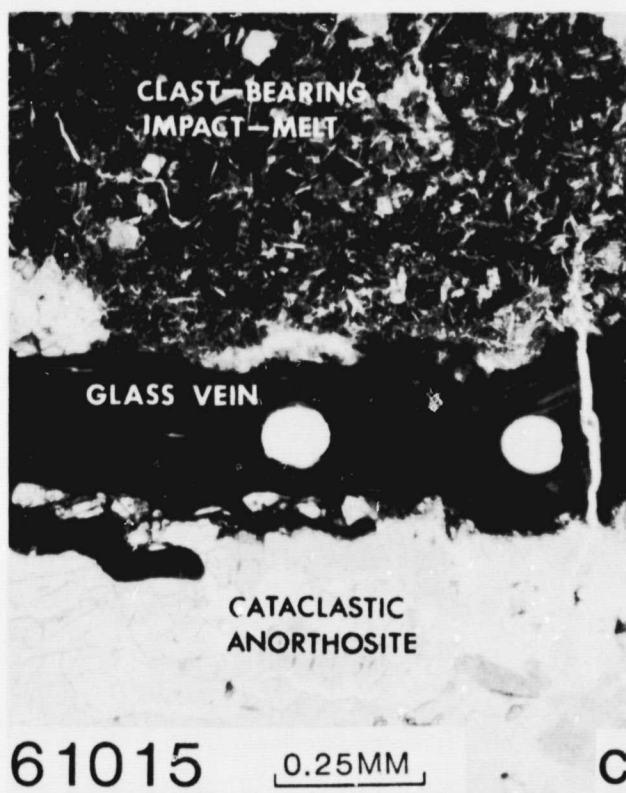
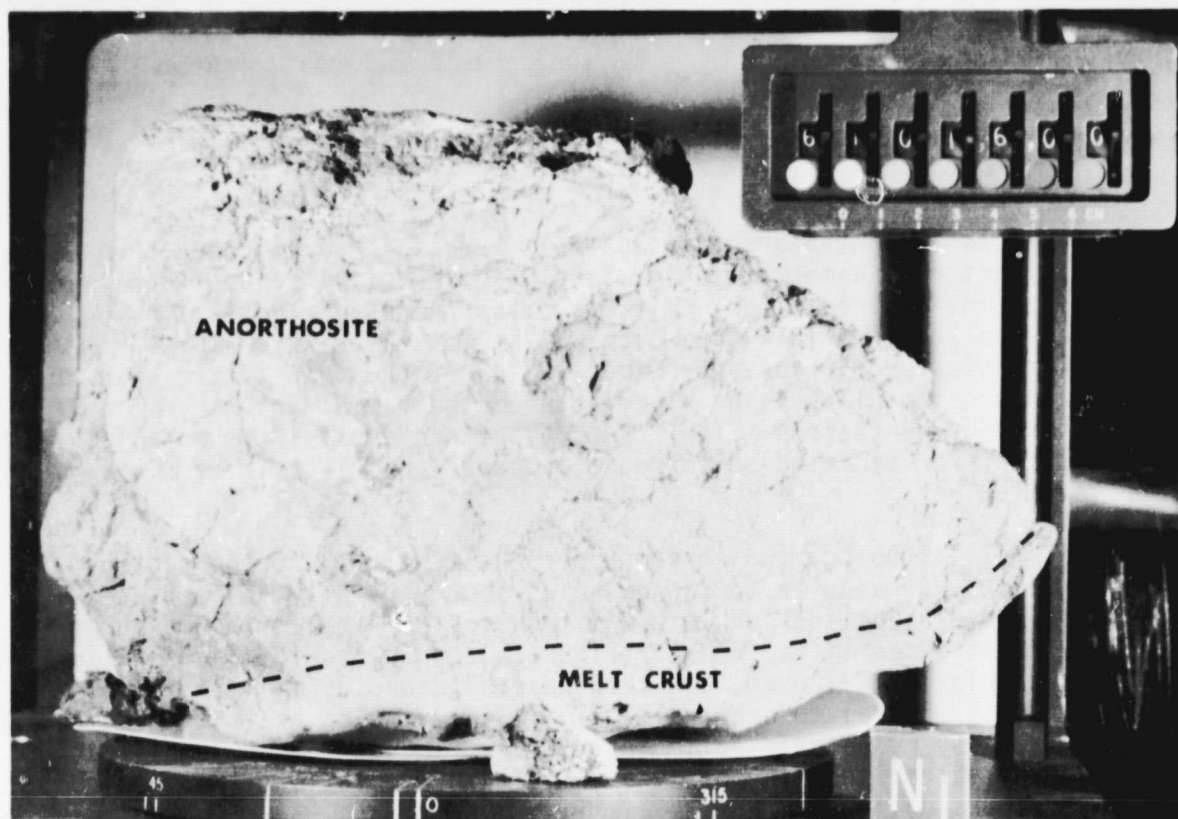
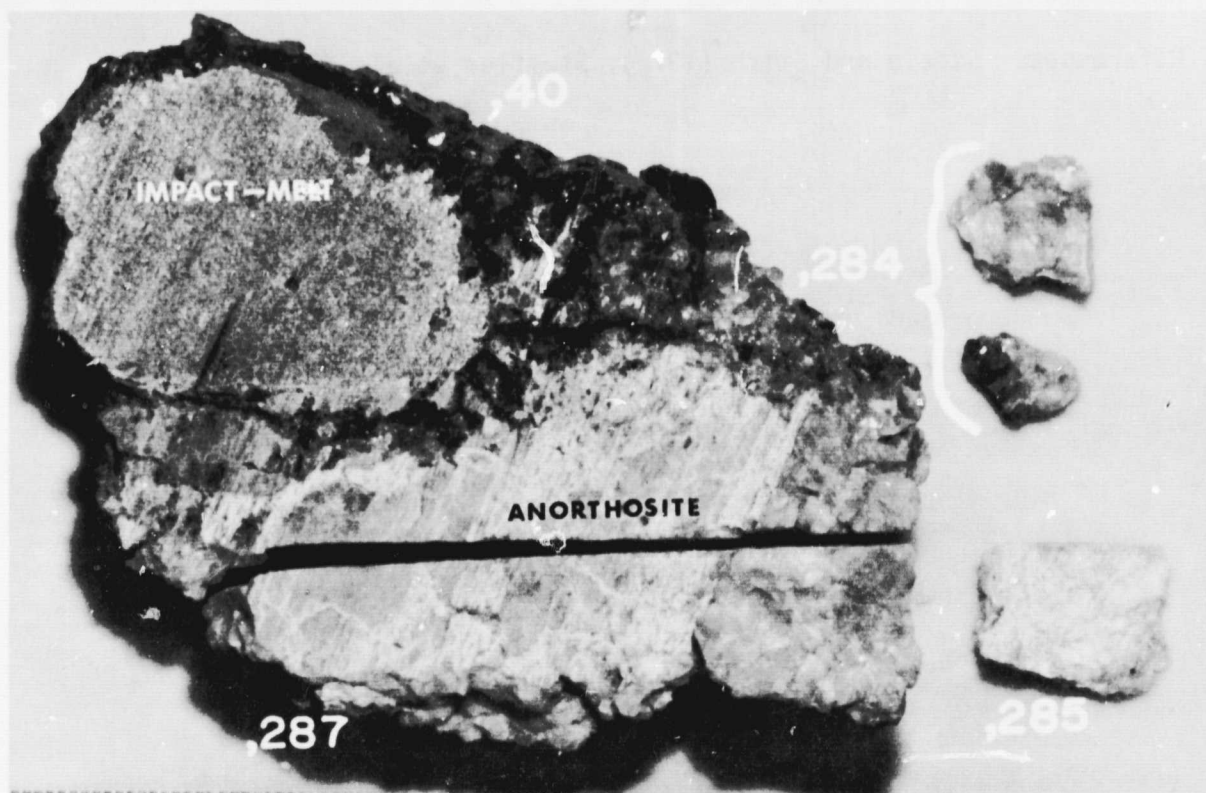


Figure 61015c. Flow-banded brown glass; transmitted light.



61016- A clast-bearing impact-melt breccia consisting of a large clast of cataclastic, chemically pristine anorthosite in a highly feldspathic impact-melt. The rock is the largest single lunar sample returned by the Apollo missions.



Sample 61016 is a medium to dark-grey rounded rock (28x18x16) cm) with white clasts which was collected at Station 1, 1400 meters west of the lunar module near the rim of Plum crater.

61016 CLAST-BEARING IMPACT-MELT BRECCIA

Sample 61016 is a clast-bearing impact-melt breccia characterized by a 15 cm diameter, fractured, almost totally maskelynitized clast of anorthosite enclosed by a fine-grained impact-melt breccia (Figure a). Both lithologies are present in section 61016,218 which was selected for this study. The anorthositic clast comprises approximately 1/3 of the area of the thin section. Although the clast is highly fractured individual grains remain in their original orientations. The fracture pattern consists of parallel fractures. Except for isolated anisotropic patches, the clast is completely maskelynitized.

The impact-melt lithology (which comprises the final 2/3 of the section) is characterized by subangular to rounded clasts of partially to completely maskelynitized plagioclase (up to 2.0 mm across) together with glassy and partially devitrified lithic clasts (Figure b) contained in a subophitic matrix of tabular (.10-.20 mm) and lath-shaped (2.0x0.05 mm) maskelynite intergrown with subhedral to euhedral (0.10 mm) olivine crystals (Figure c). A dark-brown glassy mesostasis fills interstices and at higher magnification (400x) in reflected light is observed to contain needles of ilmenite (.015-.025 mm) (Figure d).

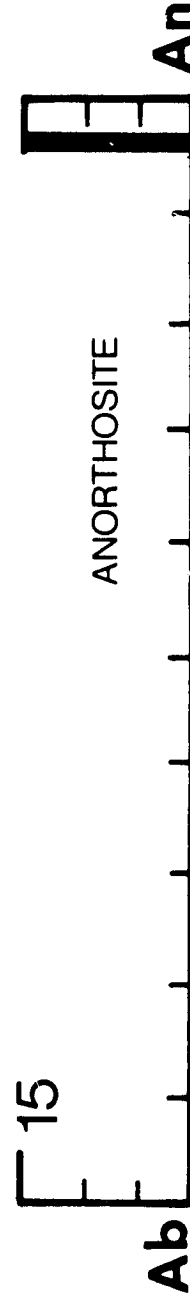
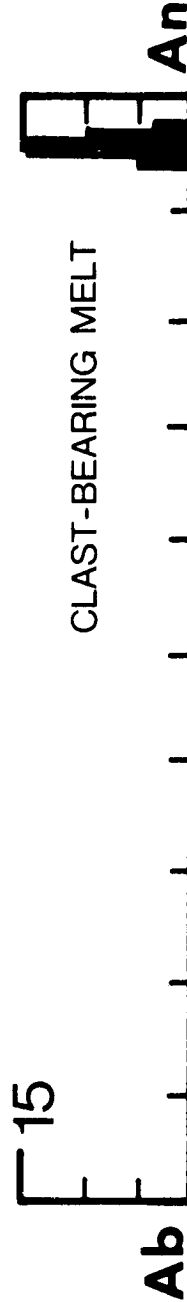
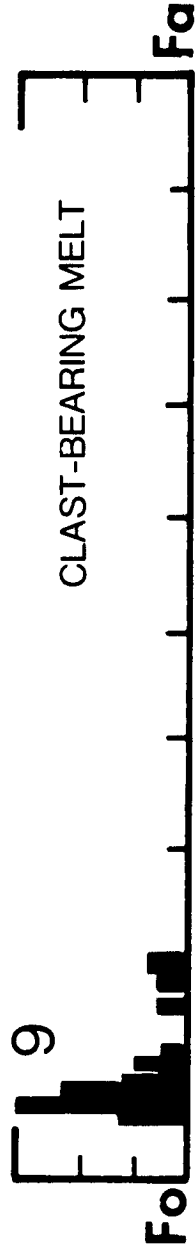
A coating of vesicular glass with an anorthositic-noritic composition forms a crust around a portion of sample 61016 (see labeled "mug" photograph). In thin section the glass is light brown and displays devitrification features (Figure e). Veins of brown and black glass extend from the melt crust and penetrate into the impact melt.

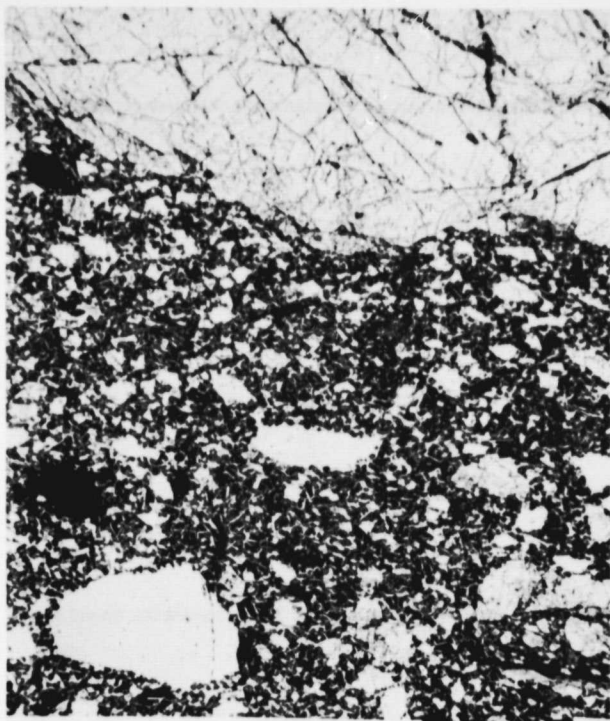
References: Steele and Smith (1973); Stoffler et al. (1975)

61016,219
 MODAL ANALYSES (VOL. %)

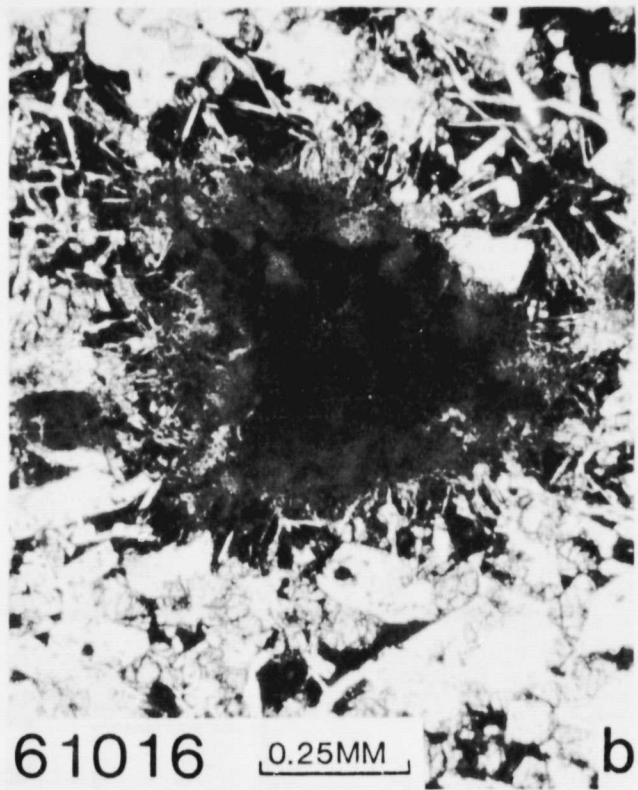
MATRIX (<39 μ) (Impact-melt)	52.82
CLASTS (>39 μ):	
PLAGIOCLASE (maskelynite)	42.38
MAFIC	—
OPAQUE	—
HETEROGENEOUS GLASS	—
HOMOGENEOUS GLASS	—
DEVITRIFIED LITHIC	4.78
FRAGMENTAL BRECCIA	—
CRYSTALLINE BRECCIA	—
GRANULITIC	—
OTHER METAMORPHIC	—
MARE BASALT	—
HIGHLAND BASALT	—
CRUSHED	—
PORE SPACE	—
OTHER	—

61016





61016 2.0MM



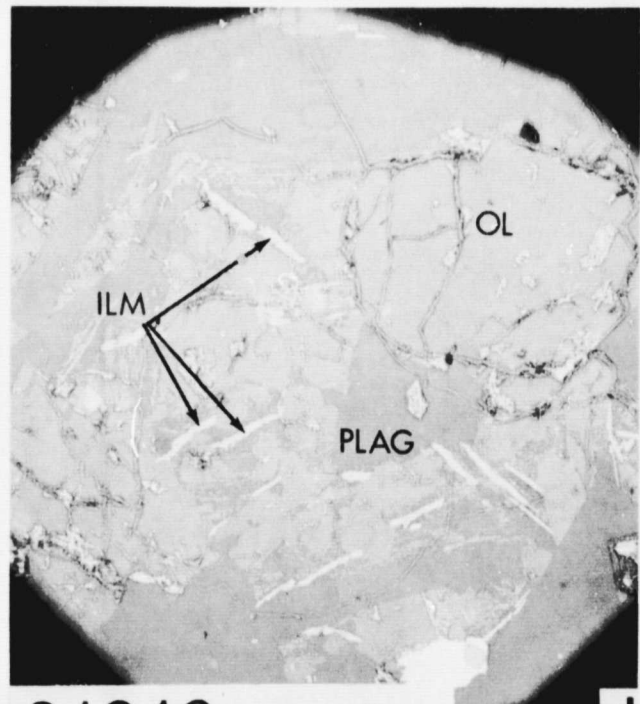
61016 0.25MM

Figure 61016a. Typical view of 61016; transmitted light.

Figure 61016b. Devitrified lithic clast; transmitted light.



61016 0.10MM



61016 0.05MM

Figure 61016c. Impact-melt lithology; transmitted light.

Figure 61016d. Ilmenite needles in mesostasis of impact-melt lithology; reflected light. Dark-grey, plagioclase; light-grey, olivine; white, ilmenite.

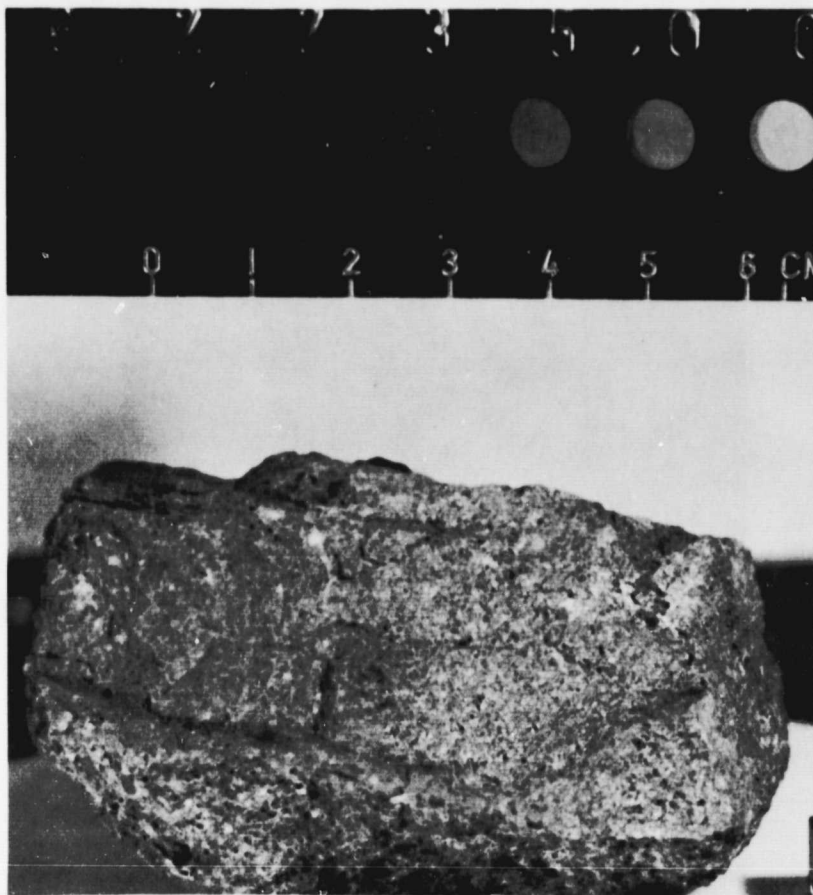
61016

126

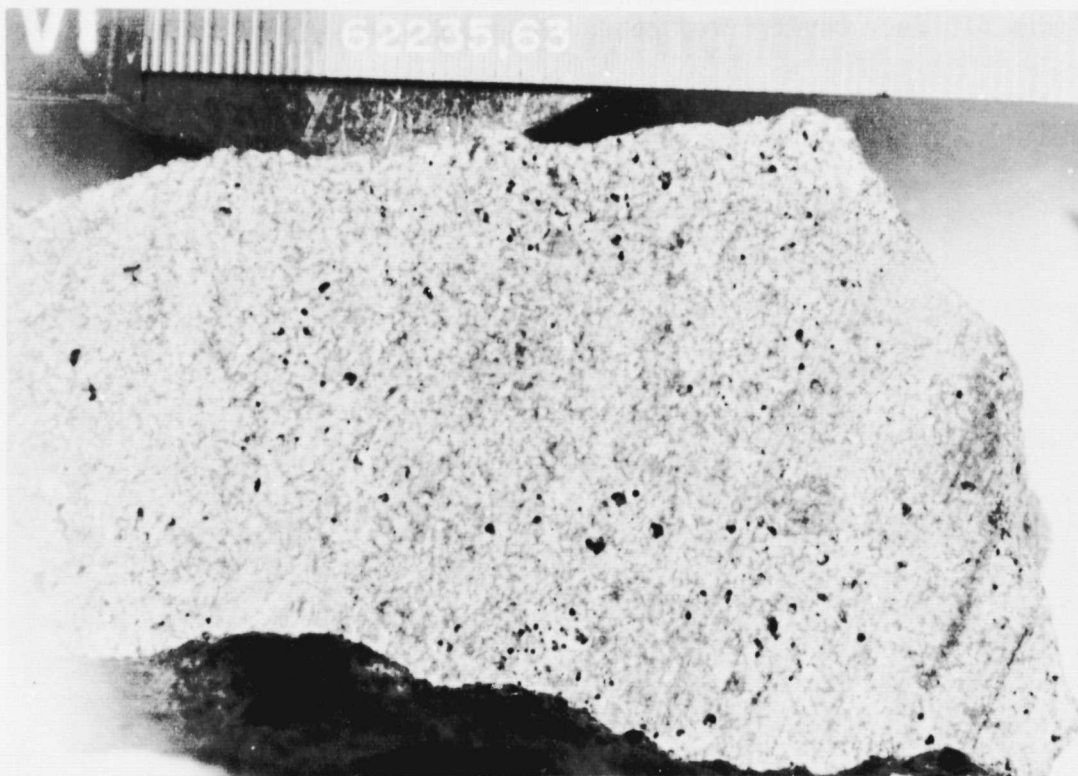


61016 0.10MM | e

Figure 61016e. Devitrified brown glass melt crust; transmitted light.



62235- A clast-bearing impact-melt breccia of noritic composition (often called low K KREEP). The rock has a poikilitic texture which is characteristic of many clast-bearing melt rocks of the same composition from all landing sites.



Sample 62235 is a grey angular rock (8x7x5.5 cm) collected at Station 2, 550 meters west of the lunar module, just north of Spook crater.

62235 CLAST-BEARING IMPACT-MELT BRECCIA

Sample 62235 is a clast-bearing impact-melt breccia characterized predominantly by coalescing oikocrysts of orthopyroxene enclosing laths of plagioclase. Poikilitic ilmenite (with included plagioclase tablets) and small amounts of phosphate, Fe-Ni metal, troilite and K-spar are concentrated between the oikocrysts (Figure a). Mineral clasts, dominantly plagioclase, together with less commonly occurring lithic clasts are scattered randomly throughout the sample. Irregularly shaped vugs (up to 0.6 mm across) are relatively common; spherical vesicles (typically 0.25 mm and less) are also present but are less abundant.

Orthopyroxene oikocrysts typically display rectangular outlines (up to 2.0 mm in length) although rounded and irregular shapes are also present (Figure b). Oikocrysts are commonly observed to have grown around spherical vesicles. Plagioclase is present as anhedral or tablet-shaped crystals (.01-.05 mm) and as lath-shaped crystals (.05-.10 mm) both enclosed within orthopyroxene oikocrysts and located between the oikocrysts (Figure c).

Ilmenite is the dominant opaque phase, occurring as poikilitic crystals (up to 0.4 mm), typically with silicate inclusions, which occur interstitial to orthopyroxene oikocrysts. Rare, needle-like laths of ilmenite (.025-.05 mm) are present and occur in association with poikilitic ilmenite grains. Troilite and Fe-Ni metal occur as micron size blebs or irregularly shaped crystals also in association with poikilitic ilmenite. Irregularly shaped troilite grains may be as large as 0.25 mm.

Plagioclase clasts are present as subangular to subrounded grains (up to 0.6 mm) enclosed within and interstitial to orthopyroxene oikocrysts. The clasts are typically unfractured and rarely display twinning.

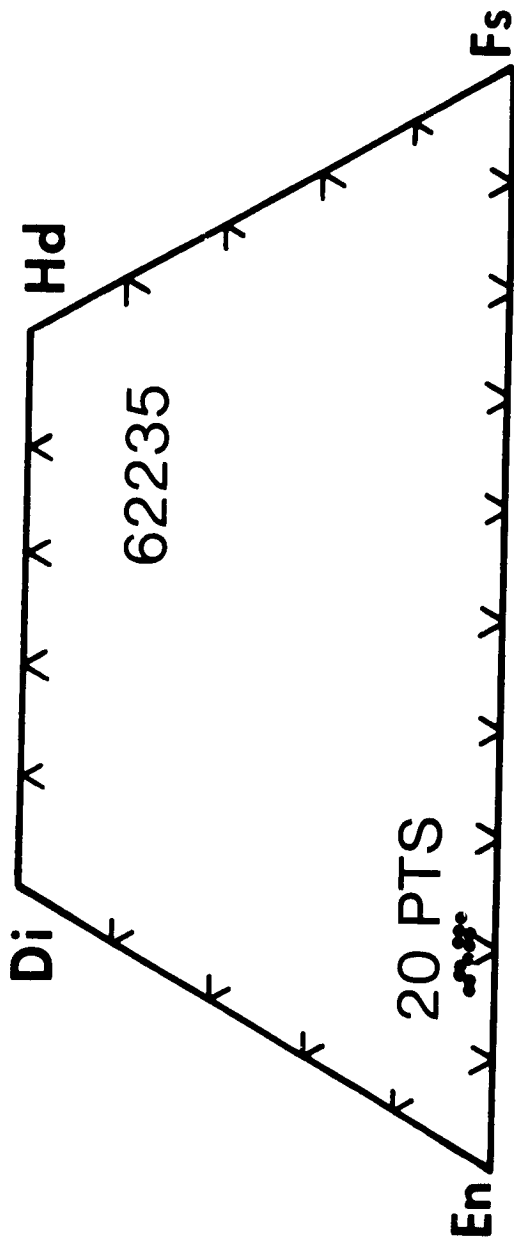
Lithic clasts constitute a small percentage (typically <10%) of the total clast population in sample 62235. Basaltic clasts are present and typically display ophitic textures. One small (0.40 mm across) anorthositic clast was observed in section 62235,39 (Figure d); no breccia clasts were observed.

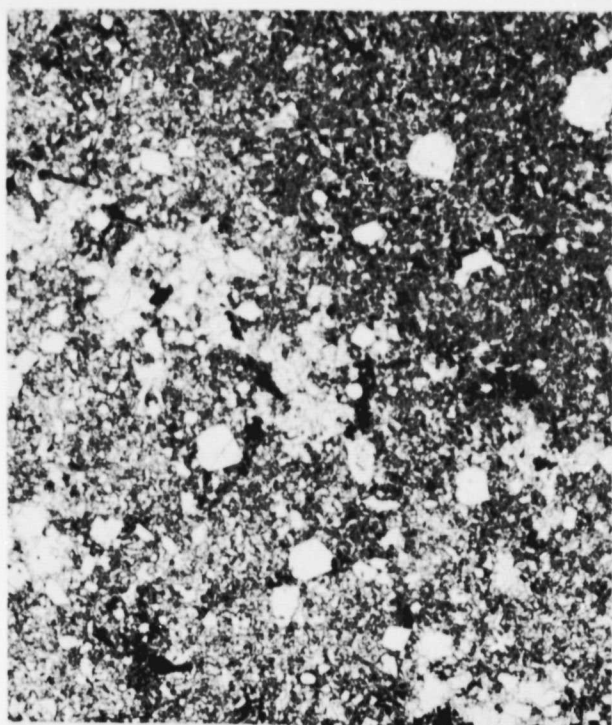
References: Warner et al. (1973); Crawford and Hollister (1974).

62235,7

MODAL ANALYSES (VOL. %) :

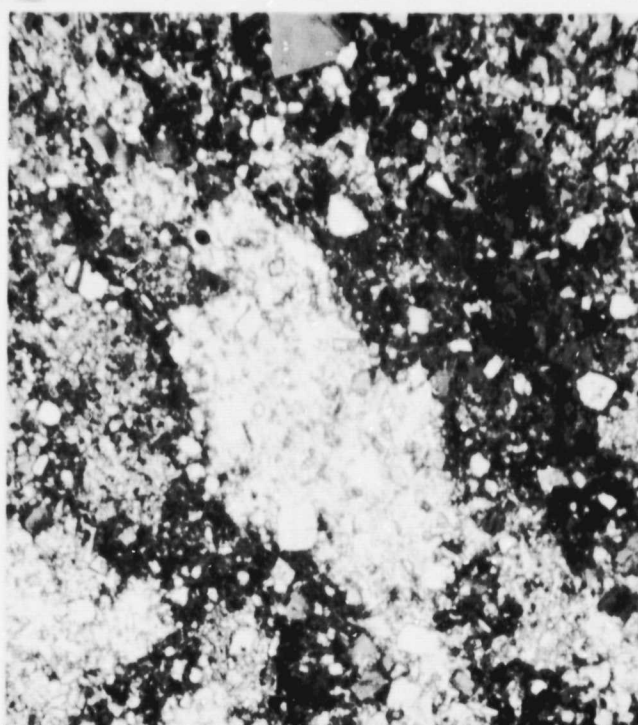
MATRIX (<39μ)	83.0
CLASTS (>39μ) :	
PLAGIOCLASE	9.1
MAFIC	—
OPAQUE	.3
HETEROGENEOUS GLASS	—
HOMOGENEOUS GLASS	—
DEVITRIFIED GLASS	—
FRAGMENTAL BRECCIA	—
CRYSTALLINE BRECCIA	—
GRANULITIC	—
OTHER METAMORPHIC	1.1
MARE BASALT	—
HIGHLAND BASALT	1.0
CRUSHED	—
PORE SPACE	5.5
OTHER	—





62235 0.5MM

a

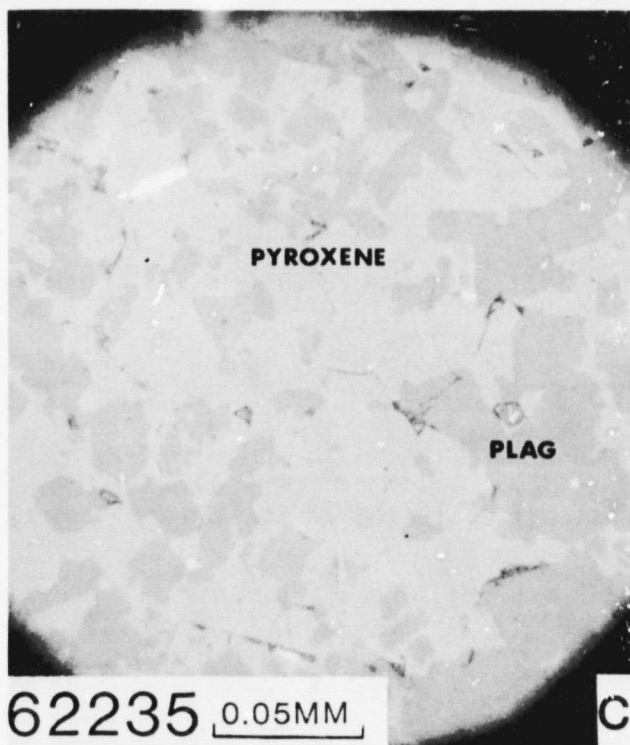


62235 0.25MM

b

Figure 62235a. Typical view of 62235; transmitted light.

Figure 62235b. Pyroxene oikocrysts; transmitted light (crossed polarizers).



62235 0.05MM

c



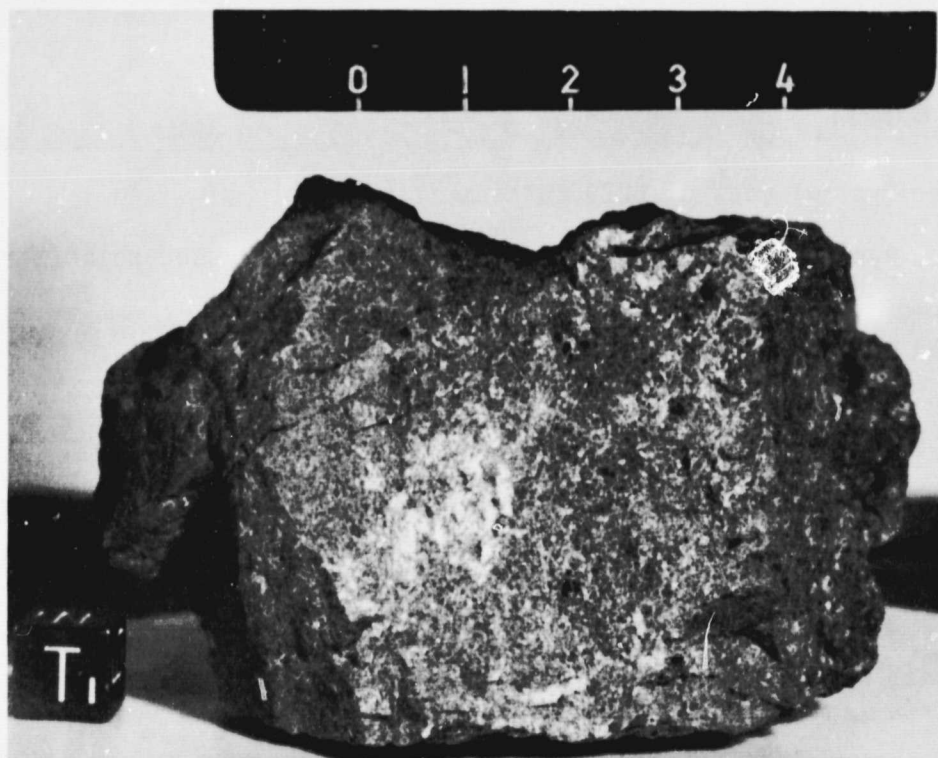
62235 0.10MM

d

Figure 62235c. Plagioclase chadacrysts (dark-grey) enclosed within pyroxene oikocrysts (light-grey); reflected light.

Figure 62235d. Anorthosite clast in 62235; transmitted light (crossed polarizers).

62295- A clast-free impact-melt breccia of unique composition and mode which is enriched in spinel and olivine relative to most highland rocks.



Sample 62295 is a grey angular rock (8.5x6.5x4 cm) collected at Station 2.

62295 CLAST-BEARING IMPACT-MELT BRECCIA

Sample 62295 is a clast-bearing impact-melt breccia characterized by randomly oriented plagioclase laths (up to 0.8 mm) intergrown with skeletal olivine crystals resulting in a variolitic texture (Figure a); interstices are filled with a complex mesostasis. Relict clasts of plagioclase (up to 1.0 mm), rare lithic clasts and conspicuous barred olivine-like bodies are scattered randomly throughout the section. Octahedra of colorless spinel (.03-.05 mm) commonly occur within plagioclase laths. Pore space is relatively common, occurring as irregularly shaped vugs (up to 0.8 mm), as angular voids enclosed by silicate minerals, and as spherical vesicles up to 0.4 mm in diameter.

Mesostasis areas in sample 62295 are characterized by complex intergrowths of feathery to acicular crystals of plagioclase, olivine and ilmenite together with brown glass (Figure b). Sub-micron size blebs of Fe-metal and troilite occur randomly in the mesostasis. Mesostasis material commonly occurs as cores within skeletal olivine and plagioclase crystals.

The chondrule-like bodies (up to 1.2 mm in diameter in 62295,75) are characterized by crystals of barred olivine with interstitial stringers of plagioclase separating the individual bars (Figure c). The plagioclase stringers rarely penetrate into the outer 20 μ m of the chondrule, giving the appearance of a narrow olivine rim around the outer edge of the sphere. The entire crystal of olivine goes to extinction at the same time and several adjoining stringers of plagioclase also go to extinction simultaneously.

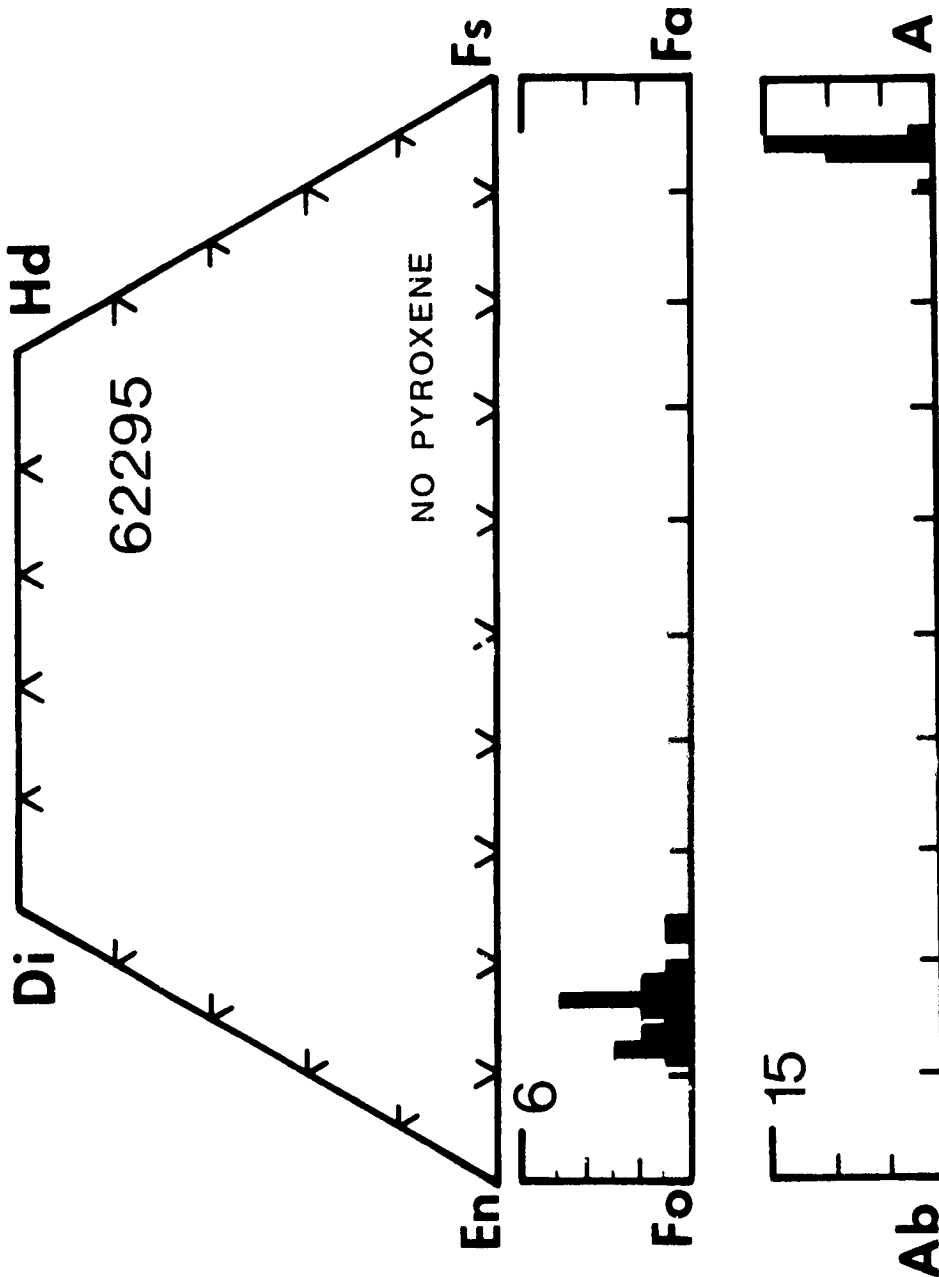
Relict clasts of plagioclase (up to 1.0 mm) occur only rarely in sample 62295. They are typically subangular and fractured; lamellae are present and possibly represent some episode of shock.

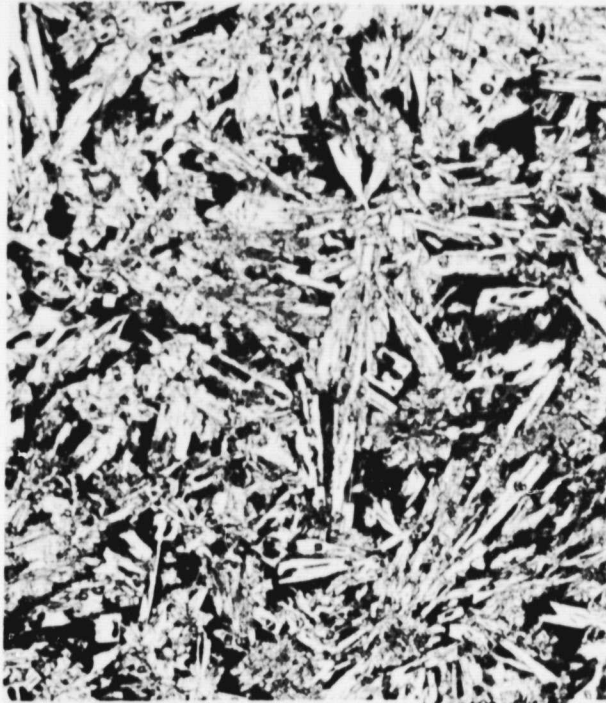
One lithic clast, a partially annealed breccia clast, was observed in section 62295,75. It is characterized by a seriate texture with clasts of plagioclase up to 0.45 mm. The clast lacks distinct boundary relations with the matrix.

References: Brown et al. (1973); Weiblen and Roedder (1973); Hodges and Kushiro (1973); Agrell et al. (1973).

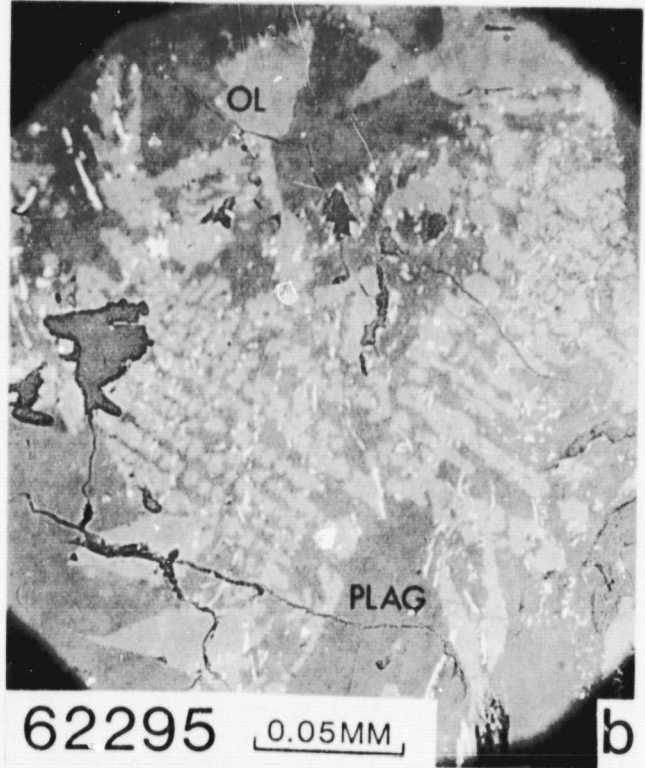
62295
MODAL ANALYSIS (VOL. %)

MATRIX (<39%)	
PLAGIOCLASE	55.0
MAFIC	26.0
OPAQUE	4.0
OTHER	15.0
CLASTS (>39%):	
PLAGIOCLASE	TR
MAFIC (chondrules)	<1.0
OPAQUE	
FRAGMENTAL BRECCIA	
CRYSTALLINE BRECCIA	TR
GRANULITIC	
OTHER METAMORPHIC	
MARE BASALT	
HIGHLAND BASALT	
CRUSHED	
PORE SPACE	





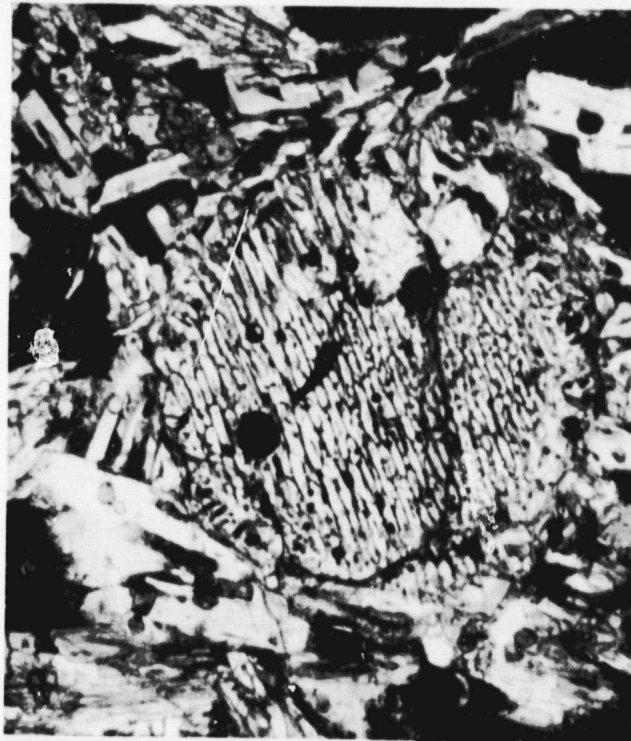
62295 0.50MM a



62295 0.05MM b

Figure 62295a. Typical view of 62295; transmitted light.

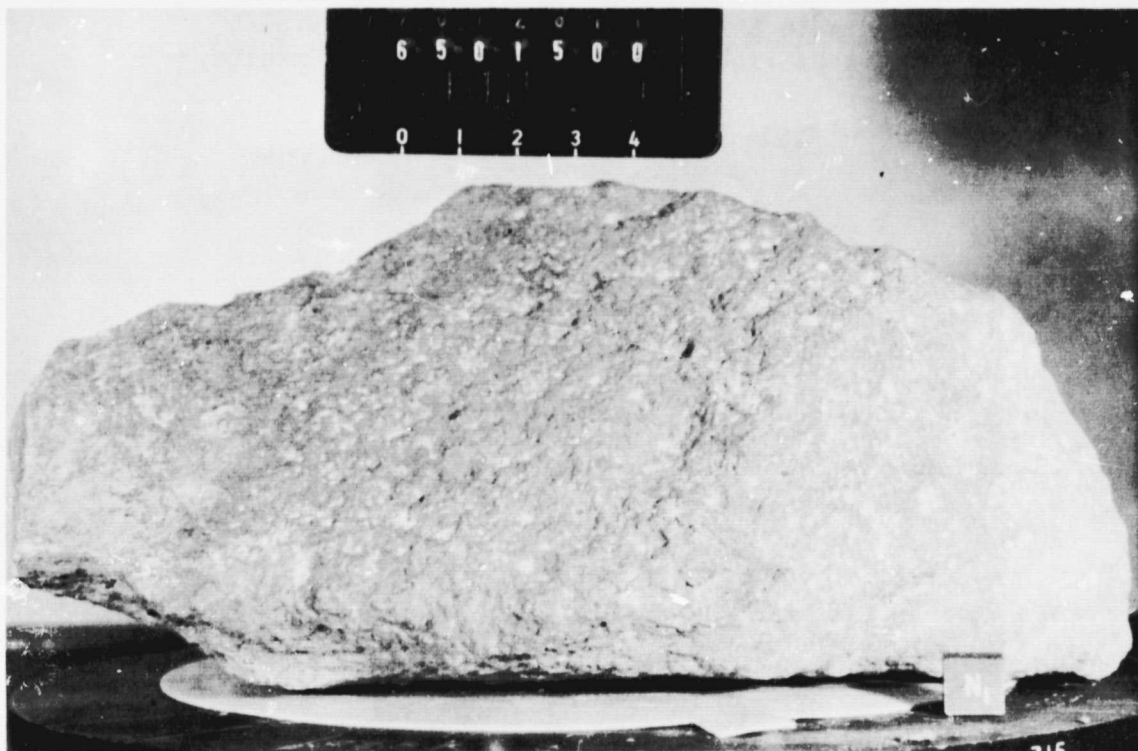
Figure 62295b. Mesostasis in 62295; reflected light. Dark-grey, plagioclase; light-grey, olivine; white, ilmenite.



62295 0.25MM c

Figure 62295c. Olivine chondrule in 62295; transmitted light.

65015- A clast-bearing impact-melt breccia with a noritic (low K KREEP) composition and a poikilitic texture.



Sample 65015 is a grey angular rock (19x9x10 cm) collected at Station 5, probably within 15 meters of the Lunar Roving Vehicle during station activities.

65015 CLAST-BEARING IMPACT-MELT BRECCIA

Sample 65015 is a clast-bearing impact-melt breccia characterized by pigeonite oikocrysts (up to 0.6 mm) which enclose numerous chadacrysts of feldspar, together with less commonly occurring chadacrysts of mafic silicates (Figure a). The inter-oikocryst region is characterized by mineral relics of feldspar, olivine, spinel and opaques together with K-rich feldspar, silica and phosphate phases. Vugs also tend to be concentrated in the inter-oikocryst regions.

Interlocking oikocrysts of pigeonite dominate section 65015,91. They typically display rounded outlines although some are distinctly rectangular in shape. Plagioclase is the most common type of chadacryst enclosed within the oikocrysts and occurs as euhedral equant crystals .04-.05 mm in size (Figure b). Chadacrysts of mafic minerals are rare; when present they occur as subrounded to rounded grains less than .05 mm across.

Inter-oikocryst regions are characterized by lath-shaped plagioclase (up to 0.06 mm.), granular olivine (up to .06 mm) and accessory ilmenite, Fe-Ni metal, troilite, phosphates and K-bearing phases. The ilmenite (0.05-0.2 mm) typically occurs as discontinuous chains composed of poikilitic plates of ilmenite (Figure c); most grains display rutile and ulvospinel lamellae. Fe-Ni metal and troilite occur as rounded and irregular blebs scattered throughout the inter-oikocryst regions. Round pores and irregular shaped vugs (0.4 to 1.0 mm) occur in the inter-oikocryst area, although the pores are not restricted to this region. Several oikocrysts were observed to have grown around the pores.

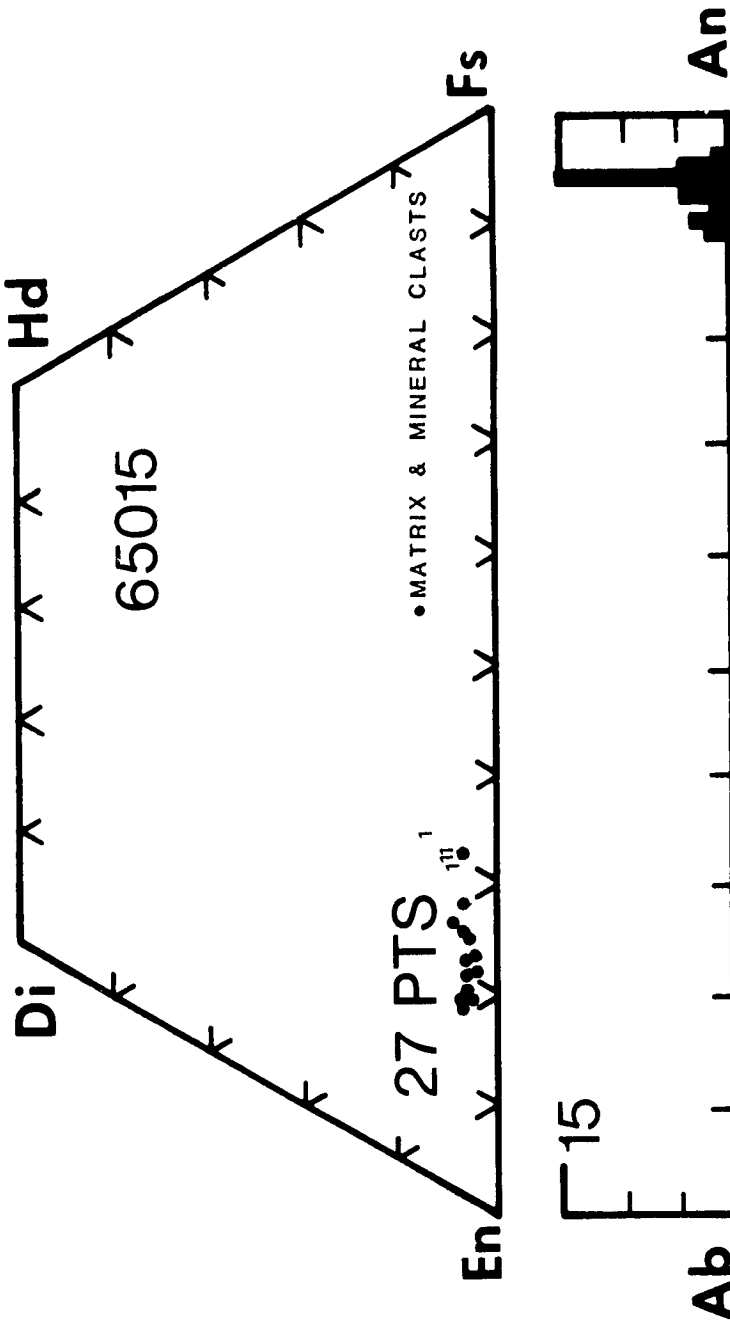
Subrounded grains of plagioclase (up to 1.5 mm) are the most abundant relic clast type in sample 65015,91. Many grains display twin lamellae and several grains are characterized by devitrification features. Overgrowth rims with compositions closely matching the matrix typically surround each plagioclase clast. Rare relics of plagioclase are enclosed within the pigeonite oikocrysts. Relics of angular olivine occur exclusively in the inter-oikocryst regions. Grains of pink-spinel are also observed in the inter-oikocrysts region and are possibly relict.

Several lithic clasts are observed in section 65015,91. One was characterized by lath-shaped plagioclase with only rare equant olivine grains. Another clast was anorthositic and displayed rounded grains of plagioclase meeting at 120° triple junctions.

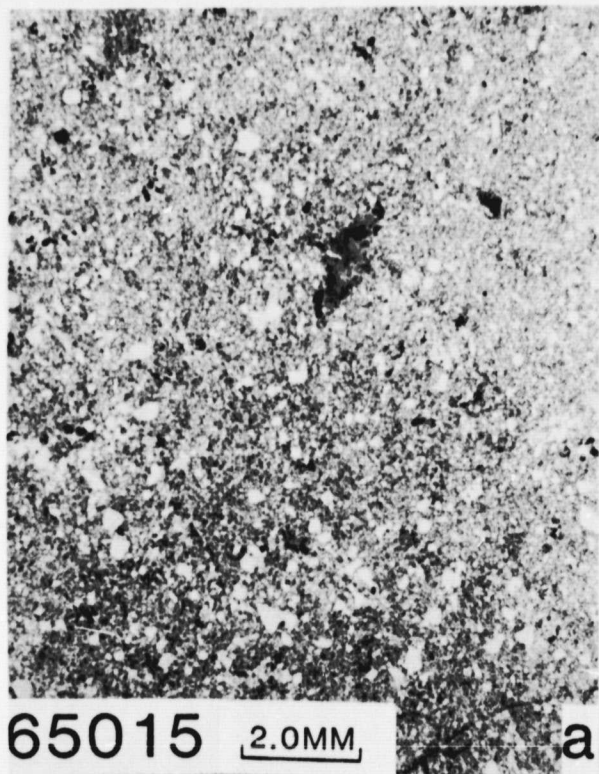
References : Simonds et al. (1973); Albee et al. (1973); Warner et al. (1973).

Age Data: Rb-Sr isochron - $3.93 \pm .02$; I_{Sr} - $.69920 \pm 3$ (Papanastassiou and Wasserburg, 1972b)

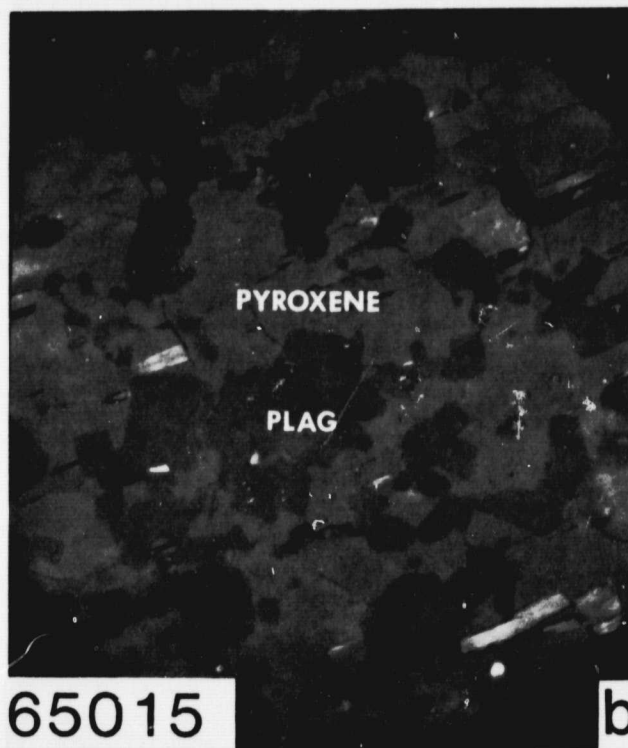
65015	
MODAL ANALYSES (VOL. %)	
MATRIX (<39 μ)	82.1
CLASTS (>39 μ):	
PLAGIOCLASE	13.8
MAFIC	.3
OPAQUE	TR
HETEROGENEOUS GLASS	—
HOMOGENEOUS GLASS	—
DEVITRIFIED GLASS	—
FRAGMENTAL BRECCIA	—
CRYSTALLINE BRECCIA	—
GRANULITIC	—
OTHER METAMORPHIC	—
MARE BASALT	.40
HIGHLAND BASALT	—
CRUSHED	—
PORE SPACE	3.1
OTHER	—



REFLECTED LIGHT

65015 2.0MM

a

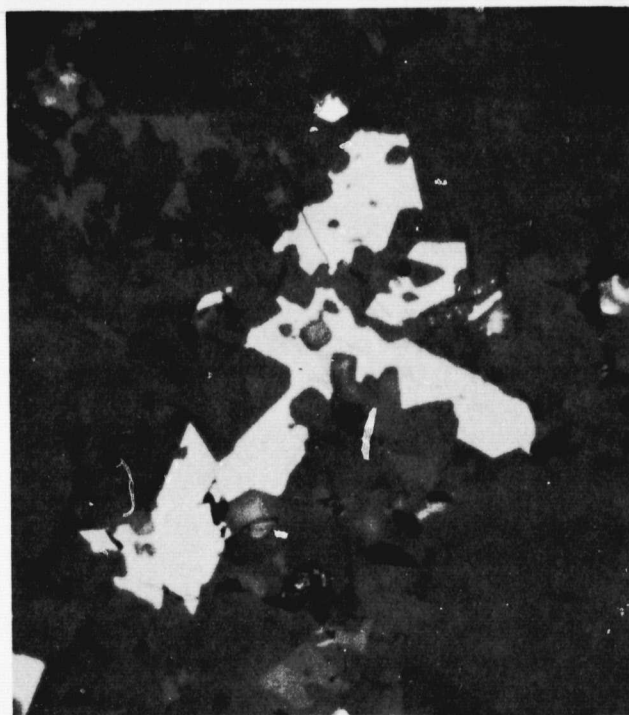


65015

b

Figure 65015a. Typical view of 65015; transmitted light.

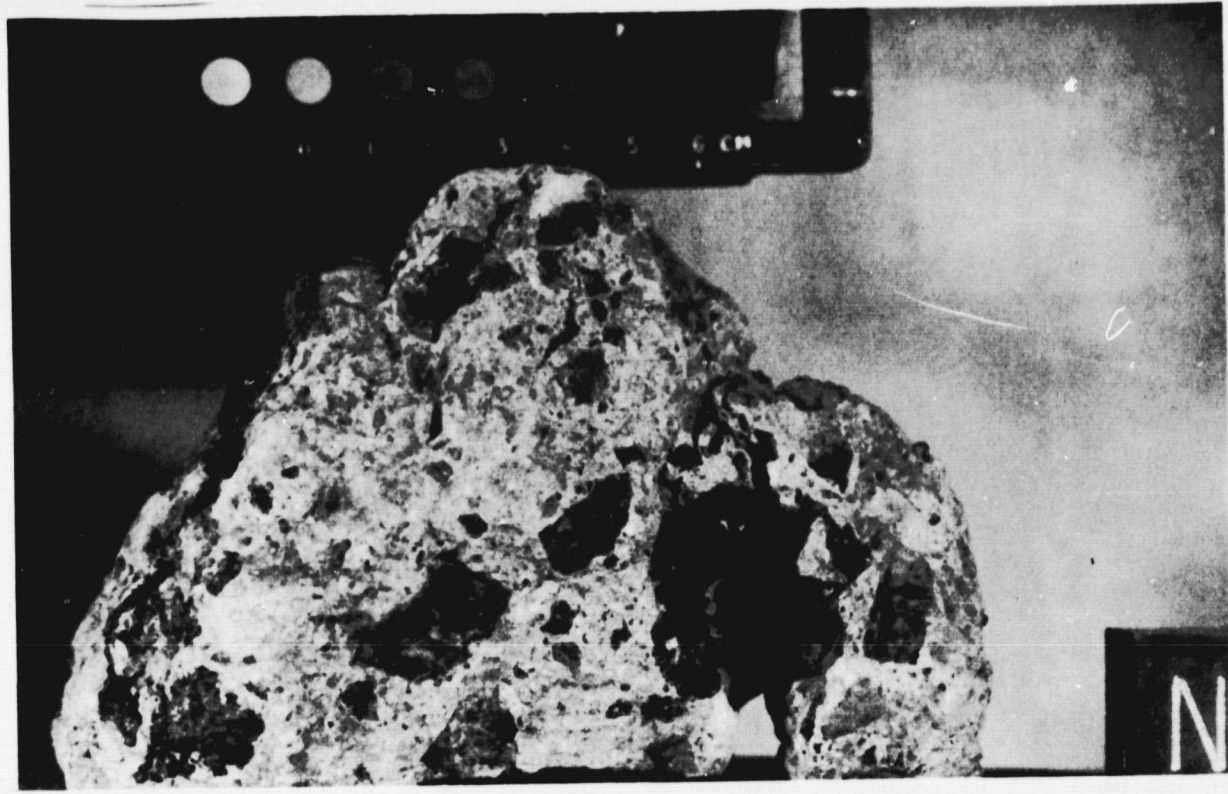
Figure 65015b. Plagioclase chadacrysts (dark-grey) in pyroxene oikocrysts (light-grey); reflected light.

65015 0.05 MM

c

Figure 65015c. Poikilitic ilmenite (white) in 65015; reflected light; color key same as in (b).

67015- One of a number of friable polymict breccias with a highly feldspathic matrix found in abundance on the rim of North Ray crater. Ar³⁹/Ar⁴⁰ analyses of these rocks suggest that they may be older than other breccias.



Sample 67015 is a white to light grey sub-angular rock (13x10x8 cm) collected at Station 11, probably 30 to 40 meters south-southwest of the lunar module Y footpad.

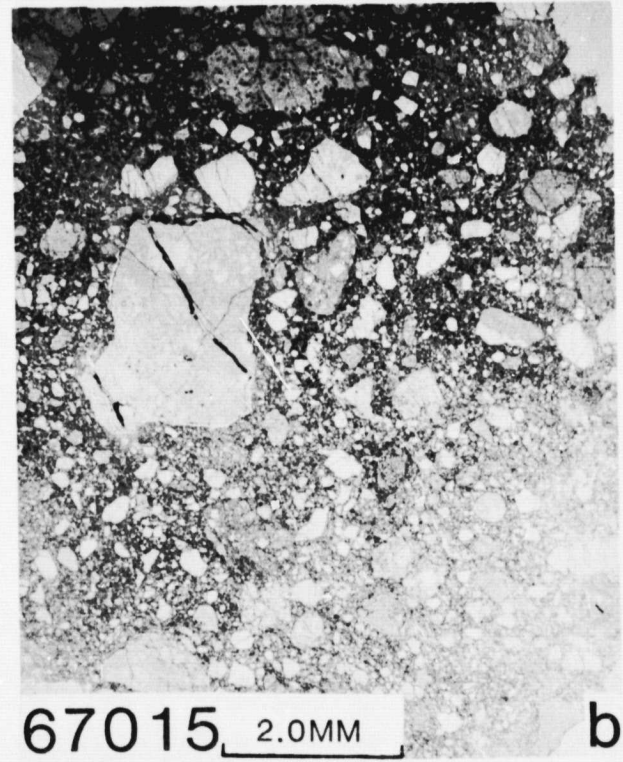
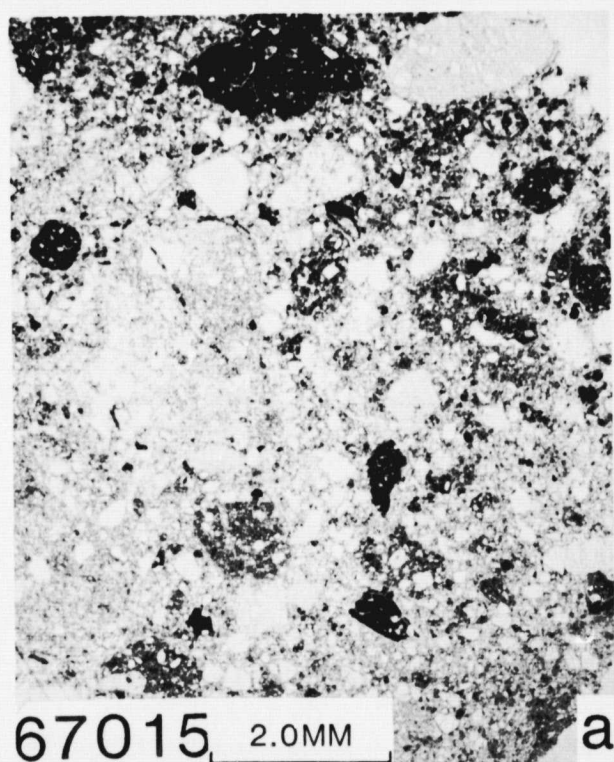


Figure 67015a. Typical view of 67015; transmitted light.

Figure 67015b. Same view as (a); reflected light.

67015 LIGHT-MATRIX BRECCIA

Sample 67015 is a light-matrix breccia characterized by mineral, lithic and glass clasts contained in an unrecrystallized matrix of mineral grains, (predominantly plagioclase, with minor mafic and opaque minerals) and orange-brown glass (Figures a and b); spinel grains are observed in the matrix of 67015,74 but are relatively rare. The texture of 67015 is seriate with components ranging in size from the limit of resolution up to 1.5 mm. Sample 67015 is porous, with micron-size intergranular voids which may be viewed in reflected light at a high (400X) magnification. Pore space is also present as non-connecting veinlets (10-25 μm wide) and as rare, irregularly shaped vugs.

Glass clasts in section 67015,74 are rare and are typically orange-brown in color and partially to completely devitrified. One large (0.45 mm across) round clast was observed which contained anhedral crystals of plagioclase and pyroxene (Figure c).

The mineral clast population is dominated by plagioclase clasts (95%). They range from rounded to angular in outline (up to 0.6 mm) and are typically unfractured and lack mineral inclusions. No overgrowths are observed around clasts. Rare clasts display interdigitating contacts with the matrix but the majority of clasts display sharp contacts. Mafic clasts are commonly rounded in outline and rarely exceed 0.50 mm in size; they are typically unfractured. Ilmenite is the most commonly occurring opaque mineral clast and is present as irregularly shaped grains typically less than 25 μm in size. Two small (less than 30 μm) pink spinel grains were observed in section 67015,74.

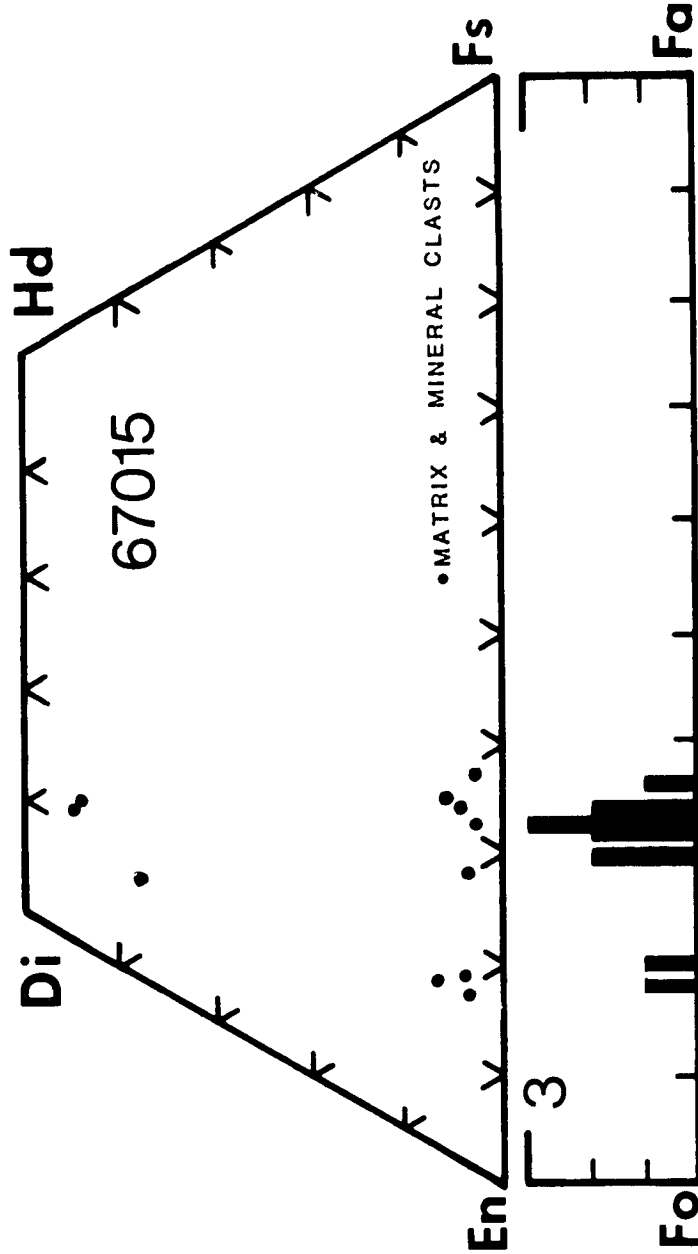
The most common lithic clast type in section 67015,74 is a crystalline matrix breccia characterized by mineral clasts (mainly plagioclase) and only rare lithic clasts in a matrix of plagioclase and pyroxene grains (Figure d). Vitric matrix breccia clasts are also common and typically occur as rounded or ovoid shapes (Figure e) up to 1.4 mm across. Clasts of anorthosite (0.3 mm) are present and are characterized by polygonal grains of plagioclase which meet at 120° triple junctions. Several large (0.9 mm) clasts of cataclastic anorthosite and gabbroic anorthosite are also present. One clast in section 67015,74 with 0.20 mm plagioclase and minor interstitial mafic grains and mesostasis is similar to sample 68415 (described in this volume). A unique clast in section 67015,74 is composed of plagioclase and opaque mineral laths, together with anhedral mafic grains contained in a brown glassy matrix.

References: Warner et al. (1973); Delano et al. (1973).

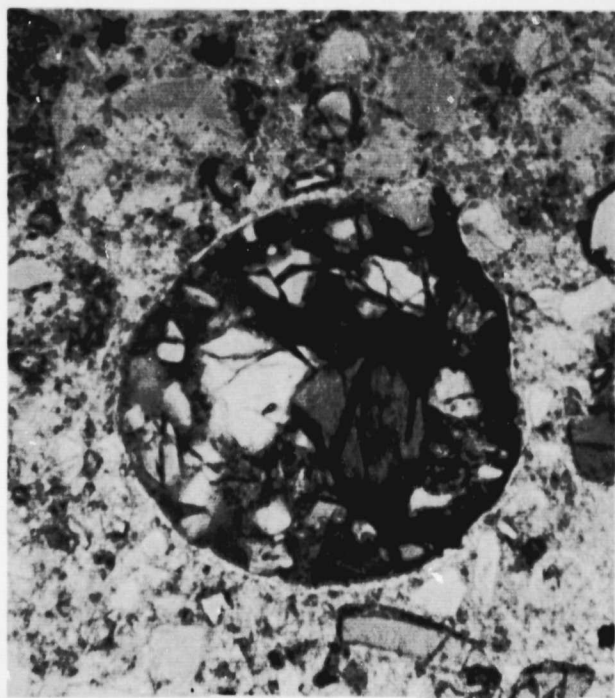
67015

MODAL ANALYSES (VOL. %)

MATRIX (<39.1):	55.35
CLASTS (>39.1):	
PLAGIOCLASE	12.39
MAFIC	.50
OPAQUE	—
HETEROGENEOUS GLASS	—
HOMOGENEOUS GLASS	—
DEVITRIFIED GLASS	TR
FRAGMENTAL BRECCIA	4.77
CRYSTALLINE BRECCIA	17.04
GRANULITIC (anorthosite)	2.80
OTHER METAMORPHIC (gabbroic anorthosite)	7.13
MARE BASALT	—
HIGHLAND BASALT	—
CRUSHED	—
PORE SPACE	—
OTHER	—

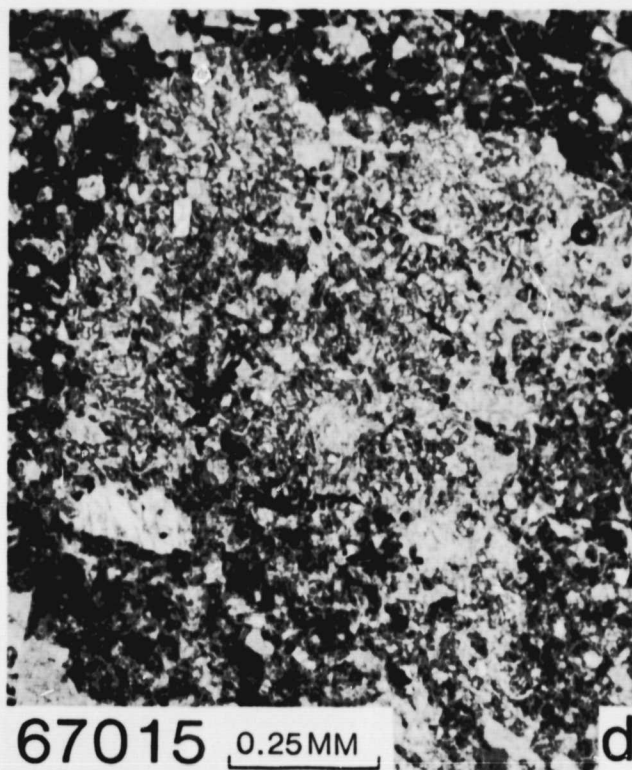


REFLECTED LIGHT



67015 0.10MM

c

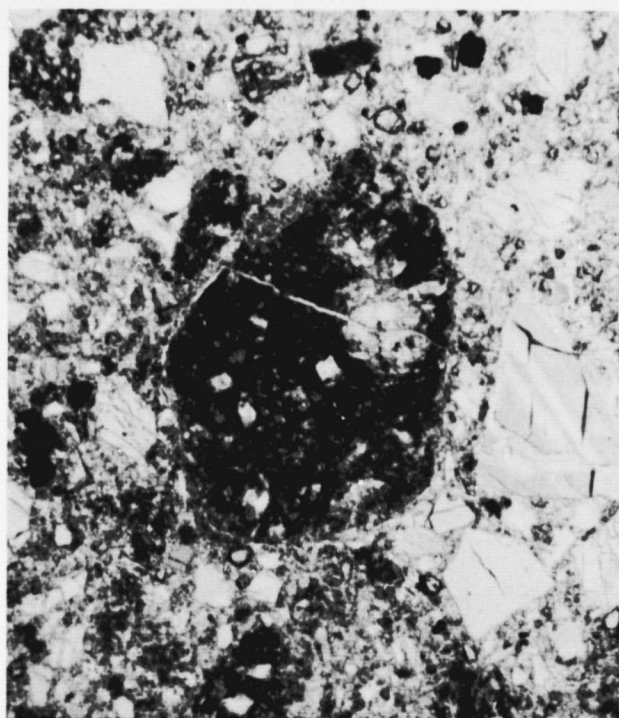


67015 0.25MM

d

Figure 67015c. Glass clast with enclosed plagioclase and pyroxene grains; transmitted light.

Figure 67015d. Crystalline matrix breccia in 67015; transmitted light.

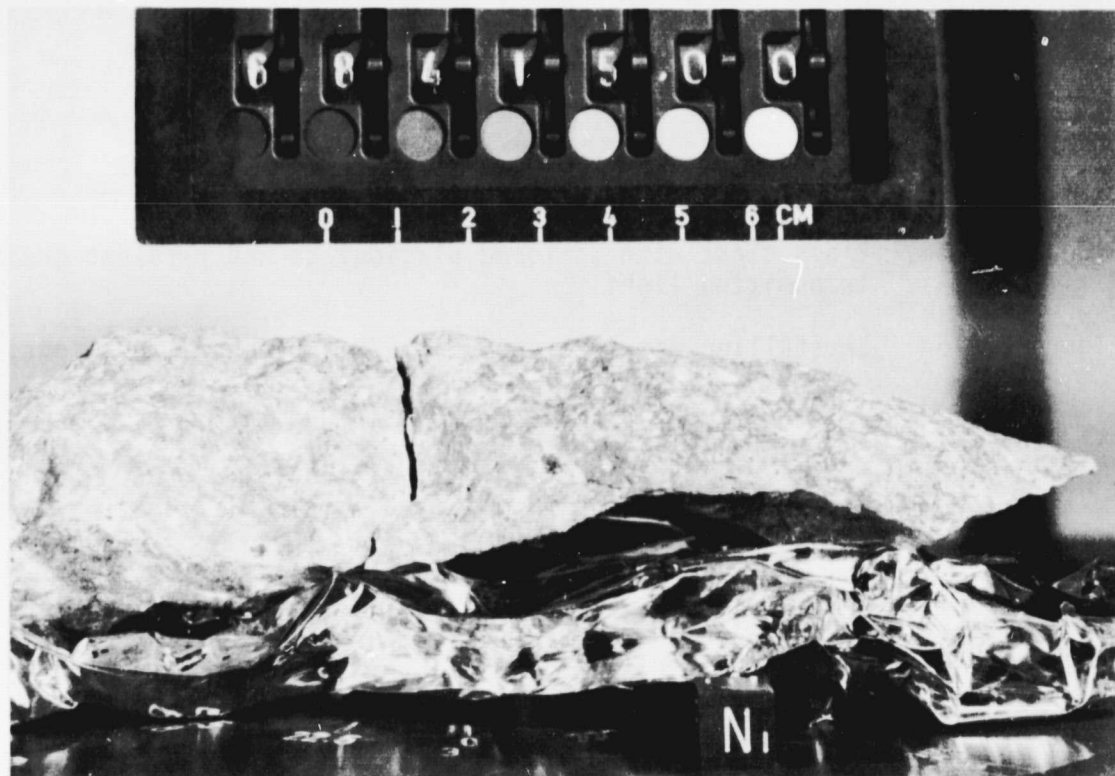


67015 0.25MM

e

Figure 67015e. Vitric matrix breccia clast; transmitted light.

68415- A clast-free impact-melt breccia with a more feldspathic composition than most impact melts. The 3.84 AE crystallization age is one of the youngest for impact-melt rocks from the highlands.



Sample 68415 is a light-grey to white subrounded rock (10x2x3.5 cm) collected at Station 8 on a bright-ray from South Ray crater. The rock was collected near two 15 to 20 meter craters, 2.8 kilometers south-southwest of the lunar module.

68415 CLAST-FREE IMPACT-MELT BRECCIA

Sample 68415 is a clast-free impact melt breccia with an igneous texture characterized by randomly oriented plagioclase laths with interstitial olivine and pyroxene and minor occurrences of opaques, phosphates and granitic glass (Figure a). Discrete grains of anhedral plagioclase (0.4-1.5 mm) and polycrystalline aggregates of anhedral plagioclase grains (up to several millimeters occur rarely throughout the sample and are interpreted as xenocrysts). Pore space is rare; when present it occurs as irregularly shaped voids bounded by plagioclase grains.

Lath-shaped plagioclase dominates the sample and accounts for approximately 75% of the mode. It is characteristically highly twinned and occurs as subhedral to euhedral laths ranging from 0.10 millimeters to several millimeters in length (Figure b); average plagioclase lengths range from 0.20 to 0.40 millimeters. Plagioclase laths are typically normally zoned with compositions ranging from An_{98} to An_{71} (Helz and Appleman, 1973). The larger laths (several millimeters) rarely display reverse zoning. Smaller laths (0.20-0.40 mm) may be strongly zoned (An_{94} - An_{77}) or may have sodic compositions throughout.

The large anhedral xenocrysts display poorly-developed twinning which is commonly distorted or offset by fracturing; many grains display undulatory extinction. The xenocrysts have calcic compositions and are virtually unzoned.

Interstitial minerals include olivine and pyroxene which occur as anhedral, irregular grains (0.1 up to 1.0 mm) between plagioclase laths. The grains are typically discrete with pyroxene and olivine rarely intergrown. Olivine is never found in association with potassic granitic residual glass. Pyroxene crystals display complex zoning trends and commonly have orthopyroxene cores and pigeonite rims. The crystals lack exsolution lamellae and are typically fractured.

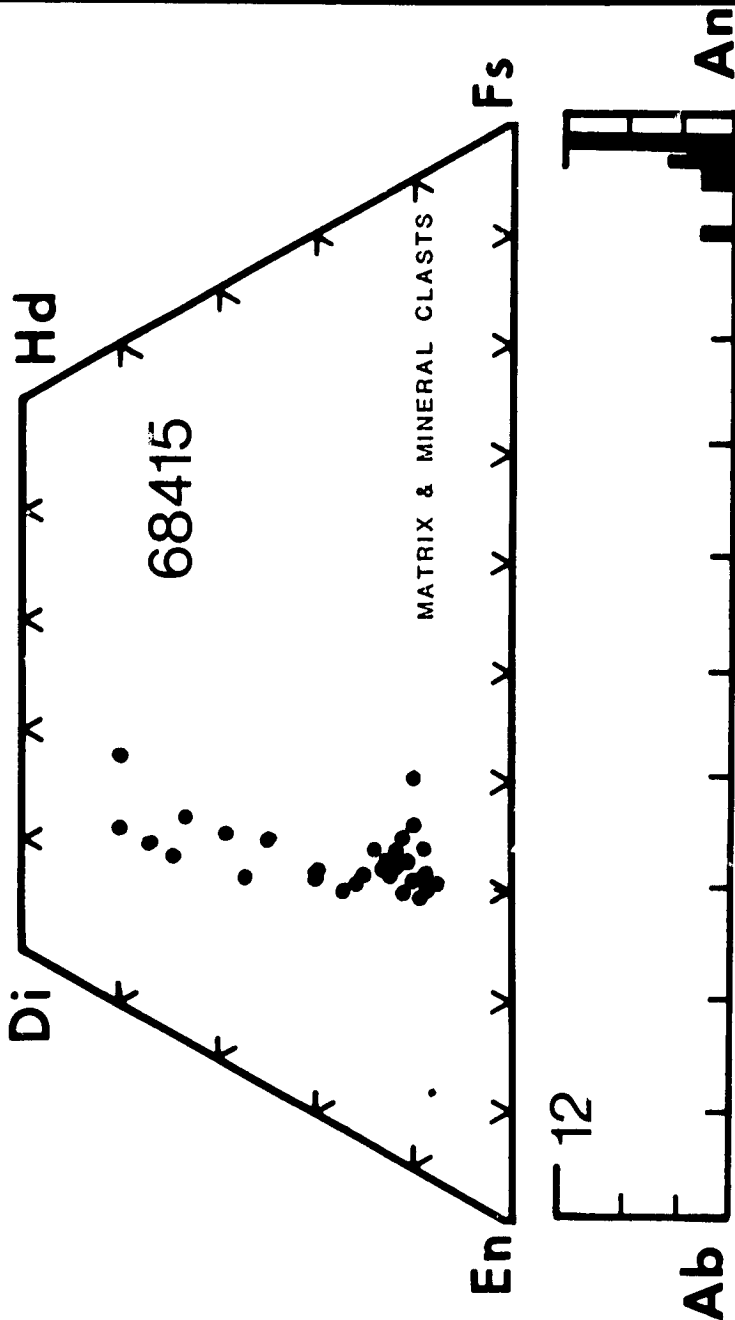
Ilmenite is the most abundant opaque phase in sample 68415 and occurs as irregularly-shaped grains in association with the residual glass phase. Other opaques include troilite and Fe-Ni metal which occur intergrown together or as discrete micron-size blebs in association with the glassy mesostasis. Patches of residual granitic glass (Figure c) are common and occur interstitial to plagioclase laths. The glassy patches commonly contain the opaque phases discussed above together with apatite and Fe-rich pigeonites.

References: Helz and Appleman (1973); Walker et al. (1973); Meyer et al. (1974); Gancarz et al. (1972)

Age Data: Rb-Sr isochron - $3.84 \pm .01$; $I_{Sr} - 7003 \pm 2$ (Papanastassiou and Wasserbarg, 1972a)

68415
MODAL ANALYSIS(VOL. %)

MATRIX (<39%)	80.0
PLAGIOCLASE	17.0
MAFIC	TR
OPAQUE	2.0
OTHER(mesostasis)	<1.0
CLASTS (>39%):	
PLAGIOCLASE	
MAFIC	
OPAQUE	
FRAGMENTAL BRECCIA	
CRYSTALLINE BRECCIA	
GRANULITIC	
OTHER METAMORPHIC	
MARE BASALT	
HIGHLAND BASALT	
CRUSHED	
PORE SPACE	



REFLECTED LIGHT



68415 0.50MM

a

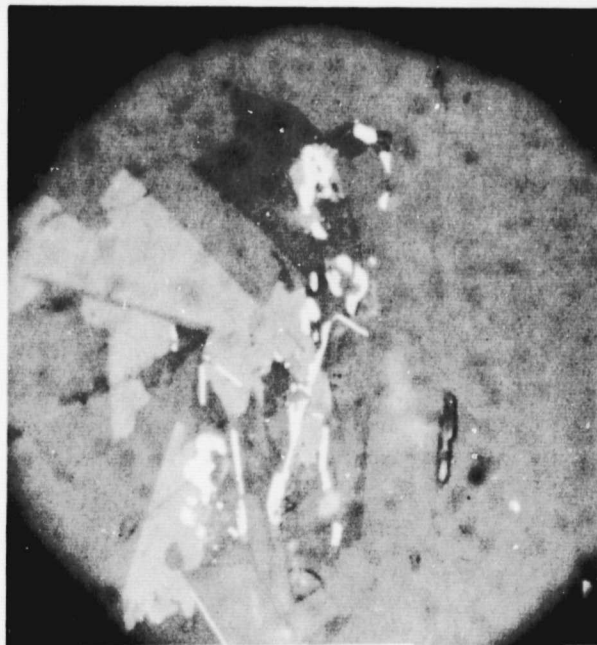


68415 0.50MM

b

Figure 68415a. Typical view of 68415; transmitted light (crossed polarizers).

Figure 68415b. Plagioclase laths in 68415; transmitted light (crossed polarizers).



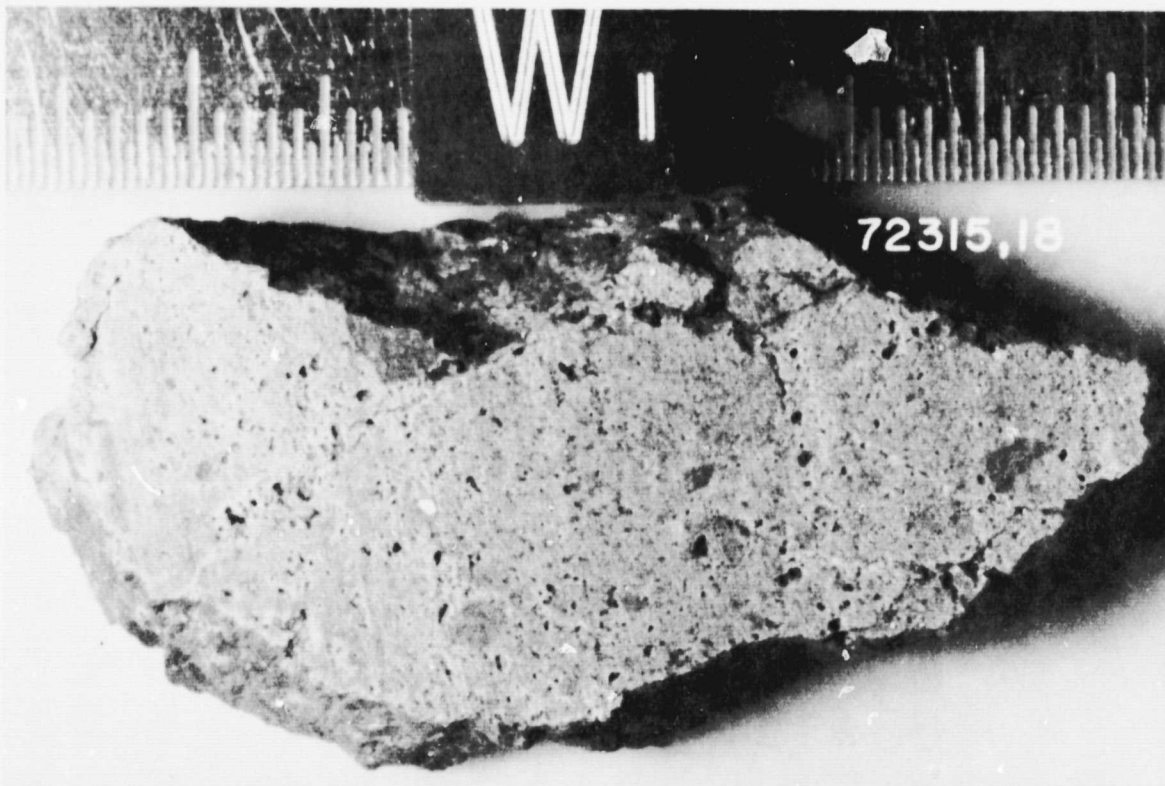
68415 0.05MM

c

Figure 68415c. Mesostasis in matrix; reflected light.



72315- A clast-bearing impact-melt breccia which is compositionally similar to rocks from both the North and South Massif at Apollo 17 but which displays a slightly different texture from other rocks in the suite. The rocks may have been produced by the Serenitatis impact.



Sample 72315 is a light-grey angular rock (10x5.5x2 cm) collected from a 2 meter boulder on the lower slopes of South Massif.

72315 CLAST-BEARING IMPACT-MELT BRECCIA

Sample 72315 is a clast-bearing impact-melt breccia texturally transitional between the Apollo 17 clast-bearing impact-melts and the Apollo 14 clast-rich impact-melts. Although plagioclase in the matrix occurs rarely as lath-shaped grains which may be intergrown with pyroxene to form ophitic-textured zones, the grains commonly display an anhedral morphology so that an ophitic texture does not persist throughout the matrix. The matrix texture is more commonly characterized by a mosaic of anhedral interlocking grains of plagioclase, pyroxene, and olivine with randomly occurring poorly-developed pyroxene oikocrysts (Figure a). Pyroxene oikocrysts rarely exceed 0.2 mm in length and enclose plagioclase tablets .015-.025 mm in size. Ilmenite is the dominant opaque phase in the matrix and occurs as irregularly shaped, embayed crystals (0.1-0.5 mm) with sieve texture (Figure b). Rutile and ulvospinel lamellae and rounded inclusions of armalcolite are commonly observed in the ilmenite grains. Troilite and native iron occur as aggregates of micron size blebs in the matrix. Pore space is common in sample 72315 and occurs as irregularly-shaped vugs (up to 0.6 mm) some of which outline large lithic clasts. Isolated areas in the matrix appear to display an alignment of vugs but the overall sample displays no such alignment.

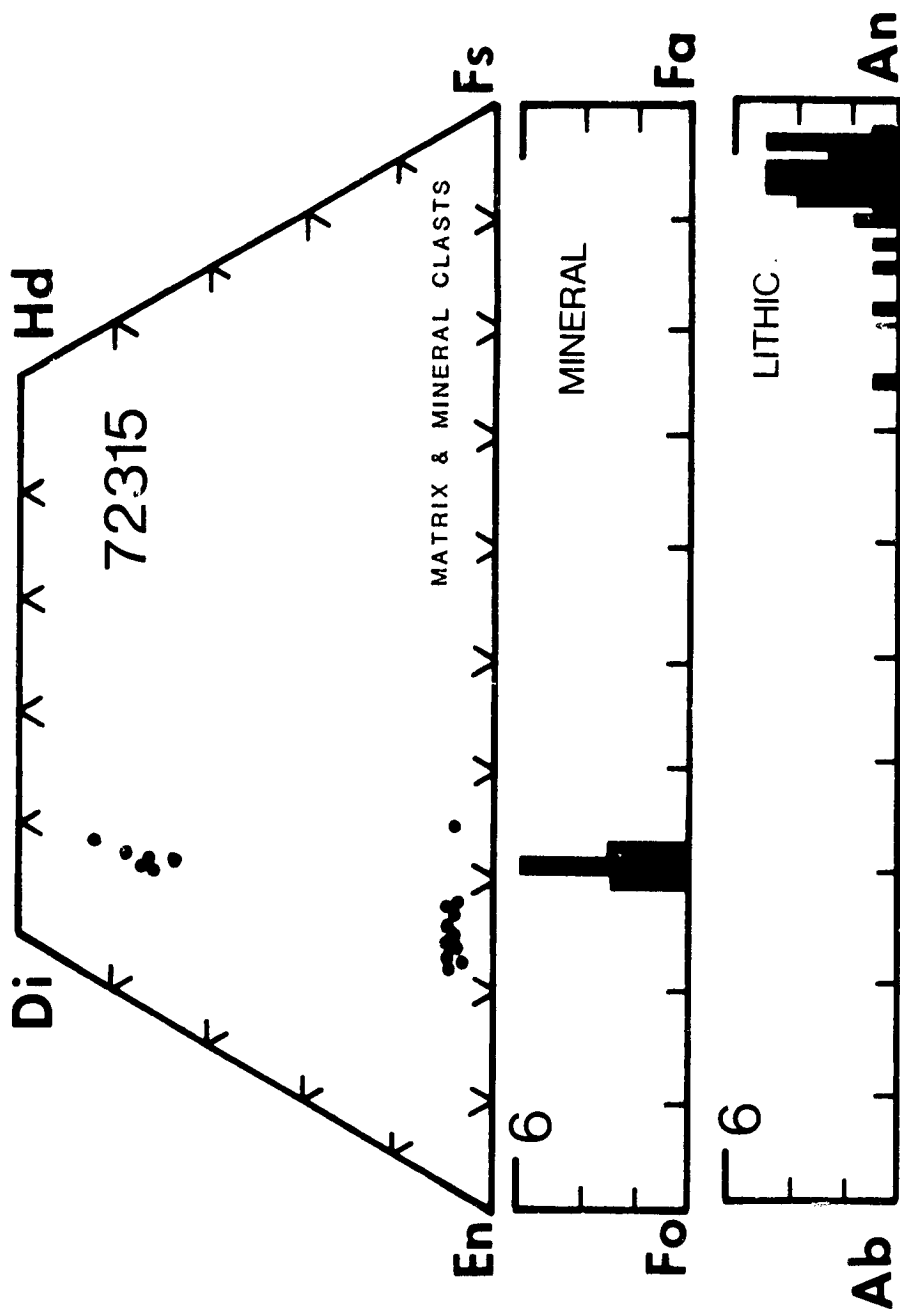
Mineral clasts in 72315 include plagioclase, olivine, pyroxene, opaques and rare pink spinel clasts. Plagioclase clasts are typically subangular (up to 0.6 mm) and commonly display features indicative of shock including fractures, undulatory extinction and anisotropy. Several grains display a flame texture, possibly the result of maskelynite devitrification. Overgrowth rims (15-20 μm) occur on many of the clasts and may or may not be associated with an olivine "necklace". Olivine clasts are both angular and rounded (up to 0.5 mm) and many display zoning. Although most olivine grains are inclusion free, several display a clouded appearance due to sub-micron size inclusions of opaques. Clasts of pyroxene are rounded to subrounded (up to 0.2 mm) and many display rims composed of intergrowths of plagioclase and pyroxene. Many pyroxene clasts are clouded by sub-micron size inclusions of opaque phases, typically native iron. Ilmenite occurs as ameboid-shaped grains (up to 0.4 mm) which may be mineral clasts.

Lithic clasts in sample 72315 are representative of the DANT suite (described by Bence et al. 1974) which include dunites, anorthosites, norites and troctolites. Small clasts (0.1-0.2 mm) of anorthosite are relatively common (Figure c) and display subhedral grains of plagioclase which meet at 120° triple junctions. One igneous-textured spinel troctolite clast (1.5 mm long) was observed in section 72315,78. It consists of subhedral to anhedral olivine grains intergrown with laths of plagioclase. Spinel occurs as aggregates of pink grains (5-20 μm) enclosed within plagioclase grains. The largest lithic clast in section 72315,78 is a 4.0 mm feldspathic norite with poikilitic pyroxene (Figure d).

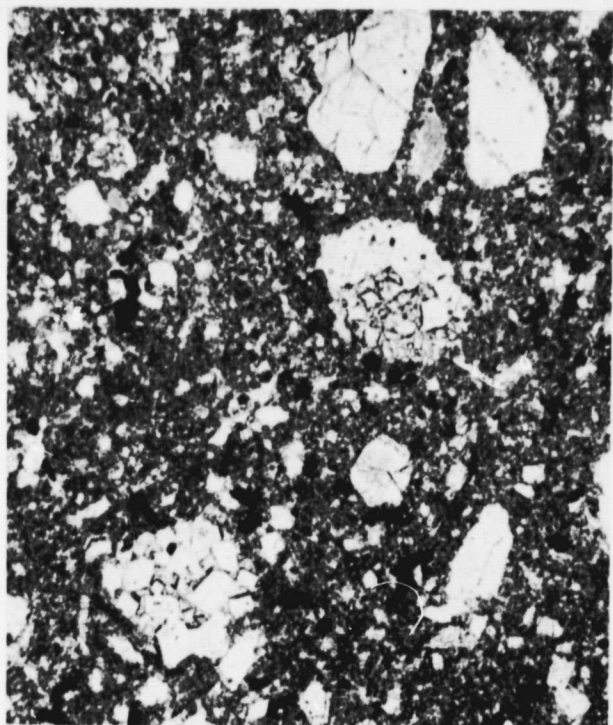
References: Simonds et al. (1974); Wilshire (LPSET, 1973); Dymek et al. (1976)

72315
MODAL ANALYSES (VOL. %)

MATRIX (<39%):	80.0
CLASTS (>39%):	
PLAGIOCLASE	14.0
MAFIC	1.0
OPAQUE	TR
HETEROGENEOUS GLASS	
HOMOGENEOUS GLASS	
DEVITRIFIED GLASS	
FRAGMENTAL BRECCIA	
CRYSTALLINE BRECCIA	
GRANULITIC	
OTHER METAMORPHIC	5.0
MARE BASALT	
HIGHLAND BASALT	
CRUSHED	
PORE SPACE	
OTHER (spinel)	TR

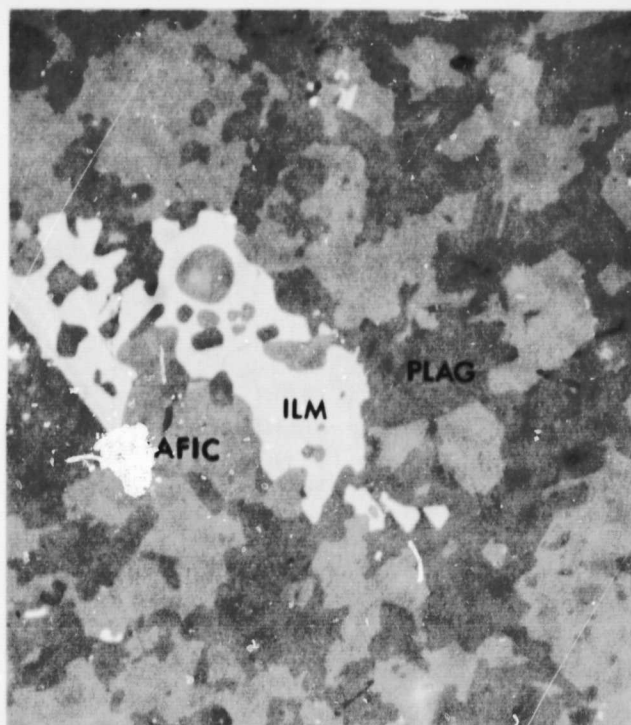


REFLECTED LIGHT



72315 1.00MM

a



72315 0.05MM

b

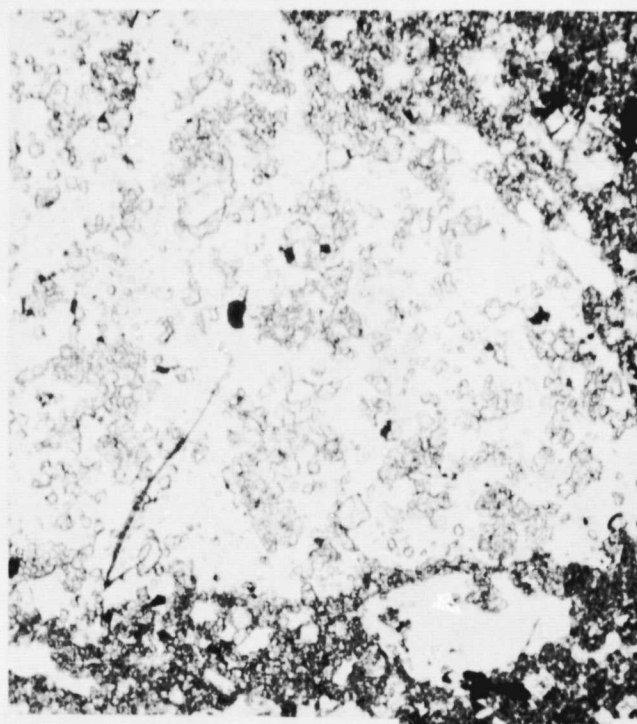
Figure 72315a. Typical view of 72315; transmitted light.

Figure 72315b. Ilmenite grain with sieve texture; reflected light.
Dark-grey, plagioclase; light-grey, mafics; white, ilmenite.



72315 0.10MM

c



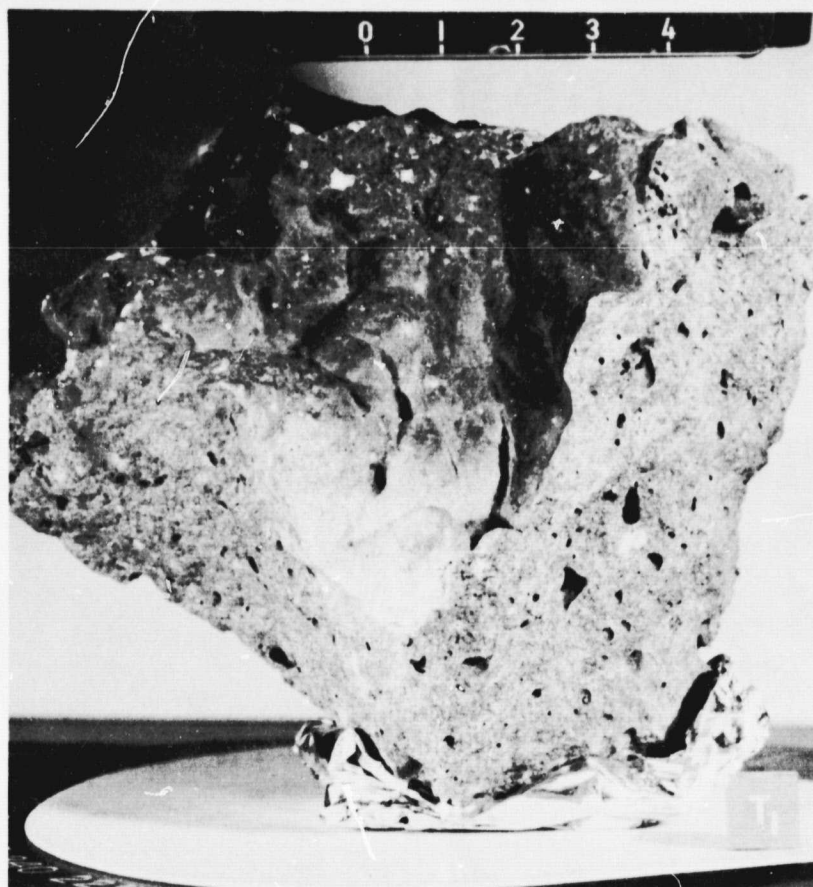
72315 0.5MM

d

Figure 72315c. Recrystallized plagioclase clast; transmitted light.

Figure 72315d. Feldspathic nortie clast; transmitted light.

Sample 76215 is a light-grey angular rock (10.5x8x6 cm) broken from a block adjacent to and probably spalled from a boulder at Station 6. The boulder was fourth downhill in a group of five boulders located 10 meters east of the lunar roving vehicle.



76215 CLAST-BEARING IMPACT-MELT BRECCIA

Sample 76215 is a clast-bearing impact-melt breccia characterized by two distinct matrix textures — both poikilitic and ophitic — which display sharp boundary relationships (Figure a). Over 90% of the matrix is poikilitic (Figure b) and consists of a network of coalescing pigeonite and augite oikocrysts (0.5-2.0 mm) which enclose abundant tabular feldspar chadacrysts (10-30 μm). Isolated regions with ophitic textures, similar to but finer-grained than sample 14310 (included in this publication) occur less commonly and are interpreted as textural variations within the matrix and not as clasts. They are characterized by ophitic intergrowths of euhedral plagioclase (0.25-0.35 mm) and anhedral to subhedral pyroxene (0.20-0.80 mm) (Figure c). Compositionally the two regions are the same and the mineral chemistries are approximately equivalent. Round, smooth walled vesicles (0.5 mm up to several millimeters) are common in the poikilitic regions; vugs with irregular outlines (typically bounded by feldspar grains) occur between the oikocrysts.

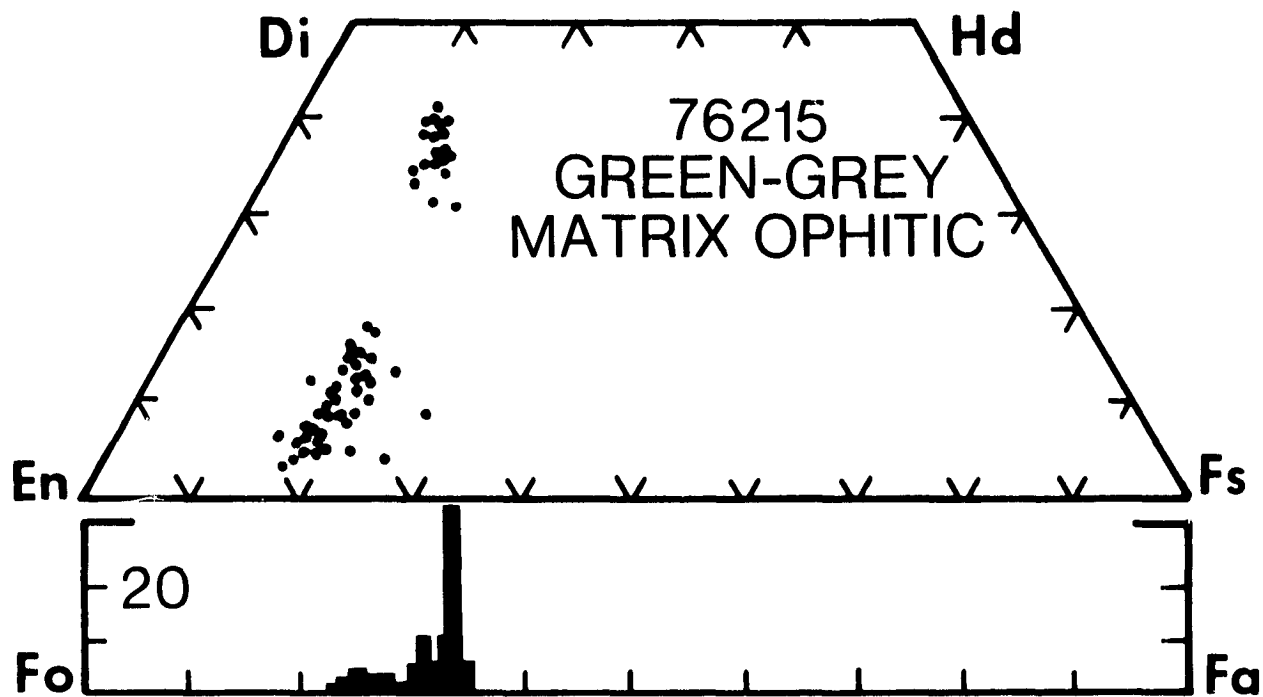
Mineral and lithic clast populations differ between the two textural regions with the majority of clasts concentrated in the poikilitic region. Plagioclase clasts in the poikilitic region are typically unshocked and display 10 μm -wide overgrowths (Figure d) with chemical compositions which match matrix plagioclase grains and differ from the core.

Plagioclase clasts in the ophitic regions are also shock free and have overgrowths up to 30 μm thick. In these clasts however the cores of the grains have compositions which match that of the matrix grains. The only mafic clasts present in the ophitic region are rare olivine clasts (100 μm) with nearly equant morphologies. Both pyroxene and olivine are present in the poikilitic regions but pyroxene is rare. Olivine occurs as anhedral grains typically less than 100 μm across although some grains may be as large as 0.45 mm.

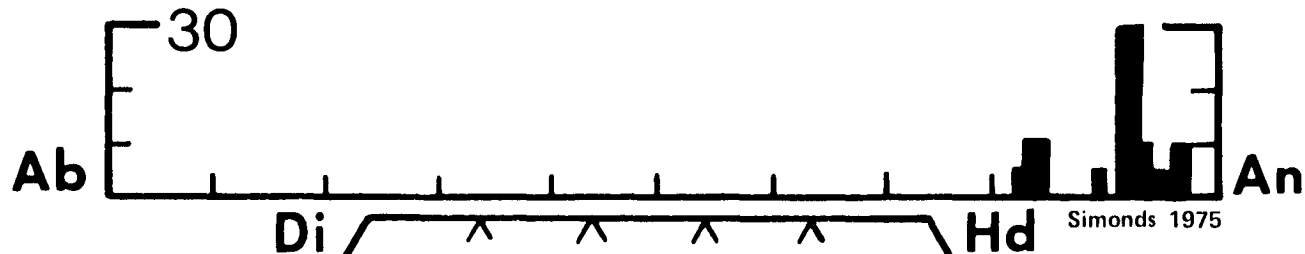
Lithic clasts were not observed in the ophitic textured lithology of sample 76215. Lithic clasts in the poikilitic region include a cm-size anorthosite clast in section 76215,70 (Figure e) displaying polygonal feldspar grains up to 2.0 mm across and a smaller (0.3 mm) anorthosite clast with 120° triple junctions. The dunite clast described by Simonds (1975) was not observed in any sections of 76215 described by the author.

References: Simonds et al. (1974); Simonds (1975); Onorato et al. (1976).

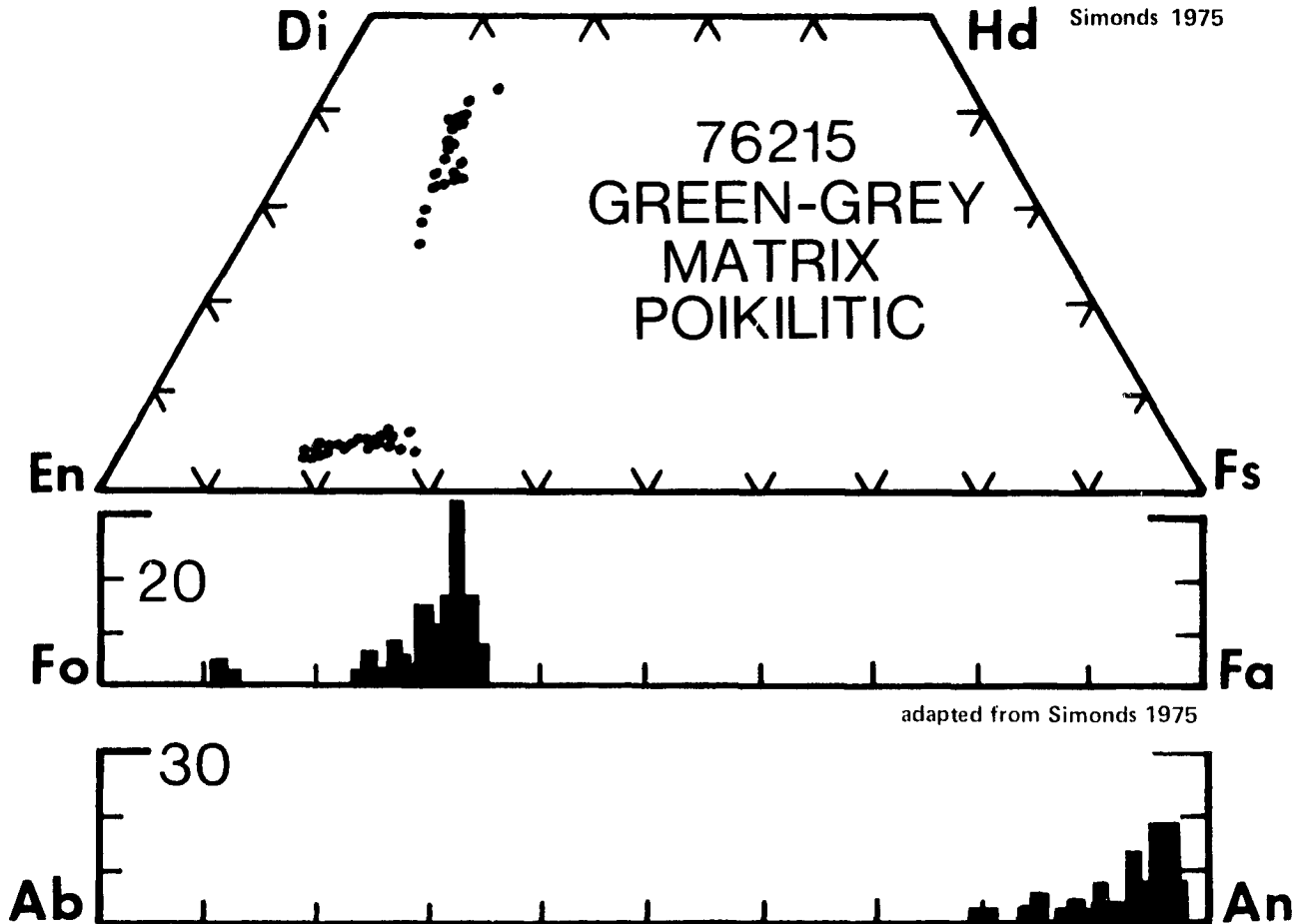
Age Data: ^{40}Ar - ^{39}Ar plateau - 3.94 ± 0.04 (Cadogen and Turner, 1976).



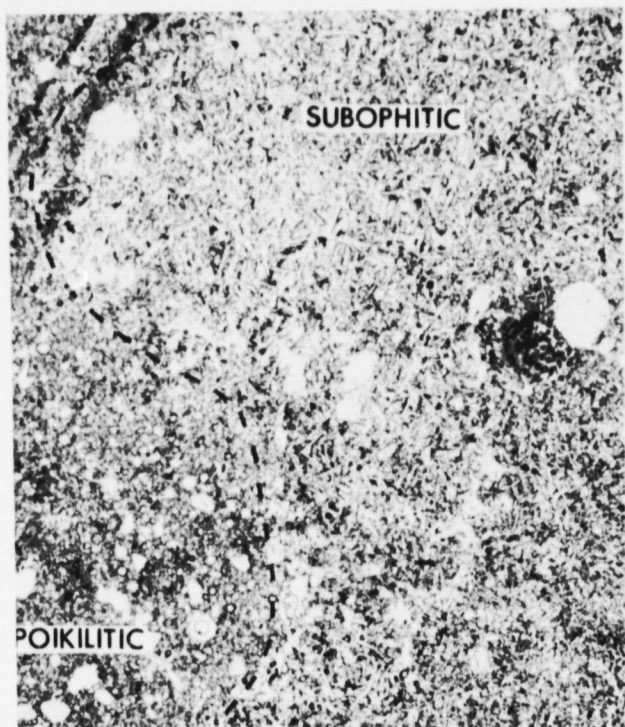
adapted from Simonds 1975



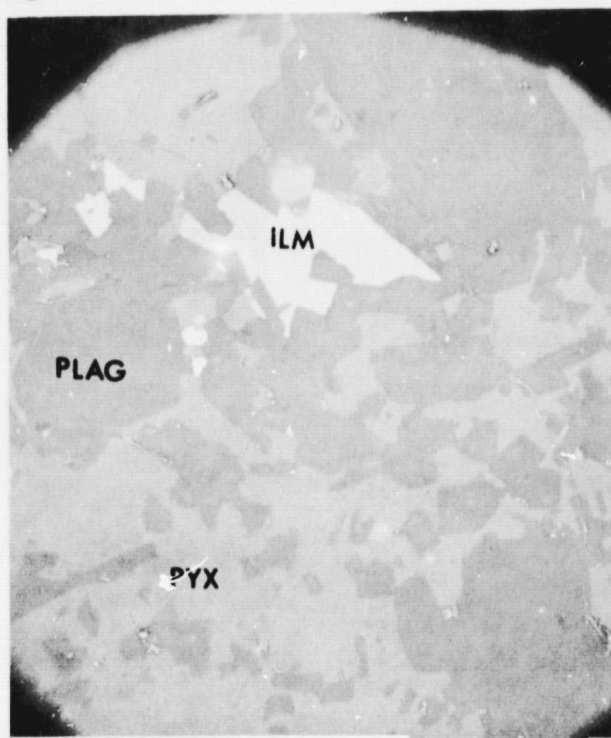
Simonds 1975



Simonds 1975



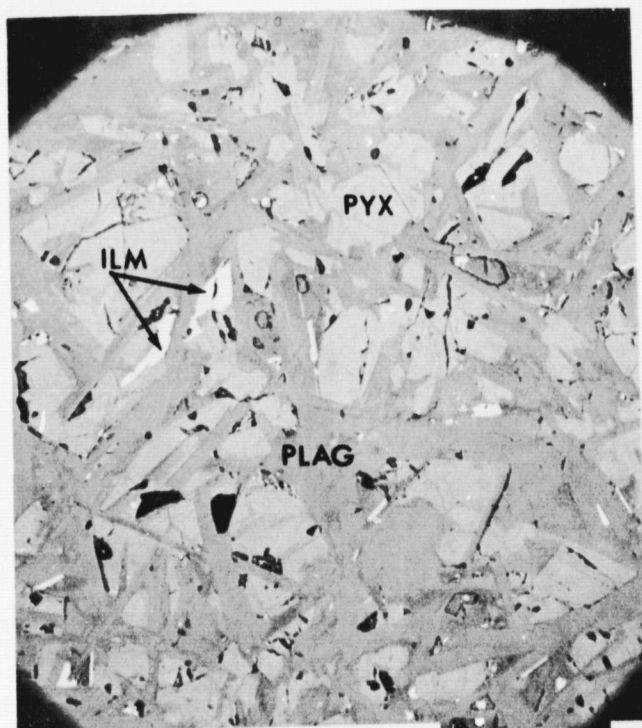
76215 2.0MM a



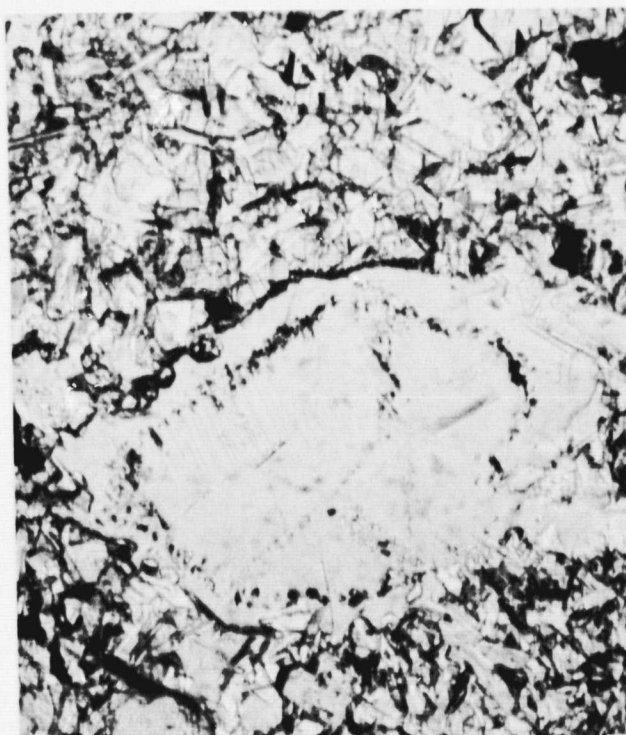
76215 0.05MM b

Figure 76215a. Typical view of 76215 showing two lithologies: poikilitic (lower left) and subophitic (upper right); transmitted light.

Figure 76215b. Poikilitic lithology; reflected light. Dark-grey, plagioclase; light-grey, pyroxene; white, ilmenite.



76215 0.05MM c



76215 0.10MM d

Figure 76215c. Ophitic lithology; reflected light. Color key same as in (b)

Figure 76215d. Plagioclase clast with overgrowth rim; transmitted light.

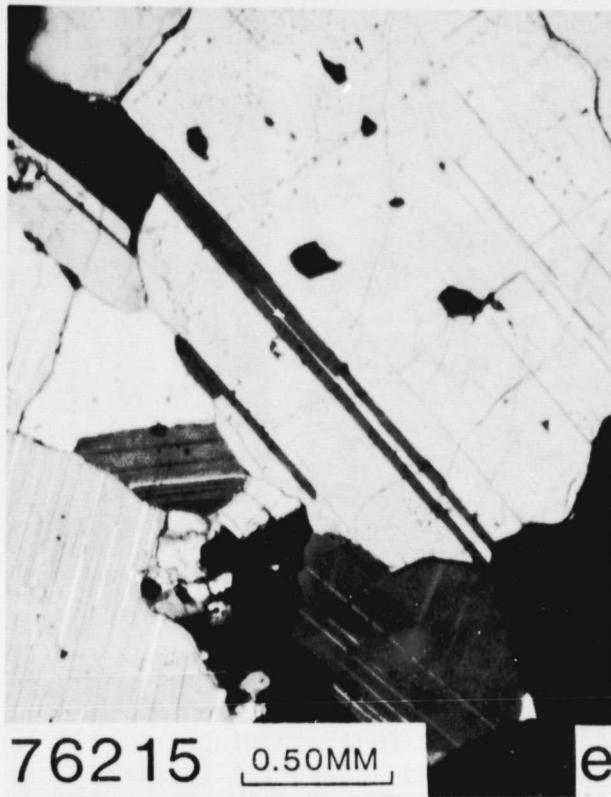
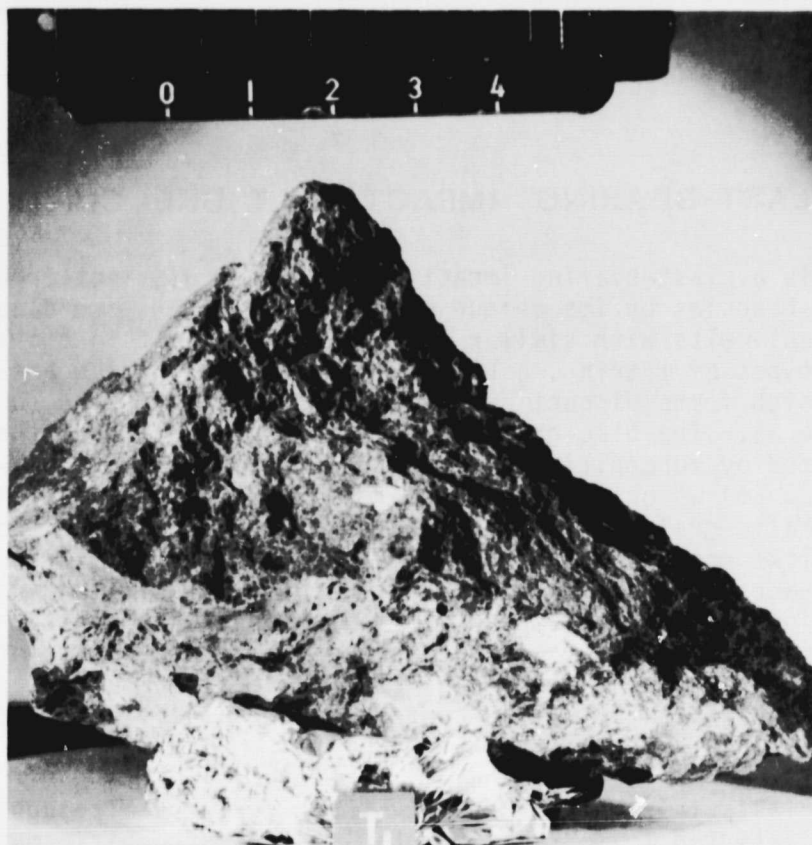


Figure 76215e. Anorthosite clast; transmitted light (crossed polarizers).



76295- A clast-bearing impact-melt breccia which is compositionally similar to the other clast-bearing rocks from Apollo 17 believed to be derived from the Serenitatis impact. The rock comes from the finest-grained most clast-rich part of Station 6 boulder which forms part of a cross section through the melt sheet.



Sample 76295 is a light to medium bluish-grey, wedge-shaped rock (10x6x3.5 cm) which was chipped from the boulder farthest upslope in a group of five boulders at Station 6.

76295 CLAST-BEARING IMPACT-MELT BRECCIA

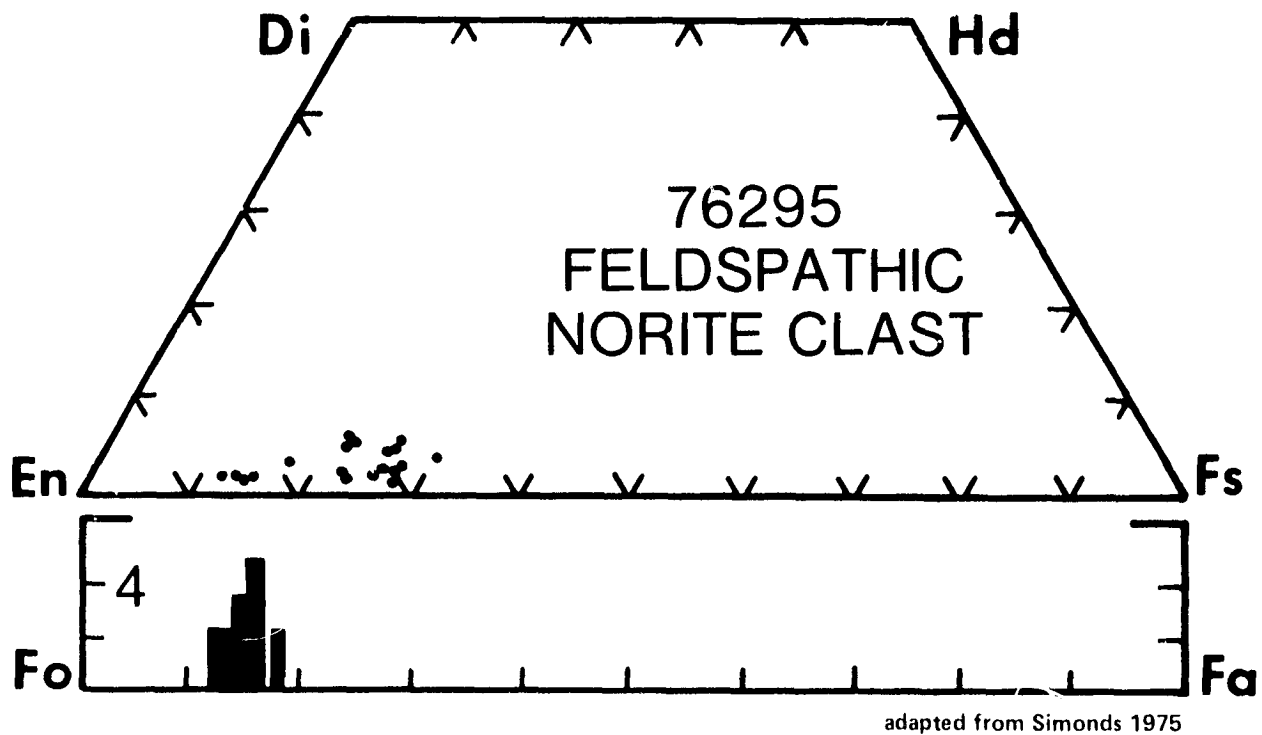
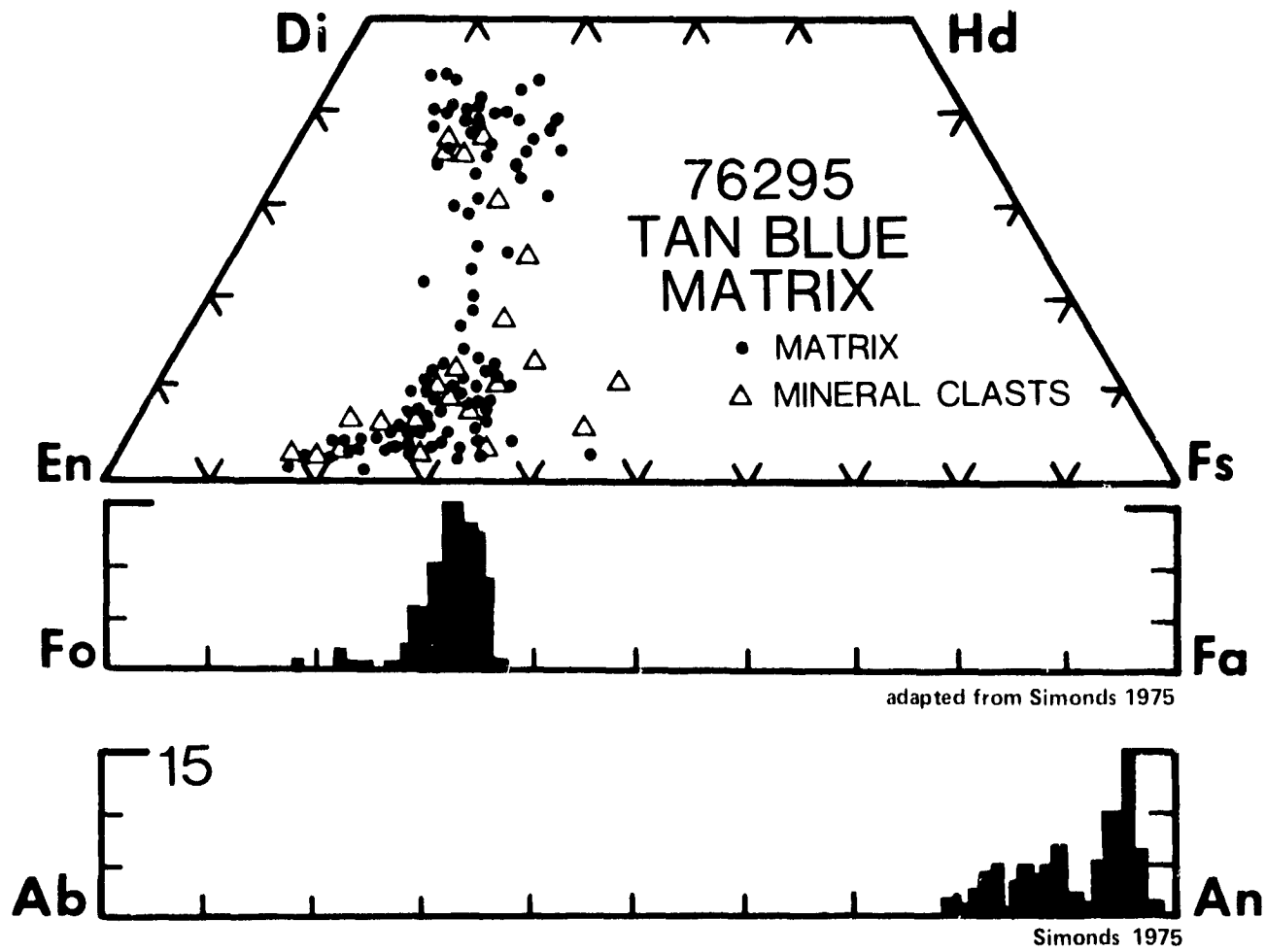
Sample 76295 is a clast-bearing impact-melt breccia distinct from the Apollo 14 clast-rich breccias by its unique matrix texture yet more clast-rich than Apollo 17 impact-melts with similar matrix textures. It is characterized by two distinct types of matrix, a blue-grey subophitic region and a tan clast-rich region which forms discontinuous vein-like masses in the subophitic matrix (Figure a). The blue-grey subophitic matrix dominates the sample and is characterized by subophitic intergrowths of plagioclase (15 μm) and mafic minerals (10-25 μm) which include low-calcium pyroxene, augite and olivine (Figure b). Mafic grains may also completely enclose plagioclase grains. The tan vein-like regions are typically extremely porous with irregularly shaped pore spaces enclosed by silicate minerals. Clast abundances for the vein-like regions are about twice as great as for the subophitic matrix regions (Figure c). Both matrix types contain about equal amounts of plagioclase ($\sim 50\%$) but the clast-rich veins lack olivine and contain abundant augite while the subophitic matrix contains abundant olivine and only minor augite.

Most mineral clasts in sample 76295 lack shock features although several large plagioclase clasts (up to 1.2 mm) in the blue-grey subophitic matrix display devitrification features. Plagioclase mineral clasts in both regions are typically subrounded to subangular (0.05-1.5 mm) and unfractured; rare plagioclase grains contain rounded inclusions of olivine (Figure d). Mafic minerals include olivine and pyroxene; olivine clasts are restricted to regions of subophitic matrix. Pyroxene clasts (up to 0.4 mm) are typically angular and lack zoning. Several large ilmenite grains (up to 0.45 mm) with irregular shapes are present in the sample and are possibly clasts. Rare rounded clasts (50 μm) of pink spinel occur in the blue-grey subophitic matrix of sample 76295.

Lithic clasts in section 76295,91 examined here included a feldspathic olivine norite clast at least one centimeter across (Figure e). The clast is characterized by abundant rounded plagioclase grains (0.1-0.8 mm) which have been shocked and recrystallized. Several smaller clasts (0.3-0.5 mm) of feldspathic norite with poikilitic pyroxene were also observed.

References: Simonds et al. (1974); Simonds (1975); Onorato et al. (1976).

Age Data: ^{40}Ar - ^{39}Ar plateau - 3.95 ± 0.04 (Cadogan and Turner, 1976).



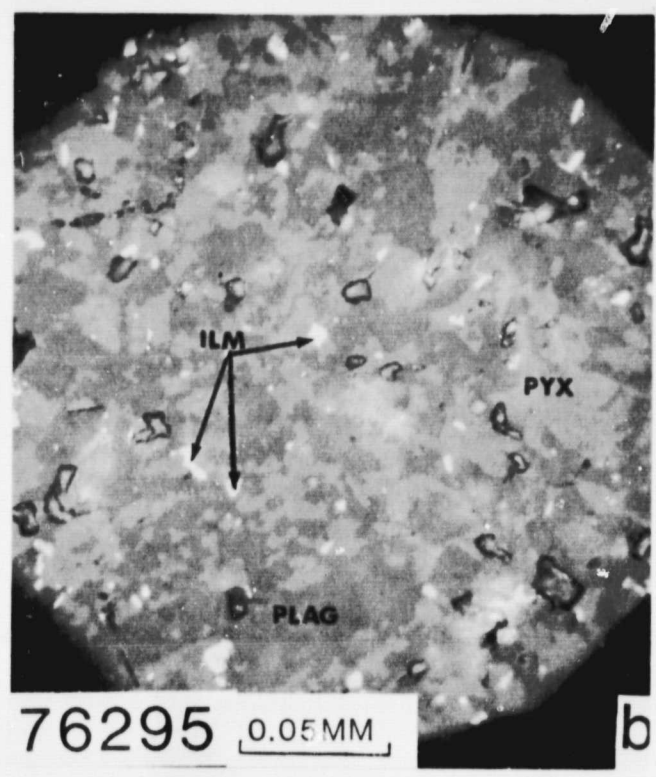
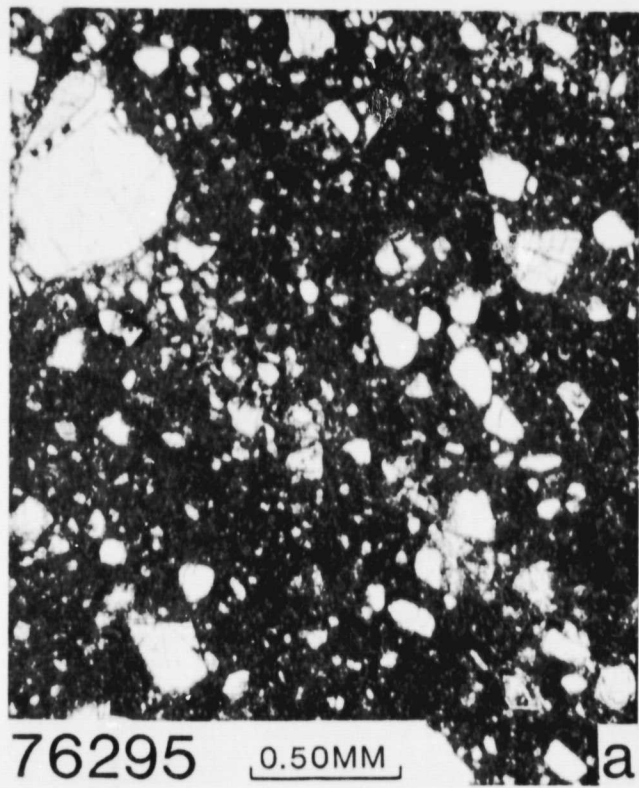


Figure 76295a. Typical view of 76295 showing clast-rich vein; transmitted light.

Figure 76295b. Typical view of matrix; reflected light. Dark-grey, plagioclase; light-grey, pyroxene; white, ilmenite.

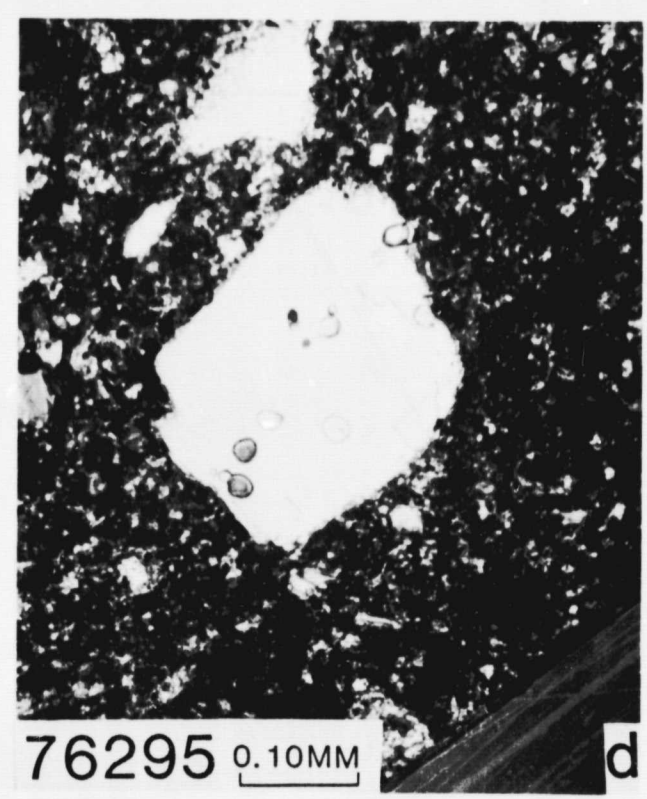
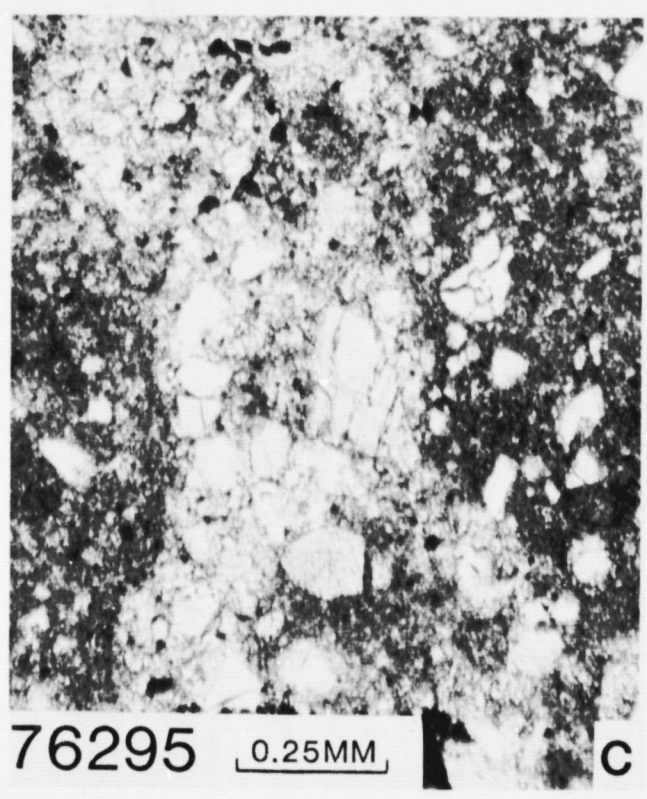
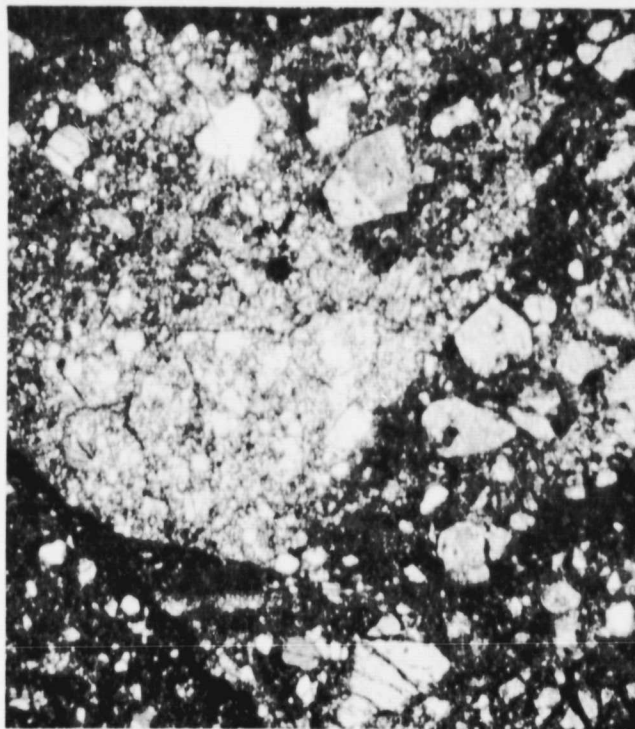


Figure 76295c. Close up view of clast-rich vein; transmitted light.

Figure 76295d. Olivine inclusions in plagioclase clast; transmitted light.

76295

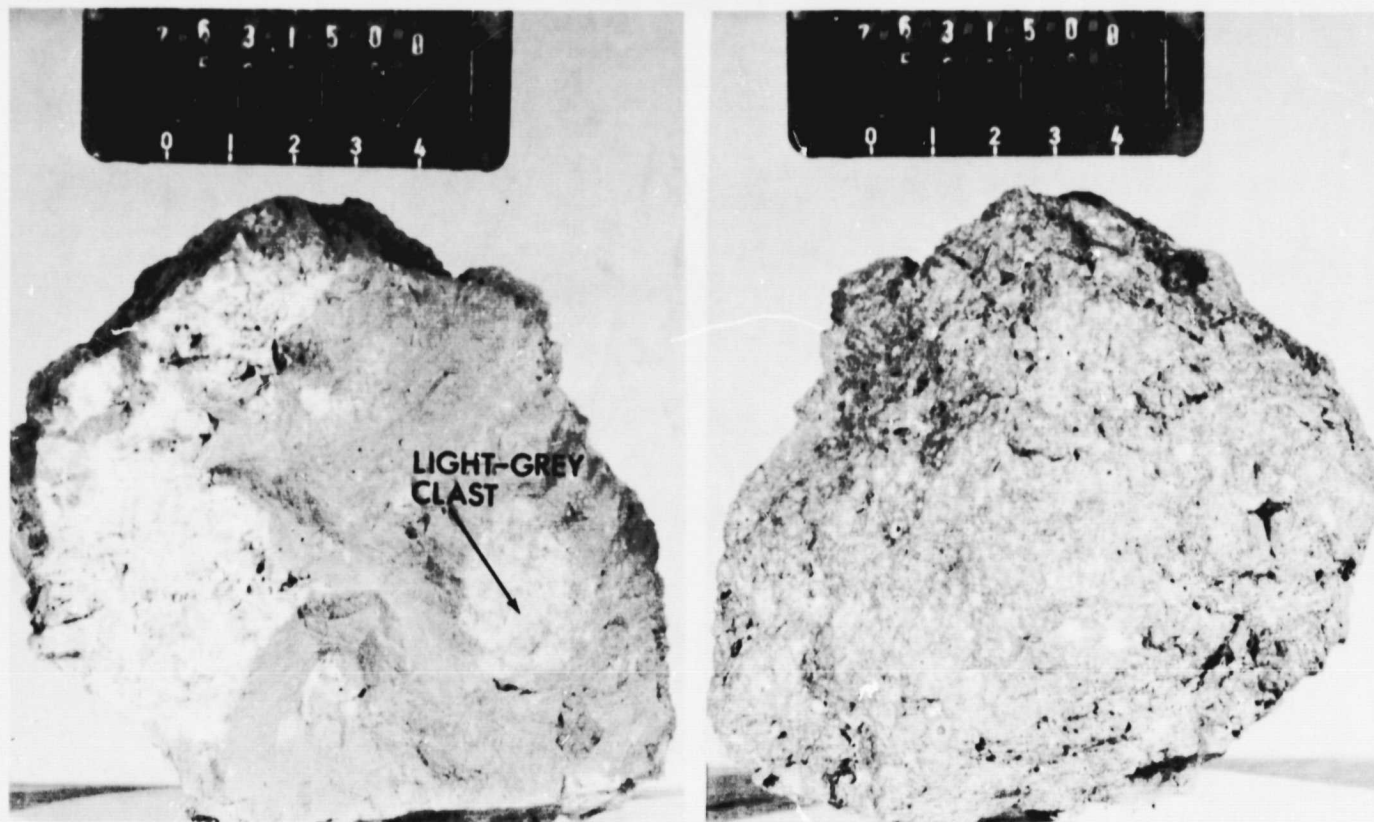
160



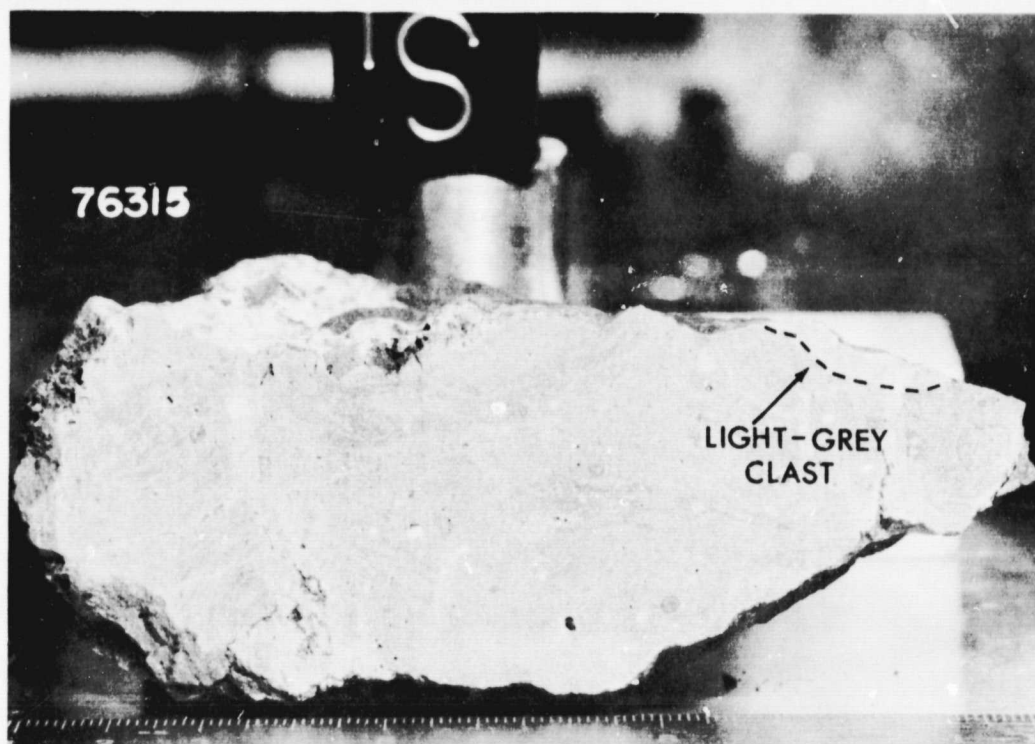
76295 0.50MM e

Figure 76295e. Feldspathic olivine norite clast; transmitted light.

76315- One of the clast-bearing impact-melt breccias of low K KREEP composition which is part of the Apollo 17, Station 6 boulder. It is intermediate between 76215 and 76295 in clast content and texture.



Sample 76315 is a light-greenish grey and dark grey (two lithologies) rock (10x12x4.5 cm) which was originally an inclusion in a vesicular "anorthositic gabbro" in the second boulder downslope at Station 6.



76315 CLAST-BEARING IMPACT-MELT BRECCIA

Sample 76315 is a clast-bearing impact-melt breccia (Figure a) characterized by a micro-poikilitic matrix (Figure b) with pyroxene oikocrysts (up to 100 μm) grading into a fine-grained subophitic matrix (Figure c) which occurs in isolated patchy regions up to several millimeters in length. Clast abundances appear to be evenly distributed between the two types of matrix although several of the subophitic zones are slightly more clast-rich and porous than the rest and resemble the clast-rich tan veins in sample 76295. Pore space in sample 76315 takes the form of smooth-walled, round vesicles typically 0.10 mm or less in diameter and as interstitial vugs <.01 mm across.

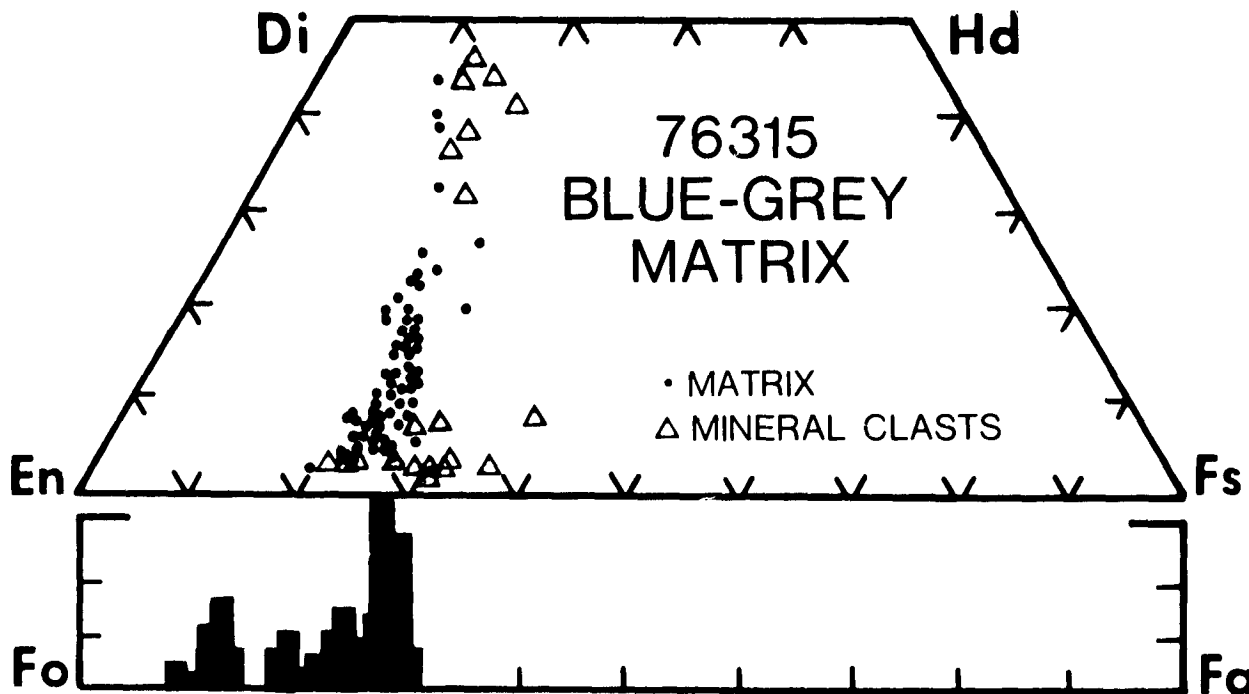
The mineral clast population is characterized by unshocked grains of plagioclase, pyroxene, olivine, and rare grains of pink spinel. Plagioclase clasts are subrounded to subangular (0.50-0.4 mm) and rare plagioclase clasts display inclusions of rounded olivine. Pyroxene clasts are angular and anhedral and commonly fractured; olivine clasts (up to 0.2 mm) are angular and rarely display zoning. Simonds (1975) reports the occurrence of pink spinel but no spinel was observed in sections 76315,95 or 76315,97.

The lithic clast population in section 76315,95 is dominated by a portion of the light-grey clast described by Simonds (1975) which is characterized by a seriate size distribution of subangular and subrounded plagioclase grains with less abundant pyroxene and olivine. The largest plagioclase grains (0.8-1.0 mm) typically display olivine necklaces (Figure d) and 50 to 60 μm overgrowths.

Smaller plagioclase grains (0.2-0.4 mm) are commonly characterized by olivine inclusions. Pyroxene and olivine oikocrysts (up to 1.0 mm) are present. Troilite and Fe-Ni metal blebs occur throughout the clast. A 1 mm basalt clast with acicular plagioclase and subhedral olivine was also observed in section 76315,95. Section 76315,97 contains a 2 mm dunite clast with polygonal olivine grains and a symplectite between several of the grains. Other lithic clast types noted by Simonds (1975) but not observed in the sections discussed above include spinel troctolites, crushed troctolites and crushed anorthosites.

References: Simonds et al. (1974); Simonds (1975); Onorato et al. (1976).

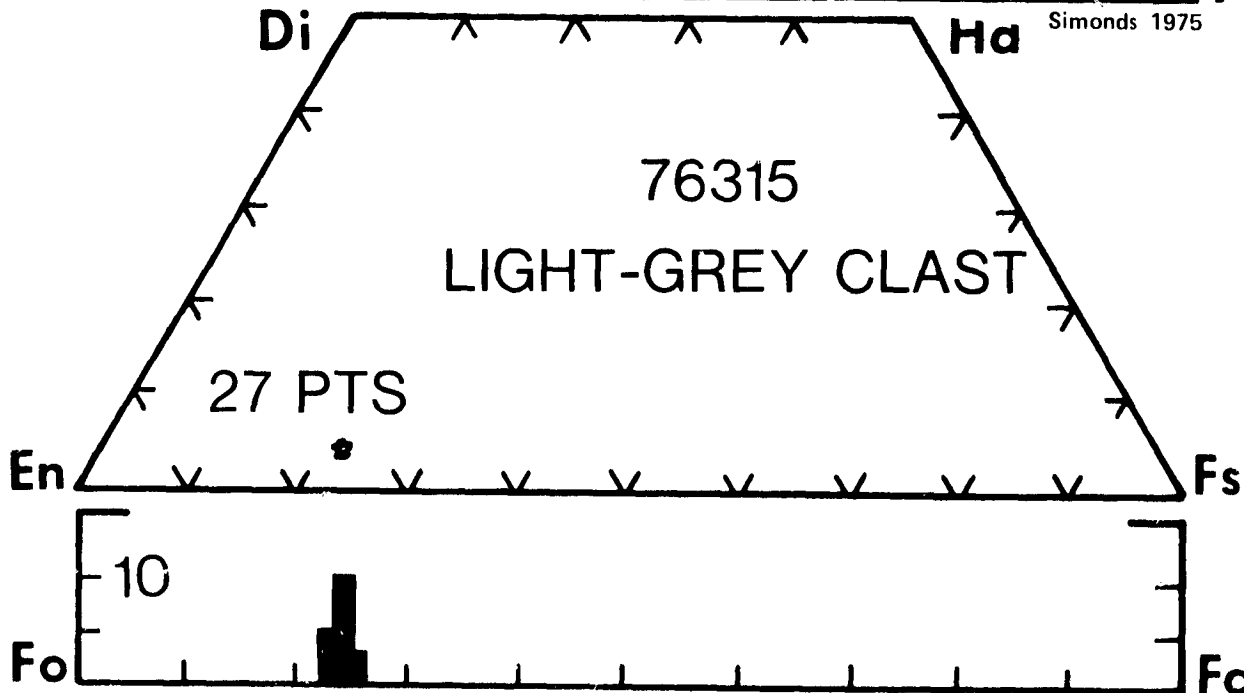
Age Data: ^{40}Ar - ^{39}Ar plateau - 3.98 ± 0.04 (Turner and Cadogan, 1975).
(Cadogan and Turner, 1976)



adapted from Simonds 1975



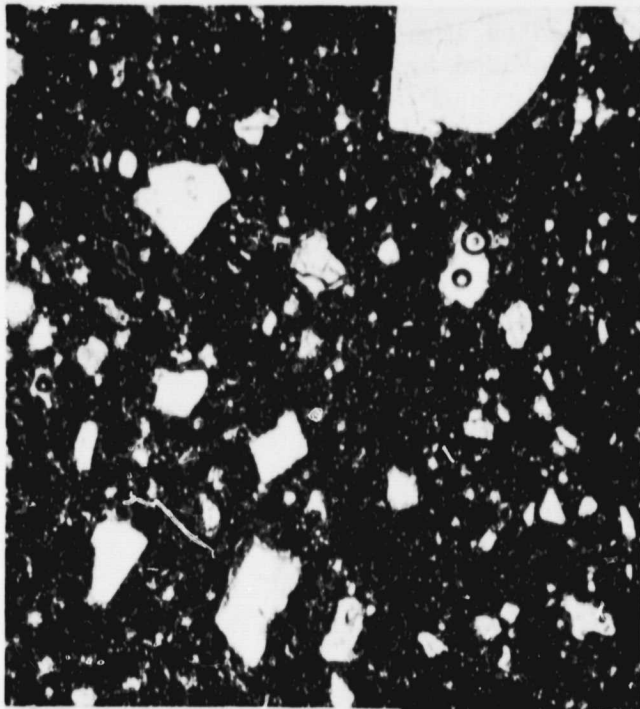
Simonds 1975



adapted from Simonds 1975

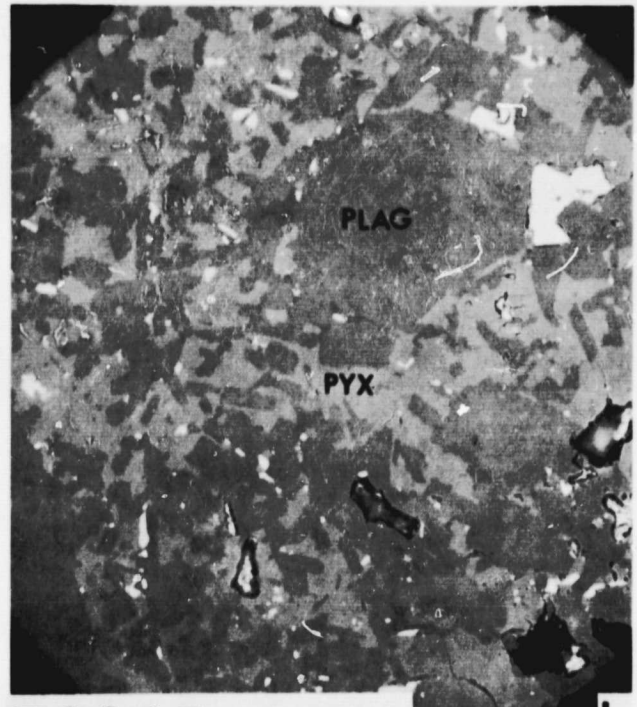


Simonds 1975



76315 0.5MM

a

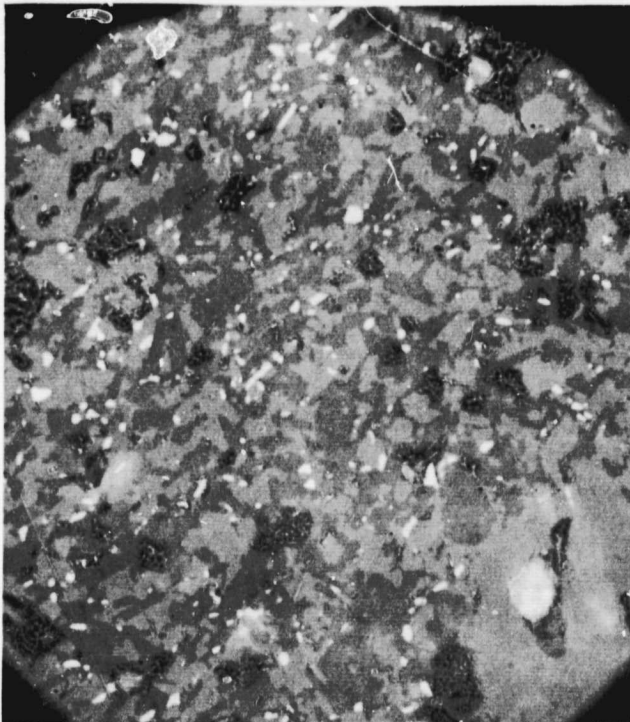


76315 0.05MM

b

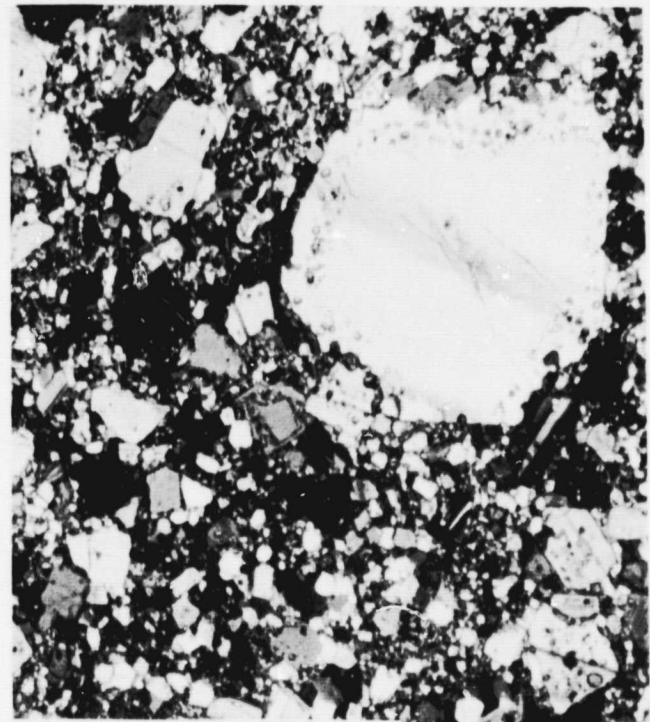
Figure 76315a. Typical view of 76315; transmitted light.

Figure 76315b. Micro-poikilitic matrix in 76315; reflected light. Dark-grey plagioclase; lt-grey, pyroxene; white, ilmenite.



76315 0.05MM

c



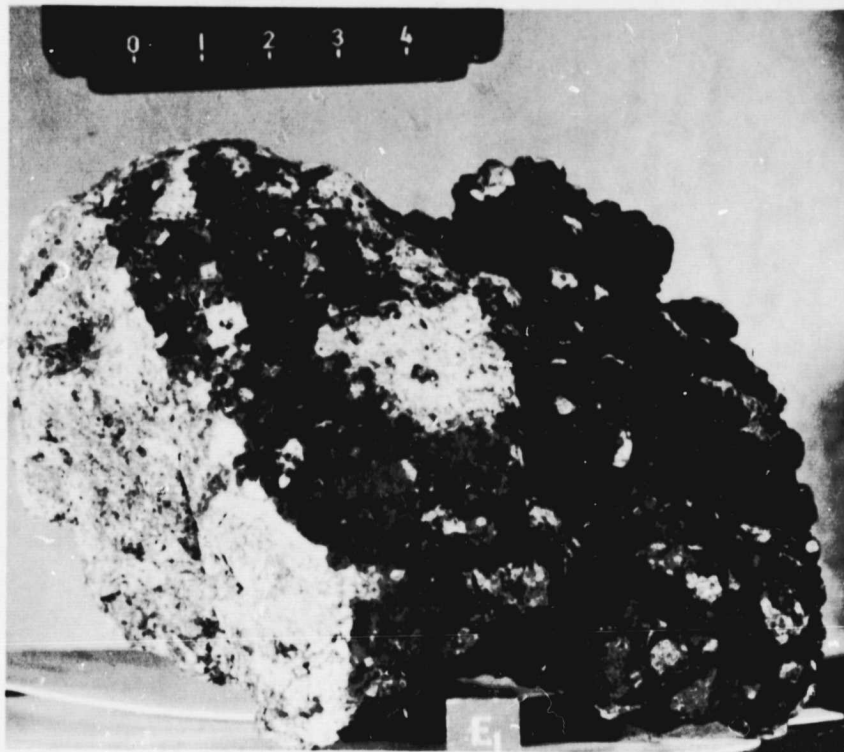
76315 0.5MM

d

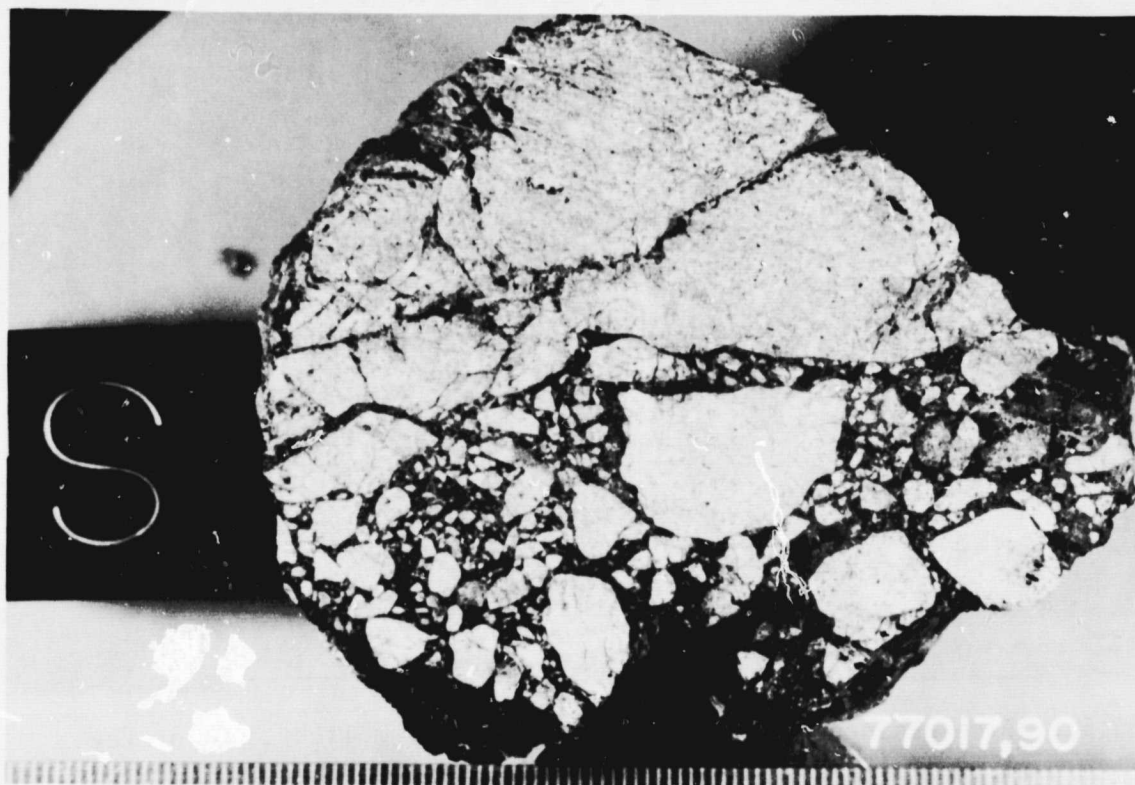
Figure 76315c. Fine-grained subophitic matrix; reflected light. Color key same as (b).

Figure 76315d. Plagioclase clast with olivine necklace; transmitted light (crossed polarizers).

77017- One of a group of high grade metamorphosed impact breccias. The meta-impactite has been subsequently invaded by black vesicular glass.



Sample 77017 is a light-grey to greenish-grey subrounded rock (17x12.5x9 cm) collected at Station 7 near the base of North Massif approximately 70 meters southwest of the lunar roving vehicle.



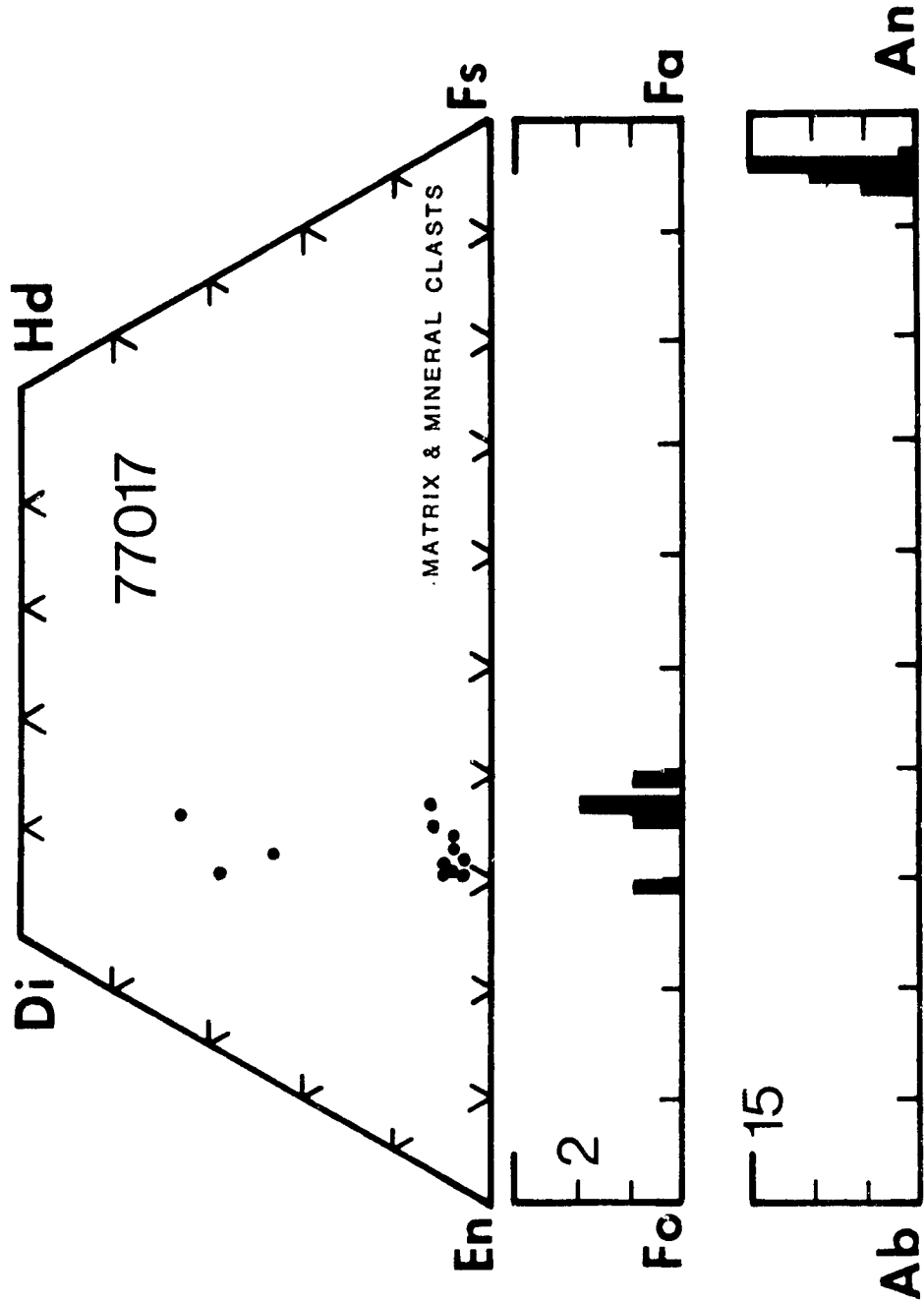
77017 GRANULITIC IMPACTITE

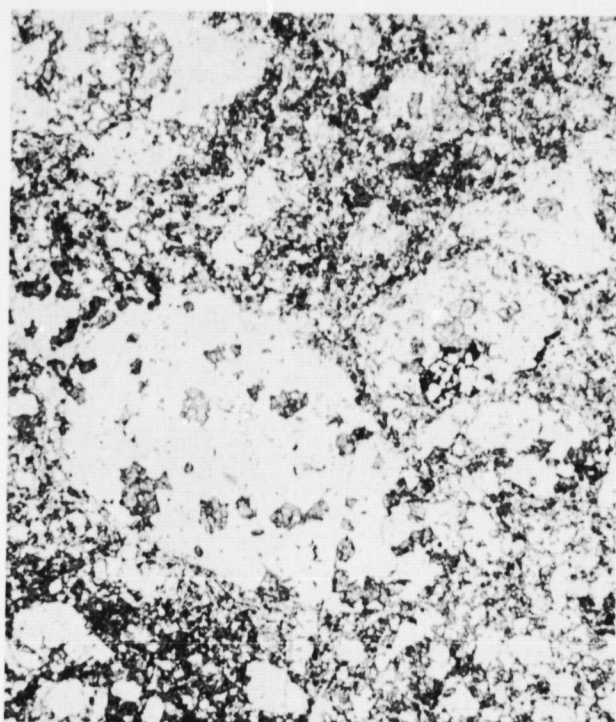
Sample 77017 is a coarse-grained granulitic impactite characterized by plates of poikilitic augite and pigeonite (up to millimeters across) which enclose large (up to 1.0 mm) subhedral to euhedral plagioclase grains and subhedral to rounded grains of olivine (Figure a); rounded olivine grains (.02-.20 mm) also commonly occur as inclusions within plagioclase grains. Lithic clasts of anorthosite and troctolite described by McCallum et al. (1974) were not observed by the author. Numerous zones of more finely comminuted material occur throughout the sample and are compositionally indistinct from the uncrushed areas. Section 77017,66 is partially surrounded by a rind (0.10-0.40 mm wide) of light-brown debris-laden vesicular glass (Figure b). In Section 77017,72 the brown glass veins also penetrate into the center of the sample.

Plagioclase grains in 77017 are characteristically highly fractured and display offset twinning, undulatory extinction and mosaicism. Pyroxene and olivine are also highly fractured; augite oikocrysts commonly display closely-spaced lamellae of low-Ca-pyroxene.

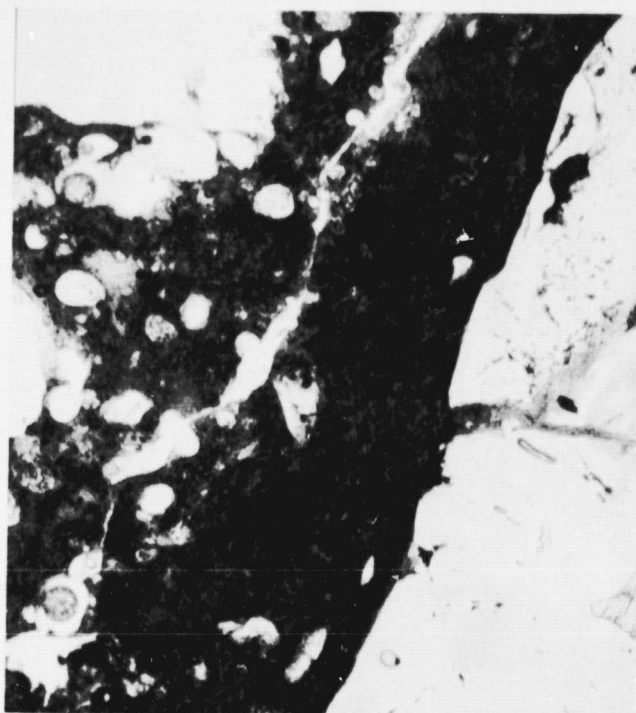
Troilite and Fe-Ni metal are common constituents of sample 77017 occurring both as discrete grains (up to 0.08 mm) as well as in association. Ilmenite is also quite common and occurs as poikilitic grains (up to 0.8 mm) which enclose plagioclase and mafic minerals (Figure c).

References: McCallum et al. (1974)



77017 2.0MM

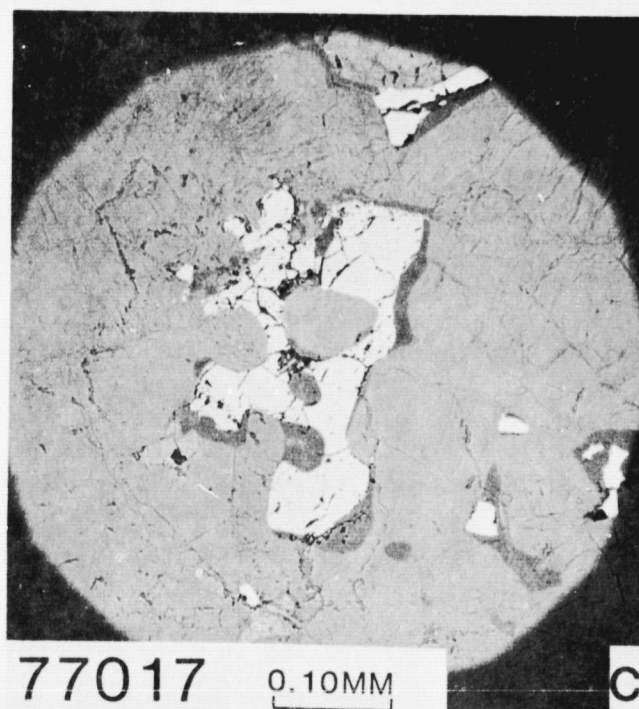
a

77017 0.10MM

b

Figure 77017a. Typical view of 77017; transmitted light.

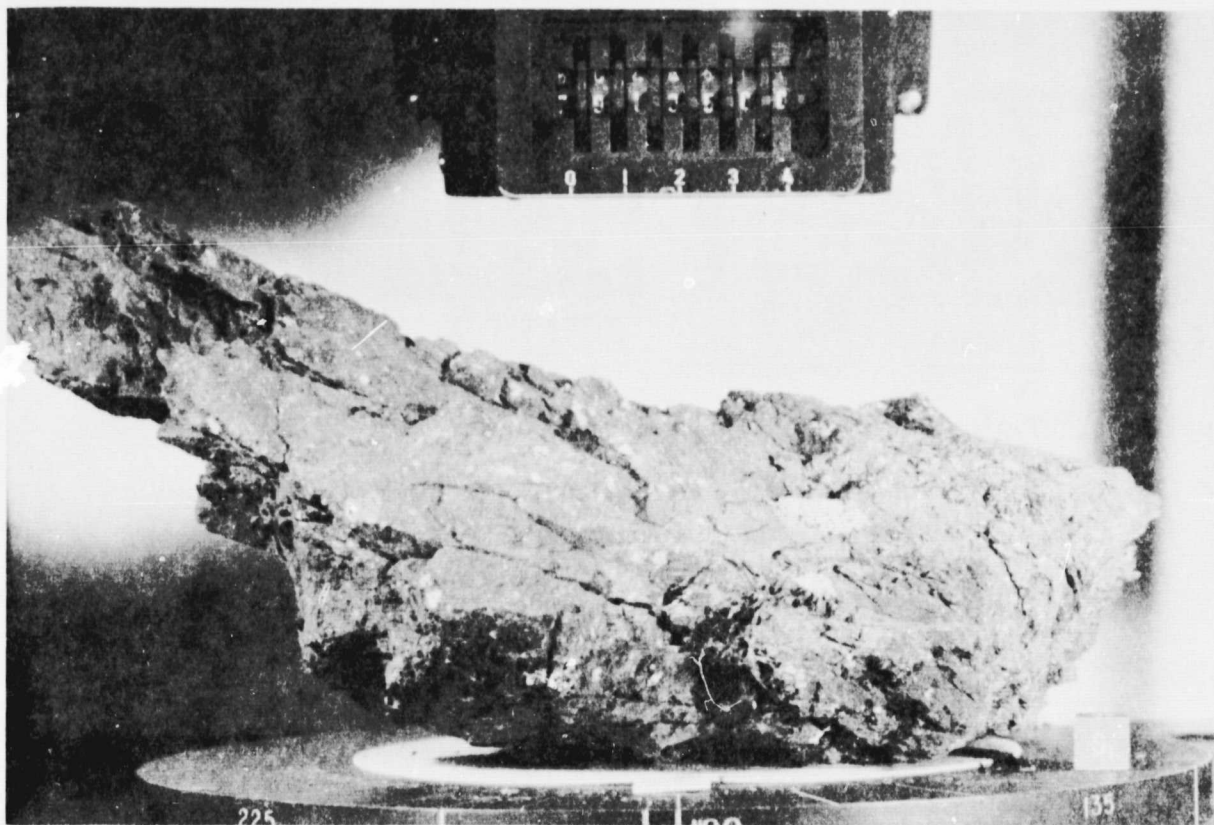
Figure 77017b. Debris-laden vesicular glass rind; transmitted light.

77017 0.10MM

c

Figure 77017c. Poikilitic ilmenite grain; reflected light.

79135- A typical Apollo 17 "soil" breccia. The restricted locale and established age of many of its constituents suggest that the crater associated with its formation is <1km across.



Sample 79135 is a medium to dark grey angular rock (20x12x10 cm) collected at Station 9 from a boulder on the southeast rim of Van Serg crater.

79135 DARK-MATRIX BRECCIA

Sample 79135 is a fragmental matrix breccia characterized by diverse populations of mineral, lithic and glass clasts in a homogeneous matrix of mineral debris and partially to completely devitrified opaque glass (Figure a). The texture is seriate with fragments ranging in size from the limit of resolution up to 2.0 mm. Porosity in the section is limited to rare fractures and irregularly shaped vugs which account for less than 5 percent of the section.

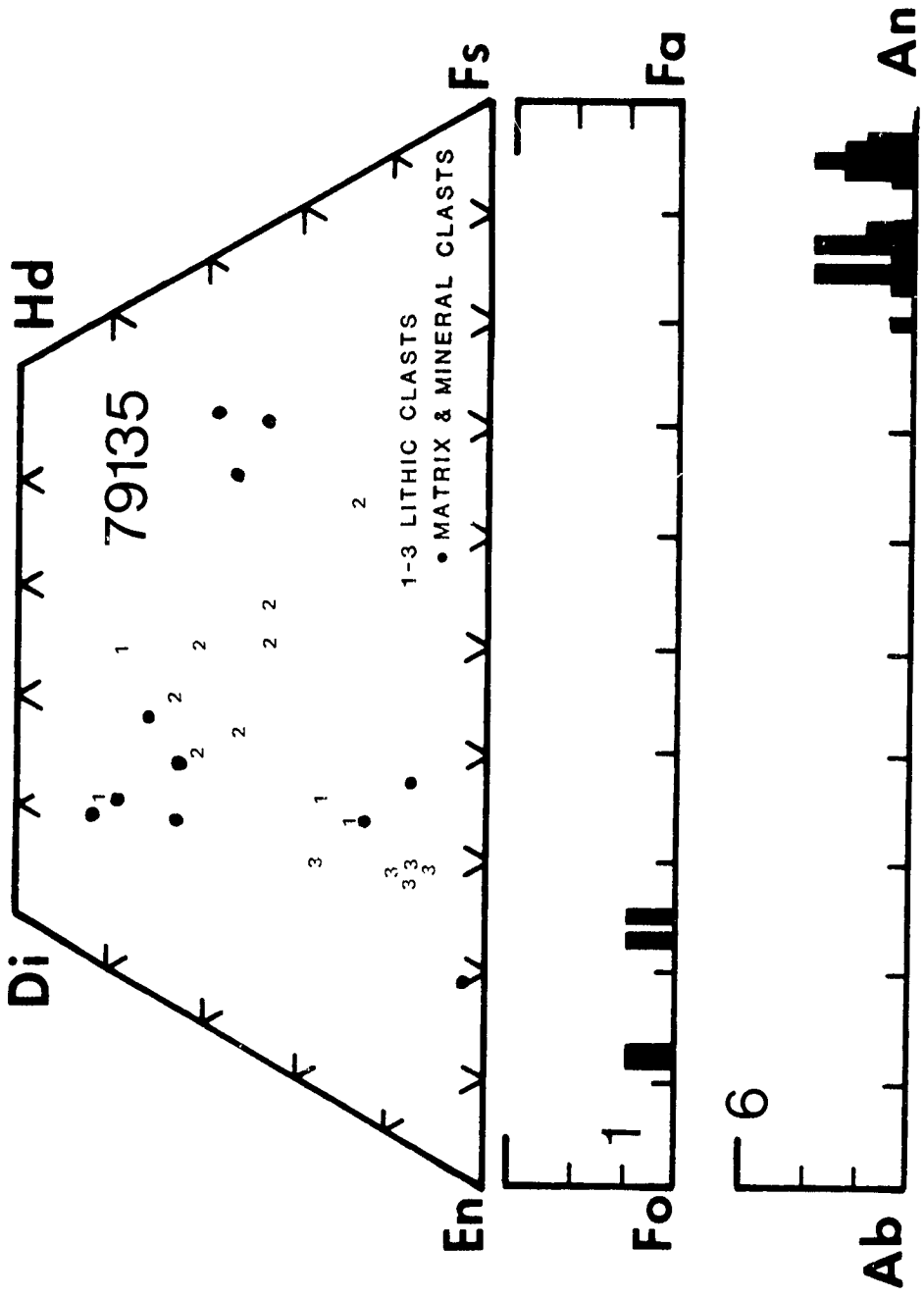
As with most fragmental matrix breccias, plagioclase dominates the mineral clast population and is present as subangular and angular clasts (up to 0.5 mm) which display fracturing and undulatory extinction. Mafic mineral clasts are less abundant than plagioclase clasts. Clinopyroxene is most common and occurs as angular fractured clasts up to 0.5 mm; olivine is present only in minor amounts. Opaque mineral clasts are relatively abundant and consist of a variety of phases. Ilmenite occurs as angular clasts up to 0.25 mm and as feathery intergrowths in devitrified glasses. Armalcolite is present as angular clasts up to 0.1 mm. Fe-Ni metal and troilite are present as angular fragments (0.15 mm) and as blebs in the matrix; ulvospinel is rare.

Glass clasts are the most abundant constituent in sample 79135. Spheres, fragments of spheres and shards of homogeneous, undevitrified orange glass up to 0.3 mm are a conspicuous feature of section 79135,102 (Figure b). Partially devitrified orange glass clasts are abundant and form a gradational sequence between the undevitrified clasts and the opaque, completely devitrified glass clasts. Schlieren and debris-filled glass "bombs" are common, some as large as 2.0 mm. Colorless glass spheres and shards (up to 0.4 mm) are also abundant. A distinctive feature of section 79135,102 is the presence of "ropy" glasses (Figure c) in a variety of colors which commonly contain microclites and mineral debris.

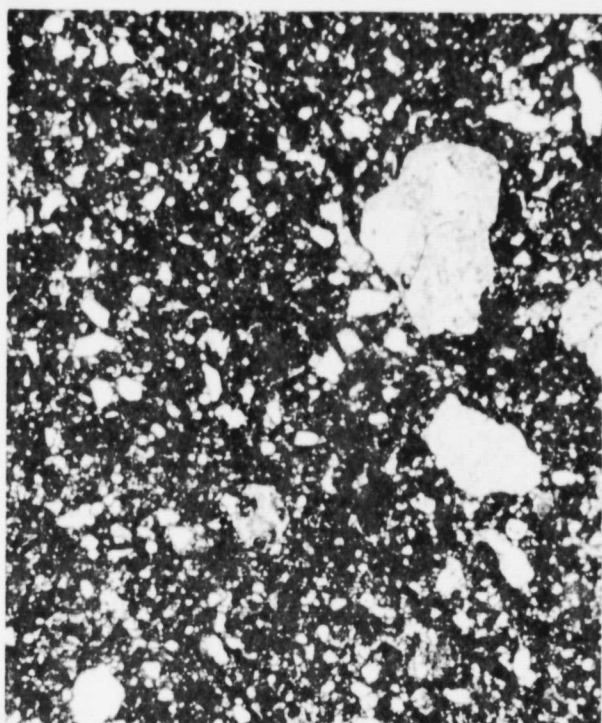
Basalt clasts (up to 2.0 mm) are quite common and display a variety of textures including porphyritic, subophitic and ophitic textures (illustrated in the companion volume). Several clasts of annealed breccia are present (Figure d). Anorthosite fragments are relatively common, occurring as clasts up to 1.5 mm; some of the clasts are polygonalized plagioclase.

79135
MODAL ANALYSES (VOL. %)

MATRIX (<39%)	69.0
CLASTS (>39%):	
PLAGIOCLASE	4.1
MAFIC	2.7
OPAQUE	1.1
HETEROGENEOUS GLASS	6.3
HOMOGENEOUS GLASS	4.2
DEVITRIFIED GLASS	3.4
FRAGMENTAL BRECCIA	1.0
CRYSTALLINE BRECCIA	3.0
GRANULITIC	TR
OTHER METAMORPHIC	—
MARE BASALT	4.2
HIGHLAND BASALT	.5
CRUSHED	TR
PORE SPACE	TR
OTHER	—

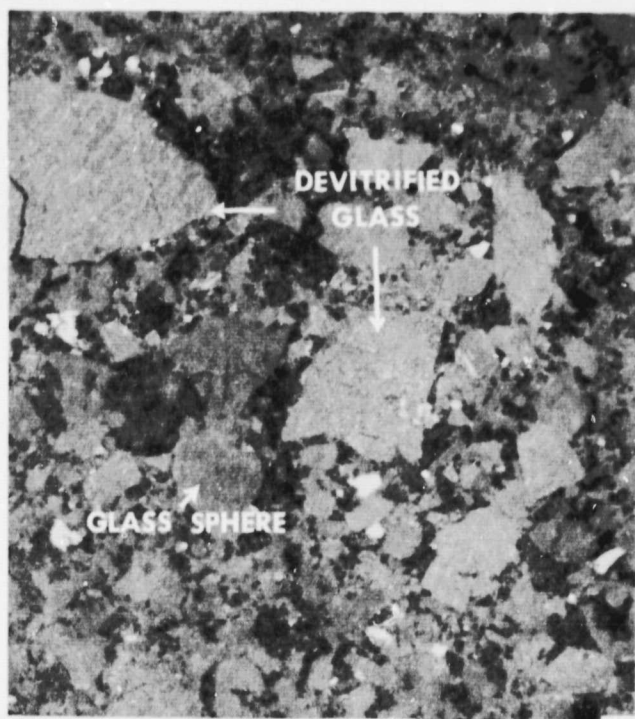


REFLECTED LIGHT



79135 1.0 MM

a

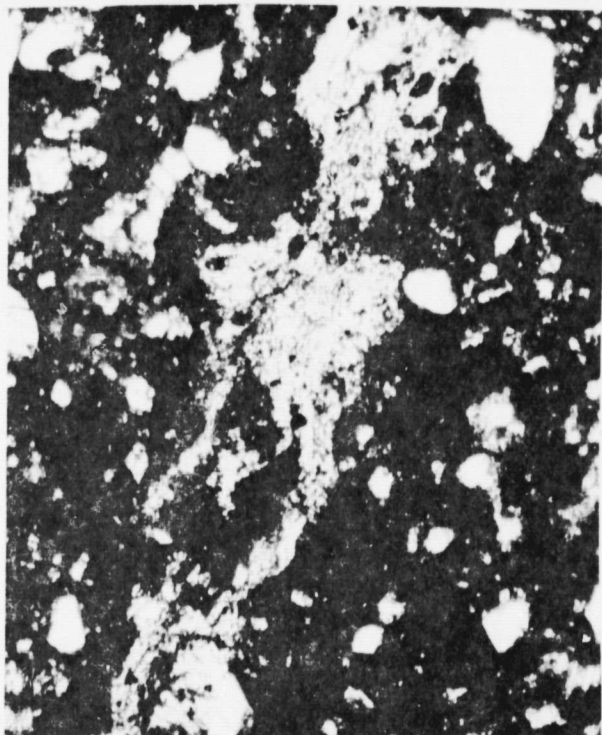


79135 0.05MM

b

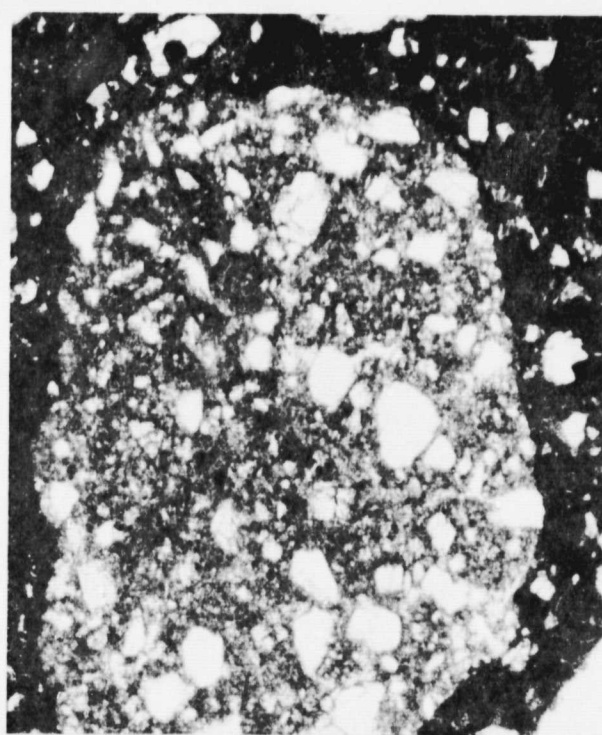
Figure 79135a. Typical view of 79135; transmitted light.

Figure 79135b. Typical view of matrix; reflected light.



79135 0.25 MM

c



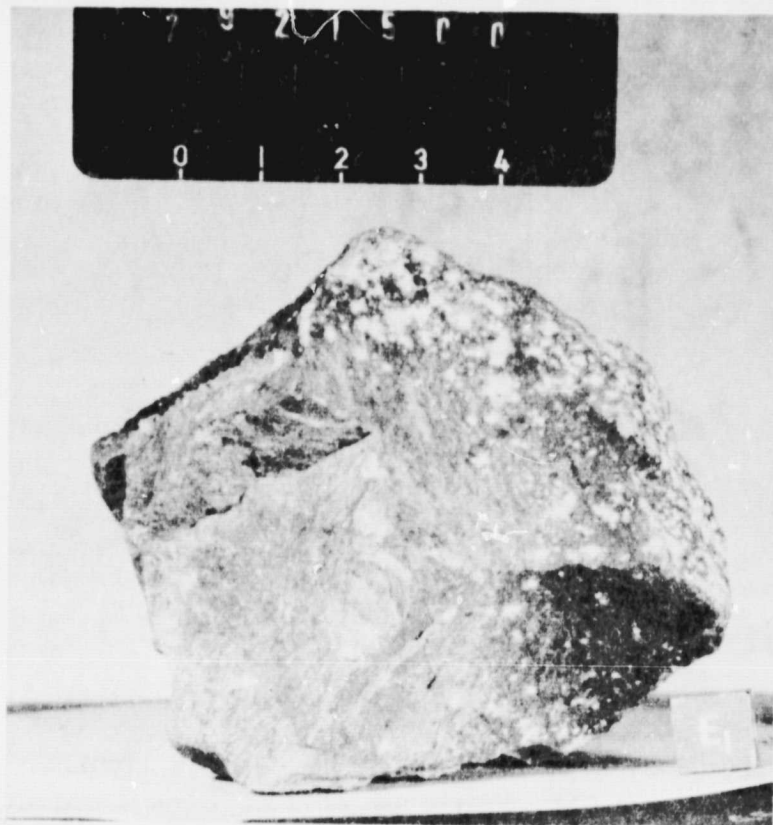
79135 0.10 MM

d

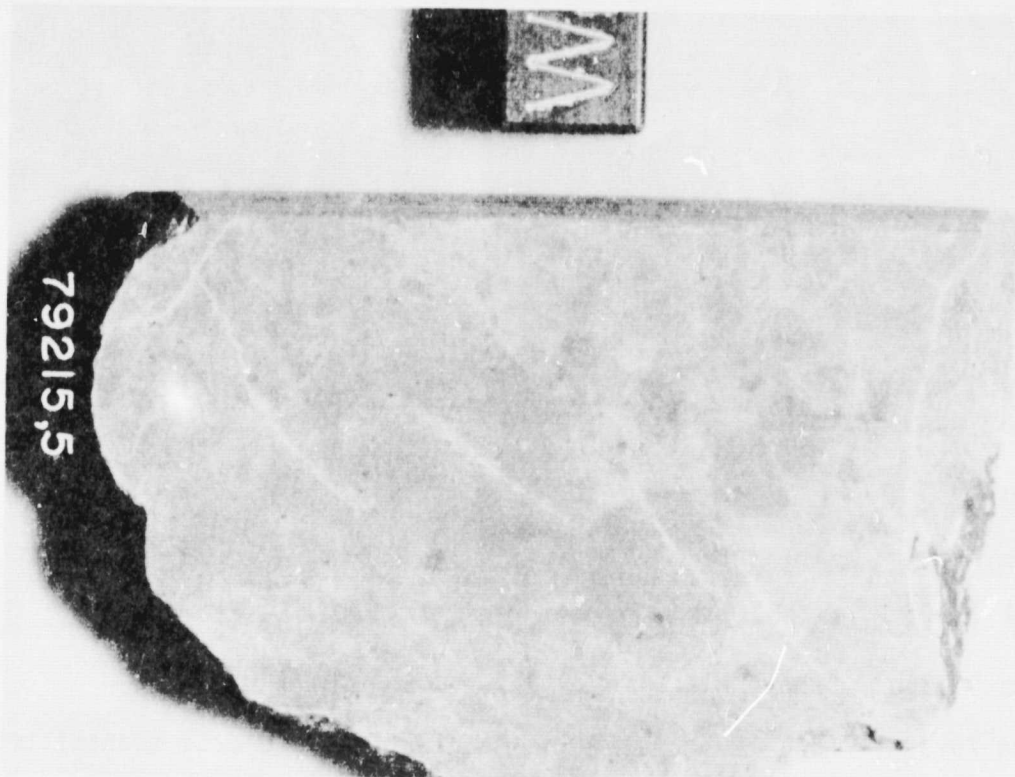
Figure 79135c. "Ropy" glass in 79135; transmitted light.

Figure 79135d. Annealed crystalline matrix breccia clast; transmitted light.

79215- A feldspathic impact breccia subjected to prolonged very high grade metamorphism.



Sample 79215 is a medium light-grey blocky rock (9x8x7.5 cm) collected at Station 9 near the southeast flank of the Van Serg crater ejecta blanket.



79215 GRANULITIC IMPACTITE

Sample 79215 is a granulitic impactite, most of which is characterized by a granoblastic matrix composed of equant anorthite grains (.03-0.1 mm) which meet at 120° triple junctions with smaller (.01-.02 mm) interstitial grains of olivine, pyroxene and opaque minerals (Figure a). Local coarser-grained aggregates of mono- and polycrystalline anorthite, olivine and pyroxene relics are present together with apatite megacrysts up to 1.5 mm across; rare poly-mineralic relics are also present.

Single grains of anorthite or aggregates of polygonal grains are the most abundant relics. Anorthite grains (up to 1.5 mm long) typically display twin lamellae and have distinct boundaries with the matrix. Many grains display olivine or pyroxene "necklaces" (Figure b) similar to those noted in other lunar highland rocks. Polycrystalline relics are characterized by 20-30 micron grains of anorthite which meet at 120° triple junctions. They are typically larger (up to 3.5 mm) than the monocrystalline varieties and lack mafic silicate minerals, a feature which easily distinguishes them from the matrix.

Fine-grained concentrations of polygonalized olivine are rarely observed (Figure c) and display distinct boundaries with the matrix. The clusters range from rounded shapes 0.7 mm across to elongated shapes up to 1.2 mm long and are associated with anorthite relics. Discrete grains of olivine (up to 0.8 mm) are more common, are typically rounded and have irregular contacts with the surrounding matrix. Several grains contain colorless, less refractory inclusions, probably anorthite. Curious aggregates 0.1-0.2 mm in diameter, consisting of Cr-spinel and ilmenite surrounded by anorthite rims (Figure d), are observed in the matrix. Ilmenite crystals, rarely intergrown with troilite, metal, and rutile, surround the central core of Cr-spinel and radially project into the anorthite rims. Blebs and irregular grains of troilite and Fe-Ni-Co metal occur both intergrown and as discrete grains randomly distributed in the matrix. Ilmenite, with exsolved rutile, is also present. Together, these opaque phases make up less than 1% of the sample.

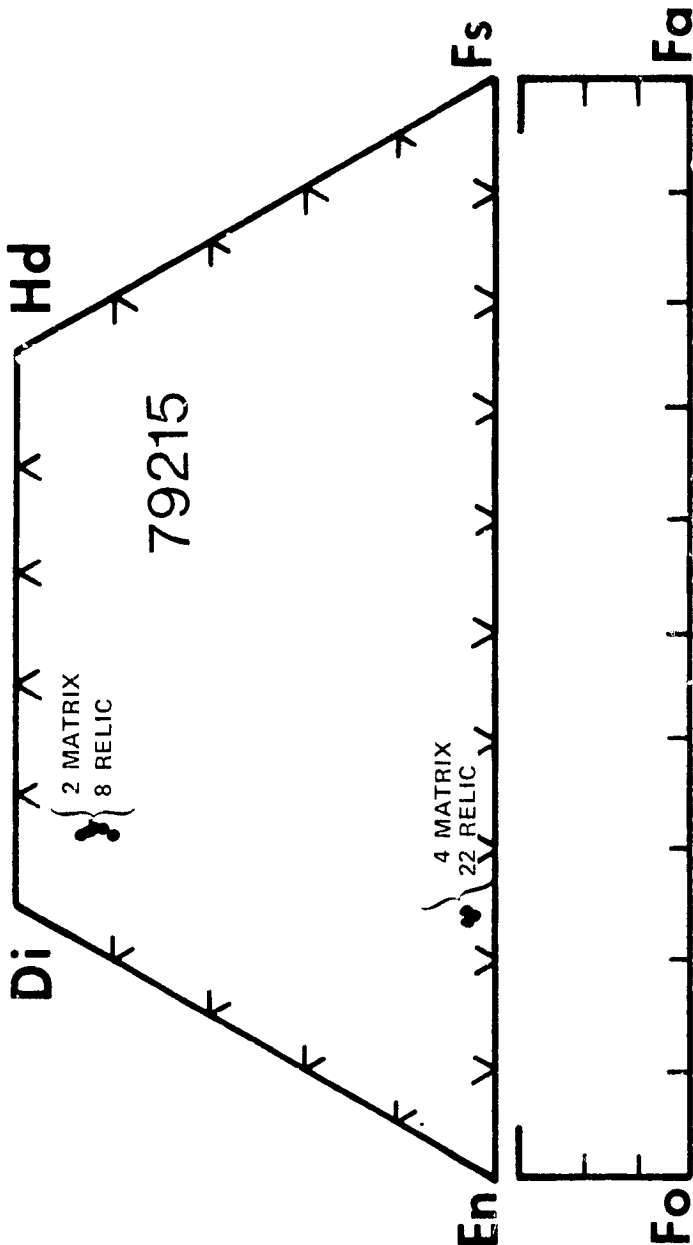
Rare polymineralic relics are less commonly occurring than the mono-mineralic varieties. Most display rounded or elongate shapes and consist of polygonal grains of anorthite and olivine which are coarser-grained than the matrix. One such relic, in section 79215,67, is characterized by equal proportions of anorthite and olivine, together with lath-shaped ilmenite (Figure e) and is possibly a lithic clast.

Megacrysts of subhedral apatite (up to 1.5 mm) are observed in many of the sections; they enclose surrounding matrix minerals and are believed to have formed during annealing.

References: Bickel et al. (1976); Higuchi and Morgan (1975).

79215
MODAL ANALYSIS (VOL. %)

MATRIX (~39%)	
PLAGIOCLASE	81.3
MAFIC	17.5
OPAQUE	0.4
OTHER (apatite)	0.8
CLASTS (>39%):	
PLAGIOCLASE	
MAFIC	
OPAQUE	
FRAGMENTAL BRECCIA	
CRYSTALLINE BRECCIA	
GRANULITIC	
OTHER METAMORPHIC	
MARE BASALT	
HIGHLAND BASALT	
CRUSHED	
PORE SPACE	



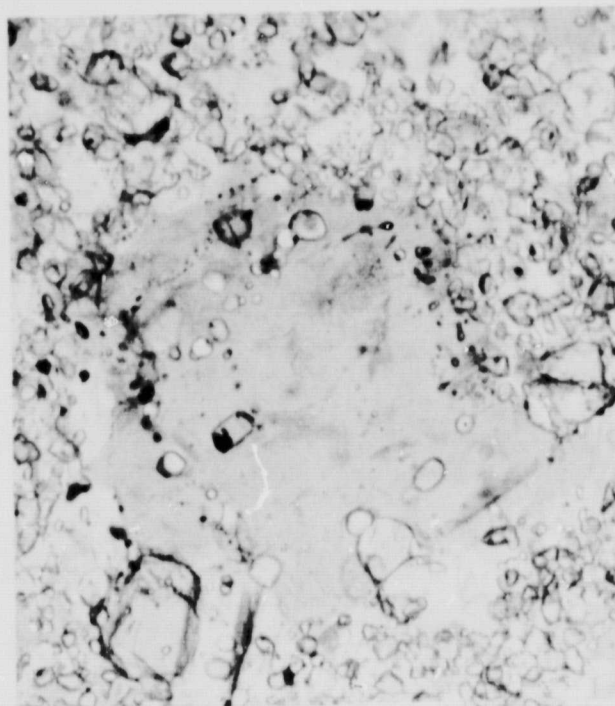
Bickel et al. 1976

adapted from Bickel et al. 1976



79215 0.5MM

a

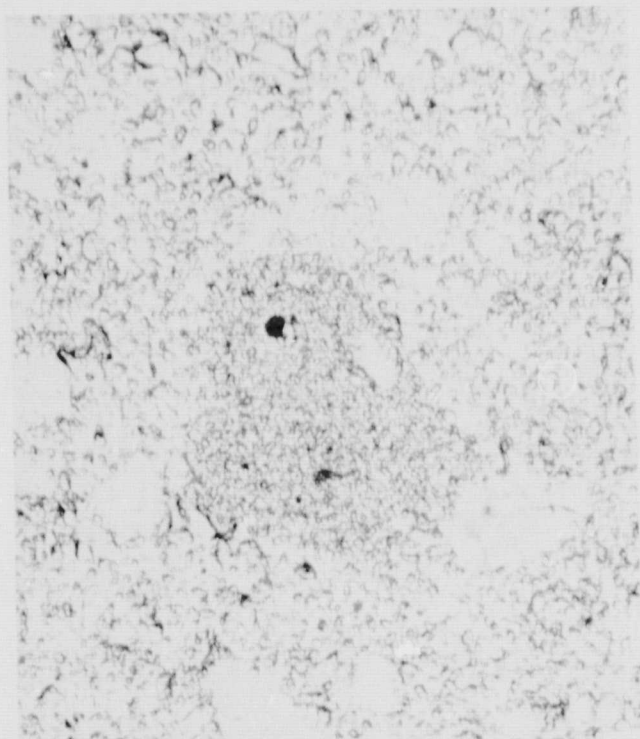


79215 0.10MM

b

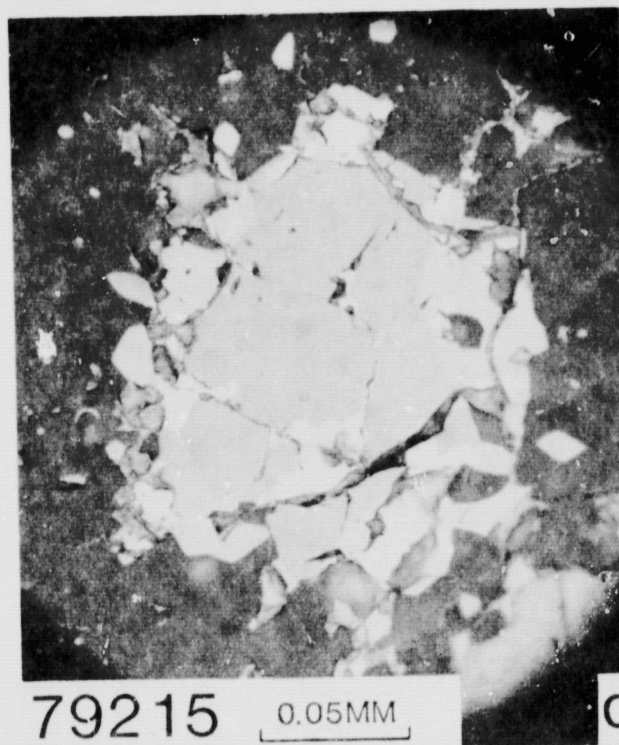
Figure 79215a. Typical view of 79215; transmitted light.

Figure 79215b. Plagioclase clast with olivine "necklace;" transmitted light.



79215 0.25MM

c



79215 0.05MM

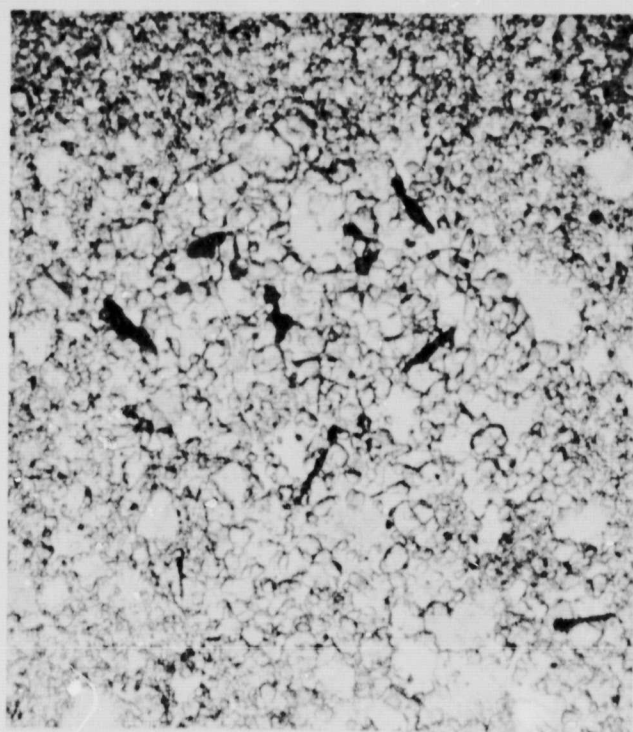
d

Figure 79215c. Olivine "cluster" in 79215; transmitted light.

Figure 79215d. Cr-spinel aggregate in 79215; reflected light.

79215

177



79215 0.25MM e

Figure 79215e. Polymineralic relic in 79215; transmitted light.

GEOCHEMISTRY TABLES

Table . Geochemistry of Soils from Apollo Landing Sites

	Apollo 11 10084	Apollo 12 12070	Apollo 14 14163	Apollo 15 15081	Apollo 16 605C1	Apollo 17 79221
SiO ₂	42.16	45.7	47.97	46.50	44.95	41.67
TiO ₂	7.75	2.78	1.77	1.58	0.60	6.52
Al ₂ O ₃	13.6	13.0	17.57	13.6	26.45	13.57
Cr ₂ O ₃	.30	.42	.26	.44	.11	.42
FeO	15.34	16.4	10.41	15.28	5.38	15.37
MnO	.20	.23	.14	.20	.08	.21
MgO	7.76	10.5	9.18	10.86	6.05	10.22
CaO	11.94	10.4	11.15	10.66	15.42	11.18
Na ₂ O	.47	.48	.68	.34	.44	.34
K ₂ O	.16	.23	.58	.13	.13	.09
P ₂ O ₅	.05	.32	.52	.157	.12	.06
S	.12	—	—	.078	—	.12
Total	100.50	100.46	100.23	99.82	99.73	99.77
Reference	1	26	126	34	130	85
Li ppm	—	15.	—	—	—	—
Rb ppm	—	5.2	15.3	3.9	3.6	1.7
Sr ppm	—	115.	186.	160.	126.	156.
Ba ppm	140.	420.	926.	220.	130.	80.
Sc ppm	58.9	38.	—	31.7	11.	48.
La ppm	16.9	34.9	68.2	18.4	11.6	8.2
Ce ppm	47.3	86.3	176.	51.	33.	30.
Nd ppm	41.	57.	103.	29.	—	24.
Sm ppm	31.66	18.1	29.0	8.50	—	7.1
Eu ppm	1.74	1.79	2.54	1.20	1.22	1.44
Gd ppm	1.3	17.6	—	—	—	—

Tb ppm	3.03	3.7	—	1.85	1.2	1.5
Dy ppm	21.0	24.3	38.3	11.4	8.6	10.
Er ppm	4.5	18.	23.8	—	—	—
Yb ppm	11.35	12.9	23.6	6.03	4.2	—
Lu ppm	1.69	1.9	—	.86	.7	.81
Zr ppm	290.	462.	—	290.	196.	193.
Hf ppm	10.2	—	—	6.53	4.4	5.6
Th ppm	—	—	—	2.58	2.2	1.0
U ppm	.45	—	—	—	—	.4
Reference	51	52	62	169	14	78
Ir ppb	7.62	8.5	13.6	7.1	—	2.
Re ppb	—	—	.93	—	—	—
Au ppb	4.15	2.4	5.4	2.3	—	3.
Co ppb	26.8	49.	—	46.	59.	35.
Ni ppm	—	2.5	—	200.	618.	236.
Sb ppb	—	—	—	—	—	—
Ge ppb	—	—	—	233.	—	—
Se ppb	—	—	—	—	—	—
Te ppb	—	100.	—	—	—	—
Ag ppb	8.89	46.	16.6	13.	—	—
Bi ppb	—	2.4	1.7	2.9	—	—
Zn ppm	21.1	6.9	31.	14.	29.0	51.
Cd ppb	53.3	—	140.	28.	—	—
Tl ppb	1.65	1.6	30.	1.8	—	—
Reference	41	76	98	42	14	78

Table Geochemistry of Lunar Breccias

	10060	12013, 10,12A Light-gray breccia	12013, 10,01 Dark-grey breccia	12034	14063, 46	14063, 37 Finest Matrix	14082	14301	14304
SiO ₂	41.96	—	—	45.8	44.69	—	—	48.26	45.91
TiO ₂	9.02	.3	3.3	2.7	1.48	1.5	—	2.06	2.08
Al ₂ O ₃	11.85	10.1	14.6	15.7	22.31	22.0	—	16.52	13.44
Cr ₂ O ₃	.31	.25	.162	.27	.21	.180	—	.21	.44
FeO	16.89	14.0	13.70	13.3	6.71	7.0	—	10.29	16.56
MnO	.23	.15	.166	.16	.08	.081	—	.14	.24
MgO	7.63	8.50	9.0	9.60	10.80	—	—	9.98	9.62
CaO	11.38	4.60	9.7	11.20	12.70	13.1	—	10.29	10.36
Na ₂ O	.49	1.12	1.45	.79	.76	.835	—	.84	.57
K ₂ O	.20	2.60	.40	—	.15	.17	.25	.75	.68
P ₂ O ₅	.07	—	—	—	.22	—	—	.64	.31
S	.15	—	—	—	—	—	—	—	—
Total	100.18	—	—	99.52	100.11	—	—	99.98	100.21
Reference	1	121	121	166	126	77	69	126	20
Li ppm	70-220	—	—	—	24.	—	—	—	—
Rb ppm	—	66.5	13.5	11.	5.	—	13.4	21.7	—
Sr ppm	—	—	—	—	205.	—	—	185.	—
Ba ppm	—	3760.	390.	.7	250.	360.	—	959.	—
Sc ppm	—	25.	28.	31.	13.	13.6	—	—	—
La ppm	20.8	56.5	135.7	70.	27.	26.5	—	71.8	—
Ce ppm	58.	151.	347.	172.	—	—	—	201.	—
Nd ppm	46.	74.	215.	100.	—	—	—	121.	—
Sm pm	15.4	19.0	59.	30.	—	10.6	—	34.7	—
Eu ppm	2.06	2.14	3.89	2.7	—	2.4	—	2.69	—
Gd ppm	24.	—	—	33.3	4.8	—	—	40.3	—

Tb ppm	3.6	5.2	12.5	5.51	---	---	---	---	---
Dy ppm	26.3	33.	75.	34.0	---	---	---	46.	---
Er ppm	16.0	---	---	31.7	---	---	---	28.	---
Yb ppm	13.2	30.	39.	22.4	6.8	10.	---	25.5	---
Lu ppm	2.0	4.2	5.2	2.74	---	1.4	---	---	---
Zr ppm	---	690.	2070.	640.	260.	---	---	---	---
Hf ppm	---	27.	63.	27.	---	---	---	---	---
Th ppm	---	47.5	24.5	13.2	---	---	4.2	---	---
U ppm	---	14.2	10.4	---	---	1.1	1.880	4.32	---
Reference	51	121	121	166	126	77	69	62	n.d.
Ir ppb	---	.15	.06	---	---	---	---	---	---
Re ppb	---	.047	4.6	---	---	.71	.834	---	---
Au ppb	---	.21	3.10	---	---	.22	.562	---	---
Co ppb	29.1	24.	31.	35.	16.	19.	---	---	---
Ni ppm	.02	---	---	---	110.	---	64.	---	---
Sb ppb	---	---	---	---	---	---	---	---	---
Ge ppb	---	---	---	---	---	23.	36.2	---	---
Se ppb	---	54.	99.	---	---	---	---	---	---
Te ppb	---	---	---	---	---	---	---	---	---
Ag ppb	---	.88	31.4	---	---	.80	64.	---	---
Si ppb	---	.46	.63	---	---	---	---	---	---
Zn ppm	---	2.06	4.10	---	<4	5.9	3.2	---	---
Cd ppb	---	91.	34.	---	---	---	---	---	---
Ti ppb	---	18.	1.9	---	---	4.0	---	---	---
Reference	51	75	75	166	126	98	48	n.d.	n.d.

	14310	14311	14312, 27,61	14321 9A MATRIX	14321 14A microbreccia clast	14321 15 microbreccia clast	14321 1B basalt clast	15086	15405, 26,117 breccia
SiO ₂	47.2	47.24	—	—	—	—	—	47.5	51.49
TiO ₂	1.24	1.81	—	2.27	1.58	1.73	2.20	1.67	1.80
Al ₂ O ₃	20.1	18.05	—	13.2	16.7	15.24	11.96	11.01	15.44
Cr ₂ O ₃	.18	.15	—	.43	—	.17	.46	.42	.22
FeO	8.38	11.13	10.5	15.4	10.7	10.54	16.3	17.49	11.17
MnO	.11	.14	—	.21	—	.13	.22	.26	.19
MgO	7.87	9.59	—	—	—	—	—	10.55	7.33
CaO	12.3	10.16	—	—	—	—	—	10.26	9.98
Na ₂ O	.63	.85	.77	.59	.81	.88	.53	.35	.81
K ₂ O	.49	.81	.56	.17	.51	.95	.13	.14	.82
P ₂ O ₅	.34	.76	—	—	—	—	—	.17	.72
S	.02	.06	—	—	—	—	—	—	—
Total	98.86	100.75	—	—	—	—	—	99.82	99.97
Reference	62	138	*	35	35	35	35	130	20
Li ppm	—	—	—	—	—	—	—	13.	24.
Rb ppm	12.8	—	—	3.6	12.9	—	2.7	4.1	29.
Sr ppm	188.	—	—	—	—	—	—	83.	190.
Ba ppm	617.	—	—	—	1070.	1140.	—	230	1200.
Sc ppm	—	—	18.1	52.8	—	21.4	54.6	33.	21.4
La ppm	56.4	—	67.	27.3	88.6	97.1	19.0	21.	77.0
Ce ppm	144.	—	182.	82.	260.	260.	56.	59.	200.0
Nd ppm	87.0	—	—	—	125.	150.	—	—	—
Sm ppm	24.0	—	30.4	14.7	42.	46.9	10.8	10.	35.3
Eu ppm	2.15	—	2.19	1.55	3.42	3.34	1.34	.035	2.33
Gd ppm	28.1	—	—	—	—	—	—	—	—

Tb ppm	—	—	6.5	3.1	9.6	9.4	2.34	2.1	5.9
Dy ppm	32.7	—	—	—	—	—	—	—	—
Er ppm	19.7	—	—	—	—	—	—	—	—
Yb ppm	18.4	—	22.5	9.3	30.5	32.6	6.5	6.9	25.5
Lu ppm	—	—	5.25	1.6	4.3	4.35	1.15	1.13	3.6
Zr ppm	700.	—	—	—	720.	1070.	—	260.	—
Hf ppm	—	—	25.3	9.8	29.5	32.1	7.7	7.4	30.
Th ppm	11.	—	13.9	3.6	19.0	21.9	2.3	3.7	14.1
U ppm	—	—	—	—	—	—	—	—	4.690
Reference	62	n.d.	*	35	35	35	35	40	
Ir ppb	10.5	—	—	.71	7.8	.044	—	—	.63 1.28
Re ppb	1.02	—	—	.056	.70	.0051	—	—	.121
Au ppb	4.31	—	—	.70	6.06	.30	—	—	.525
Co ppb	—	—	31.3	33.2	31.4	34.3	—	42.	19.2
Ni ppm	64-410	—	280.	—	—	—	—	79.	83.
Sb ppb	4.5	—	—	15.3	2.2	.78	—	—	1.06
Ge ppb	130.	—	—	240.	50.	640.	—	—	62.6
Se ppb	120.	—	—	162.	128.	338.	—	33.	78.
Te ppb	4.	—	—	—	11.	6.	—	—	4.9
Ag ppb	10.780	—	—	1.1	.88	.60	—	—	2.22
Bi ppb	2.5	—	—	.55	.34	.39	—	—	.25
Zn ppm	2.3	—	28.	2.8	6.6	2.9	—	28.	4.2
Cd ppb	2.6	—	—	7.3	298.	24.	—	—	17.7
Tl ppb	10.0	—	—	1.7	8.1	1.7	—	—	3.4
Reference	98	n.d.	*	101	101	101	n.d.	40	48

* Blanchard, unpublished

	15405 26,63,85,11: quartz- monzodiorite clast	15445 matrix	15445 olivine-bearing White clast	15445 spinel clast	60255	61015	61016 matrix	61016 anorthosite clast	62235
SiO ₂	—	44.6	—	—	45.24	—	43.82	44.15	47.05
TiO ₂	—	1.47	—	—	.69	—	.69	.20	1.19
Al ₂ O ₃	—	16.66	—	7.2	26.11	—	25.06	33.19	18.88
Cr ₂ O ₃	.181	.26	.25	1.074	.10	—	.11	.03	.19
FeO	15.1	9.83	3.9	6.4	5.85	—	4.97	1.40	9.45
MnO	—	.14	—	—	.06	—	.05	.02	.13
MgO	—	16.0	—	31.1	6.39	—	10.48	2.51	10.0
CaO	—	10.04	—	1.9	15.14	—	14.31	18.30	11.80
Na ₂ O	.89	.55	.32	.14	.46	—	.36	.34	.42
K ₂ O	1.85	.17	—	—	.12	—	.07	.02	.33
P ₂ O ₅	—	.21	—	—	.12	—	.12	.05	.39
S	—	.06	—	—	.04	—	—	.01	.10
Total	—	99.99	—	—	100.32	—	100.04	100.22	99.93
Reference	*	135a	124	124	139	63	63	63	63
Li ppm	—	14.1	—	—	—	—	7.3	2.2	—
Rb ppm	—	3.56	1.14	.661	—	—	2.84	.446	8.39
Sr ppm	164	160.	—	—	—	—	130.	177.91	152.
Ba ppm	1310.	237.	—	25.0	140.	—	160.	40.7	530.
Sc ppm	30.7	—	7.1	3.43	16.7	—	6.6	—	16.5
La ppm	211.	22.1	4.02	2.86	12.6	—	16.7	3.47	60.3
Ce ppm	545.	57.6	10.8	3.2	35.	—	46.	8.61	160.
Nd ppm	—	35.7	—	2.89	—	—	—	5.60	94.
Sm ppm	92.6	10.1	1.81	1.19	—	—	6.9	1.56	25.2
Eu ppm	2.66	1.85	.87	.31	1.35	—	1.38	.926	1.93
Gd ppm	—	11.9	—	2.09	—	—	9.5	1.84	31.7

* Blanchard unpublished

Tb ppm	15.6	—	.46	.26	—	1.5	—	5.56
Dy ppm	—	13.2	—	4.88	—	9.7	1.91	35.0
Er ppm	—	7.71	—	4.04	—	4.8	1.16	21.0
Yb ppm	62.7	6.90	1.72	.90	4.6	4.4	1.01	19.4
Lu ppm	8.9	1.02	.28	.136	0.70	.61	.149	2.59
Zr ppm	—	—	—	—	—	209.	51.2	858.
Hf ppm	50.2	—	1.36	.74	5.2	4.9	1.06	20.7
Th ppm	40.0	—	.82	.27	5.2	1.6	.486	7.83
U ppm	—	—	.135	.024	2.4	.46	.101	2.08
Reference *	124	—	*	*	14	168	168	170
Ir ppb	—	6.21	.072	.34	—	11.5	.0099	17.0
Re ppb	—	.668	.0097	.174	—	1.28	.0022	1.7
Au ppb	—	6.02	.022	.319	—	9.55	.02	17.6
Co ppb	—	47.4	10.3	50.4	35.0	36.7	—	54.2
Ni ppm	—	396.	11.4	901.	—	515.	<1	830.
Sb ppb	—	244.	.42	18.9	—	3.13	.15	—
Ge ppb	—	630.	5.09	338.	—	620.	13.	.8
Se ppb	—	91.	4.6	1.3	—	181.	.40	260.
Te ppb	—	—	—	—	—	4.8	<.4	—
Ag ppb	—	2.0	.5	1.7	—	21.4	.29	—
Bi ppb	—	.24	.25	.22	—	7.3	.22	—
Zn ppm	—	2.5	1.5	13.4	—	.84	1.45	11.0
Cd ppb	—	5.3	2.8	2.0	—	29.5	190.	—
Tl ppb	—	.59	3.5	2.7	—	45.3	131.	—
Reference n.d.	49	49	49	49	14	74	74	170

* Blanchard, unpublished

	62295	65015, 45,51	67015	68415	72315	76215, 28,29,48	76295, 14,37	76315, 35,65,73 matrix	76315, 62 light-grey clast
SiO ₂	44.73	47.18	45.79	45.4	—	46.13	47.03	46.21	45.10
TiO ₂	.68	1.04	.48	.32	1.4	1.24	1.39	1.50	.36
Al ₂ O ₃	20.28	19.98	29.46	28.63	19.2	18.73	18.25	18.14	26.37
Cr ₂ O ₃	.11	.34	.06	—	.187	—	—	.20	—
FeO	6.29	7.91	3.62	4.25	8.5	8.08	9.09	8.95	5.29
MnO	.10	.12	.05	.06	.111	—	—	0.12	0.07
MgO	15.06	10.34	3.84	4.38	.2	12.43	10.78	12.02	7.46
CaO	11.78	12.03	15.39	16.39	11.3	11.50	11.54	11.32	15.12
Na ₂ O	.43	.44	.51	.41	.70	—	—	0.60	0.47
K ₂ O	.08	.32	.082	.06	.35	0.25	0.26	0.26	0.10
P ₂ O ₅	.13	.40	—	.07	—	0.24	0.32	0.29	0.06
S	.07	.13	—	.04	—	—	—	.97	—
Total	99.74	100.23	99.28	100.01	—	98.60	98.66	100.58	100.40
Reference	63	63	169	64	79	146	146	146	146
Li ppm	—	—	—	5.1	—	22.6	19.4	13.9	9.5
Rb ppm	4.59	9.09	1.42	1.704	9.6	6.10	5.43	5.78	2.336
Sr ppm	139.	164.	195.	182.4	165.	—	—	174.	153.
Ba ppm	187.	492.	86.2	76.2	280.	294.	376.	337.	72.
Sc ppm	—	—	—	—	16.	—	—	—	—
La ppm	18.6	49.5	4.9	6.81	31.	27.3	37.8	31.6	5.41
Ce ppm	45.9	125.	11.6	18.3	77.	68.9	95.7	82.3	13.7
Nd ppm	29.0	78.0	7.9	10.9	50.	43.7	60.0	52.7	8.60
Sm ppm	8.30	22.2	2.14	3.09	12.9	12.3	16.9	14.8	2.42
Eu ppm	1.18	1.91	1.16	1.11	1.83	1.70	1.91	1.95	0.94
Gd ppm	10.1	26.6	2.6	3.78	—	15.9	21.3	18.8	2.99

77017 79135 79215,
24,28

SiO ₂	44.09	42.29	44.8
TiO ₂	.41	5.15	.3
Al ₂ O ₃	26.59	15.08	27.6
Cr ₂ O ₃	.13	.39	.098
FeO	6.19	14.01	4.15
MnO	.08	.19	.054
MgO		10.42	5.84
CaO	15.43	11.44	16.3
Na ₂ O	.30	.40	.549
K ₂ O	.05	.10	.107
P ₂ O ₅	.03	.07	—
S	.15	.10	—
Total		99.64	99.79
Reference	64	122	12
Li ppm	4.4	10.6	—
Rb ppm	1.31	2.1	.489
Sr ppm	141.	171.	—
Ba ppm	49.0	123.	—
Sc ppm	—	—	7.14
La ppm	3.48	—	2.5
Ce ppm	8.90	29.2	6.5
Nd ppm	5.56	21.7	—
Sm ppm	1.60	7.51	1.03
Eu ppm	.794	1.64	.77
Gd ppm	2.01	—	—

Tb ppm	—	—	—	.23
Dy ppm	2.34	11.7	—	—
Er ppm	1.5	—	—	—
Yb ppm	1.5	5.85	1.07	—
Lu ppm	—	.712	.16	—
Zr ppm	59.1	185.	—	—
Hf ppm	1.6	—	1.34	—
Th ppm	—	—	.21	—
U ppm	.22	—	.190	—
Reference	64	115	12	—
Ir ppb	17.0	5.8	21.3	—
Re ppb	1.73	—	1.9	—
Au ppb	5.65	4.7	8.27	—
Co ppb	—	—	18.8	—
Ni ppm	443.	160.	255.	—
Sb ppb	.72	—	2.79	—
Ge ppb	110.	285.	33.	—
Se ppb	68.	—	176.	—
Te ppb	1.9	—	17.0	—
Ag ppb	.87	—	1.16	—
Bi ppb	.22	—	.16	—
Zn ppm	2.5	97.	2.3	—
Cd ppb	9.0	120.	.98	—
Tl ppb	.77	—	.41	—
Reference	100	8	97	—

References

1. Agrell S.O., Scoon J.H., Muir I.D., Long J.V.P., McConnell J.D., and Peckett A. (1970). Observations on the chemistry, mineralogy, and petrology of some Apollo 11 lunar samples. Proc. Apollo 11 lunar Sci. Conf., p. 120-134.
2. Agrell S.O., Agrell J.E., Arnold A.R. and Long J.V.P. (1973). Some observations on rock 62295. Lunar Science IV, p. 15-17.
3. Ahrens T.J. and O'Keefe J.D. (1972). Shock melting and vaporization of lunar rocks and minerals. The Moon 4 p. 214-219.
4. Albee A.L., Gancarz A.J. and Chodos A.A. (1973). Metamorphism of Apollo 16 and 17 and Luna 20 metaclastic rocks at about 3.95 AE: Samples 61156, 64423,14-2, 65015, 67483,15-2, 76055, 22006, and 22007. Proc. Lunar Sci. Conf. 4th, p. 569-595.
5. Anders E., Ganapathy R., Krähenbühl U. and Morgan J.W. (1973). Meteoritic material on the moon. The Moon 8, p. 3-24.
6. Anderson A.T., Braziunas T.F., Jacoby J. and Smith J.V. (1972). Thermal and mechanical history of breccias 14306, 14063, 14270 and 14321. Proc. Lunar Sci. Conf. 3rd, p. 819-835.
7. Ashwal L.D. (1975). Petrologic evidence for a plutonic igneous origin of anorthositic norite clasts in 67955 and 77017. Proc. Lunar Sci. Conf. 6th, p. 221-230.
8. Baedeker P.A., Chou C.-L., Sundberg L.L., and Wasson J.T. (1975). Volatile and siderophile trace elements in the soils and rocks of Taurus-Littrow. Proc Lunar Sci. Conf. 5th, p. 1625-1644.
9. Bence A.E. and Papike J.J. (1972). Pyroxenes as recorders of lunar basalt petrogenesis: Chemical trends due to crystal-liquid interaction. Proc. Lunar Sci. Conf. 3rd, p. 431-469.
10. Bickel C.E., Warner J.L. and Phinney W.C. (1976). Petrology of 79215: Brecciation of a lunar cumulate. Proc. Lunar Sci. Conf. 7th, p. 1793-1819.
11. Bickel C.E. (1977). Petrology of 78155: An early, thermally metamorphosed polymict breccia. Proc. Lunar Sci. Conf. 8th, p. 2007-2027.
- 11a. Bickel C.E. and Warner J.L. (1978). Survey of lunar plutonic and granulitic lithic fragments. Proc. Lunar Sci. Conf. 9th, p. 629-652.
12. Blanchard D.B., Jacobs J.W. and Brannon J.C. (1977). Chemistry of the ANT-suite and felsite clasts from consortium breccia 73215 and of gabbroic anorthosite 79215. Proc. Lunar Sci. Conf. 8th, p. 2507-2524.

13. Bogard D.D. and Nyquist L.E. (1973). $^{40}\text{Ar}/^{39}\text{Ar}$ variations in Apollo 15 and 16 regolith. Proc. Lunar Sci. Conf. 4th, p. 1975-1985.
14. Boynton W.", Baedeker P.A., Chou C.-L., Robinson K.L. and Wasson J.T. (1975). Mixing and transport of lunar surface materials: Evidence obtained by the determination of lithophile, siderophile, and volatile elements. Proc. Lunar Sci. Conf. 6th, p. 2241-2259.
15. Brown G.M., Peckett A., Phillips R., and Emeleus C.H. (1973). Mineral chemical variations in the Apollo 16 magnesio-feldspathic highland rocks. Proc. Lunar Sci. Conf. 4th, p. 505-518.
16. Cadogan P.H. and Turner G. (1976). The chronology of the Apollo 17 Station 6 boulder. Proc. Lunar Sci. Conf. 7th, p. 2267-2285.
- 16a. Cameron E.N. (1970). Opaque minerals in certain lunar rocks from Apollo 11. Proc. Apollo 11 Lunar Sci. Conf., p. 221-245.
17. Cameron K.L. and Fisher G.W. (1975). Olivine-matrix reactions in thermally metamorphosed Apollo 14 breccias. Earth and Planetary Science Letters, Vol. 25, p. 197-207.
18. Chao E.C.T., Boreman J.A. and Desborough G.A. (1971). The petrology of unshocked and shocked Apollo 11 and Apollo 12 microbreccias. Proc. Lunar Sci. Conf. 2nd, p. 797-816.
19. Chao E.C.T., Minkin J.A. and Best J.A. (1972). Apollo 14 breccias: General characteristics and classification. Proc. Lunar Sci. Conf. 3rd, p. 645-661.
20. Christian A.P., Berman S., Dwornik E.J., Rose H.J. Jr., and Schnepfe M.M. (1976) Composition of some Apollo 14, 15 and 16 lunar breccias and two Apollo 15 Fines. Lunar Science VII, p.141-142. The Lunar Science Institute, Houston.
21. Christie J.M., Griggs D.T., Heuer A.H., Nord G.L., Radcliffe S.V., Lally J.S. and Fisher R.M. (1973). Electron petrography of Apollo 14 and 15 breccias and shock-produced analogs. Proc. Lunar Sci. Conf. 4th, p. 365-382.
22. Compston W., Chappell B.W., Arriens P.A. and Vernon M.J. (1970). The chemistry and age of Apollo 11 lunar material. Proc. Apollo 11 Lunar Sci. Conf., p. 1007-1027.
23. Compston W., Vernon M.J., Berry H., and Rudowski R. (1971). Age of Fra Maura formation - radiometric older limit. Earth and Planetary Science Letters, Vol. 12, p. 55.
24. Cooper H.F. Jr. and Sauer F.M. (1977). Crater-related ground motions and implications for crater scaling. Impact and Explosion Cratering - Planetary and Terrestrial Implications, p. 1133-1163.
25. Crawford M.L. and Hollister L.S. (1974). KREEP Basalt: A possible partial melt from the lunar interior. Proc. Lunar Sci. Conf. 5th, p. 399-419.

26. Cuttitta F., Rose H.J., Ansell C.S., Carron M.K., Christian R.P., Dwornik E.J., Greenland L.P., Helz A.W., Ligon D.T., Jr. (1971). Elemental composition of some Apollo 12 lunar rocks and soils. Proc. Lunar Sci. Conf. 2nd, p. 1217-1229.
27. Delano J.W., Bence A.E., Papike J.J. and Cameron K.L. (1973). Petrology of the 2-4 mm soil fraction from the Descartes region of the moon and stratigraphic implications. Proc. Lunar Sci. Conf. 4th, p. 537-553.
28. Dence M.R., Innes, M.J.S. and Robertson P.B. (1968). Recent geological and geophysical studies at Canadian craters. Shock Metamorphism of Natural Materials, p. 339-362.
29. Dence M.R., Grieve R.A.F., and Robertson P.B. (1977). Terrestrial impact structures: Principal characteristics and energy considerations. Impact and Explosion Cratering - Planetary and Terrestrial Implications, p. 247-275.
30. Dowty E., Keil K., Prinz M., Gros J. and Takahashi H. (1976). Meteorite-free Apollo 15 crystalline KREEP. Proc. Lunar Sci. Conf. 7th, p. 1833-1844.
31. Drake M.J., McCallum I.S., McKay G.A., and Weill D.F. (1970). Mineralogy and petrology of Apollo 12 sample 12013: a progress report. Earth Planet. Sci. Letters, Vol. 9, p. 103-123.
32. Drake J.C. and Klein C. Jr. (1973). Lithic fragments and glasses in microbreccia 15086: Their chemistry and occurrence. Proc. Lunar Sci. Conf. 4th, pp. 467-479.
33. Duke M.B., Woo C.C., Sellers G.A., Bird M.L. and Finkelman R.B. (1970). Genesis of lunar soil at Tranquillity Base. Proc. Apollo 11 Lunar Sci. Conf., p. 347-361.
34. Duncan A.R., Sher M.K., Abraham Y.C., Erlank A.J., Willis J.P. and Ahrens L.H. (1975a). Interpretation of the compositional variability of Apollo 15 soils. Proc. Lunar Sci. Conf. 6th, p. 2309-2320.
35. Duncan A.R., McKay S.M., Stoesser J.W., Lindstrom M.M., Lindstrom D.J., Fruchter J.S. and Goles G.G. (1975b). Lunar polymict breccia 14321 - Compositional study of its principal components. Geochim. et Cosmochim. Acta, Vol. 39 (3), p. 247.
36. Dymek R.F., Albee A.L. and Chodos A.A. (1976). Petrology and origin of Boulders #2 and #3, Apollo 17 Station 2. Proc. Lunar Sci. Conf. 7th, p. 2335-2378.
37. El Goresy A. (1965). Baddelyite and its significance in impact glasses. J. Geophys. Res. 70, p. 3453-3456.
38. Engelhardt W.v., Arndt J., Muller W.F. and Stöffler D. (1971). Shock metamorphism and origin of regolith and breccias at the Apollo 11 and 12 landing sites. Proc. Lunar Sci. Conf. 2nd, p. 833-854.
39. Engelhardt W.v., Arndt J., Stoffler D. and Schneider H. (1972). Apollo 14 regolith and fragmental rocks, their compositions and origin by impact. Proc. Lunar Sci. Conf. 3rd, p. 753-770.

40. Fruchter J.S., Stoesser J.W., Lindstrom M.M., and Goles G.G. (1973). Apollo 15 clastic materials and their relationship to local geologic features. Proc. Lunar Sci. Conf. 4th, Vol. 2, p. 1227-1238.
41. Ganapathy R., Reid K.R., Laul J.C. and Anders E. (1971). Trace elements in Apollo 11 lunar rocks: Implications for meteorite influx and origin of moon. Proc. Apollo 11 Lunar Sci. Conf., p.1117-1142.
42. Ganapathy R., Morgan J.W., Krähenbühl U., and Anders E. (1973). Ancient meteoritic components in lunar highland rocks - clues from trace elements in Apollo 15 and 16 samples. Proc. Lunar Sci. Conf. 4th, Vol. 2, p. 1239-1262.
43. Gancarz A.J., Albee A.L. and Chodos A.A. (1972). Comparative petrology of Apollo 16 sample 68415 and Apollo 14 samples 14276 and 14310. Earth Planet. Sci. Lett. 16, p. 307-330.
44. Gast P.W. (1972). The chemical composition and structure of the Moon. The Moon 5, p. 121-148.
- 44a. Gault D.E., Quaide W.L. and Oberbeck V.R. (1968). Impact cratering mechanics and structures. In Shock Metamorphism of Natural Materials (B.M. French and N.M. Short, eds.). Mono Book Corp., Baltimore.
45. Gray C.M., Compston W., Foster J.J. and Rudowski R. (1974). Rb-Sr ages of clasts from within Boulder 1, Station 2, Apollo 17. In Interdisciplinary Studies of Samples From Boulder 1, Station 2, Apollo 17, Vol. 2 (J.A. Wood, ed.) LSI Contr. 211D, Section VII, p. 1-10. Center for Astrophysics, Cambridge.
46. Grieve R.A., McKay G.A., Smith H.D., and Weill D.J. (1975). Lunar polymict breccia 14321: A petrographic study. Geochim. Cosmochim. Acta 39, p. 229-245.
47. Grieve R.A.F., Dence M.R. and Robertson P.B. (1977). Cratering processes: As interpreted from the occurrence of impact melts. Impact and Explosion Cratering - Planetary and Terrestrial Implications, p. 791-814.
48. Gros J., Takahashi H., Hertogen J., Morgan J.W. and Anders E. (1976a). Composition of the projectiles that bombarded the lunar highlands. Proc. Lunar Sci. Conf. 7th, p. 2403-2425.
49. Gros J., Takahashi H., Morgan J.W., and Anders E. (1976b) Siderophile and volatile elements in Apollo 14 and 15 rocks of the Imbrium Consortium. In Interdisciplinary Studies by the Imbrium Consortium, Vol. 1, (J.A. Wood, ed.). LSI Contr. 267D, p. 125-131. Center for Astrophysics, Cambridge.
50. Hartung J.B., Hörz F. and Gault D.E. (1972). Lunar microcraters and interplanetary dust. Proc. Lunar Sci. Conf. 3rd, p. 2735-2753.
51. Haskin L.A., Allen P.O. Jr., Helmke P.A., Paster T.P., Anderson M.R., Korotev R.L., and Zweifel K.A. (1970). Rare-earths and other trace elements in Apollo 11 lunar samples. Proc. Apollo 11 Lunar Sci. Conf. Geochim et Cosmochim Acta, p. 1213-1232.

52. Haskin L.A., Helmke P.A., Allen R.O., Anderson M.R., Korotev R.L. and Zweifel K.A. (1971). Rare-earth elements in Apollo 12 lunar materials. Proc. Lunar Sci. Conf. 2nd, p. 1307-1317.
53. Haskin L.A., Helmke P.A., Blanchard D.P., Jacobs J.W. and Telander K.M. (1973). Major and trace element abundances in samples from the lunar highlands. Proc. Lunar Sci. Conf. 4th, Vol. 2, p. 1275-1296.
54. Haskin L.A., Blanchard D.P., Korotev R., Jacobs J.W., Brannon J.A., Clark R.S., and Hermann A.G. (1974) Major and trace element concentrations in samples from 72275 and 72255. In Interdisciplinary Studies of Samples from Boulder 1, Station 2, Apollo 17, Vol. 1 (J.A. Wood, ed.). LSI Contr. 210D, p. 121-130. Center for Astrophysics, Cambridge.
55. Heiken G.H. (1974). A catalogue of lunar soils. NASA Johnson Space Center, Curators Office. 220p.
- 55a. Heiken G.H., McKay D.S. and Brown R.W. (1974). Lunar deposits of possible pyroclastic origin. Geochim. Cosmochim. Acta 38, p. 1703-1718.
56. Heiken G.H. (1975). Petrology of Lunar Soils Rev. Geophys. and Space Physics, Vol. 13 No. 4, p. 567-587.
57. Helz R.T. and Appleman D.E. (1973). Mineralogy, petrology, and crystallization history of Apollo 16 rock 68415. Proc. Lunar Sci. Conf. 4th., p. 643-661.
58. Higuchi H. and Morgan J.W. (1975). Ancient meteoritic component in Apollo 17 boulders. Proc. Lunar Sci. Conf. 6th, p. 1625-1651.
59. Hodges F.N. and Kushiro I. (1973). Petrology of Apollo 16 lunar highland rocks. Proc. Lunar Sci. Conf. 4th, p. 1033-1048.
60. Hörz F. (1965). Untersuchungen an Riesglasern. Beitrag Mineral. Petrog. 11, p. 621-661.
61. Hubbard N.J. and Gast P.W. (1971). Chemical composition and origin of nonmare lunar basalts. Proc. Lunar Sci. Conf. 2nd, p. 999-1020.
62. Hubbard N.J., Gast P.W., Rhodes J.M., Bansal B.M. and Wiesmann H. (1972). Nonmare basalts: Part II. Proc. Lunar Sci. Conf. 3rd, p. 1161-1179.
63. Hubbard N.J., Rhodes J.M., Gast P.W., Bansal B.M., Shih C.-Y., Wiesmann H. and Nyquist L.E. (1973). Lunar rock types: The role of plagioclase in non-mare and highland types. Proc. Lunar Sci. Conf. 4th, p. 1297-1312.
64. Hubbard N.J., Rhodes J.M., Wiesmann H., Shih C.-Y. and Bansal B.M. (1974). The chemical definition and interpretation of rock types returned from the non-mare regions of the moon. Proc. Lunar Sci. Conf. 5th, p. 1227-1247.
65. Irving A.J. (1977). Chemical variation and fractionation of KREEP basalt magmas. Proc. Lunar Sci. Conf. 8th, p. 2433-2448.
66. James O.B. (1970). Petrology of lunar microbreccia 12013,6. U.S. Geol. Survey Interagency Report: Astrogeology 23.

67. James O.B. (1973). Crystallization history of lunar feldspar basalt 14310. U.S.G.S. Prof. Paper 841, 22p.
68. James O.B. and Hammarstrom J.G. (1977). Petrology of four clasts from consortium breccia 73215. Proc. Lunar Sci. Conf. 8th, p. 2459-2494.
69. Keith J.E., Clark R.S. and Richardson K.A. (1972). Gamma-ray measurements of Apollo 12, 14 and 15 lunar samples. Proc. Lunar Sci. Conf. 3rd, p. 1671-1681.
70. Kieffer S.W. (1975). From Regolith to rock by shock. The Moon 13, p. 301-320.
71. Kieffer S.W. and Simonds C.H. (1979). The role of volatiles in the cratering process. Submitted to Rev. Geophys. and Space Phys.
72. King Elbert A. Jr., Carman Max F., Butler John C. (1970). Mineralogy and petrology of coarse particulate material from the lunar surface at Tranquillity Base. Proc. Apollo 11 Lunar Sci. Conf., p. 599-606.
73. King E.A. Jr., Butler J.C. and Carman M.F. (1972). Chondrules in Apollo 14 samples and size analyses of Apollo 14 and 15 fines. Proc. Lunar Sci. Conf. 3rd, p. 673-686.
74. Krahenbuhl U., Ganapathy R., Morgan J.W. and Anders E. (1973). Volatile elements in Apollo 16 samples - implications for highland volcanism and accretion history of the moon. Proc. Lunar Sci. Conf. 4th, Vol. 2, p. 1325-1348.
75. Laul J.C., Morgan J.W., Ganapathy R. and Anders E. (1970). Abundances of 14 trace elements in lunar rock 12013,10. Earth Planet. Sci. Lett. 9, p. 211-215.
76. Laul J.C., Morgan J.W., Ganapathy R., and Anders E. (1971). Meteoritic material in lunar samples: Characterization from trace elements. Proc. Lunar Sci. Conf. 2nd, p. 1139-1158.
77. Laul J.C., Wakita H., Showalter D.L., Boynton W.V., and Schmitt R.A. (1972). Bulk, rare earth, and other trace elements in Apollo 14 and 15 and Luna 16 samples. Proc. Lunar Sci. Conf. 3rd, p. 1181-1200.
78. Laul J.C. and Schmitt R.A. (1973). Chemical composition of Apollo 15, 16, and 17 samples. Proc. Lunar Sci. Conf. 4th, p. 1349-1367.
79. Laul J.C. and Schmitt R.A. (1974). Chemical composition of Boulder 2 rocks and soils, Apollo 17, Station 2. Earth Planet. Sci. Lett. 23, p. 206-219.
80. Lindstrom M.M., Duncan A.R., Fruchter J.S., McKay S.M., Stoesser J.W., Goldes G.G. and Lindstrom D.J. (1972). Compositional characteristics of some Apollo 14 clastic materials. Proc. Lunar Sci. Conf. 3rd, p. 1201-1214.
81. Lofgren G. (1974). An experimental study of plagioclase crystal morphology: isothermal crystallization. Amer J. Sci. 274, p.243-273.

82. LSPET (Lunar Sample Preliminary Examination Team) (1971). Preliminary examination of lunar samples from Apollo 14. Science 173, p. 681-693.
83. LSPET (Lunar Sample Preliminary Examination Team) (1972). The Apollo 15 Lunar samples. Science 175. p. 363-374.
84. LSPET (Lunar Sample Preliminary Examination Team) (1973). The Apollo 16 lunar samples: Petrographic and chemical description. Science 179; p. 23-24.
85. LSPET (Lunar Sample Preliminary Examination Team) (1973). Apollo 17 lunar samples: Chemical and petrographic description. Science 182, p. 659-672.
86. Lunatic Asylum (1970). Mineralogic and isotopic investigations on lunar rock 12013. Earth Planet. Sci. Lett. 9, p. 137-163.
87. McCallum I.S., Mathez E.A., Okamura F.P. and Ghose S. (1974). Petrology and crystal chemistry of poikilitic anorthositic gabbro 77017. Proc. Lunar Sci. Conf. 5th, p. 287-302.
88. McCallum I.S. and Mathez E.A. (1975). Petrology of noritic cumulates and a partial melting model for the genesis of Fra Mauro basalts. Proc. Lunar Sci. Conf. 6th, p. 395-414.
89. McGee J.J., Bence A.E. and Schaeffer O.A. (1978). Feldspathic granulite 79215: Conditions of metamorphism and age. Lunar Science IX, p. 720-722.
90. McKay David S., Greenwood William R., Morrison Donald A. (1970). Origin of small lunar particles and breccia from the Apollo 11 site. Proc. Apollo 11 Lunar Sci. Conf., p. 673-694.
91. McKay D.S. and Morrison D.A. (1971). Lunar breccias. Jour Geophys. Res. Vol. 76, No. 23, p. 5658-5669.
92. Mark R.K., Lee-Hu C. and Wetherill G.W. (1974). Rb-Sr measurements on lunar igneous rocks and breccia clasts. Lunar Science V. Part II, p. 490-492. The Lunar Science Institute, Houston.
93. Mason B., Fredriksson K., Henderson E.P., Jarosewich E., Melson W.G., Towe K.M. and White J.S. Jr. (1970). Mineralogy and petrology of lunar samples. Proc. Apollo 11 Lunar Sci. Conf., p. 655-660.
94. Melosh H. Jay (1976). On the origin of fractures radial to lunar basins. Proc. Lunar Sci. Conf. 7th, p. 2967-2982.
95. Meyer C. Jr., Anderson D.H. and Bradley J.G. (1974). Ion microprobe mass analysis of plagioclase from "non-mare" lunar samples. Proc. Lunar Sci. Conf. 5th, p. 685-706.
96. Meyer C. Jr. (1977). Petrology, mineralogy, and chemistry of KREEP basalt. Phys. Chem. Earth, Vol. 10, p. 506-508.
97. Morgan J.W., Higuchi H., Ganapathy R. and Anders E. (1975). Meteoritic material in four terrestrial meteorite craters. Proc. Lunar Sci. Conf. 6th, p. 1609-1623.

98. Morgan J.W., Laul J.C., Krähenbühl U., Ganapathy R. and Anders E. (1972). Major impacts on the moon: Characterization from trace elements in Apollo 12 and 14 samples. Proc. Lunar Sci. Conf. 3rd, Vol. 2, p. 1377-1397.
99. Morgan J.W., Ganapathy R., Higuchi H., Krähenbühl U., and Anders E. (1974a) Siderophile and volatile elements in 72255 and 72275. In Interdisciplinary Studies of Samples from Boulder 1, Station 2, Apollo 17, Vol. 1 (J.A. Wood, ed.). LSI Contr. 210D p. 131-138. Center for Astrophysics, Cambridge.
100. Morgan J.W., Ganapathy R., Higuchi H., Krähenbühl U. and Anders E. (1974b). Lunar Basins: Tentative characterization of projectiles, from meteoritic elements in Apollo 17 boulders. Proc. Lunar Sci. Conf. 5th, pp. 1703-1736.
101. Morgan J.W., Ganapathy R. and Krahenbuhl U. (1975). Meteoritic trace elements in lunar rock 14321,184. Geochim. et Cosmochim. Acta, Vol. 39, p. 261-264.
102. Muehlberger W.R., Batson R.M., Boudette E.L., Duke C.M., Eggleton R.E., Elston D.P., England A.W., Freeman V.L., Hait M.H., Hall T.A., Head J.W., Hodges C.A., Holt H.E., Jackson E.D., Jordon J.A., Larson K.B., Milton D.J., Reed U.S., Rennilson J.J., Schaber G.G., Schafer J.P., Silver L.T., Stuart-Alexander D., Sutton K.L., Swann G.A., Tyner R.L., Ulrich G.E., Wilshire H.G., Wolfe E.W. and Young J.W. (1972). Preliminary geologic investigation of the Apollo 16 landing site. Apollo 16 Preliminary Science Report. NASA SP-315, pp. 6-1 through 6-81.
103. Muehlberger W.R., Batson R.M., Cernan E.A., Freeman V.L., Hait M.H., Holt H.E., Howard K.A., Jackson E.D., Larson K.B., Reed U.S., Rennilson J.J., Schmitt H.H., Scott D.H., Sutton R.L., Stuart-Alexander D., Swann G.A., Trask N.J., Ulrich G.E., Wilshire H.G., and Wolfe E.W. (1973). Preliminary geologic investigation of the Apollo 17 landing site. Preliminary Science Report, NASA-SP-330, pp. 6-1 through 6-91.
- 103a. Nyquist L.E. (1977). Lunar Rb-Sr Chronology. Phys. Chem. Earth 10, p. 103-142.
104. Nyquist L.E., Hubbard N.J., Gast P.W., Church S.E., Bansal B.M. and Wiesmann H. (1972). Rb-Sr systematics for chemically defined Apollo 14 breccias. Proc. Lunar Sci. Conf. 3rd, p. 1515-1530.
105. Nyquist L.E., Hubbard N.J., Gast P.W., Bansal B.M., Wiesmann H. and Jahn B.M. (1973). Rb-Sr systematics for chemically defined Apollo 15 and 16 materials. Proc. Lunar Sci. Conf. 4th p. 1823-1846.
106. Nyquist L.E., Bansal B.M., Wiesmann H. and Jahn B.M. (1974). Taurus-Littrow chronology: some constraints on early lunar crustal development. Proc. Lunar Sci. Conf. 5th, p. 1515-1539.
107. Nyquist L.E., Bansal B.M., Wooden J.L. and Wiesmann H. (1977). Sr-isotopic constraints on the petrogenesis of Apollo 12 mare basalts. Proc. Lunar Sci. Conf. 8th, p. 1383-1415..
108. O'Keefe J.D. and Ahrens T.J. (1975). Shock effects from a large impact on the moon. Proc. Lunar Sci. Conf. 6th, p. 2831-2844.
109. Onorato P.I.K. and Uhlmann D.R., (1976). Heat flow in impact melts: Apollo 17 Station 6 boulder and some applications to other breccias and xenolith laden melts. Proc. Lunar Sci. Conf. 7th, p. 2449-2467.

110. Onorato P.I.K., Uhlmann D.R., and Simonds C.H. (1977). Numerical calculations of thermal history of Manicouagan impact-melt sheet. Submitted to J. Geophys. Res.
111. Papanastassiou D.A. and Wasserburg G.J. (1972a). The Rb-Sr age of a crystalline rock from Apollo 16. Earth Planet. Sci. Lett. 16, p. 289-298.
112. Papanastassiou D.A. and Wasserburg G.J. (1972b). Rb-Sr systematics of Luna 20 and Apollo 16 samples. Earth Planet. Sci. Lett. 17, p. 52-63.
113. Papike J.J. and Bence A.E. (1972). Apollo 14 inverted pigeonites: Possible samples of lunar plutonic rocks. Earth Planet. Sci. Lett. 14, p. 176-182.
114. Pepin R.O., Nyquist L.E., Phinney D. and Black D.C. (1970). Rare gases in Apollo 11 lunar material. Proc. Apollo 11 Lunar Sci. Conf., p. 1435-1454.
115. Philpotts J.A., Schuhmann S., Kouns C.W., Lum-Staab R.K.L. and Winzer S.R., (1974). Origin of Apollo 17 rocks and soils. Proc. Lunar Sci. Conf. 5th, Vol. 2, p. 1255-1267.
116. Phinney W.C., Warner J.L., Simonds C.H. and Lofgren G.E. (1972). Classification and distribution of rock types at Spur Crater. Apollo 15 Lunar Samples, Lunar and Planetary Institute, Houston, p. 149-153.
117. Phinney W.C., McKay D.S., Simonds C.H. and Warner J.L. (1976). Lithification of vitric- and clastic-matrix breccias: SEM petrography. Proc. Lunar Sci. Conf. 7th, p. 2469-2493.
118. Prinz M., Dowty E., Keil K. and Bunch T.E. (1973). Mineralogy, petrology and chemistry of lithic fragments from Luna 20 fines: Origin of the cumulate ANT suite and its relationship to high-alumina basalts. Geochim. Cosmochim. Acta, Vol. 37, p. 979-1006.
119. Quaide William and Bunch Theodore (1970). Impact metamorphism of lunar surface materials. Proc. Apollo 11 Lunar Sci. Conf., p. 711-729.
120. Quaide W. and Wrigley R. (1972). Mineralogy and origin of Fra Mauro fines and breccias. Proc. Lunar Sci. Conf. 3rd, p. 771-784.
121. Quick J.E., Albee A.L., Ma M.-S., Murali A.V. and Schmitt R.A. (1977). Chemical compositions and possible immiscibility of two silicate melts in 12013. Proc. Lunar Sci. Conf. 8th, p. 2153-2189.
122. Rhodes J.M., Rodgers K.V., Shih C.-Y., Bansal B.M., Nyquist L.E., Wiesmann H. and Hubbard N.J. (1974). The relationships between geology and soil chemistry at the Apollo 17 landing site. Proc. Lunar Sci. Conf. 5th, p. 1097-1119.
123. Ridley W.I., Brett R., Williams R.J., Takeda H. and Brown R. (1972). Petrology of Fra Mauro basalt 14310. Proc. Lunar Sci. Conf. 3rd, p. 159-170.
124. Ridley W.I., Hubbard N.J., Rhodes J.M., Wiesmann H. and Bansal B. (1973). The petrology of lunar breccia 15445 and petrogenetic implications. Jour. Geol., Vol. 81, p. 621-631.

125. Rose H.J. Jr., Cuttita F., Dwornik E.J., Carron M.K., Christian R.P., Lindsay J.R., Ligon D.T. Jr. and Larson R.R. (1970). Semimicro x-ray fluorescence analysis of lunar samples. Proc. Apollo 11 Lunar Sci. Conf. Geochim et Cosmochim Acta, p. 1493-1498.
126. Rose H.J. Jr., Cuttita F., Ansell C.S., Carron M.K., Christian R.P., Dwornik E.J., Greenland L.P., and Ligon D.T. Jr. (1972) Compositional data for twenty-one Fra Mauro lunar materials. Proc. Lunar Sci. Conf. 3rd, Vol. 2, p. 1215-1231.
127. Rose H.J. Jr., Cuttita F., Berman S., Carron M.K., Christian R.P., Dwornik E.J., Greenland L.P. and Ligon D.T. Jr. (1973). Compositional data for twenty-two Apollo 16 samples. Proc. Lunar Sci. Conf. 4th, Vol. 2, p. 1149-1159.
128. Rose H.J., Cuttitta F. Jr., Berman S., Brown F.W., Carron M.K., Christian R.P., Dwornik, E.J. and Greenland, L.P. (1974). Chemical composition of rocks and soils at Taurus-Littrow. Proc. Lunar Sci. Conf. 5th, p. 1119-1135.
129. Rose H.J. Jr., Christian R.P., Dwornik E.J., and Schnepfe M.M. (1975a). Major elemental analysis of some Apollo 15, 16, and 17 samples. Lunar Science VI, LSI, p. 686-688.
130. Rose H.J. Jr., Baedeker P.A., Berman S., Christian R.P., Dwornik E.J., Finkleman R.B. and Schnepfe M.M. (1975b). Chemical composition of rocks and soils returned by the Apollo 15, 16, and 17 missions. Proc. Lunar Sci. Conf. 6th, p. 1363-1375.
131. Ryder G. (1976). Lunar sample 15405: Remnant of a KREEP basalt — granite differentiated pluton. Earth Planet. Sci. Lett. 29, p. 255-268.
132. Ryder G. and Bower J.F. (1976a). Sample 14082 petrology. In Interdisciplinary Studies by the Imbrium Consortium, Vol. 1 (J.A. Wood, ed.). LSI contr. No. 267D, p. 41-50.
133. Ryder G. and Bower J.F. (1976b). Sample 15405 petrology. In Interdisciplinary Studies by the Imbrium Consortium, Vol. 1 (J.A. Wood, ed.) LSI Contr. 267D, p. 77-94.
134. Ryder G. and Bower J.F. (1976c). Sample 15405 petrology. In Interdisciplinary Studies by the Imbrium Consortium, Vol. II (J.A. Wood, ed.). LSI Contr. No. 268D, p. 23-26
135. Ryder G. and Bower J.F. (1976d). Sample 14312 petrology. In Interdisciplinary Studies by the Imbrium Consortium, Vol. I (J.A. Wood, ed.). LSI Contr. No. 267D, p. 55-66.
- 135a. Ryder G. and Bower J.F. (1976e). Sample 15445 petrology. In Interdisciplinary Studies by the Imbrium Consortium, Vol. II (J.A. Wood, ed.) LSI Contr. No. 268D, p. 42-60.
136. Ryder G. and Bower J.F. (1977). Petrology of Apollo 15 black-and-white rocks 15445 and 15455 — Fragments of the Imbrium impact melt sheet? Proc. Lunar Sci. Conf. 8th, p. 1895-1923.

137. Schonfeld E. (1974). The contamination of lunar highland rocks by KREEP: Interpretation by mixing models. Proc. Lunar Sci. Conf. 5th, p. 1269-1286.
138. Scoon J.H. (1972). Chemical analyses of lunar samples 14003, 14311, and 14321. Proc. Lunar Sci. Conf. 3rd, Vol. 2, p. 1335-1337.
139. Scoon J.H. (1974). Chemical analysis of lunar samples from the Apollo 16 and 17 collections. Lunar Science V, L.S.I. and J.S.C., p. 690-692.
140. Shih C.-Y. (1977). Origin of KREEP basalts. Proc. Lunar Sci. Conf. 8th, p. 2375-2401.
141. Shoemaker E.M. (1963). Impact mechanics at Meteor Crater, Arizona. The Moon, Meteorites and Comets, p. 301-336.
142. Shoemaker E.M., Bailey N.G., Batson R.M., Dahlem D.H., Foss T.H., Grolier M.J., Goddard E.N., Hait M.H., Holt H.E., Larson K.B., Rennilson J.J., Schaber G.G., Schleicher D.L., Schmitt H.H., Sutton R.L., Swann G.A., Waters A.C. and West M.N. (1969). Geologic setting of the lunar samples returned by the Apollo 11 mission. Apollo 11 Preliminary Science Report, NASA SP-214, p. 41-83.
143. Shoemaker E.M., Batson R.M., Bean A.L., Conrad C. Jr., Dahlem D.H., Goddard E.N., Hait M.H., Larson K.B., Schaber G.G., Schleicher D.L., Sutton R.L., Swann G.A. and Waters A.C. (1970). Preliminary geologic investigation of the Apollo 12 landing site. Apollo 12 Preliminary Science Report, NASA SP-235, p. 113-156.
- 143a. Simonds C.H. (1973). Sintering and hot pressing of Fra Mauro composition glass and the lithification of lunar breccias. Amer. J. Sci. 273, p. 428-439.
144. Simonds C.H., Warner J.L. and Phinney W.C. (1973). Petrology of Apollo 16 poikilitic rocks. Proc. Lunar Sci. Conf. 4th, p. 613-132.
145. Simonds C.H., Phinney W.C. and Warner J.L. (1974). Petrography and classification of Apollo 17 non-mare rocks with emphasis on samples from the Station 6 boulder. Proc. Lunar Sci. Conf. 5th, p. 337-353.
146. Simonds C.H. (1975). Thermal regimes in impact melts and the petrology of the Apollo 17 Station 6 boulder. Proc. Lunar Sci. Conf. 6th, p. 641-672.
147. Simonds C.H., Warner J.L., Phinney W.C. and McGee P.E. (1976). Thermal model for impact breccia lithification: Manicouagan and the Moon. Proc. Lunar Sci. Conf. 7th, p. 2509-2528.
148. Simonds C.H., Phinney W.C., Warner J.L., McGee P.E., Geeslin J., Brown R.W. and Rhodes M.J. (1977). Apollo 14 revisited, or breccias aren't so bad after all. Proc. Lunar Sci. Conf. 8th, p. 1869-1893.
149. Simonds C.H., Phinney W.C., McGee P.E., and Cochran A. (1978). West Clearwater, Quebec impact structure, Part I: Field geology, structure and bulk chemistry. Proc. Lunar Sci. Conf. 9th, p. 2633-2658.
150. Smith J.V., Anderson A.T., Newton R.C., Olsen E.J., Wyllie P.J., Crewe A.V., Isaacson M.S. and Johnson D. (1970). Petrologic history of the moon inferred from petrography, mineralogy, and petrogenesis of Apollo 11 rocks. Proc. Apollo 11 Lunar Sci. Conf., p. 897-925.

151. Steele I.M. and Smith J.V. (1973). Mineralogy and petrology of some Apollo 16 rocks and fines: General petrologic model of moon. Proc. Lunar Sci. Conf. 4th, p. 519-536.
152. Steele I.M. and Smith J.V. (1976). Mineralogy and petrology of complex breccia 14063,14. Proc. Lunar Sci. Conf. 7th, p. 1949-1964.
153. Stöffler D., Knoll H.-D., Reimold W.-U. and Schülen S. (1976). Grain size statistics, composition, and provenance of fragmental particles in some Apollo 14 breccias. Proc. Lunar Sci. Conf. 7th, p. 1965-1985.
154. Sutton R.L., Hait M.H. and Swann G.A. (1972). Geology of the Apollo 14 landing site. Proc. Lunar Sci. Conf. 3rd, p. 27-38.
155. Swann G.A., Bailey N.G., Batson R.M., Eggleton R.E., Hait M.H., Holt H.E., Larson K.B., McEwen M.C., Mitchell E.D., Schaber G.G., Schafer J.P., Shepard A.B., Sutton R.L., Trask N.J., Ulrich G.E., Wilshire H.G. and Wolfe E.W. (1971). Preliminary geologic investigations of the Apollo 14 landing site. Apollo 14 Preliminary Science Report. NASA SP-272, p. 39-85.
156. Swann G.A., Bailey N.G., Batson R.M., Freeman V.L., Hait M.H., Head J.W., Holt H.E., Howard K.A., Irwin J.B., Larson K.B., Muehlburger W.R., Reed V.S., Rennilson J.J., Schaber G.G., Scott D.R., Silver L.T., Sutton R.L., Ulrich G.E., Wilshire H.G. and Wolfe E.W. (1972). Preliminary geologic investigation of the Apollo 15 landing site. Apollo 15 Preliminary Science Report, NASA SP-289, p. 5-1 through 5-112.
157. Taylor G.J., Drake M.J., Hallam M.E., Marvin U.B. and Wood J.A. (1973). Apollo 16 stratigraphy: The ANT hills, the Cayley Plains, and a pre-Imbrium regolith. Proc. Lunar Sci. Conf. 4th, p. 553-569.
158. Taylor G.J. (1976) Further petrological studies of the KREEP-rich quartz-monzodiorite. In Interdisciplinary Studies by the Imbrium Consortium, Vol. 1 (J.A. Wood, ed.). LSI Contr. 267D pp. 94-95. Center for Astrophysics, Cambridge.
159. Taylor S.R. and Jakes (1974). The geochemical evolution of the moon. Proc. Lunar Sci. Conf. 5th, p. 1287-1307.
160. Taylor S.R. (1976). Geochemical constraints on the composition of the moon. Proc. Lunar Sci. Conf. 7th, p. 3461-3477.
161. Tera F. and Wasserburg G.J. (1974). U-Th-Pb systematics on lunar rocks and inferences about lunar evolution and the age of the moon. Proc. Lunar Sci. Conf. 5th, p. 1571-1599.
162. Tilton G.R. (1973). Isotopic lead ages of chondritic meteorites. Earth Planet. Sci. Lett. 19, p. 321-329.
163. Turner G., Cadogen P. and Yonge C.J. (1973). Argon selenochronology. Proc. Lunar Sci. Conf. 4th, p. 1889-1914.

164. Uhlmann D.R., Klein L., Onorato P.I.K. and Hopper R.W. (1975). The formation of lunar breccias: Sintering and crystallization kinetics. Proc. Lunar Sci. Conf. 6th, p. 693-705.
165. Ulrich G.E. (1973). A geologic model for North Ray Crater and stratigraphic implications for the Descartes region. Proc. Lunar Sci. Conf. 4th, p. 27-41.
166. Wakita H. and Schmitt R.A. (1971). Bulk elemental composition of Apollo 12 samples - Five igneous and one breccia rocks and four soils. Proc. Lunar Sci. Conf. 2nd, p. 1231-1236.
167. Walker D., Longhi J., Grove T.L., Stolper E. and Hays J.F. (1973). Experimental petrology and origin of rocks from the Descartes Highlands. Proc. Lunar Sci. Conf. 4th, p. 1013-1032.
168. Wänke H., Palme H., Baddenhausen H., Dreibus G., Jagoutz E., Kruse H., Spettel B., Teschke F. and Thacker R. (1974). Chemistry of Apollo 16 and 17 samples: Bulk composition, late stage accumulation and early differentiation of the moon. Proc. Lunar Sci. Conf. 5th, p. 1307-1337.
169. Wänke H., Palme H., Baddenhausen H., Dreibus G., Jagoutz E., Kruse H., Palme C., Spettel B., Teschke F., and Thacker R. (1975). New data on the chemistry of lunar samples: Primary matter in the lunar highlands and the bulk composition of the moon. Proc. Lunar Sci. Conf. 6th, Vol. 2, p. 1313-1340.
170. Wänke H., Palme H., Kruse H., Baddenhausen H., Cendales M., Dreibus G., Hofmeister H., Jagoutz E., Palme C., Spettel B., and Thacker R. (1976). Chemistry of lunar highland rocks: A refined evaluation of the composition of the primary matter. Proc. Lunar Sci. Conf. 7th, Vol. 3, p. 3479-3499.
171. Warner J.L. (1972). Metamorphism of Apollo 14 breccias. Proc. Lunar Sci. Conf. 3rd, p. 623-643.
172. Warner J.L., Simonds C.H. and Phinney W.C. (1973). Apollo 16 rocks: Classification and petrogenetic model. Proc. Lunar Sci. Conf. 4th, p. 481-504.
173. Warner J.L., Simonds C.H. and Phinney W.C. (1974). Impact-induced fractionation in the lunar highlands. Proc. Lunar Sci. Conf. 4th, p. 481-504.
174. Warner J.L., Phinney W.C., Bickel C.E. and Simonds C.H. (1977). Feldspathic granulitic impactites and pre-final bombardment lunar evolution. Proc. Lunar Sci. Conf. 8th, p. 2051-2066.
175. Warren P.H. and Wasson J.T. (1977). Pristine nonmare rocks and the nature of the lunar crust. Proc. Lunar Sci. Conf. 8th, p. 2215-2235.
176. Waters A.C., Fisher R.V., Garrison R.E. and Wax D. (1971). Matrix characteristics and origin of lunar breccia samples 12034 and 12073. Proc. Lunar Sci. Conf. 2nd, p. 893-907.

177. Weiblen P.W. and Roedder E. (1973). Petrology of melt inclusions in Apollo samples 15598 and 62295, and of clasts in 67915 and several soils. Proc. Lunar Sci. Conf. 4th, p. 681-703.
178. Weill D.F., McKay G.A., Kridelbaugh S.J., and Grutzeck M. (1974). Modeling the evolution of Sm and Eu abundances during lunar igneous differentiation. Proc. Lunar Sci. Conf. 6th, p. 1337-1352.
179. Wetherill G.W. (1975). Late heavy bombardment of the moon and terrestrial planets. Proc. Lunar Sci. Conf. 6th, p. 1539-1561.
180. Wilshire H.G., Stuart-Alexander D.E., and Jackson E.D. (1973). Petrology and classification of the Apollo 16 samples. Lunar Science IV, p. 784-786. The Lunar Science Institute, Houston.
181. Winzer S.R., Lum R.K.L., Schuhmann S., and Philpotts J.A. (1975). Large-ion-lithophile trace element abundances in phases from 78235,34, a lunar norite cumulate. Lunar Science VI, p. 872-875. The Lunar Science Institute, Houston.
182. Wood John A., Dickey John S. Jr., Marvin Ursula B. and Powell Benjamin N. (1970). Lunar anorthosites and a geophysical model of the moon. Proc. Apollo 11 Lunar Sci. Conf., p. 965-988.
183. Wood J.A. (1975). Lunar petrogenesis in a well-stirred magma ocean. Proc. Lunar Sci. Conf. 6th, p. 1087-1102.